



---

# DISSIPATIVE EFFECTS IN THE EARLY UNIVERSE

Rafael Cerezo Balsera

Universidad de Granada

Julio 2015

---

Directora:  
Dra. Mar Bastero Gil

*Programa de Doctorado en Física y Ciencias del Espacio*

Editorial: Universidad de Granada.Tesis Doctorales  
Autor: Rafael Cerezo Balseira  
ISBN: 978-84-9125-192-7  
URI: <http://hdl.handle.net/10481/40610>

---

El doctorando, Rafael Cerezo Balsera, y la directora de la tesis, Mar Bastero Gil, profesora titular de universidad,

**GARANTIZAMOS** al firmar esta tesis doctoral, *Dissipative effects in the early Universe*, que el trabajo ha sido realizado por el doctorando bajo la dirección de la directora de la tesis. Y hasta donde nuestro conocimiento alcanza, en la realización del trabajo se han respetado los derechos de otros autores y otras autoras a ser citadas, cuando se han utilizado sus resultados o publicaciones, así como que el doctorando ha disfrutado de una estancia en el extranjero, durante un periodo de tres meses, en la *School of Physics and Astronomy* de la Universidad de Edimburgo (Reino Unido).

Granada, 20 de mayo de 2015.

Directora de la tesis

Doctorando

Fdo: Mar Bastero Gil

Fdo: Rafael Cerezo Balsera



# Contents

---

|                                                                                                         |            |
|---------------------------------------------------------------------------------------------------------|------------|
| <b>Introduction</b>                                                                                     | <b>IX</b>  |
| <b>Introducción</b>                                                                                     | <b>XII</b> |
| <b>1 Particle physics and the early universe</b>                                                        | <b>1</b>   |
| 1.1 To the Standard Model, and beyond! . . . . .                                                        | 1          |
| 1.2 The bang of the Big Bang: inflation . . . . .                                                       | 4          |
| 1.3 Warming up inflation . . . . .                                                                      | 10         |
| <b>I Background</b>                                                                                     | <b>15</b>  |
| <b>2 Warm inflation in a potential with an inflection point</b>                                         | <b>17</b>  |
| 2.1 Cold inflation near an inflection point . . . . .                                                   | 19         |
| 2.2 Warm inflation near an inflection point . . . . .                                                   | 21         |
| 2.3 Results . . . . .                                                                                   | 23         |
| <b>3 Viscous effects in warm inflation I: background</b>                                                | <b>31</b>  |
| 3.1 Warm Inflation in a bulk viscous radiation fluid . . . . .                                          | 33         |
| 3.1.1 Eckart theory for the bulk pressure . . . . .                                                     | 34         |
| 3.1.2 Israel-Stewart theory for the bulk pressure . . . . .                                             | 35         |
| 3.1.3 Nonlinear causal dissipative hydrodynamics theory for the<br>bulk pressure . . . . .              | 37         |
| 3.2 The dynamical system of equations for warm inflation in a bulk<br>viscous radiation fluid . . . . . | 38         |
| 3.3 Numerical analysis . . . . .                                                                        | 42         |
| 3.4 Model building . . . . .                                                                            | 44         |
| 3.4.1 Chaotic model . . . . .                                                                           | 48         |
| 3.4.2 Hybrid models . . . . .                                                                           | 50         |
| 3.4.3 Hilltop models . . . . .                                                                          | 53         |
| 3.4.4 Bulk viscosity coefficients from quantum field theory . . . . .                                   | 54         |

|            |                                                                    |            |
|------------|--------------------------------------------------------------------|------------|
| <b>II</b>  | <b>Perturbations</b>                                               | <b>59</b>  |
| 4          | Dynamics of the linear perturbations in warm inflation             | 61         |
| 5          | Viscous effects in warm inflation II: perturbations                | 67         |
| 5.1        | Bulk and shear viscous effects in a radiation fluid . . . . .      | 68         |
| 5.2        | Perturbations in warm inflation with viscous effects . . . . .     | 71         |
| 5.3        | Numerical Results . . . . .                                        | 75         |
| 5.3.1      | Amplitude of the power spectrum . . . . .                          | 75         |
| 5.3.2      | Spectral index . . . . .                                           | 81         |
| 6          | Warm inflation in the weak dissipation regime                      | 85         |
| 6.1        | The weak dissipation regime . . . . .                              | 86         |
| 6.2        | Chaotic warm inflation . . . . .                                   | 88         |
| 6.3        | Warm inflation in a hilltop model . . . . .                        | 94         |
| <b>III</b> | <b>Reheating</b>                                                   | <b>97</b>  |
| 7          | WIMPlaton: inflation and dark matter unification                   | 99         |
| 7.1        | Minimal model . . . . .                                            | 101        |
| 7.1.1      | Basic properties and dynamics . . . . .                            | 101        |
| 7.1.2      | Condensate evaporation: the WIMPlaton scenario . . . . .           | 108        |
| 7.1.3      | Reheating the Standard Model . . . . .                             | 111        |
| 7.2        | Hybrid model . . . . .                                             | 115        |
| 7.2.1      | Basic properties and dynamics . . . . .                            | 115        |
| 7.2.2      | Condensate evaporation: the WIMPlaton scenario . . . . .           | 121        |
| 7.3        | Embedding in a consistent inflationary model . . . . .             | 123        |
|            | <b>Conclusions</b>                                                 | <b>127</b> |
|            | <b>Conclusiones</b>                                                | <b>131</b> |
| A          | Stability analysis for the viscosity descriptions                  | 135        |
| A.1        | Dynamical system for the Eckart case . . . . .                     | 135        |
| A.2        | Dynamical system for the NLCDH case . . . . .                      | 139        |
| B          | Semianalytic function for the spectral index with bulk viscosity   | 141        |
| C          | Radiative corrections to the minimal model of inflaton dark matter | 143        |
|            | List of figures                                                    | 145        |
|            | List of tables                                                     | 149        |





*Estamos hechos de átomos, según dicen los científicos, pero un pajarito me contó que también estamos hechos de historias.*

Eduardo Galeano

## Introduction

---

Every society at each moment in its his- or herstory develops a unique world view encompassing a model for the description of their cosmos. Modern Western society founds its cosmological notion on scientific laws bringing together observational astronomy, general relativity and particle physics; thus governing the origin, evolution, and eventual fate of the universe. The Big Bang model has been an outstanding achievement of the 20th century for the understanding in scientific terms of the cosmos. It answers old questions ranging from the infant to the present universe, while unveiling new mysteries regarding its composition. There are strong indirect evidences of a Dark Side of the Universe, comprised of dark matter, dark energy and inflation; however a confirmed description of such phenomena is still elusive.

The work contained in this thesis aims to further develop the understanding of the role of inflation and dark matter in the early universe. Our framework is the study of dissipation in such context, a natural outcome of the presence interactions in the models describing the system. Therefore, a better comprehension of dissipative processes may help in building more realistic representations of the physics of the early universe. For a clearer presentation of the results, the contents of the thesis are divided in three distinct parts, with part I and II devoted to the study of dissipation during inflation, while part III is dedicated to the connection of inflation and dark matter through dissipation in the reheating era.

Chapter 1 gives an overview of the present view of the modern cosmology, summarizing the most relevant results. In part I we will concentrate on the effects of dissipation at the background level of warm inflation, the inflationary scenario where interactions of the inflaton with other degrees of freedom are described in terms of quantum field theory. Such description consistently incorporates dissipative effects during inflation. In chapter 2 we will study the aftermath of including interactions in a class of inflationary models characterized by the existence of an inflection point in the inflationary potential [1]. These potentials arise in a variety of contexts, such as supersymmetry or string theory, providing desirable connections to low-energy phenomenology. The inflection point result from the interplay of different terms contributing to the scalar potential, but it usually requires the

fine-tuning of such terms. We will show that the situation can be alleviated in the context of warm inflation, due to the dissipation induced by the interactions of the inflaton with other degrees of freedom. Furthermore, we will analyse the dynamics of warm inflation in such a flat potential shape, and extract information regarding the field multiplicities required in the low momentum limit of the two stage (LOTS) realization of warm inflation. In chapter 3 we follow a different line in the investigation of dissipative effects, and focus on the consequences of the self interactions of the light fields in the thermal bath of warm inflation [2]. Such interactions preclude the bath from being in a perfect thermal equilibrium state, thus inducing viscous effects. In a FLRW background these effects are described by the bulk viscosity, which enhances radiation production and may help in realizing warm inflation. Nevertheless, it may also lead to the overproduction of light particles, such that the radiation bath becomes the dominant contribution to the total energy density and inflation is spoiled. Therefore, we will study the stability of the system with different hydrodynamic descriptions of the bulk viscosity, from the simplest to more realistic ones. Then, we will apply the results to the canonical  $\lambda\phi^4$  model and analyse the enlargement of the parameter space compatible with warm inflation in the presence of bulk viscosity.

Part II will be devoted to the examination of the dissipative dynamics of the perturbations at linear order in warm inflation. In chapter 4 we will discuss the details of the calculation of the power spectrum in warm inflation and the region of applicability of its analytical approximation. We will show that the coupling between the equations for the perturbations of the inflaton and the radiation bath induces a *growing mode* in the power spectrum in the strong dissipation regimen, which renders the analytical approximation invalid. The chapters included in part II try to address this feature of the LOTS realization of warm inflation. Chapter 5 follows the line initiated in chapter 3 of investigating the effect of self interaction in the radiation fluid. At the perturbation level of the FLRW metric both bulk and shear viscosities are required to describe the departures from thermal equilibrium. We will analyse the region of the parameter space where the perturbative dynamics are modified by the presence of viscosities, and whether they can control the effect of the growing mode in the power spectrum. In chapter 6 we take a different approach to deal with the growing mode. We will research the observational implications of warm inflation in the weak dissipation regimen, where there is no growing mode [3]. At the time when we carried out this work, data from the *Planck* collaboration was made available, hence we could make use of it to show the effect of dissipation even in the weak regimen. As an example, we will consider the  $\lambda\phi^4$  model, which is in tension with *Planck* data in the renormalizable single field models of inflation, and will show that the tension can be solved when embedding the model in the LOTS realization of warm inflation.

In Part III we will explore dissipation in the reheating period subsequent to inflation. Dissipation plays the key role in the energy transfer from the inflaton

to radiation bath that defines the reheating period, therefore it has been widely studied in the literature. Chapter 7 will be dedicated to the study of a particular dissipation mechanism such that the inflaton field can play the role of a dark matter candidate [4]. We will propose a configuration of interactions that will lead to a successful reheating period producing a universe dominated by radiation, while leaving a remnant of the inflaton field. The remnant will behave as an additional matter component in the universe, and we will find solutions such that the inflaton remnant is compatible the current bounds on dark matter. We will show that the mechanism is consistent with different inflationary potentials by analysing two canonical models of inflation.



*Estamos hechos de átomos, según dicen los científicos, pero un pajarito me contó que también estamos hechos de historias.*

Eduardo Galeano

## Introducción

---

Toda sociedad en cada momento de su historia desarrolla una cosmovisión única que incluye una descripción de su universo. La sociedad occidental moderna basa su cosmología en leyes científicas que parten de la astronomía observacional, la relatividad general y la física de partículas para gobernar el origen, la evolución y el posible destino del universo. El modelo del Big Bang ha sido un logro fundamental del siglo XX para la comprensión en términos científicos del cosmos. Es capaz de dar respuesta a preguntas fundamentales que van desde el universo temprano hasta el actual, al mismo tiempo que revela nuevos misterios sobre sus componentes. Hay evidencias indirectas muy significativas de la existencia de un lado oscuro en el universo, compuesto de materia oscura, energía oscura e inflación; sin embargo una explicación comprobada observacionalmente sigue siendo elusiva.

Los trabajos que contiene esta tesis aspiran a contribuir al desarrollo de la comprensión del papel que juegan inflación y la materia oscura en el universo temprano. Nuestro marco de trabajo es el estudio de disipación en ese contexto, una consecuencia natural de la presencia de interacciones en los modelos que describen en sistema. Por lo tanto, una mejor intelección de los procesos disipativos puede ayudar a la construcción de representaciones más precisas de la física del universo temprano. Para una mayor claridad en la presentación de los resultados, hemos dividido la tesis en tres partes diferenciadas. Las partes I y II están dedicadas al estudio de disipación durante inflación, mientras que en la parte III analizamos la conexiones entre inflación y materia oscura a través de disipación en la era de recalentamiento.

El capítulo 1 da una visión del conjunto del enfoque de la cosmología moderna, resumiendo los resultados más relevantes. En la parte I nos centraremos en los efectos de disipación al nivel cero en teoría lineal de perturbaciones de inflación templada, el escenario de inflación en el que las interacciones del inflatón con otros grados de libertad se describen en términos de teoría cuántica de campos. Esta descripción incorpora de forma consistente los efectos de disipación durante inflación. En el capítulo 2 estudiaremos las repercusiones de la inclusión de interacciones en una categoría de modelos de inflación caracterizada por la existencia

de un punto de inflexión en el potencial inflacionario [1]. Este tipo de potenciales aparece en contextos muy variados, como pueden ser supersimetría o teoría de cuerdas, por lo que generan conexiones muy interesantes con fenomenología a bajas energías. La aparición del punto de inflexión es debida a la combinación de distintos términos que contribuyen al potencial escalar, de modo que usualmente requiere un ajuste fino de esos términos. Mostraremos que esta problemática puede desaparecer en el contexto de inflación templada, debido a la disipación inducida por la interacción del inflatón con los demás grados de libertad. Además analizaremos las dinámicas de inflación templada en este tipo de potenciales tan planos y extraeremos información sobre las multiplicidades de los campos que son necesarias en el límite de bajo momento de la realización en dos etapas (LOTS) de inflación templada. En el capítulo 3 seguiremos una línea diferente en la investigación de los efectos disipativos y nos centraremos en las consecuencias de las autointeracciones de los campos ligeros en el baño térmico de inflación templada [2]. Estas interacciones impiden que el baño térmico esté en un estado de equilibrio térmico, por lo que induce efectos viscosos. En el nivel cero de un universo descrito por la métrica FLRW, estos efectos se describen en términos de viscosidad de volumen, que aumenta la producción de radiación y puede contribuir a inflación templada. Sin embargo, también puede conducir a una producción excesiva de partículas ligeras tal que el baño térmico se convierta en la contribución dominante a la densidad de energía total, lo que produciría el fin del periodo inflacionario. Por tanto, estudiaremos la estabilidad del sistema con diferentes descripciones hidrodinámicas de la viscosidad de volumen, desde las más simples hasta descripciones más realistas. Una vez hecho esto, aplicaremos los resultados al modelo canónico de inflación  $\lambda\phi^4$  y analizaremos el incremento del espacio de parámetros compatible con inflación templada en presencia de la viscosidad de volumen.

La parte II estará dedicada al examen de las dinámicas disipativas de las perturbaciones a orden lineal en inflación templada. En el capítulo 4 discutiremos los detalles del cálculo de espectro de potencias en inflación templada y la región en la que se puede aplicar su aproximación analítica. Mostraremos que el acoplo entre las ecuaciones para las perturbaciones del inflatón y el baño térmico induce un modo creciente del espectro de potencias en el régimen de disipación fuerte, lo que invalida la aproximación analítica en ese régimen. Los capítulos recogidos en la parte II tratan de resolver este problema de la realización LOTS de inflación templada. El capítulo 5 continúa la línea iniciada en el capítulo 3 en la que investigamos el efecto de las autointeracciones en el fluido de radiación. A nivel de perturbaciones en la métrica FLRW tanto la viscosidad de volumen como la de cizña aparecen en la descripción de las desviaciones del equilibrio térmico. Analizaremos la región del espacio de parámetros en la que la dinámica de las perturbaciones se modifica debido a la presencia de las perturbaciones y la posibilidad de controlar el efecto del modo creciente del espectro de potencias. En el

capítulo 6 seguiremos un enfoque distinto para tratar el problema del modo creciente. Investigaremos las implicaciones observacionales de inflación templada en el régimen de disipación débil, donde no se manifiesta el modo creciente [3]. En el momento en el que realizamos este trabajo, se publicaron los datos de la colaboración *Planck*, de modo que pudimos utilizarlos para mostrar el efecto que tiene la presencia de disipación incluso en el régimen de disipación débil. Como ejemplo consideraremos el modelo  $\lambda\phi^4$ , que está en tensión con los datos de *Planck* en los modelos inflacionarios renormalizables con un solo campo y demostraremos que la tensión puede eliminarse al introducir el modelo en la realización LOTS de inflación templada.

En la parte III exploraremos los efectos de disipación en el periodo de recalentamiento que sigue a inflación. La disipación juega un papel fundamental en la transferencia de energía del inflatón al baño de radiación que define el periodo de recalentamiento, de modo que ha sido estudiada muy extensamente en la literatura. El capítulo 7 estará dedicado al estudio de un mecanismo de disipación concreto que permite que el inflatón sea un candidato a materia oscura [4]. Propondremos una configuración de las interacciones tal que conducirá un periodo de recalentamiento capaz de producir un universo dominado por la radiación, al mismo tiempo que un remanente del inflatón sobrevive al proceso. El remanente se comportará como una componente de materia adicional en el universo, así que buscaremos soluciones en las que este remanente es compatible con los límites actuales de materia oscura. Mostraremos que el mecanismo es consistente con diferentes modelos inflacionarios mediante el análisis de dos modelos canónicos de inflación.



*If you don't understand, ask questions. Here's to possibilities of friendship and connection and understanding.*

Chimamanda Ngozi Adichie

# Particle physics and the early universe

# 1

## 1.1 To the Standard Model, and beyond!

A major scientific effort during the 20th century led to the building of the Standard Model (SM) of particle physics [5, 6, 7]. The theory is classifying all the subatomic particles known to date as well as describing their electromagnetic, weak and strong nuclear interactions. The Standard Model is a renormalizable non-abelian gauge theory based on the local symmetry group  $SU(3)_C \otimes SU(2)_L \otimes U(1)_Y$  whose associated gauge bosons characterize the interactions included. The strong interaction is represented by the gauge bosons  $G_\mu^a; a = 1, 2, \dots, 8$  of the group  $SU(3)_C$  while the weak and electromagnetic interactions are described by a combination of the gauge bosons  $W_\mu^I, I = 1, 2, 3$  and  $B_\mu$  of the groups  $SU(2)_L$  and  $U(1)_Y$  respectively. The symmetry group is spontaneously broken to  $SU(3)_C \otimes U(1)_Q$  below the electroweak scale by the vacuum expectation value of a complex scalar field, the (Brout-Englert-Guralnik-Hagen-Kibble) Higgs field [8, 9, 10, 11], with gauge quantum numbers  $(SU(3), SU(2))_{U(1)} = (1, 2)_{1/2}$ . The matter content of the theory is organized in a threefold family structure of fermions with identical gauge quantum numbers which are shown for one family in Table 1.1 together with its field content. The lagrangian of the SM is

$$\begin{aligned} \mathcal{L} = & -\frac{1}{4} (G_{\mu\nu}^a G_a^{\mu\nu} + W_{\mu\nu}^I W_I^{\mu\nu} + B_{\mu\nu} B^{\mu\nu}) \\ & + \bar{q}_{Li} i \not{D} q_{Li} + \bar{u}_{Ri} i \not{D} u_{Ri} + \bar{d}_{Ri} i \not{D} d_{Ri} + \bar{l}_{Li} i \not{D} l_{Li} + \bar{e}_{Ri} i \not{D} e_{Ri} \\ & + (D_\mu H)^\dagger (D^\mu H) - \lambda (H^\dagger H - v^2/2)^2 \\ & - (y_{ij}^u \bar{q}_{Li} i \sigma_2 H^* u_{Rj} + y_{ij}^d \bar{q}_{Li} H d_{Rj} + y_{ij}^l \bar{l}_{Li} H e_{Rj} + \text{h.c.}), \end{aligned} \quad (1.1)$$

where Einstein summation convention is assumed,  $a$  and  $I$  are gauge indices while  $i, j$  are family subscripts. The covariant derivative is defined by

$$D_\mu = \partial_\mu - ig_s \frac{\lambda_a}{2} G_\mu^a - ig \frac{\sigma_I}{2} W_\mu^I - ig' y B_\mu, \quad (1.2)$$

|                                                  |                                  |                                   |                                                    |                                 |
|--------------------------------------------------|----------------------------------|-----------------------------------|----------------------------------------------------|---------------------------------|
| $q_L = \begin{pmatrix} u_L \\ d_L \end{pmatrix}$ | $u_R$                            | $d_R$                             | $l_L = \begin{pmatrix} \nu_L \\ e_L \end{pmatrix}$ | $e_R$                           |
| $(\mathbf{3}, \mathbf{2})_{1/6}$                 | $(\mathbf{3}, \mathbf{1})_{2/3}$ | $(\mathbf{3}, \mathbf{1})_{-1/3}$ | $(\mathbf{1}, \mathbf{2})_{-1/2}$                  | $(\mathbf{1}, \mathbf{1})_{-1}$ |

Table 1.1: Chirality and gauge quantum numbers of one family of fermions of the SM.

with  $g_s$ ,  $g$  and  $g'$  being the SU(3), SU(2) and U(1) gauge constants,  $\lambda_a$  ( $\sigma_I$ ) are the Gell-Mann (Pauli) matrices and  $y$  is the hypercharge. The field strength tensors appearing in the lagrangian are

$$G_{\mu\nu}^a = \partial_\mu G_\nu^a - \partial_\nu G_\mu^a - g_s f_{bc}^a G_\mu^b G_\nu^c \quad (1.3)$$

$$W_{\mu\nu}^I = \partial_\mu W_\nu^I - \partial_\nu W_\mu^I - g \epsilon_{JK}^I W_\mu^J W_\nu^K \quad (1.4)$$

$$B_{\mu\nu} = \partial_\mu B_\nu - \partial_\nu B_\mu \quad (1.5)$$

In addition, there is an accidental global symmetry that leaves the SM Lagrangian invariant even at the quantum level, the combination of the baryon and lepton number U(1) $_{B-L}$ . The baryon number is  $B = (-)1/3$  for (anti)quarks and  $B = 0$  for leptons while the total lepton number is  $L = L_e + L_\mu + L_\tau$  with  $L_i = (-)1$  for (anti)leptons of the  $i$ -th family and zero otherwise.

In spite of the extreme success of the SM predictions compared to the particle accelerators and cosmic rays experimental data results [12], the measurements of solar [13], atmospheric [14], reactor [15] and beam [16] neutrino oscillations along with the observations of modern cosmology showed that the SM might not be a complete theory of nature. Neutrino oscillation experiments proved that neutrinos are massive and non degenerate. Because of the lack of right handed neutrinos, neutrino masses cannot be generated within the gauge structure of the SM. Therefore, an extension of the SM is required to explain the existence of massive neutrinos.

The paradigm of modern cosmology, the Hot Big Bang scenario (BB) was developed concurrently with the SM, posing new questions the SM cannot address. The cornerstones giving rise to the BB scenario are the advent of general relativity [17] together with the observations of the expansion of the universe [18, 19], the development of the theory explaining the relative abundance of light nuclei [20, 21] and the discovery of Cosmic Microwave Background radiation (CMB)[22]. This scenario describes the evolution of the universe and its content from its beginning to the present era. It relies on the observed homogeneity and isotropy which can be described by the Friedmann-Lemaître-Robertson-Walker (FLRW) metric:

$$ds^2 = -dt^2 + a^2(t) \left[ \frac{dr^2}{1 - kr^2} + r^2(d\theta^2 + \sin^2\theta d\varphi^2) \right], \quad (1.6)$$

with  $a(t)$  being the scale factor,  $k$  the curvature and comoving spherical coordinates have been used. As for today the version of the BB scenario preferred by the observations is the  $\Lambda$ CDM model which contains six free parameters  $\{\Omega_b h^2, \Omega_c h^2, \theta_{MC}, A_s, n_s, \tau\}$ . Two of them represent the matter content of the universe: the baryonic matter density  $\Omega_b h^2$  and the cold dark matter density  $\Omega_c h^2$ . The acoustic scale  $\theta_{MC}$  contains the geometrical structure of the universe which is related to its other component, the density of dark energy. The amplitude of the primordial spectrum of perturbations  $A_s$  and the spectral index  $n_s$  encompass information about inflation, an era of accelerated expansion in the early universe that will be discussed in detail in the following section. The optical depth  $\tau$  describes the epoch of reionization when galaxies and quasars began to form. Table 1.2 shows the cosmological parameter values measured by *Planck* [23].

|                    |                       |
|--------------------|-----------------------|
| $\Omega_b h^2$     | $0.02226 \pm 0.00016$ |
| $\Omega_c h^2$     | $0.1193 \pm 0.0014$   |
| $100\theta_{MC}$   | $1.04087 \pm 0.00032$ |
| $\tau$             | $0.063 \pm 0.014$     |
| $n_s$              | $0.9653 \pm 0.0048$   |
| $\ln(10^{10} A_s)$ | $3.059 \pm 0.025$     |

Table 1.2: 68% limits on the cosmological parameter values measured by *Planck* using the CMB power spectra in combination with lensing reconstruction.

The cosmological budget poses a hint of the necessity of a grander theory describing the components of the universe. A number of observations at very different energy scales indicate that the matter content of the SM can only account for the baryonic matter representing the 4 – 5% of the total energy density, while dark matter (24 – 27%) and dark energy (68 – 72%) cannot be understood in the context of the SM with general relativity. Observations include light chemical elements abundances [24], galactic rotation curves [25, 26], weak gravitational lensing of distant galaxies by foreground structures [27, 28], weak modulation of strong lensing around individual massive elliptical galaxies [29], acceleration of the universe through observations of type Ia supernovae [30, 31], baryon acoustic oscillations in the large scale structure [32] and anisotropies [33, 23] and late-time integrated Sachs-Wolfe effect [34, 35] in the CMB. There are extensions beyond the SM proposing dark matter and dark energy candidates, with supersymmetry [36, 37], Kaluza-Klein models [38, 39, 40] and quintessence models [41, 42, 43, 44] being among the most popular proposals. Modifications of general relativity such as  $f(R)$  gravities [45, 46] or DPG braneworld models [47] also try to explain the nature of dark matter and dark energy. Nevertheless, no hypothesis have been experimentally confirmed up to date and the origin of dark matter and dark energy remains an open question.

A complementary cosmological observation evidencing the shortcomings of the SM is the absence of antibaryons in the today universe. The lack of a strong signal of solar winds annihilating with antimatter precludes its presence within the solar system [48]. Material from other parts of our entire galaxy arriving at the Earth in the form cosmic rays contains positrons and antiprotons. However its abundance is consistent with secondary production mechanisms such as collisions of matter with the interstellar medium [49, 50]. The presence of antimatter on larger scales is severely disfavoured by the measurements of  $\gamma$ -ray flux from the intergalactic medium [51, 52]. Therefore, there are no signs of traces of antibaryons in the present day observable universe while baryons are ubiquitous in all tested scales. This difference in the abundances of matter and antimatter is commonly referred to as the baryon asymmetry. Within the  $\Lambda$ CDM model the baryon asymmetry can be determined from *Planck* observations of the CMB to be  $\eta = (6.4 \pm 0.1) \times 10^{-10}$  [53] in concordance with measurements from the relative abundance of light elements [54]. The discovery of violations of parity invariance (P) [55] and its combination with charge conjugation invariance (CP) [56] suggested that the asymmetry might have been created by a dynamical process in the early universe, *baryogenesis*, from a symmetric initial state. Sakharov [57] formulated the three necessary conditions for a successful baryogenesis: baryon number violation, C and CP violation and deviation from thermal equilibrium. The SM fulfills all three conditions, however the values of the CP-violating Cabibbo-Kobayashi-Maskawa exclude a plausible baryogenesis, motivating research of physics beyond the SM. Models of particle physics beyond the SM generally contain new sources of CP violation, the most studied examples including for example electroweak baryogenesis [58, 59, 60] and leptogenesis [61, 62, 63, 64]. There are not conclusive experimental tests supporting these ideas and the subject is under current intense investigation.

Other clue about the structure of new physics beyond the SM arises from the study of the inflationary period in the early universe. Inflation is the main topic of the works included in this thesis, hence it will be minutely described in the next section.

## 1.2 The bang of the Big Bang: inflation

The original BB cosmology proposal was remarkably successful, providing a reliable description of the history of the universe from the synthesis of the light chemical elements ( $t \simeq 1\text{s}$  and  $T \simeq 100\text{MeV}$ ) until today ( $t \simeq 13.8\text{Gyr}$  and  $T \simeq 2.75\text{K}$ ). Nevertheless, the ‘old’ standard cosmology proved to suffer severe shortcomings in the predictive power. The drawbacks of the old picture are known as the *cosmological puzzles* and motivated a major change of paradigm resulting in the present understanding of cosmology. Hence our interest in briefly revisiting the cosmolog-

ical puzzles in the following paragraphs.

The horizon problem [65] is related to the causal structure of the theory. In a FLRW universe the region that is or was causally connected at some point in the history of the universe with a certain position, e.g. the position of the Earth, a time  $t$  after the Big Bang is a sphere centered at that position with radius given by the particle horizon

$$d_H \equiv \int_0^t \frac{dt}{a(t)} = \int_0^a \left( \frac{1}{aH} \right) d \ln a, \quad (1.7)$$

where  $H$  is the Hubble parameter

$$H = \frac{\dot{a}}{a}, \quad (1.8)$$

defining the horizon or Hubble radius  $(aH)^{-1}$ . In the case of the Earth, the horizon today defines the region we can currently observe, the *observable universe*. The subtle difference between the particle horizon and the horizon lies in the moment when the causal connection is made: the former takes into account the whole history of the observer while the latter only considers a specific time. The contrast will prove useful if the two quantities evolve in a different manner. By definition the horizon is always a positive quantity, hence the particle horizon in Eq. (1.7) grows with time. The evolution of the horizon depends on the component dominating the energy density of the universe. For a fluid with density  $\rho$ , pressure  $p$  and equation of state  $p = \omega\rho$ , the horizon evolves as

$$(aH)^{-1} \propto a^{\frac{1}{2}(1+3\omega)}. \quad (1.9)$$

In the old BB model, the universe was believed to be dominated by either relativistic (radiation) or non-relativistic (matter) species for the most part of the evolution, the dark energy only coming to dominate at a very late epoch. The combination  $(1 + 3\omega)$  is positive for both matter and radiation causing the horizon to monotonically increase. The consequence of this behaviour is that regions beginning to establish causal contact at the present era were never causally connected in the past. In this context, it is very hard to understand why we observe regions at opposite directions in the sky with the exact same measured temperature in the CMB. As they just established causal contact with the Earth, they could not have communicated yet with each other according to the old BB picture, hence no physical mechanism could establish thermal equilibrium between them. Following this line of reasoning, the old BB model could not explain the observed homogeneity in the universe, but rather had to impose it as an initial condition in an unnatural large amount of causally disconnected regions.

The flatness problem [66, 67] refers to the spatial geometry of the observed universe. Geometry is described in terms of the density parameter, the ratio of the

actual energy density of the universe,  $\rho$  to the critical energy density,  $\rho_c$ , defined as the energy density for the universe to be spatially flat,

$$\Omega \equiv \left( \frac{\rho}{\rho_c} \right) = \frac{\rho}{3H^2 m_P^2}, \quad (1.10)$$

where  $m_P$  is the reduced Planck mass,  $m_P \simeq 2.435 \times 10^{18} \text{GeV}$ . Boomerang[68] and Maxima[69] collaborations measured the present density parameter to be very close to a flat geometry solution with the most accurate result up to date,  $|\Omega_0 - 1| = 0.001 \pm 0.006$ , given by the combination of the *Planck*, WMAP and baryon acoustic oscillation results [53]. This fact might be problematic because of the time dependence of the density parameter, whose evolution is given by the differential equation

$$\frac{d\Omega}{d \ln a} = (1 + 3\omega)\Omega(\Omega - 1). \quad (1.11)$$

In the old version of the BB model the flat solution is an unstable fixed point due to the positive combination  $(1 + 3\omega)$ . Therefore, for the universe to be as close to the flat solution as observed after 13.8Gyr of evolution, the initial conditions must be unacceptably fine tuned, e.g.  $|\Omega(t = 1s) - 1| \lesssim 10^{-16}$ . The fine tuning is even more unreasonable when the horizon problem is taken into account, as the initial conditions for each of the enormous number of causally disconnected region must be fine tuned separately.

The problem of the origin of the inhomogeneities is related to the formation of the structures observed in the universe. Despite the measured large scale homogeneity, a plethora of small scale structure is observed, such as stars, galaxies, clusters and superclusters. The standard picture for the formation of such rich abundance of structure defends the process of gravitational collapse of small primordial overdense regions into the array of structure present today. The CMB photons did not participate in the gravitational collapse, therefore they carry today an imprint of the primeval density inhomogeneity, which was discovered to be of one part in  $10^5$  by the COBE satellite[70]. The old BB paradigm was not able to propose a mechanism producing such inhomogeneities in the energy density, and also consigned it to the realm of initial conditions.

The solution of the cosmological puzzles inspired the development of the inflationary paradigm [71, 72, 73], modifying the picture of the early universe provided by the BB model. The idea behind inflation is an epoch during the first stages of the history of the universe when the space expanded with positive acceleration,  $\ddot{a}(t) > 0$ . The simplest and most common way to achieve such acceleration is through a single scalar field dominating the energy density of the universe during inflation. Not surprisingly, the scalar field is known as the *inflaton*,  $\phi$ . Scalar fields can mimic different equations of state depending on their dynamics, as their energy density and pressure are defined by

$$\rho_\phi = \dot{\phi}^2 + V(\phi), \quad p_\phi = \dot{\phi}^2 - V(\phi), \quad (1.12)$$

where a dot indicates time derivative and  $V(\phi)$  is the potential of the inflaton. Therefore, the equation of state is given by

$$\omega_\phi = \frac{\dot{\phi}^2 - V(\phi)}{\dot{\phi}^2 + V(\phi)}. \quad (1.13)$$

In a FLRW universe dominated by the inflaton, the acceleration of the expansion is given by

$$\frac{\ddot{a}}{a} = -\frac{\rho_\phi}{6m_P^2}(1 + 3\omega_\phi). \quad (1.14)$$

For the acceleration to be positive, the combination  $(1 + 3\omega_\phi)$  must be negative. This requirement could not be fulfilled in the BB model without inflation, as we saw in the review of the cosmological puzzles. Nevertheless, a scalar field with a negligible kinetic energy compared to the potential,  $V(\phi) \gg \dot{\phi}^2$ , mimics a cosmological constant with equation of state  $\omega \simeq -1$ . In that case, the combination  $(1 + 3\omega_\phi)$  is negative and the universe expands with a positive acceleration. The condition  $V(\phi) \gg \dot{\phi}^2$  is a constraint in the possible shapes of the inflationary potential, in this sense the potentials suitable for a prosperous inflation are said to be *flat*.

Inflation provides an elegant resolution for the cosmological puzzles. The horizon and flatness problems can be avoided due to the negative combination  $(1 + 3\omega_\phi)$  during the inflationary epoch. According to Eq.(1.9) the horizon shrinks during inflation, therefore if the inflationary era was long enough, the horizon in the early universe was larger than in the present age. Hence the particle horizon today is much larger than the Hubble radius because the particle horizon got most of its contribution from early times. As a consequence, regions that currently are not in causal contact were causally connected in the past, so that physical mechanisms could establish the observed homogeneity. The flatness problem is evaded because the  $\Omega = 1$  solution is turned into an attractor of Eq. (1.11), for that reason a different set of initial conditions will generate a flat space time today and no fine tuning is required. The problem of the origin of the inhomogeneities is solved due to quantum effects in the scalar field. The inflaton takes slightly different values in different regions of the space, providing a profile of over- and underdense sectors that will evolve later on in the small scale structure of the universe through gravitational collapse.

In order to describe dynamics during inflation, the scalar field is split in a spatially homogeneous background component and spatially inhomogeneous perturbations around it,

$$\Phi(x, t) = \phi(t) + \delta\phi(x, t) + \dots \quad (1.15)$$

The background evolution is governed by the Klein-Gordon equation combined

with the Friedmann equation

$$\ddot{\phi} + 3H\dot{\phi} + V_\phi = 0, \quad (1.16)$$

$$H^2 = \frac{\rho_\phi}{3m_P^2}, \quad (1.17)$$

where  $V_\phi$  is the derivative of the potential with respect to the field. The standard approximation technique for studying the inflationary solutions of Eq. (1.16) is the slow-roll approximation. It is assumed that the potential is flat enough for the motion of the inflaton to be overdamped, so that the nearly constant potential is the dominant source of energy density in the early universe. Under the slow-roll approximation the system of Eqs. (1.16,1.17) simplifies to

$$\dot{\phi} \simeq \frac{-V_\phi}{3H}, \quad (1.18)$$

$$H^2 \simeq \frac{V(\phi)}{3m_P^2}. \quad (1.19)$$

The slow-roll approach is accurate when two conditions hold

$$\epsilon(\phi) \ll 1, \quad |\eta(\phi)| \ll 1, \quad (1.20)$$

where the slow roll parameters  $\epsilon$  and  $\eta$  are defined by<sup>1</sup> [74, 75]

$$\epsilon(\phi) = \frac{m_P^2}{2} \left( \frac{V_\phi}{V} \right)^2, \quad (1.23)$$

$$\eta(\phi) = m_P^2 \frac{V_{\phi\phi}}{V}. \quad (1.24)$$

In the majority of the models inflation ends when the slow-roll conditions are violated. The duration of the inflationary period is quantified by the logarithm of the ratio of the scale factor at the end to its initial value, the number of e-folds,

$$N_e = \ln \frac{a(t_{\text{end}})}{a(t)} = \int_t^{t_{\text{end}}} H dt. \quad (1.25)$$

The exact number of e-folds required to solve the horizon and flatness problem depends on the details of the evolution subsequent to the inflationary epoch. After

<sup>1</sup>There is an alternative definition in terms of the Hubble parameter

$$\epsilon_H = 2m_P^2 \left( \frac{H_\phi}{H} \right)^2, \quad (1.21)$$

$$\eta_H = 2m_P^2 \frac{H_{\phi\phi}}{H}, \quad (1.22)$$

in slow-roll  $\epsilon_H \rightarrow \epsilon$  and  $\eta_H \rightarrow \eta - \epsilon$ .

inflation an era of *reheating* is believed to take place [76, 77, 78, 79], where the energy density stored in the inflaton field was dissipated into other degrees of freedom and the tested features of the old BB paradigm were recovered. The specifics of reheating are not known yet, however, we can place limits on the minimum number of e-folds required to solve the puzzles. Assuming that the energy density is constant during inflation, this number is given by [80]:

$$N_e^{\min} \simeq 62 - \ln \frac{10^{16} \text{GeV}}{\rho_f^{1/4}} - \frac{1}{3} \ln \frac{\rho_f^{1/4}}{\rho_{\text{reh}}^{1/4}}, \quad (1.26)$$

where  $\rho_f$  and  $\rho_{\text{reh}}$  are the energy densities at the end of inflation and at the end or reheating respectively. The minimum number of e-folds varies between  $N_e^{\min} = [25, 70]$ , with the upper limit arising from inflation at the Planck scale and instantaneous reheating, and the lower limit coming from low scale inflation and a long reheating period. Most popular models in the literature consider the intermediate range  $N_e = [50, 60]$ .

There are two observable magnitudes that can be extracted from the inflaton perturbations. The power spectrum  $\mathcal{P}_{\mathcal{R}}$  represents the power of the scalar fluctuations at each comoving scale. The tensor-to-scalar ratio  $r$  measures the amplitude of the gravitational waves  $r$  produced during inflation by the tensor perturbations relative to the amplitude of the scalar fluctuations. In the slow-roll approximation, the power spectrum of a comoving scale  $\lambda$  with comoving wave number  $k$  can be computed from background quantities to be

$$\mathcal{P}_{\mathcal{R}}(k) = \left[ \left( \frac{H}{\dot{\phi}} \right) \left( \frac{H}{2\pi} \right) \right]_{k=aH}^2, \quad (1.27)$$

where this expression is understood to be evaluated when the scale *crosses the horizon* during inflation,  $k = aH$ . Before horizon crossing, the scale is *inside the horizon*,  $k > aH$  and the curvature perturbation induced by the quantum fluctuation evolves according to the dynamics of the particular model of inflation. After horizon crossing the scale is *outside the horizon*,  $k < aH$ , with the curvature perturbation remaining constant in single field models. Inflation predicts the scale dependence of the power spectrum to be

$$\mathcal{P}_{\mathcal{R}}(k) = A_s \left( \frac{k}{k_0} \right)^{n_s - 1}, \quad (1.28)$$

where  $A_s$  is the amplitude of the power spectrum,  $k_0$  is a reference scale and  $n_s$  is the spectral index. The most common models of slow-roll inflation predict the spectral index to be

$$n_s - 1 = -6\epsilon + 2\eta. \quad (1.29)$$

During inflation  $\epsilon \ll 1$  and  $|\eta| \ll 1$ , therefore the spectral index is predicted to be very close to  $n_s = 1$  implying a nearly scale invariant power spectrum. The slow-roll approach also allows to compute the spectrum of gravitational waves

$$\mathcal{P}_{\text{grav}}(k) = \frac{2}{m_P^2} \left( \frac{H}{2\pi} \right)_{k=aH}^2, \quad (1.30)$$

which is parametrized as

$$\mathcal{P}_{\text{grav}}(k) = A_t \left( \frac{k}{k_0} \right)^{n_t}. \quad (1.31)$$

The spectral index of the tensor modes in single field inflation is also predicted to be nearly scale invariant,  $n_t = -2\epsilon$ . Experiments looking for traces of primeval gravitational waves describe its amplitude as a ratio to the amplitude of the scalar perturbations through the tensor-to-scalar ratio

$$r = \frac{A_t}{A_s}. \quad (1.32)$$

The nearly scale invariant spectrum of scalar perturbations and the non-zero amplitude of the tensor perturbations are the two most outstanding predictions of the inflationary paradigm. The former was confirmed by the observations of the COBE satellite and the balloon experiments Boomerang and Maxima[70, 81]. The most accurate current estimation of the spectral index is  $n_s = 0.9616 \pm 0.0094$  made by the *Planck* collaboration[53]. The BICEP2 collaboration claimed the discovery of gravitational waves through measurements of the CMB polarization [82], however as for today it is not yet clear whether the polarization they found is due to a real signal of gravitational waves or a background signal of dust emission [83].

Inflation is so far the only paradigm solving the cosmological puzzles consistent with observations. This fact in combination with the confirmation of its prediction of a nearly scale invariant power spectrum prompted the incorporation of inflation in the standard BB model. Inflation answered some of the old questions of cosmology and proposed new challenges. The SM together with general relativity is not able to nominate a successful candidate to play the role of the inflaton, therefore motivating research beyond known physics.

### 1.3 Warming up inflation

The main features of inflation such as the accelerated expansion, the nearly scale invariant power spectrum and the generation of gravitational waves are well understood. However the details of the particle physics model underlying inflation are still a mystery, because the observational data cannot choose a preferred candidate in the plentiful zoo of proposals. Realistic particle physics descriptions of

inflation should include couplings of the inflaton to other species, so that it can decay during the reheating epoch and repopulate the universe with the matter content of the SM. Nevertheless, the standard picture of inflation assumes that the role of the interactions is negligible during the inflationary era. Any other component present along with the inflaton is diluted away by the spurt of acceleration and the universe ends in a supercooled state. This behaviour inspires us to refer to this picture as *cold inflation*.

An alternative picture is *warm inflation*, originally proposed in [84, 85] following on earlier work in [86, 87]. In this scenario the interactions of the inflaton field with other degrees of freedom are taken into account during inflation, with dissipation of energy from the inflaton to the other species as a natural outcome. The concomitant particle production may balance the dilution effect of the accelerated expansion if dissipation is strong enough, resulting in an inflationary state that is far from the supercooled vacuum that is conventionally considered. In particular, if the resulting particles have sufficiently strong interactions between them, they can possibly reach a nearly-thermal state at a temperature  $T > H$ , thus potentially changing the dynamics of inflation.

The quantum field theory origin of the dissipation needed to realize warm inflation was first examined in [88]. This investigation proposed that solutions relevant to warm inflation should be explored within an adiabatic approximation of quantum field theory, which is the approximation that has been followed by all subsequent research in this area. The works [88, 89] showed that couplings of the inflaton to light degrees of freedom in a thermal bath will induce thermal corrections to the inflationary potential that may spoil its flatness, thus ending inflation. Therefore, they proved that not every interaction pattern is compatible with inflation. Most scenarios considered in the literature so far in the context of quantum field theory are based on the two-stage interaction pattern first proposed in [90]. The supersymmetric version of this pattern is described in terms of the chiral superfields  $\Phi$ ,  $X$  and  $Y$  with the superpotential [91, 92]

$$W = g\Phi X^2 + hXY^2 + f(\Phi). \quad (1.33)$$

The scalar component of the superfield  $\Phi$  describes the inflaton field, with an expectation value  $\phi = \varphi/\sqrt{2}$ , which we assume to be real, and the generic holomorphic function  $f(\Phi)$  describes the self-interactions in the inflaton sector. The expectation value of the inflaton field gives large masses to the bosonic and fermionic components of the intermediate superfields  $X$ . They catalyze the production of the components of the superfields  $Y$ , which remain light, producing a nearly-thermal bath of radiation. Renormalizable superpotentials of the form in Eq. (1.33) are ubiquitous in supersymmetric models, such as for example the NMSSM, where the additional singlet could play the role of the inflaton and dissipate its energy into (s)quarks and (s)leptons through the Higgs portal, e.g.  $W = g\Phi H_u H_d + hQ H_u U + \dots$ . Notice, however, that a much larger number of fields

is required to achieve a sufficient number of e-folds of inflation than in the MSSM. Such a superpotential also arises in D-brane constructions, where dissipative effects have been shown to play an important role in overcoming the associated eta-problem [93].

In the region where the microphysical dynamics determining dissipation are faster than the macroscopic motion of the background inflaton and the expansion,

$$\Gamma_\chi > \left| \frac{\dot{\phi}}{\phi} \right|, H, \quad (1.34)$$

with  $\Gamma_\chi$  being the decay width of the heavy bosonic field, the non-local effects of dissipation yield, to leading order, an additional friction term in the inflaton's equation of motion

$$\ddot{\phi} + (3H + \Upsilon)\dot{\phi} + V_\phi = 0. \quad (1.35)$$

The dissipative coefficient  $\Upsilon$  helps overdamping the inflationary trajectory, thus allowing for longer periods of slow-roll inflation. It can be computed microscopically in the particular particle physics realization of inflation in Eq.(1.33) and may in general depend on the value of the inflaton field and the properties of the multi-particle state produced by dissipation. The leading contribution to the dissipation coefficient has the following form [94]:

$$\Upsilon = \frac{4}{T} (2g^2)^2 \varphi^2 \int \frac{d^4p}{(2\pi)^4} \rho_\chi^2 n_B(1 + n_B), \quad (1.36)$$

where  $n_B(p_0) = [e^{p_0/T} - 1]^{-1}$  is the Bose-Einstein distribution and  $\rho_\chi$  is the spectral function for the scalar component,  $\chi$ , of the  $X$  field,

$$\rho_\chi(p_0, p) = \frac{4\omega_p \Gamma_\chi}{(p_0^2 - \omega_p^2)^2 + 4\omega_p^2 \Gamma_\chi^2}, \quad (1.37)$$

where  $\omega_p = \sqrt{\tilde{m}_\chi^2 + p^2}$  for modes of 3-momentum  $|\mathbf{p}| = p$  and energy  $p_0$ , and  $\tilde{m}_\chi$  is the effective mass of the  $\chi$  scalars including the thermal corrections induced by the  $Y$  fields

$$\tilde{m}_\chi^2 = m_\chi^2 + \frac{h^2 N_Y}{4} T^2. \quad (1.38)$$

The integral in Eq. (1.36) receives contributions from virtual  $\chi$  modes with low momentum and real  $\chi$  modes with momentum near the pole. The solution can be written as the sum of both contributions [95, 94, 96, 97]

$$\begin{aligned} \Upsilon &\simeq \Upsilon_{LM} + \Upsilon_P \\ &\simeq \frac{h^2}{16\pi} N_X N_Y \frac{T^3}{\phi^2} + \frac{8}{\sqrt{2\pi}} \frac{g^2 N_X}{h^2 N_Y} \sqrt{T m_\chi} e^{-m_\chi/T}, \end{aligned} \quad (1.39)$$

In this thesis, we will focus our analysis in the region of the parameter space where the low momentum contribution is the dominant contribution to the dissipative coefficient,  $m_\chi/T \geq 10$  and  $h\sqrt{N_Y} \simeq 1$  [96]. For convenience, we will write the low momentum contribution in terms of an effective dissipation parameter  $C_\phi$  containing the information about the field couplings and multiplicities

$$\Upsilon \simeq C_\phi \frac{T^3}{\phi^2}, \quad C_\phi \simeq \frac{h^2 N_Y}{16\pi} N_X. \quad (1.40)$$

Thermal corrections to the inflaton potential are under control in the region  $m_\chi/T \geq 10$  due to the Boltzmann suppression caused by the mass of the heavy fields being larger than the temperature [98]

$$\frac{\Delta V_T}{T^4} \sim - \left( \frac{m_X}{T} \right)^{3/2} \exp \left[ -\frac{m_X}{T} \right]. \quad (1.41)$$

The thermalized radiation fluid has an energy density

$$\rho_r \simeq \frac{\pi^2}{30} g_* T^4, \quad (1.42)$$

where  $g_*$  is the effective number of light degrees of freedom, and is sourced by the dissipative motion of the inflaton field, yielding

$$\dot{\rho}_r + 3H(\rho_r + p_r) = \Upsilon \dot{\phi}^2 \quad (1.43)$$

where  $p_r$  is the pressure associated with the radiation fluid. In warm inflation the radiation bath is not redshifted by the expansion, due to the additional dissipative source term [84, 85]. The radiation energy density needs, however, to be subdominant to achieve a period of accelerated expansion, i.e.  $\rho_r \ll \rho_\phi$ . Nevertheless, the associated temperature may be larger than the expansion rate,  $T > H$ , which makes the effects of expansion negligible in computing the dissipation coefficient in Eq.(1.40). Otherwise, when  $T \ll H$ , dissipative effects can be disregarded and the standard cold inflation scenario is recovered. In the intermediate region,  $T \sim H$ , both dissipative effects and the expansion of the universe need to be taken into account in computing the dissipation coefficient, and the region has not been explored so far.

In warm inflation the additional friction term  $\Upsilon$  may help to achieve the overdamped evolution characterizing the slow roll approximation. Once the field  $\phi$  is in the slow-roll regime, the evolution of the radiation fluid is also generically overdamped, and the equations of motion reduce to

$$3H(1+Q)\dot{\phi} \simeq -V_\phi, \quad (1.44)$$

$$4\rho_r \simeq 3Q\dot{\phi}^2, \quad (1.45)$$

where we have introduced the dissipative ratio  $Q = \Upsilon/(3H)$ , which may increase or decrease during inflation depending on the particular model [91]. In the limit of *strong dissipation*,  $Q \gg 1$ , the evolution of the inflaton will be severely affected by its interactions with other species while in the *weak dissipation* regime,  $Q \ll 1$ , the cold inflation solution will be recovered. The cold inflation slow-roll conditions in Eq. (1.20) are corrected in warm inflation by the dissipative ratio

$$\epsilon(\phi) \ll 1 + Q, \quad |\eta(\phi)| \ll 1 + Q, \quad (1.46)$$

and supplemented by two additional conditions[99]

$$\beta_\Upsilon = m_P^2 \left( \frac{\Upsilon_\phi V_\phi}{\Upsilon V} \right) \ll 1 + Q, \quad (1.47)$$

$$\delta = \frac{TV_{T\phi}}{V_\phi} < 1, \quad (1.48)$$

where  $\beta_\Upsilon$  measures the variation of the dissipation coefficient with respect to the inflaton field and  $\delta$  ensures that thermal corrections to the potential are under control. Dissipation modifies the inflaton perturbations in warm inflation through the effect of the thermal bath even in the weak dissipation limit. A thermal gaussian noise term  $\xi_k$  described by the fluctuation-dissipation theorem is added to the perturbations evolution equation turning it into a Langevin equation [100, 101, 102], whose form at zero order in the metric perturbations is

$$\delta\ddot{\phi}_k + 3H(1+Q)\delta\dot{\phi}_k + \frac{k^2}{a^2}\delta\phi_k \simeq \sqrt{2\Upsilon T}a^{-3/2}\xi_k, \quad (1.49)$$

for the Fourier transform  $\delta\phi_k$  of a inflaton perturbation with wavenumber  $k$ . The presence of interactions during inflation can drastically alter the inflationary observables of warm inflation compared to those of cold inflation. The computation of such observables is very involved, and usually requires numerical techniques. An analytical approximation was calculated in [99, 101, 102]

$$\mathcal{P}_{\mathcal{R}}^{1/2} \simeq \left( \frac{H}{2\pi} \right) \left( \frac{3H^2}{V_\phi} \right) (1+Q)^{5/4} \left( \frac{T}{H} \right)^{1/2}, \quad (1.50)$$

however, later works [103, 104] proved that this approximation was only valid in the weak dissipation regime, and in the case where interactions are not sufficiently strong for the inflaton perturbations to thermalize. We will come back to this subject in part II of this thesis.

# Background

---



*We all have different understandings of what truth is, and we are in danger of each believing that our truth is the one and only absolute truth. I think a search for understanding is much more serviceable to humankind.*

Jocelyn Bell Burnell

## Warm inflation in a potential with an inflection point

---

The slow-roll inflationary paradigm requires a particular shape of the scalar potential, such that the motion of the inflaton is overdamped and the nearly constant potential is the dominant source of energy density in the early universe. While a profusion of phenomenological potentials with this concept of flatness have been constructed in the literature, the main challenge has been to embed the inflationary dynamics within a more fundamental theory that reduces to the Standard Model at low energies. This is important not only in establishing a connection between inflation and low-energy particle phenomenology but also due to the sensitivity of the inflationary dynamics to ultraviolet effects close to the Planck scale.

This has motivated a search for inflaton candidates in supersymmetric (SUSY) theories, in particular in the context of supergravity/string theory (see e.g. [105]), which provides the best-known candidate for a fundamental theory of quantum gravity. These scenarios have the appealing feature of naturally including several additional scalar fields, in particular the superpartners of the Standard Model fermions and also the Higgs fields, as well as a variety of extra-dimensional moduli. Moreover, these models generically exhibit a multitude of directions in field space along which the scalar potential is completely flat in the supersymmetric limit and which are uplifted by different SUSY breaking effects. For example, even the simplest supersymmetric extension of the Standard Model, the MSSM, includes nearly 300 flat directions corresponding to gauge invariant combinations of the matter and Higgs superfields [106].

Flat directions can be lifted by different effects, including soft terms from SUSY breaking in a hidden/sequestered sector, renormalizable and non-renormalizable terms in the superpotential, as well as non-perturbative effects (e.g. gaugino condensation). In the context of string theory, these effects are generically related to the geometry and topology of the compactified extra-dimensions, which typically involves different fluxes and/or D-brane configurations. All these different effects may *a priori* yield both attractive and repulsive contributions to the scalar poten-

tial, which may conspire to produce an inflection point or even a saddle point in the potential.

The resulting flatness thus provides a very attractive setup for inflationary dynamics, and several successful models have been constructed in the literature. In the context of the MSSM flat directions, inflection points may for example result from the interplay between repulsive soft trilinear  $A$ -terms and (non-)renormalizable terms in the superpotential, providing not only inflationary models consistent with observational data but also interesting connections to low-energy phenomenology, such as neutrino masses, natural dark matter candidates and the recent Higgs mass from LHC [107, 108, 109, 110, 111, 112, 113, 114, 115, 116, 117, 118]. Several different flat directions in the MSSM field space have been analyzed so far, including simple extensions such as additional singlet fields leading to hybrid inflation models [119], as well as taking into account supergravity corrections [120, 121] and possible embeddings within the string theory landscape [122]. In the context of string theory, several new possibilities arise, as for example the case of warped D-brane inflation [123, 124, 125, 126, 127], where the D-brane potential receives a broad array of contributions such as Coulomb-like interactions in brane-antibrane pairs, couplings to the four-dimensional scalar curvature and several different moduli stabilization effects in the bulk of the compactification. A recent statistical analysis of these contributions has shown that successful models typically occur near an inflection point in the potential [128]. Such features may also be found in closed-string moduli dynamics, for example in the context of racetrack models [129] and the so-called accidental inflation scenarios [130, 131].

Inflection point inflation thus appears in a broad range of different setups, being quite successful in terms of consistency with observational data [132], as well as providing a natural embedding within ultraviolet completions of the Standard Model and desirable links to low-energy phenomenology. However, these models are far from generic and typically require a fine-tuning of the different contributions to the scalar potential, making inflation rather special within the vast landscape of different possibilities.

We will revisit inflationary dynamics near an inflection point in the potential taking into account the effects of dissipation in the inflaton's motion. The friction term representing dissipation in the inflaton's equation of motion helps overdamping its trajectory, thus allowing for longer periods of slow-roll inflation and alleviating the need for a very flat potential (see e.g. [91]), which is particularly important in the context of supergravity and string theory [133, 134, 135, 93], where one typically finds a severe 'eta-problem'. In this sense, we expect the inclusion of dissipative effects to minimize the fine-tuning of different terms in the scalar potential required for a sufficiently long period of inflation near an inflection point. We consider as a working example a renormalizable flat direction in a  $U(1)_{B-L}$  extension of the MSSM.

## 2.1 Cold inflation near an inflection point

As discussed earlier, scalar potentials exhibiting an inflection point may arise in a variety of models in supersymmetric theories and supergravity/string theory models. For concreteness, we will consider throughout most of our discussion a simple example introduced in [107, 111] and also considered in [119], consisting of a low-scale extension of the MSSM with an additional  $U(1)_{B-L}$  symmetry and right-handed neutrino superfields. In particular, we focus on the scalar potential induced for the  $NH_u L$  flat direction, parametrized by a scalar field  $\phi$  that plays the role of the inflaton and which, without loss of generality, we take to be real. This flat direction is lifted by a renormalizable term in the superpotential and by soft-SUSY breaking terms, yielding:

$$V(\phi) = \frac{1}{2}m_\phi^2\phi^2 + \frac{h^2}{12}\phi^4 - \frac{Ah}{6\sqrt{3}}\phi^3. \quad (2.1)$$

For  $A \simeq 4m_\phi$ , this potential exhibits an approximate saddle point for a field value  $\phi_0 \simeq \sqrt{3}m_\phi/h$ , such that  $V'(\phi_0) \simeq V''(\phi_0) \simeq 0$ , which is thus suitable for inflation. We may then define [119]:

$$A = 4m_\phi\sqrt{1 - \frac{\beta^2}{4}} \quad (2.2)$$

and expand the potential about the generic point of inflection, yielding for  $\beta \ll 1$ , to lowest order:

$$V(\phi) \simeq V_0 \left( 1 + 3\beta^2 \left( \frac{\phi - \phi_0}{\phi_0} \right) + 4 \left( \frac{\phi - \phi_0}{\phi_0} \right)^3 \right), \quad (2.3)$$

where  $V_0 = V(\phi_0)$ . This clearly shows that, for  $\beta = 0$ ,  $\phi_0$  is a saddle point in the potential, with  $\beta$  determining the deviations from this case, i.e. the fine-tuning of the parameters in the potential required for a sufficiently flat inflationary potential. Note that for real values of  $\beta$ , the potential exhibits an inflection point at  $\phi_0$ , whereas for imaginary values of  $\beta$  it develops a local minimum at  $\phi > \phi_0$ , as illustrated in Fig. 2.1. This latter option could be suited for inflation with the field trapped in the false vacuum and then tunneling into the true minimum, as in the old inflationary picture. However, this does not lead to a graceful exit into a radiation-dominated era, so we will not consider this case in the remainder of our discussion.

The inflationary dynamics, in the absence of dissipation, is determined by the slow-roll parameters, which are in this case given by:

$$\begin{aligned} \epsilon_\phi &= \frac{1}{2}m_P^2 \left( \frac{V_\phi(\phi)}{V(\phi)} \right)^2 \simeq \frac{1}{2} \left( \frac{m_P}{\phi_0} \right)^2 (3\beta^2 + 12\Delta_\phi^2)^2, \\ \eta_\phi &= m_P^2 \frac{V_{\phi\phi}(\phi)}{V(\phi)} \simeq 24 \left( \frac{m_P}{\phi_0} \right)^2 \Delta_\phi, \end{aligned} \quad (2.4)$$

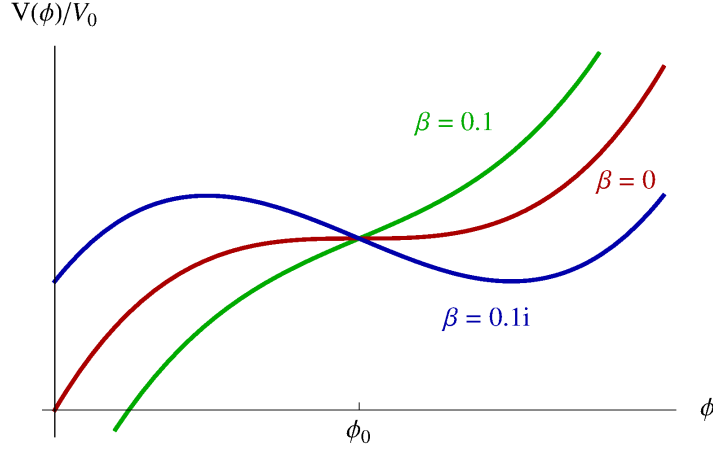


Figure 2.1: Normalized scalar potential for different values of the fine-tuning parameter  $\beta$ .

where  $m_P = 2.4 \times 10^{18}$  GeV is the reduced Planck mass,  $\Delta_\phi = (\phi - \phi_0)/\phi_0$  and we have taken  $V(\phi) \simeq V_0$ , which holds for  $\Delta_\phi, \beta \ll 1$ . From these quantities we may determine the amplitude and tilt of the resulting spectrum of density perturbations, given by:

$$\begin{aligned} \mathcal{P}_R &\simeq \left(\frac{H}{\dot{\phi}}\right)^2 \left(\frac{H}{2\pi}\right)^2 \simeq \frac{1}{24\pi^2} \frac{V_0/m_P^4}{\epsilon_{\phi_*}}, \\ n_s &\simeq 1 + 2\eta_{\phi_*} - 6\epsilon_{\phi_*} \simeq 1 + 48 \left(\frac{m_P}{\phi_0}\right)^2 \Delta_{\phi_*}, \end{aligned} \quad (2.5)$$

where  $\phi_*$  denotes the value of the field when the relevant CMB scales left the horizon about 40-60 e-folds before the end of inflation, and we have used that  $|\eta_{\phi_*}| \gg \epsilon_{\phi_*}$  for  $\Delta_\phi, \beta \ll 1$ . These two conditions can be used to determine the constant term in the potential  $V_0$  and  $\phi_*$ , leaving  $\phi_0$  and  $\beta$  as the only undetermined parameters.

The dynamics of inflation is governed by the slow-roll equation:

$$3H\dot{\phi} \simeq -V_\phi(\phi), \quad (2.6)$$

with  $H^2 \simeq V(\phi)/3m_P^2$ . Inflation ends in this case when the slow-roll condition  $|\eta_\phi| < 1$  is violated, such that  $\Delta_{\phi_e} \simeq -(\phi_0/m_P)^2/24$ . This allows us to compute the total number of e-folds of inflation from horizon-crossing, which is then given by:

$$N_e = \int_{t_*}^{t_e} H dt \simeq - \int_{\phi_*}^{\phi_e} \frac{3H^2}{V_\phi(\phi)} d\phi \simeq \frac{1}{\xi} [\arctan(1/2\xi) + \arctan((n_s - 1)/4\xi)], \quad (2.7)$$

where  $\xi = 6\beta(m_P/\phi_0)^2$ . We can invert this expression to determine the value of  $\beta$

required for 40-60 e-folds of inflation with  $n_s = 0.967$  [136], yielding:

$$\beta \simeq (3.1 - 5.2) \times 10^{-3} \left( \frac{\phi_0}{m_P} \right)^2, \quad (2.8)$$

with smaller values of  $\beta$  yielding longer periods of inflation, since the resulting potential is flatter. This illustrates the generic fine-tuning problem of inflection point models, and in this particular case the soft inflaton mass and the trilinear term in Eqs. (2.1) and (2.2) have to compensate each other to at least one part in  $10^6$  for a successful model with sub-planckian inflaton values, as can be seen by inserting Eq. (2.8) in Eq. (2.2).

## 2.2 Warm inflation near an inflection point

Slow-roll inflation, whether cold or warm, requires an overdamped evolution of the inflaton field. In warm inflation this can be achieved due to the friction term  $\Upsilon$  in addition to Hubble damping. Once the field  $\phi$  is in the slow-roll regime, the evolution of the radiation fluid is also generically damped, and the equations of motion are given by

$$3H(1 + Q)\dot{\phi} \simeq -V_\phi(\phi), \quad (2.9)$$

$$4\rho_R \simeq 3Q\dot{\phi}^2, \quad (2.10)$$

where we make use of the dissipative ratio  $Q = \Upsilon/(3H)$ , and the radiation energy density is related to the temperature through

$$\rho_r = \frac{\pi^2}{30} g_* T^4, \quad (2.11)$$

with  $g_*$  being the number of relativistic degrees of freedom. We concentrate our study in the LOTS realization of warm inflation described in chapter 1. Then the dissipative coefficient reads

$$\Upsilon \approx C_\phi \frac{T^3}{\phi^2}, \quad (2.12)$$

where  $C_\phi$  is a constant that depends on the couplings and the field multiplicities and which, for the purposes of our discussion, we will take as a free parameter of the model.

The additional friction term in Eq. (2.9) alleviates the flatness of the potential required in order to achieve a sufficient amount of inflation. In the context of inflection point inflation, we have seen that the  $\beta$  parameter determines the shape of the potential in the vicinity of the inflection point, measuring the fine-tuning of the underlying parameters. Therefore, we expect that a warm realization of these models can naturally reduce the amount of fine-tuning required.

We will use the Eq. (2.1) as a working example of a potential with an inflection point to analyze the generic dynamics of warm inflation in this context, although this does not correspond to a concrete realization of warm inflation in the MSSM. Writing Eq. (2.1) in the form of Eq. (2.3), the dynamics is described by six independent parameters, in particular the value of the field at the inflection point  $\phi_0$ , the corresponding height of the potential  $V_0$ , the fine-tuning parameter  $\beta$ , the value of the field at horizon-crossing  $\phi_*$ , the dissipative constant  $C_\phi$  and the effective number of light degrees of freedom  $g_*$ . We can use the WMAP 7-year results<sup>1</sup> giving a power spectrum with an amplitude  $\mathcal{P}_\mathcal{R} = (2.43 \pm 0.11) \times 10^{-9}$  and a spectral index  $n_s = 0.967 \pm 0.014$  [136] to determine  $V_0$  and  $\phi_*$ . In this discussion we consider of the analytical approximation to the warm inflation power spectrum calculated in [99, 101, 102]:

$$\mathcal{P}_\mathcal{R}^{1/2} \simeq \left(\frac{H}{2\pi}\right) \left(\frac{3H^2}{V_\phi(\phi)}\right) (1+Q)^{5/4} \left(\frac{T}{H}\right)^{1/2}, \quad (2.13)$$

where all quantities are implicitly evaluated at horizon-crossing. In part II of the thesis we will discuss that this expression might not be accurate in the strong dissipative regime of warm inflation. However, the results of this chapter does not depend strongly on it, as we only use Eq (2.13) to fix the value of the free parameter  $V_0$ , i.e. the scale of inflation. In order to solve Eq. (2.13), it is useful to write it in a more convenient way. Using the slow-roll equations (2.9) and (2.10), one obtains

$$Q_*(1+Q_*)^{13/2} \simeq \mathcal{P}_\mathcal{R} \left(\frac{C_\phi}{3}\right) \left(\frac{\pi C_\phi}{2C_R}\right)^2 (2\epsilon_{\phi_*})^3 \left(\frac{m_P}{\phi_*}\right)^6, \quad (2.14)$$

where  $C_R = g_*\pi^2/30$ . Eq. (2.14) and the expression for the spectral index [91]

$$(1+Q_*)(1+7Q_*)(n_s-1) + (2+9Q_*)\epsilon_{\phi_*} + 3Q_*\eta_{\phi_*} + (1+9Q_*)\beta_{\Upsilon_*} \simeq 0 \quad (2.15)$$

form a coupled system of equations for  $Q_*$  and  $\phi_*$  that needs to be solved numerically for given values of  $\phi_0$ ,  $\beta$ ,  $C_\phi$  and  $g_*$ . Once the system is solved, we can obtain the value of  $V_0$  using Eq. (2.13):

$$V_0 \simeq \left(\frac{C_R}{C_\phi}\right) \frac{144\pi^2 \mathcal{P}_\mathcal{R} \phi_*^2 m_P^2}{\sqrt{1+Q_*} \left(1 + 3\beta^2 \left(\frac{\phi_* - \phi_0}{\phi_0}\right) + 4 \left(\frac{\phi_* - \phi_0}{\phi_0}\right)^3\right)}. \quad (2.16)$$

The system has in general three possible solutions satisfying the observational constraints, and we have consistently chosen the one that maximizes the difference  $\phi_* - \phi_0$ , since as we discuss below this minimizes the amount of dissipation

<sup>1</sup>At the time of this work WMAP7 data were the latest available. Recent data do not modify significantly the central values of the observables under consideration, hence our results are essentially unaltered.

required for a sufficiently long period of inflation. To simplify the numerical procedure, one can use the approximate solutions in the strong and weak dissipative regimes,  $Q_* \ll 1$  and  $Q_* \gg 1$ , respectively, where the equations decouple, to find the initial root required to calculate numerically the full solution to the coupled system of equations. In the intermediate regime,  $Q_* \sim 1$ , it is sufficient to use an initial root in this range.

## 2.3 Results

Having determined  $V_0$  and  $\phi_*$  from the observational constraints, we may now study the evolution of the coupled inflaton-radiation system as a function of the remaining parameters,  $C_\phi$ ,  $\beta$ ,  $\phi_0$  and  $g_*$ . For concreteness, we first fix the number of relativistic degrees of freedom  $g_* = 100$ , corresponding to the order of magnitude of the number of MSSM scalar fields, although we study the effect of varying this parameter at the end of this section. Our main goal is to determine which is the lowest value of  $C_\phi$  required for a sufficiently long period of inflation as a function of the fine-tuning parameter  $\beta$  and for different values of  $\phi_0$ . The number of e-folds of warm inflation can be computed by including the effects of dissipation in Eq. (2.7):

$$N_e \simeq - \int_{\phi_*}^{\phi_e} \frac{3H^2(1+Q)}{V_\phi(\phi)} d\phi. \quad (2.17)$$

However, due to the  $T$ - and  $\phi$ -dependent dissipative ratio  $Q$ , this integral cannot be solved analytically as in the cold inflation case. Besides, the value of the field at the end of inflation cannot be calculated *a priori*. Hence, the equations of motion for both the inflaton and the radiation fluid have to be integrated numerically. In most areas of the parameter space, the inflaton field is always in the slow-roll regime and therefore we may integrate Eq. (2.9). However, in some regions of the parameter space the radiation fluid is not slow-rolling, in that case we integrate the full equation

$$\ddot{\phi} + (3H + \Upsilon)\dot{\phi} + V_\phi = 0. \quad (2.18)$$

The consistency of our analysis is determined by three main conditions:

- $\epsilon_H = -\frac{\dot{H}}{H} < 1$  is the requirement for accelerated expansion;
- $m_X \gg T$  is the definition of the low temperature regime, in which the dissipative coefficient in Eq. (2.12) has been calculated.
- $T > H$  describes the regime where inflation is warm, and dissipation modifies the evolution and/or observables of inflation.

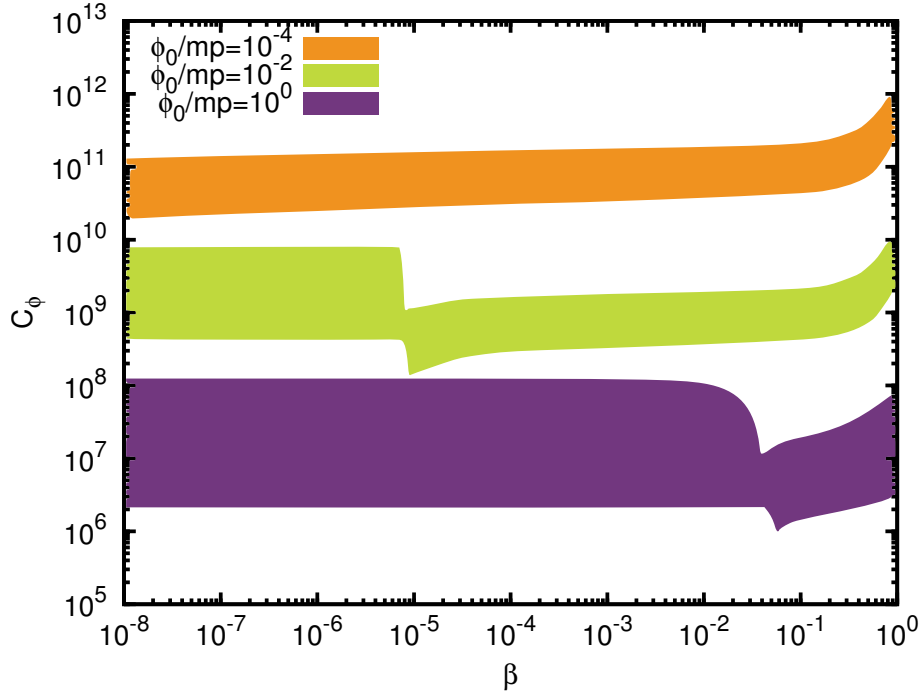


Figure 2.2: Values of  $C_\phi$  and  $\beta$  required to obtain  $N_e \in [40, 60]$  for  $g_* = 100$  and  $\phi_0/m_P = 10^{-4}, 10^{-2}, 1$  from top to bottom.

These conditions need to hold for 40 – 60 e-folds of inflation in order to solve the horizon and flatness problems, and in Fig. 2.2 we show the regions in the plane  $C_\phi - \beta$  where this is obtained for different values of the inflection point  $\phi_0$ .

As one can easily see in this figure, lower values of  $\phi_0$  require more dissipation in order to obtain the same number of e-folds, which is related to the associated increase in the slow-roll parameters in Eq. (2.4), due to a steeper shape of the potential. In addition, we find two distinct regions of parameter space in Fig. 2.2, corresponding to small and large values of the fine-tuning parameter  $\beta$ . The separation between these regions depends on the value of  $\phi_0$ , with the small- $\beta$  region moving to lower values of  $\beta$  for smaller  $\phi_0$ .

In the small- $\beta$  region, the potential is extremely flat and intuitively one would expect less friction to be required for a given period of accelerated expansion. However, Fig. 2.2 clearly shows that the required value of  $C_\phi$  becomes constant for low values of  $\beta$ , which suggests taking a closer look at the physical mechanism behind dissipation. Since it is the motion of the inflaton field that produces light particles in a quasi-thermal bath, the amount of radiation produced depends on how fast the inflaton is rolling, as can be explicitly seen in Eq. (2.10). If the potential is too flat, the inflaton will roll too slowly, which suppresses the amount of radiation produced and consequently decreases the temperature of the thermal bath. In fact, it is the condition  $T > H$  that determines the end of warm inflation

in this region of parameter space, as one can see in Fig. 2.3, where we plot the evolution of the relevant quantities in this regime. This also explains why the initial condition farther away from the inflection point yields the lowest value of  $C_\phi$ , since an initially steeper potential can more easily produce a radiation bath with  $T > H$ .

In Fig. 2.3(a), one can see that the inflaton starts above the inflection point and ends close to the latter, with the temperature dropping below the Hubble rate after 40 e-folds of inflation. Notice, however, that inflation does not necessarily end at this point, since  $\epsilon_H < 1$  and decreasing, but our analysis is no longer consistent at this stage since de Sitter effects may modify the dissipation coefficient. It may, in fact, be possible for an additional period of cold inflation to follow, thus decreasing the amount of dissipation required to achieve the desired number of e-folds. However, the computation of the dissipative coefficient in the intermediate regimen  $T \sim H$  has not been studied up to date. Finally, in Fig. 2.3 we see that  $\epsilon_H$  follows closely the evolution of the radiation energy density, which in this case is becoming more and more sub-leading compared to the inflaton field, thus requiring an additional reheating stage to recover a universe dominated by radiation.

In the large- $\beta$  region the potential is steeper, therefore the production of radiation is enhanced and  $T > H$  is no longer the dominant constraint. In fact, in this regime radiation tends to be overproduced and dominate the energy density, thus allowing for a graceful exit from inflation, as shown in Fig. 2.4 where we plot the evolution with the number of e-folds of the relevant quantities in the large- $\beta$  region.

In Fig. 2.4(a), one can see that the inflaton field starts away from the inflection point, remains close to it for a few e-folds but that, due to the slope of the potential, inflation ends beyond the point of inflection, in contrast with the small- $\beta$  behavior. Notice that  $\rho_r/\rho_\phi$  decreases sharply when the field slows down close to the inflection point, in agreement with the discussion above, but then increases as the field moves to lower values and eventually ends inflation with a smooth exit into a radiation-dominated era. In Fig. 2.4(c) it is also clear that  $T > H$  for the whole duration of inflation.

Although we have not plotted the condition  $m_X \gg T$  in Figs. 2.3 and 2.4, we have checked that it is satisfied in all the parameter space shown for couplings of the inflaton to the catalyst field  $g\Phi X^2$  around  $g \sim 1$ . On the other hand, we may consider more general potentials, associated with different SUSY breaking effects, yielding a different value for the numerical coefficient of the slow-roll parameter  $\eta_\phi$  in Eq. (2.4). We then find that, for lower values of this coefficient, the condition  $m_X \gg T$  is more stringent than  $T > H$ . However, the amount of dissipation required does not change significantly even for an order of magnitude change in this coefficient, so we do not explore this possibility in more detail.

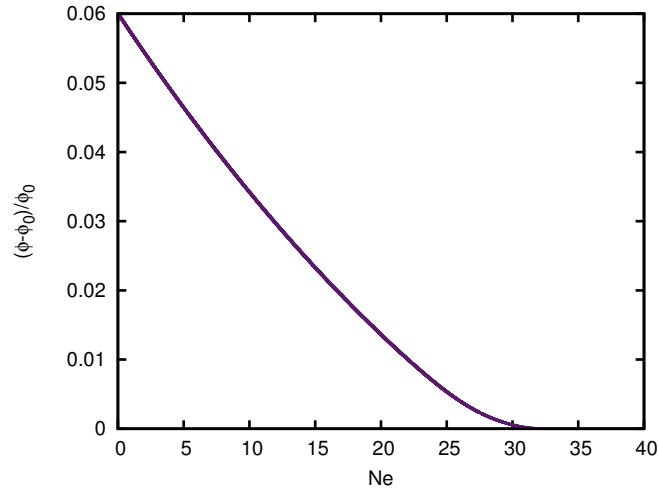
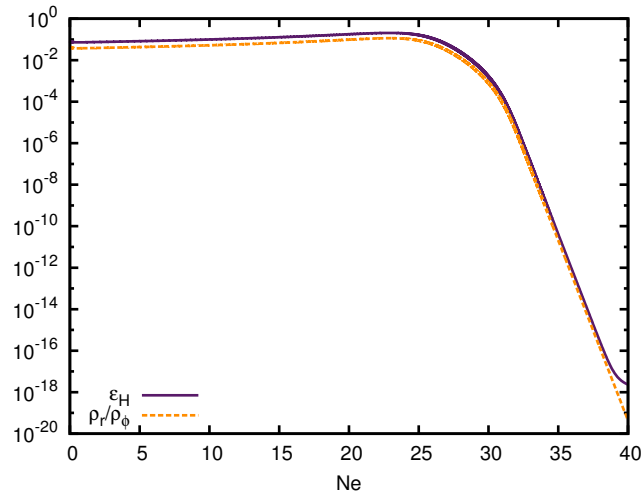
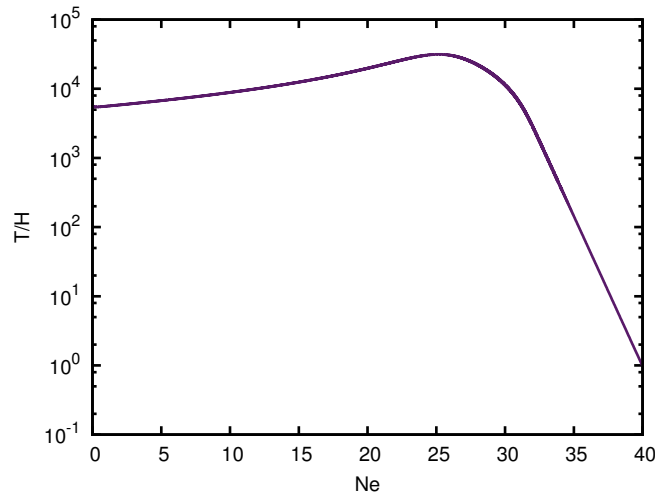
(a)  $(\phi - \phi_0)/\phi_0$ (b)  $\epsilon_H$  and  $\rho_r/\rho_\phi$ (c)  $T/H$ 

Figure 2.3: Evolution with the number of e-folds of  $(\phi - \phi_0)/\phi_0$ ,  $\epsilon_H$ ,  $\rho_r/\rho_\phi$  and  $T/H$  for  $\phi/m_P = 10^{-2}$ ,  $g_* = 100$  and  $\beta = 10^{-7}$  when inflation lasts 40 e-folds.

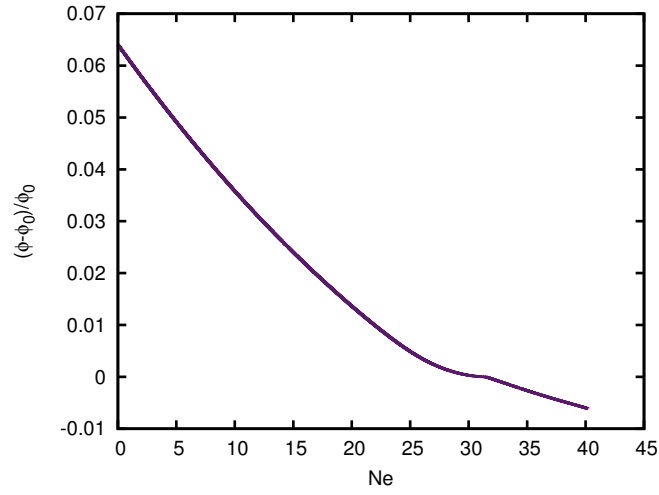
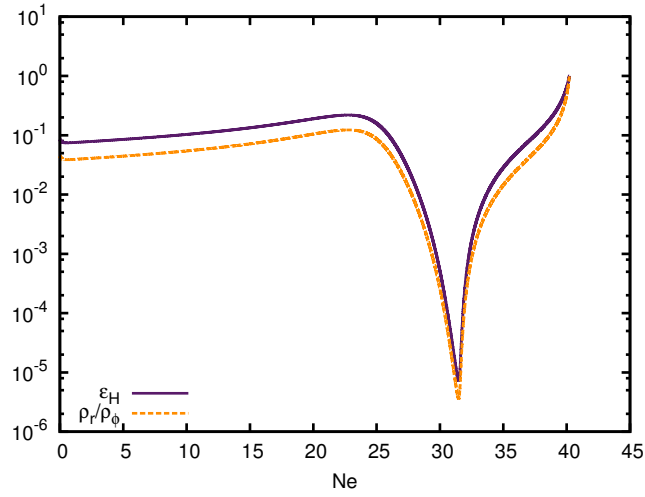
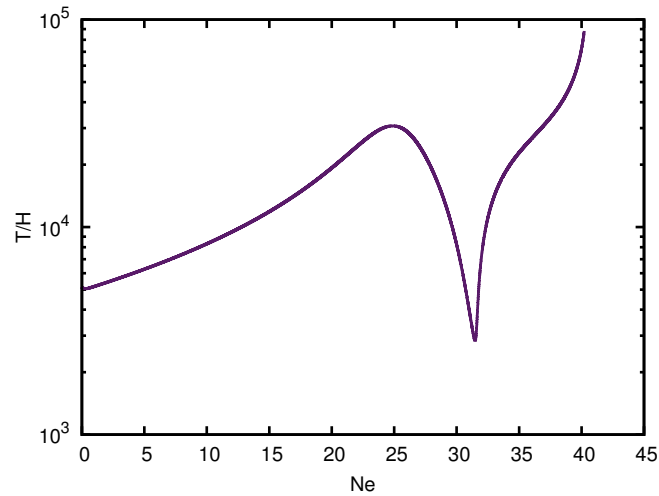
(a)  $(\phi - \phi_0)/\phi_0$ (b)  $\epsilon_H$  and  $\rho_r/\rho_\phi$ (c)  $T/H$ 

Figure 2.4: Evolution with the number of e-folds of  $(\phi - \phi_0)/\phi_0$ ,  $\epsilon_H$ ,  $\rho_r/\rho_\phi$  and  $T/H$  for  $\phi/m_P = 10^{-2}$ ,  $g_* = 100$  and  $\beta = 10^{-2}$  when inflation lasts 40 e-folds.

Finally, we analyze the effect of the number of relativistic degrees of freedom on the amount of dissipation required for successful inflation. In Fig. 2.5 we show the  $C_\phi - \beta$  region where 40-60 e-folds of inflation are obtained with different values of  $g_*$ .

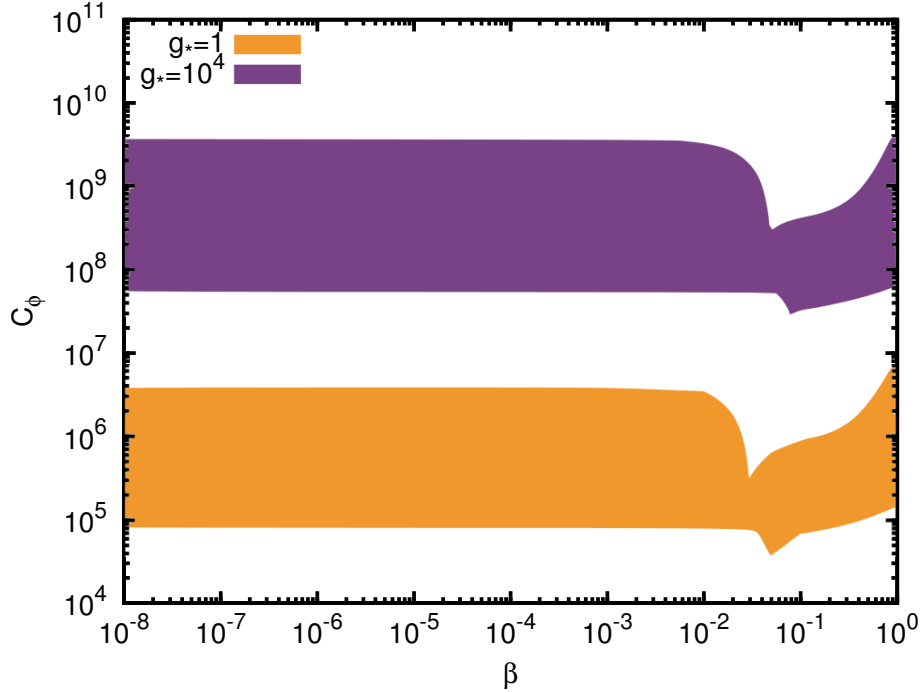


Figure 2.5: Values of  $C_\phi$  and  $\beta$  required to obtain  $N_e \in [40, 60]$  for  $\phi_0/m_P = 1$  and  $g_* = 1, 10^4$ .

In Fig. 2.5, it can be observed that the required value of  $C_\phi$  decreases for smaller  $g_*$ . In order to understand this behavior, we compute the explicit dependence of the dissipation coefficient on  $g_*$  by substituting Eq. (2.11) into Eq. (2.12):

$$\Upsilon = \frac{30^{3/4} C_\phi \rho_r^{3/4}}{\pi^{3/2} g_*^{3/4} \phi^2}. \quad (2.19)$$

Hence, the relevant quantity is an effective dissipation constant:

$$\tilde{C}_\phi = \frac{C_\phi}{g_*^{3/4}} \quad (2.20)$$

that remains constant in Fig. 2.5 for the different values of  $g_*$ , which is also the case for smaller (sub-planckian) values of the inflection point.

Our numerical simulations of the dissipative dynamics of inflation in this model have lead us to two main conclusions. Firstly, if dissipative effects are sufficiently

strong, a sufficiently long period of inflation may occur independently of the fine-tuning of the parameters in the potential, which was expected since the additional friction alleviates the need for a very flat potential. Secondly, and more surprisingly, the required amount of dissipation does not decrease arbitrarily for flatter potentials, given that if the scalar potential is too flat and the inflaton evolves too slowly, it becomes more difficult to sustain a radiation bath with a temperature above the Hubble rate, which is required for consistency of our analysis. This results in a field-dependent critical value of the fine-tuning parameter  $\beta$  below which the required dissipation parameter  $C_\phi$  becomes constant. Above this value, the potential is sufficiently steep to ensure that  $T > H$  throughout inflation, with steeper potentials requiring larger values of the dissipation parameter.

The value of  $C_\phi$  depends on the coupling between the intermediate fields and the light degrees of freedom, as well as on the multiplicities of both heavy and light fields. The minimum value of  $C_\phi \gtrsim 10^6$  obtained for  $g_* = 100$  is of the same order as that obtained for other forms of the inflaton potential, such as monomial or hybrid models [91], which implies large couplings and field multiplicities, so one may ask whether there is any gain from the model building perspective in trading a large fine-tuning in the parameters of the potential for large couplings and a large number of fields. On one hand, fine-tuning makes inflation less generic, since it isolates a small region of the available parameter space, whereas inflation should provide an explanation for the otherwise finely-tuned conditions in the early universe. On the other hand, a large number of degrees of freedom during inflation points towards more complicated beyond the Standard Model scenarios, e.g. with fields in large representations, which may be realized in generic GUT constructions or D-brane models [93].



*Ninguém educa ninguém, ninguém educa a si mesmo, os  
homens se educam entre si, mediatizados pelo mundo.*

Paulo Freire

## Viscous effects in warm inflation I: background

---

In warm inflation the transfer of energy of the inflaton field to the radiation bath is mediated by the dissipation term in the inflaton's evolution equation. Nevertheless, an additional effect can arise due to inner couplings in the radiation fluid itself. Internal decays within the radiation fluid can make it depart slightly from thermal equilibrium. Therefore, the radiation fluid can behave as a non-ideal fluid and viscosity effects must be taken into account [137]. At the background level, the relevant viscous effect is due to bulk pressure, since it is the only viscous effect appearing in the background equations for an FRW universe. There may be other dissipative effects in the radiation fluid itself, like shear viscous stresses, that may be relevant at the perturbation level in the determination of the spectrum of density perturbations, as demonstrated recently [138]

The study of bulk viscous effects in cosmology, and in particular in inflation, has some history to it, focused mainly on the effect of the bulk pressure as a negative pressure (for a partial sample of the earlier works on bulk viscous cosmologies, see for example Refs. [139, 140, 141, 142, 143, 144, 145, 146]). In addition, more recently, there has been a surge of interest in exploring the effects of the bulk pressure as the origin of the present accelerated expansion of the universe (see e.g. Refs. [147, 148, 149, 150]). Almost all of these works only use phenomenological forms for the bulk viscosity. The investigation described in this chapter differs from previous one since we will apply first principle quantum field theory computed expressions for the bulk viscosity, based on the calculations found e.g. in Refs. [151, 152], to warm inflation. There has been very little work done in studying first principles bulk viscosity expressions in application to cosmology. There is one paper we are aware of along these lines [147], where quantum field theory derived expressions of bulk viscosity are used, and it is shown how they can play the role similar to dark energy.

We are interested in determining the stability conditions of the background equations of warm inflation when coupled to the bulk viscous radiation bath. Earlier studies examining the stability properties of the warm inflation equations in-

clude Refs. [99, 153], but these studies did not include the effects of bulk viscous pressure. Preliminary studies on the inclusion of bulk viscous pressure have been done in [154, 155], where only the non-causal theory of Eckart [156] has been used. Here we extend the stability analysis of the dynamical warm inflation equations to include bulk viscous effects. Moreover our analysis will be done not just for the non-causal Eckart theory but also the causal theories of bulk pressure [157, 158, 159], with a full analysis of the differences in the resulting dynamics from these different theories.

In the study of viscous effects in cosmology it is common to use linear expressions to describe the viscous pressure, where it is assumed that the deviations are close to equilibrium. However, the viscous pressure can, in principle, take the system far from its thermodynamical equilibrium, so, we must apply suitable approaches in order to see if one really needs to use a more robust description, incorporating nonlinear effects. We consider here three different theories to describe the viscous pressure: the non-causal theory due to Eckart [156], the linear and causal theory of Israel-Stewart [157, 158] and finally we will also use a recent causal and nonlinear theory proposed by the authors in [159], named by them *Nonlinear Causal Dissipative Hydrodynamics* (NLCDH). There have been other proposals for a nonlinear theory for the bulk viscous pressure [160, 161] that make use of ad-hoc parameters, such as the time where nonlinear effects become important [160] or functions [161] that do not have an immediate interpretation from quantum field theory. In using such approaches there is no immediate understanding how to associate their parameters with first principles parameters. We have considered the theory for bulk pressure in [159] since it utilizes parameters which can readily be determined from microscopic physics, in particular from quantum field theory. The theories for the bulk pressure we analyze here are more natural to use in field theory model building, where the dissipation terms, viscosity coefficients and relaxation times are well defined and can be reliably computed once a specific field theory model is given.

We will study the effects of the inclusion of bulk viscosity in three commonly used supersymmetric realizations of warm inflation, the chaotic, hybrid and hilltop models. As the bulk viscosity modifies the background dynamics of warm inflation, it also changes the available parameter space, which will be analyzed here. The Eckart description of the bulk viscosity will be accurate enough in that part of the study, and we will study the limits on the couplings of the underlying particle physics theory for the validity of this approximation.

### 3.1 Warm Inflation in a bulk viscous radiation fluid

In the presence of a bulk viscous pressure,  $\Pi$ , the stress-energy tensor for the radiation fluid is given by [137, 162, 163],

$$\mathcal{T}_{\mu\nu}^{(r)} = (\rho_r + p_r + \Pi)u_\mu^{(r)}u_\nu^{(r)} + (p_r + \Pi)g_{\mu\nu}, \quad (3.1)$$

where  $\rho_r$  is the radiation energy density,  $p_r$  the adiabatic radiation pressure,  $u_\mu^{(r)}$  the four velocity of the radiation fluid and  $g_{\mu\nu}$  the four-dimensional metric. It happens then that the bulk pressure enters as a contribution to the radiation pressure  $p_r$ , such that we can define in general an effective pressure for the radiation,  $\tilde{p}_r$ , given by

$$\tilde{p}_r = p_r + \Pi. \quad (3.2)$$

The evolution equation for the radiation fluid energy density  $\rho_r$  then becomes

$$\dot{\rho}_r + 3H(\rho_r + \tilde{p}_r) = \Upsilon(\rho_\phi + p_\phi), \quad (3.3)$$

where  $p_\phi = \dot{\phi}^2/2 - V(\phi, T)$ , and  $\rho_\phi + p_\phi = \dot{\phi}^2$ .

It is also useful to express this in terms of the entropy density  $s$ . From the Helmholtz free energy  $f = \rho_T - Ts$ , where  $f = V(\phi, T)$ , and using  $s = -\partial f/\partial T$ , the total energy density  $\rho_T$  becomes

$$\rho_T = \frac{\dot{\phi}^2}{2} + V(\phi, T) + Ts, \quad (3.4)$$

and the Hubble rate  $H$  reads

$$H^2 = \frac{1}{3m_{\text{P}}^2} \left[ \frac{\dot{\phi}^2}{2} + V(\phi, T) + Ts \right], \quad (3.5)$$

where  $m_{\text{P}}$  is the reduced Planck mass,  $m_{\text{P}} = 1/\sqrt{8\pi G} = 2.4 \times 10^{18} \text{GeV}$ . Using also that  $p_r = (\gamma - 1)\rho_r$  and that the entropy density  $s$  is related to the radiation energy density by  $Ts = \gamma\rho_r$ , Eq. (3.3) can then be written in terms of the entropy density as

$$T\dot{s} + 3H(Ts + \Pi) = \Upsilon\dot{\phi}^2, \quad (3.6)$$

where we have used  $\gamma = 4/3$ , which is valid for a quasi-equilibrium high temperature thermal bath typical of warm inflation.

From Eq. (3.6), the dynamical effects of the bulk viscosity can be easily read. Given that the bulk viscous pressure  $\Pi$  is negative, it acts to decrease the radiation pressure, thus enhancing the effect from the source term on the RHS in the equation for the entropy density. As a consequence, the entropy density increases, and therefore the radiation energy density also grows. On the one hand, if this bulk

pressure term is too large, there is too much radiation production and the radiation energy density dominates too soon over the scalar field energy density, thus spoiling inflation. This regime is called the *unstable regime*. On the other hand, if the bulk pressure term is controlled to avoid the radiation domination until the end of inflation, the system is said to be in the *stable regime*. In this regime the bulk viscosity gives rise to an additional negative pressure, and hence, inflation is enhanced.

To account for the dynamics involving the bulk viscous pressure  $\Pi$ , as explained at the beginning of this chapter, we will consider three different theories: the non-causal theory due to Eckart [156], the linear and causal theory of Israel-Stewart (IS) [157, 158], and a recent causal and nonlinear theory, *Nonlinear Causal Dissipative Hydrodynamics* (NLCDH), proposed in [159]. The starting point to build these hydrodynamic theories is the conservation equations of the stress-energy tensor and the number density vector  $N^\mu = nu^\mu$ ,

$$\nabla_\mu \mathcal{T}^{\mu\nu} = 0, \quad \nabla_\mu N^\mu = 0, \quad (3.7)$$

with the additional condition on the 4-entropy, written in terms of the entropy density  $s$ ,  $s^\mu = su^\mu$ , that must satisfy the second law of thermodynamics in its covariant form,

$$\nabla_\mu s^\mu \geq 0. \quad (3.8)$$

The 4-entropy, just like the stress-energy tensor, gains a contribution coming from the dissipative fluxes,

$$s^\mu = su^\mu + \frac{Q^\mu}{T}, \quad (3.9)$$

where  $Q^\mu = Q^\mu(N^\mu, \mathcal{T}^{\mu\nu})$  accounts for the dissipative fluxes. The irreversible thermodynamics comprises of the dissipative forces to the hydrodynamics variables at equilibrium, the number density  $n$ , the energy density  $\rho$  and the pressure  $p$ . These quantities are able to describe the energy fluxes in a nonideal fluid. There are different ways in which this can be done, which lead to different descriptions for the dissipative fluxes, like for example for the bulk pressure. We summarize below the Eckart, IS and NLCDH theories for the bulk pressure.

### 3.1.1 Eckart theory for the bulk pressure

The Eckart theory [156] assumes that the entropy vector  $s^\mu$  is linear in the dissipative fluxes. The nonequilibrium contribution to the entropy vector,  $Q^\mu$ , to first order, should then be proportional to the dissipative fluxes. Neglecting dissipative terms other than the bulk pressure, we then have that

$$Q^\mu \simeq a(n, \rho) \Pi u^\mu, \quad (3.10)$$

where the proportionality factor is obtained from the equilibrium condition and from the covariant form of the second law of thermodynamics, Eq. (3.8). This then gives [162, 163]

$$T\nabla_\mu s^\mu \simeq -3H\Pi. \quad (3.11)$$

To ensure that the second law of thermodynamics, Eq. (3.8), is satisfied and interpreting the term  $3H$  in Eq. (3.11) as a dissipative force,  $\chi_E = 3H$ , we impose  $\Pi$  to be linear in this force, expressing bulk viscosity as

$$\Pi = -3\zeta_b H, \quad (3.12)$$

where the proportionality term  $\zeta_b \equiv \zeta_b(n, \rho) \geq 0$  is the bulk viscosity coefficient [137].

The bulk pressure expressed like Eq. (3.12) is a noncausal theory, *i.e.*, the speed of the fluxes propagation is infinite. The Eckart theory can be considered in some circumstances as a reasonable approximation for the irreversible thermodynamics. This may happen, for example, when sufficiently short relaxation time scales are involved, otherwise a causal theory would be a much better choice. We now turn to the simplest of such a causal theory, the IS one.

### 3.1.2 Israel-Stewart theory for the bulk pressure

The IS theory [157, 158] goes one step further than the Eckart theory by accounting for second order contributions beyond equilibrium, by expanding the entropy vector to second order in the dissipative fluxes. Generically this gives, by again only considering the bulk pressure contribution,

$$s^\mu \simeq su^\mu - \beta_0 \Pi^2 \frac{u^\mu}{2T}, \quad (3.13)$$

where  $\beta_0(n, \rho) \geq 0$ . From the covariant derivative of the entropy vector,

$$T\nabla_\mu s^\mu = -\Pi \left[ 3H + \beta_0 \dot{\Pi} + \frac{T}{2} \nabla_\mu \left( \frac{\beta_0}{T} u^\mu \right) \Pi \right], \quad (3.14)$$

and from the second law of thermodynamics to be satisfied, Eq. (3.8), it is imposed again, like in the Eckart case, that the dissipative fluxes be linear in the dissipative forces. For the bulk pressure  $\Pi$  this implies from Eq. (3.14) that

$$\Pi = -\zeta_b \left[ 3H + \beta_0 \dot{\Pi} + \frac{T}{2} \nabla_\mu \left( \frac{\beta_0}{T} u^\mu \right) \Pi \right]. \quad (3.15)$$

The relation (3.15) is analogous to Eq. (3.12) in the Eckart theory. The difference here being that, from Eq. (3.11), the Israel-Stewart force is expressed as

$$\chi_{IS} = 3H + \beta_0 \dot{\Pi} + \frac{T}{2} \nabla_\mu \left( \frac{\beta_0}{T} u^\mu \right) \Pi. \quad (3.16)$$

By defining  $\tau = \zeta_b \beta_0$ , which is interpreted as a relaxation time for the bulk viscous processes in the radiation fluid, then Eq. (3.15) can also be rewritten in the form

$$\tau \dot{\Pi} + \Pi = -3\zeta_b H - \frac{\zeta_b T}{2} \nabla_\mu \left( \frac{\tau}{\zeta_b T} u^\mu \right) \Pi, \quad (3.17)$$

and by expanding the derivative in the last term in Eq. (3.17) it can finally be expressed as

$$\tau \dot{\Pi} + \Pi = -3\zeta_b H - \frac{\tau \Pi}{2} \left( 3H + \frac{\dot{\tau}}{\tau} - \frac{\dot{\zeta}_b}{\zeta_b} - \frac{\dot{T}}{T} \right), \quad (3.18)$$

which is the IS equation for the bulk pressure.

As shown in Ref. [164], the propagation speed for the bulk pressure is given by

$$c_{\text{visc}}^2 = \frac{\zeta_b}{(\rho + p)\tau}, \quad (3.19)$$

and, thus, for  $\tau \neq 0$  there is a finite propagation speed for the flux, while for the Eckart theory, where  $\tau = 0$ , it is infinity (noncausal). In a quantum field theory description for the radiation bath, e.g. for example in the two-stage decay mechanism for warm inflation, both the bulk viscosity coefficient  $\zeta_b$  and the relaxation time  $\tau$  can be defined unambiguously and be computed microscopically, just like the dissipation coefficient  $\Upsilon$ . In particular, the bulk viscosity coefficient can be obtained from a Kubo formula[165, 166] for the high-temperature light particles of the radiation bath [151, 152], and  $\tau$  can be associated with the respective decay time of these particles,  $\tau = 1/\Gamma$ , where  $\Gamma$  is the decay width. For the validity of considering a quasi-equilibrium thermal radiation bath, we are then required to impose that

$$\tau H \equiv H/\Gamma < 1. \quad (3.20)$$

Likewise, the assumption of proximity with thermal equilibrium requires the dissipative fluxes to be small compared to the equilibrium pressure,

$$|\Pi| \ll p. \quad (3.21)$$

The IS equation for  $\Pi$ , Eq. (3.18), can then be seen to give a correction to the Maxwell-Cattaneo equation

$$\tau \dot{\Pi} + \Pi = -3\zeta_b H, \quad (3.22)$$

which, after Eckart, is the simplest equation for the bulk pressure including relaxation (causal) effects.

### 3.1.3 Nonlinear causal dissipative hydrodynamics theory for the bulk pressure

Next, let us consider the NLCDH theory proposed by the authors of Ref. [159]. This theory assumes the Eckart force term,  $\chi_E = \nabla_\mu u^\mu = 3H$ , plus a memory effect, so as to respect causality. Since this theory in principle makes no assumptions about the linearity of the dissipative fluxes in the bulk pressure, as it was assumed in the IS theory for instance, it has been regarded as a nonlinear theory for the bulk pressure. The memory effect adds a relaxation to the system. Recall that the Maxwell-Cattaneo theory Eq. (3.22) is obtained by adding a relaxation time directly to  $\Pi$ . In the NLCDH instead, the memory effect is added to the quantity  $\tilde{\Pi} = \Pi\mathcal{V}$  (where  $\mathcal{V}$  is the volume), which is then integrated in a cell of the fluid<sup>1</sup>. This is done by imposing the relation  $\tilde{\Pi} = -\zeta_b\mathcal{V}\chi_E$ . Through the addition of the memory effect, we are lead to [159]

$$\tau\dot{\tilde{\Pi}} + \tilde{\Pi} = -3H\zeta_b\mathcal{V}. \quad (3.23)$$

The first term in the above equation results in  $\tau(\dot{\Pi}\mathcal{V} + \Pi\dot{\mathcal{V}})$ . After using the conservation law for the volume in a cell of the fluid,  $\nabla_\mu(u^\mu/\mathcal{V}) = 0$ , it can be shown that [159]

$$\nabla_\mu \frac{u^\mu}{\mathcal{V}} = \left(\frac{1}{\mathcal{V}}\right)' + \frac{1}{\mathcal{V}}\nabla_\mu u^\mu = -\left(\frac{1}{\mathcal{V}}\right)^2 \dot{\mathcal{V}} + \frac{1}{\mathcal{V}}\chi = 0. \quad (3.24)$$

It follows that  $\chi = \dot{\mathcal{V}}/\mathcal{V}$  and then  $\dot{\mathcal{V}} = \chi\mathcal{V} = 3H\mathcal{V}$ . From Eq. (3.23), it then follows the NLCDH equation for the bulk pressure [159],

$$\tau\dot{\Pi} + \Pi = -3H(\zeta_b + \tau\Pi). \quad (3.25)$$

The NLCDH description suppresses the effect of the bulk viscosity in the radiation production compared to IS, being a more robust characterization of such viscosity. This feature is caused by the non-linearity nature of the NLCDH description, which translates into a larger effect of the same relaxation time, as can be observed by comparing Eqs. (3.18) and (3.25).

---

<sup>1</sup>The hydrodynamical description is based on the local equilibrium ansatz, which assumes the existence of cells at each space points: finite volume elements that are described by the thermodynamic laws in equilibrium

## 3.2 The dynamical system of equations for warm inflation in a bulk viscous radiation fluid

The relevant equations concerning warm inflation in a bulk viscous radiation fluid are given by the inflaton evolution equation,

$$\ddot{\phi} + 3H\dot{\phi} + V_\phi = \Upsilon\dot{\phi} \quad (3.26)$$

the entropy energy density evolution Eq. (3.6), with the bulk pressure  $\Pi$  given by: (a) in the Eckart case Eq. (3.12); (b) in the IS case by the evolution equation (3.18); and (c) in the NLCDH case by the evolution equation (3.25). Writing the inflaton equation of motion as two first order differential equations, we have that Eqs. (3.26) and (3.6) are equivalently written in the form:

$$\begin{aligned} \dot{\phi} &= u, \\ \dot{u} &= -3Hu - \Upsilon u - V_\phi, \\ T\dot{s} &= -3HTs - 3H\Pi + \Upsilon u^2, \end{aligned} \quad (3.27)$$

where

$$H^2 = \frac{1}{3m_{\text{P}}^2} \left( \frac{u^2}{2} + V + Ts \right), \quad V = V(\phi, T), \quad \Upsilon = \Upsilon(\phi, T), \quad (3.28)$$

with expression for the bulk pressure  $\Pi$ , given by either Eq. (3.12), (3.18) or (3.25), depending on which of the cases is treated. In all the cases, they depend on the bulk viscosity coefficient,  $\zeta_b \equiv \zeta_b(T)$ . We consider the dependence of the dissipation coefficient on the field and temperature to be

$$\Upsilon = C_\phi \frac{T^c}{\phi^{c-1}}, \quad (3.29)$$

with proportionality factor  $C_\phi$  depending on the field content of the model and the value of the power  $c$  depending on the temperature regime for the different fields involved. For example, in the LOTS realization of warm inflation, we discussed that  $c = 3$  [95, 167, 94]. Likewise, the bulk viscosity coefficient, in this same regime is [151, 152]  $\zeta_b \propto T^3$ . In the following we consider a generic power dependence  $l$  in the temperature for the bulk viscosity coefficient,  $\zeta_b \propto T^l$ , similar to that considered for the dissipation coefficient, Eq. (3.29). Treating the variables of the dynamical system in the form of a column matrix  $\mathbb{X}$ , we can express the dynamical system in the compact matrix form,

$$\dot{\mathbb{X}} = \mathbb{F}(x) \mathbb{X}, \quad (3.30)$$

where for example, for the dynamical system given by Eq. (3.27),  $\mathbb{X} = (\phi, u, s)$ . In the IS and NLCDH cases we also have the bulk pressure entering in the system as an additional function,  $\mathbb{X} = (\phi, u, s, \Pi)$ .

Writing  $x = x_0 + \delta x$ , where we assume that  $x_0$  is a stable solution of the system, which here will be taken as the slow-roll solutions that can be derived directly from Eq. (3.27) (see below), the equation for the variations in  $\delta x$  become

$$\delta \dot{\mathbb{X}} = \mathbb{M}(x_0) \delta \mathbb{X} - \dot{\mathbb{X}}_0, \quad (3.31)$$

where

$$\mathbb{M}(x_0) = \frac{\partial \mathbb{F}(x_0)}{\partial x}, \quad (3.32)$$

is the Jacobian matrix for the system, evaluated at the  $x_0$  solution, and  $\dot{\mathbb{X}}_0$  is a residual force term, which in general is small and can be neglected [99]. The general solution of Eq. (3.31) is of the form

$$\delta \mathbb{X} = \mathbb{X}_0 e^{\mathbb{M}(x_0)t}, \quad (3.33)$$

and  $\mathbb{M}(x_0)$  must be zero or negative for the system be stable, i.e., the eigenvalues  $\Lambda_i$  of  $\mathbb{M}(x_0)$  must necessarily all satisfy

$$\Lambda_i \leq 0. \quad (3.34)$$

The stability of the dynamical system can be studied directly in the time variable, but it simplifies the analysis, in particular the determination of the eigenvalues of the Jacobian matrix, if we make a change of variables and rewrite the dynamical system (3.27) using  $\phi$  as the independent variable instead of the time [99]. By doing this the dimension of the corresponding system is smaller and easier to analyze. In particular, the Jacobian matrix for the dynamical system (3.27) becomes a  $2 \times 2$  matrix; if one includes the bulk pressure as an additional function to the system, as in IS and NLCDH cases, it then makes the Jacobian matrix  $3 \times 3$ . The eigenvalues obtained by using  $\phi$  rather than time as the variable makes the analysis much simpler. As such, using that

$$\frac{d}{dt} = \frac{d\phi}{dt} \frac{d}{d\phi} = u \frac{d}{d\phi} = u (\prime), \quad (3.35)$$

where a prime indicates derivative with respect to  $\phi$ , the dynamical system Eq. (3.27) becomes equivalent to

$$\begin{aligned} u' &= -3H - \Upsilon - V_{,\phi}u^{-1}, \\ Ts' &= -3HTsu^{-1} - 3H\Pi u^{-1} + \Upsilon u, \end{aligned} \quad (3.36)$$

together with the corresponding equations for the bulk viscosity, Eqs. (3.12), (3.18) or (3.25) (these last two also transformed to the  $\phi$  variable), depending on which case we are considering. In the slow-roll regime, the system of equations can be approximated to

$$\begin{aligned} u &= -\frac{V_{,\phi}}{3H(1+Q)}, \\ Ts &= Qu^2 - \Pi. \end{aligned} \quad (3.37)$$

The Hubble rate  $H$ , in the slow-roll approximation is given by

$$H^2 = \frac{1}{3m_{\text{p}}^2}V(1 + \kappa), \quad (3.38)$$

where  $\kappa = \rho_r/V$ . Keeping the radiation energy density in Eq. (3.38) is justified because in the presence of a bulk pressure, the radiation energy density does not in general need to be much smaller than the vacuum energy density in order to have inflation. Including a bulk pressure, the acceleration equation is

$$\frac{\ddot{a}}{a} = \frac{1}{6m_{\text{p}}^2}(2V + 3|\Pi| - 2\rho_r), \quad (3.39)$$

which shows that we could in principle have  $\rho_r \sim V$  and inflation could still be sustained by the bulk pressure [160].

The general solution of Eq. (3.36) is now of the form

$$\delta\mathbb{X} = \mathbb{X}_0 e^{\mathbb{M}(x_0)\phi(t)}. \quad (3.40)$$

The stability condition on the eigenvalues  $\lambda_i$ , which are the eigenvalues of  $\mathbb{M}(x_0)$  once  $u$  is factorized, depends now on whether the inflaton field  $\phi(t)$  during slow-roll decreases with time (like in chaotic inflation), so  $\lambda_i \geq 0$ , or increases with time (like in hilltop inflation), in which case  $\lambda_i \leq 0$ . This is an important consideration when replacing the time by the inflaton as the independent variable in the dynamical system. In a  $2 \times 2$  system, stability is ensured once the determinant is positive and the trace, negative, as is done in [99, 154]. However, in a  $3 \times 3$  system, the case for the Israel-Stewart and NLCDH descriptions, further information beyond the trace and determinant is required to guarantee the stability of the system. Thus, we will make use directly of the eigenvalues for searching for the

stability of the system. Nevertheless, for all the cases we have studied, only one eigenvalue changes sign at the instability point, and therefore it would be enough to look at the determinant of the system. The full derivation of the stability conditions for the three descriptions of the bulk viscosity can be found in appendix A. In this section we will show the results for the case  $\gamma = 4/3$ .

For the Eckart description of the bulk viscosity, stability is ensured as long as

$$(c - 2b)(1 + \sigma) + 4 + l\sigma - \frac{3}{2} \frac{\sigma \tilde{\sigma}}{1 + \kappa} > 0, \quad (3.41)$$

where we have defined the quantities  $\sigma$  and  $\tilde{\sigma}$  as

$$\sigma = \frac{\Pi}{\gamma \rho_r}, \quad (3.42)$$

$$\tilde{\sigma} = \frac{\Pi}{V}, \quad (3.43)$$

and  $b$  is the slow-roll parameter ensuring that thermal corrections to the inflation potential are negligible

$$b = \frac{TV_{T\phi}}{V_\phi}. \quad (3.44)$$

The Eq. (3.41) generalizes the results in [154], which were obtained for a constant bulk pressure ( $l = 0$ ), by accounting for temperature dependence. Also for  $\sigma = 0$  and  $\tilde{\sigma} = 0$ , the case of zero bulk pressure, we reproduce the results obtained by Moss and Xiong in [99]. In [99] the stability condition was found to be  $|c| < 4$ . From Eq. (3.41), in the absence of bulk viscosity, we derive instead only the condition  $c > -4$ . We do also obtain the result  $c < 4$  if we consider the eigenvalues in the approximation of very small dissipation  $Q \ll 1$ , but this regime is not the most general situation for warm inflation.

The IS description is stable under the following condition

$$\begin{aligned} & \left[ 1 + \frac{2\sigma + \Theta b \Lambda (1 + \sigma)^2}{2 + 3\Theta} \right] c + 4 + \frac{2\sigma}{2 + 3\Theta} l - \frac{3}{2} \frac{\sigma \tilde{\sigma}}{1 + \kappa} \left[ \frac{2 - 3\Theta}{2 + 3\Theta} - \frac{2\Theta \Lambda}{2 + 3\Theta} (1 + \sigma) \right] + \\ & - \left[ 4(1 + \sigma) + 3\Theta(2 + \sigma) - 3\Theta \Lambda (1 + \sigma)^2 - \Theta(1 + \sigma)(\Lambda + \sigma \Sigma) \right. \\ & \left. + 2b\Lambda \Theta (1 + \sigma)^2 \right] \frac{b}{2 + 3\Theta} > 0. \end{aligned} \quad (3.45)$$

where we have defined the parameters

$$\begin{aligned} \Theta &= \tau H, \\ \Lambda &= 1 + l - \frac{T\tau_{,T}}{\tau}, \\ \Sigma &= \left( 1 + \frac{T\tau_{,TT}}{\tau_T} - \frac{T\tau_{,T}}{\tau} \right) \frac{T\tau_{,T}}{\tau} - \left( 1 + \frac{T\zeta_{b,TT}}{\zeta_{b,T}} - l \right) l - \Lambda \frac{TV_{\phi TT}}{V_{\phi T}}. \end{aligned} \quad (3.46)$$

From Eq. (3.45), when the relaxation time vanishes,  $\tau = 0$ , *i.e.*, for  $\Theta = \tau H \rightarrow 0$ , we recover the previous condition Eq. (3.41), obtained in the Eckart theory case.

The stability condition for the NLCDH theory for the bulk pressure is

$$\begin{aligned} \left(1 + \frac{\sigma}{1 + 3\Theta}\right) c + 4 + \frac{\sigma}{1 + 3\Theta} l - \frac{3}{2} \frac{\sigma \tilde{\sigma}}{1 + \kappa} \frac{1 - 3\Theta}{1 + 3\Theta} \\ - \left(2 + \sigma + \frac{\sigma}{1 + 3\Theta}\right) b > 0. \end{aligned} \quad (3.47)$$

If we take the relaxation time as vanishing in Eq. (3.47),  $\Theta = \tau H \rightarrow 0$ , we once again recover the result Eq. (3.41).

### 3.3 Numerical analysis

In this Section, we study numerically the system of equations for each of the three cases derived in the previous section. We will verify the corresponding stability conditions directly through the numerical time evolution of the corresponding dynamical systems. We will restrict our analysis to the to the dissipation coefficient arising from the LOTS realization of warm inflation  $\Upsilon = C_\phi T^3 / \phi^2$ , although the study can easily be extended to other dissipative coefficients. The bulk viscosity coefficient will have the form  $\zeta_b = C_b T^3$ , which is obtained for quantum field theory in [151, 152] and also is the form generically considered in hydrodynamics. This then corresponds to the case where  $c = 3$  for the dissipative coefficient in Eq. (3.29) and  $l = 3$  for the bulk viscosity, with  $C_\phi$  and  $C_b$  being (dimensionless) proportionality constants. Also for simplicity, we will analyze here the simplest case of a quadratic inflaton potential,

$$V = \frac{m_\phi^2}{2} \phi^2, \quad (3.48)$$

with a constant relaxation time. The extension to other types of potentials, such as a quartic potential or hybrid type potentials, does not offer additional difficulties and can be easily implemented.

In the example considered here, the stability conditions Eqs. (3.41), (3.45) and (3.47), for the Eckart, IS and NLCDH cases respectively, reduce to

$$C_{\text{stab}}^{\text{Eckart}} = 3(1 + \sigma) + 4 + 3\sigma - \frac{3}{2} \frac{\sigma \tilde{\sigma}}{1 + \kappa} > 0, \quad (3.49)$$

$$\begin{aligned} C_{\text{stab}}^{\text{IS}} &= 3 \left(1 + \frac{2}{2 + 3\Theta} \sigma\right) + 4 + \frac{6\sigma}{2 + 3\Theta} + \\ &- \frac{3}{2} \frac{\sigma \tilde{\sigma}}{1 + \kappa} \left[ \frac{2 - 3\Theta}{2 + 3\Theta} - \frac{8\Theta}{2 + 3\Theta} (1 + \sigma) \right] > 0, \end{aligned} \quad (3.50)$$

$$C_{\text{stab}}^{\text{NLCDH}} = 3 \left(1 + \frac{\sigma}{1 + 3\Theta}\right) + 4 + \frac{3\sigma}{1 + 3\Theta} - \frac{3}{2} \frac{\sigma \tilde{\sigma}}{1 + \kappa} \frac{1 - 3\Theta}{1 + 3\Theta} > 0. \quad (3.51)$$

In all the numerical studies using the inflaton potential Eq. (3.48), we have kept fixed the values  $m_\phi = \sqrt{8\pi} \times 10^{-6} m_{\text{P}}$ , the initial value for the dissipation factor  $Q = 100$ , the initial temperature  $T = 370 m_\phi$  and  $\phi(0) = 10.98 m_{\text{P}}$ . The values for  $H(0)$  and  $\dot{\phi}(0)$  follow from the slow-roll conditions. These values correspond to a proportionality constant  $C_\phi \simeq 1.61 \times 10^8$  for the dissipation term, which is a typical value found in the context of WI model building [91], and gives 60 e-folds of inflation without viscosities. The value of the bulk viscosity coefficient  $C_b$  is varied and also the value of the relaxation constant  $\tau H = \Theta$ , but observing that we are still in the region of validity of the thermal radiation bath at quasi-equilibrium,  $\Theta < 1$ .

By letting the system of equations evolve, we determine the critical value of  $C_b$  for which the stability conditions for each of the three theories studied here, Eqs. (3.49), (3.50) and (3.51), are violated. The corresponding results are given in Tab. 3.1.

| $\Theta$ | theory | $C_b$   |
|----------|--------|---------|
| 0.01     | Eckart | 2232.94 |
|          | IS     | 2266.48 |
|          | NCLDH  | 2300.04 |
| 0.05     | Eckart | 2232.94 |
|          | IS     | 2400.61 |
|          | NCLDH  | 2568.42 |
| 0.1      | Eckart | 2232.94 |
|          | IS     | 2568.23 |
|          | NCLDH  | 2903.79 |

Table 3.1: The critical values for the bulk viscosity constant  $C_b$ . The Eckart case is independent of  $\Theta$ , therefore the value for its critical  $C_b$  does not change.

We note from the results of Tab. 3.1 that the values for the bulk viscosity constant  $C_b$  for which the stability conditions for IS and NCLDH cases are violated increases with respect to the Eckart case as  $\Theta$  increases. In Tab. 3.2 we give the corresponding differences in percentage.

| theory | $\Theta = 0.01$ | $\Theta = 0.05$ | $\Theta = 0.10$ |
|--------|-----------------|-----------------|-----------------|
| IS     | 1.5%            | 7.5%            | 15.0%           |
| NLCDH  | 3.0%            | 15.0%           | 30.0%           |

Table 3.2: The increase of the critical value of  $C_b$  for the causal theories with respect to the Eckart theory.

Once we have the system evolving in time and also allowing the time depen-

dence for the stability parameters  $C_{\text{stab}}^{\text{Eckart}}$ ,  $C_{\text{stab}}^{\text{IS}}$  and  $C_{\text{stab}}^{\text{NLCDH}}$ , by starting from the initial conditions given above, we can explicitly check that the time where Eqs. (3.49), (3.50) and (3.51), are violated, is the time where both radiation energy density and the bulk pressure start to grow exponentially, as expected. In the Fig. 3.1 we plot the stability parameters  $C_{\text{stab}}^{\text{Eckart}}$ ,  $C_{\text{stab}}^{\text{IS}}$  and  $C_{\text{stab}}^{\text{NLCDH}}$  along side those for the radiation energy density and the bulk pressure, as a function of time, for the case of  $\Theta = 0.01$  and for the values of critical  $C_b$  shown in Tab. 3.1.

The results shown in Fig. 3.1 indicate that the time where the stability condition is violated corresponds to an inflection point in the radiation energy density and the bulk pressure evolutions. After that time, both the radiation energy density and the bulk pressure start to grow and soon after the dynamics become uncontrollable. The point where the stability conditions Eqs. (3.49), (3.50) and (3.51), are violated, corresponds then to a turnover point in the evolution of the dynamical system of equations.

We can also notice from the results for the radiation and bulk pressure shown in Figs. 3.1(b), 3.1(d) and 3.1(f), that the causal theories always lead to a smaller radiation production when compared to the noncausal case. Among the two causal theories studied here, the NLCDH theory gives a much smaller radiation production from bulk pressure effects than the IS theory. The differences between the causal theories of IS and NLCDH are also larger than the noncausal theory of Eckart as the relaxation time increases, which is clear from the results presented in Tabs. 3.1 and 3.2. Even though the difference of the Eckart theory for the bulk pressure from that of IS is around the percent level for a relatively small relaxation time of  $\tau H = 0.01$ , it is twice that (in percentage) when the NLCDH theory is considered. This difference between the IS and NLCDH theories can easily be understood once we compare the Eqs. (3.18) and (3.25) and realizes that the relaxation time in the NLCDH theory appears with an additional factor two on the right-hand-side of the equation. Among the theories for the bulk pressure we have studied here, thus, the NLCDH case is the most robust in terms of stability. It allows for relatively larger bulk viscous pressures as compared to the Eckart and IS cases.

### 3.4 Model building

We have understood how to separate, in general, between the stable and unstable regimes. Moreover, we have studied the differences between the non-causal and causal descriptions of the bulk viscosity. In this section, we are going to apply this knowledge to some generic supersymmetric (SUSY) models of warm inflation, namely, the chaotic, hybrid and hilltop (or new inflation) models.

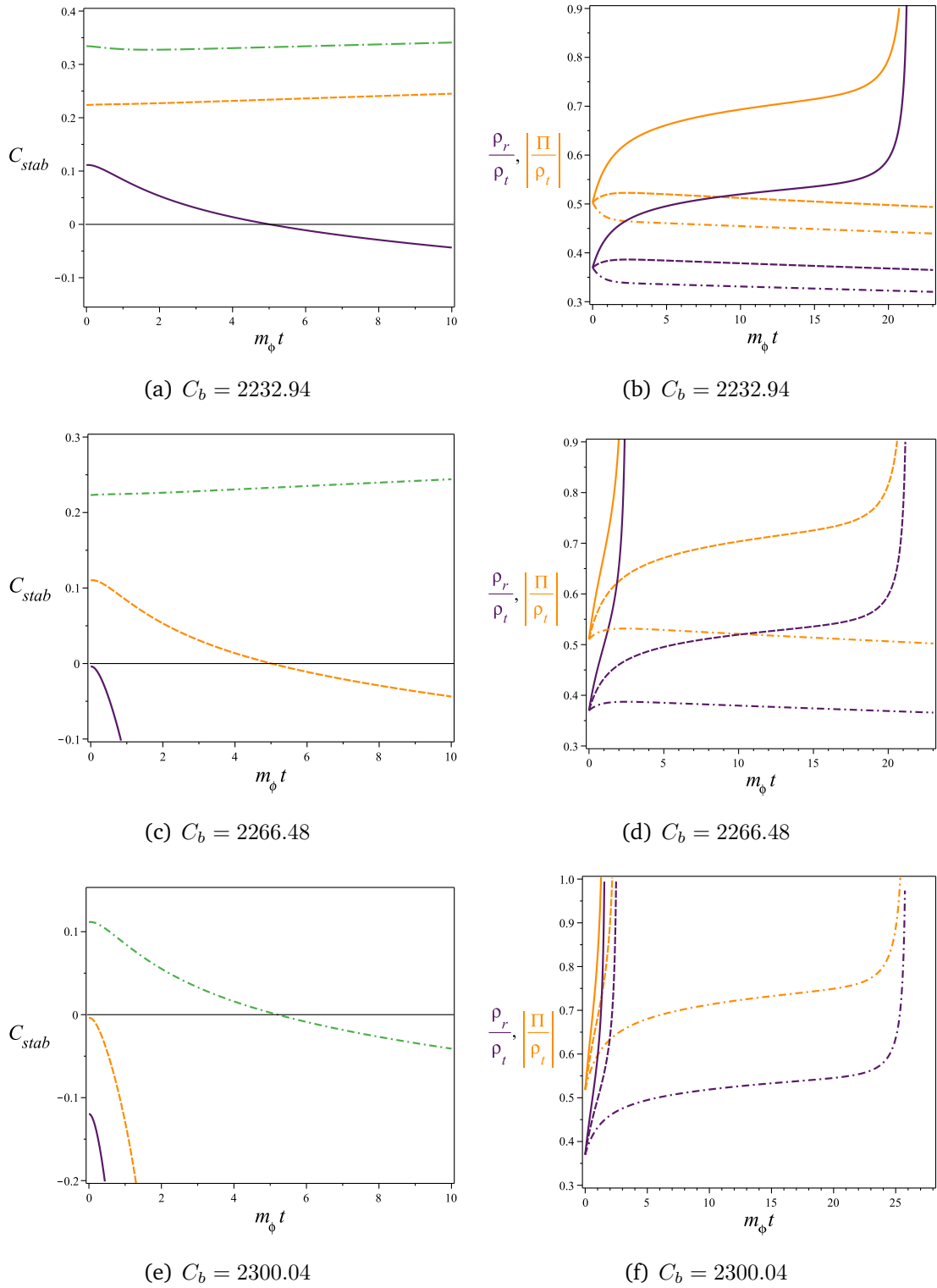


Figure 3.1: The stability condition (left) and the results (right) for the radiation energy density,  $\rho_r$  (purple curves), and bulk pressure,  $\Pi$  (orange curves), normalized by the total energy density. The solid curves are for the Eckart case, the dashed curves are for IS and the dash-dotted curves are for NLCDH. In all cases  $\Theta = 0.01$ .

As discussed in previous sections, the bulk viscous pressure decreases the radiation pressure and so allows the source term creating radiation to be more effective. Thus assuming thermalization, it raises the temperature. Given that the dissipative coefficient depends on the temperature, the bulk viscosity enhances it; and therefore, the inflaton can slow-roll down its potential with lower values of the dissipative factor  $C_\phi$ . Hence, we expect an enlargement of the parameter space in regions of low  $C_\phi$ , where warm inflation is not allowed in the absence of bulk viscosity. In addition, in the regions of the parameter space where warm inflation is allowed without bulk viscosity, its effect is to produce more e-folds of inflation. We will analyse the modification of the parameter space induced by the bulk viscosity with the stability conditions studied in the previous sections, which place limits upper limits on the value of the bulk viscosity coefficient,  $C_b \lesssim C_{\text{stab}}$ .

In addition to the standard constraints to the parameter space available for warm inflation, we also must take into account the thermodynamical condition  $|\Pi/p_r| < 1$ , as the hydrodynamic descriptions of the bulk viscosity that we are using treat the viscous pressure as a perturbation to the equilibrium one. Therefore, we define the parameter space compatible with warm inflation as the region where the following conditions hold:

1.  $\epsilon_H = -\dot{H}/H^2 < 1$ , which is the standard condition for the accelerated expansion,
2.  $\rho_\phi > \rho_r$ , which prevents the radiation energy density to dominate,
3.  $T/H > 1$ , which is required for the consistency of the LOTS description,
4.  $\phi/T \gtrsim 10$ , which is the low-T condition for  $g = \mathcal{O}(1)$ ,
5.  $|\Pi/p_r| < 1$ , which is the condition for the hydrodynamic description to hold.

These conditions need to hold for at least 40 e-folds to solve the flatness and horizon problems. Condition 2 is controlled by the stability conditions found in the previous section. From the system of Eqs. (3.37), we can relate the rest of the conditions with slow-roll parameters. Condition 1 during slow-roll simply is:

$$\epsilon_H = \frac{\epsilon}{1+Q} < 1. \quad (3.52)$$

The evolution of the ratio  $T/H$ , in the slow-roll regime, with respect to the number of e-folds is given by:

$$\frac{d \ln(T/H)}{dN_e} = \frac{2(1+\sigma)}{1+Q+6Q(1+\sigma)} \left( \frac{2+4Q}{1+Q} \epsilon - \eta + \frac{1-Q}{1+Q} \frac{m_P}{\phi} \sqrt{2\epsilon} \right). \quad (3.53)$$

$\Pi/p_r$  is directly related to  $T/H$ ,

$$\left| \frac{\Pi}{p_r} \right| = \frac{270C_b}{\pi^2 g_*} \frac{H}{T}. \quad (3.54)$$

The evolution of  $\phi/T$  by:

$$\begin{aligned} \frac{d \ln(\phi/T)}{dN_e} = & \frac{-1}{[1 + Q + 6Q(1 + \sigma)]} \left[ \frac{3 + 4\sigma + (1 + 2\sigma)Q}{1 + Q} \epsilon \right. \\ & \left. - 2(1 + \sigma)\eta + \frac{3 + 2\sigma + (5 + 4\sigma)Q}{1 + Q} \frac{m_P}{\phi} \sqrt{2\epsilon} \right]. \end{aligned} \quad (3.55)$$

In addition to these equations, the slow-roll evolution of the field  $\phi$  is given by:

$$\frac{d\phi/m_P}{dN_e} = -\frac{\sqrt{2\epsilon}}{1 + Q}. \quad (3.56)$$

For completeness, we also show the evolution of  $Q$ :

$$\frac{dQ}{dN_e} = \frac{Q}{1 + Q + 6Q(1 + \sigma)} \left[ 10 \left( 1 + \frac{6}{5}\sigma \right) \epsilon - 6(1 + \sigma)\eta + 8 \left( 1 + \frac{3}{4}\sigma \right) \frac{m_P}{\phi} \sqrt{2\epsilon} \right]. \quad (3.57)$$

These results generalize the ones obtained in [91] for the case with no bulk viscosity. Note the difference in the notation between our  $\sigma$  and the  $\sigma_\phi$  defined there, which have replaced here by  $\sqrt{2\epsilon}(\phi/m_P)$ . Nevertheless, as we have shown in (A.10),  $|\sigma| \lesssim 1$  and then the results in [91] concerning whether the conditions increase or decrease during the evolution are still valid.

The last question before entering in the particular details of each model is how we are treating the bulk viscosity. In this section we will use the non-causal description of the bulk viscosity, i.e. the Eckart theory, and place limits on the validity of this approximation. As discussed previously, the Eckart description is a good approximation for low values of  $\Theta = \tau H$ . The Hubble parameter is given by (3.5) and the relaxation time  $\tau$  is obtained from Eq. (3.70). Using for example the first expression for the bulk viscosity in Eq. (3.68) (the second expression for the bulk viscosity in Eq. (3.68) can be easily seen as obtained from the first, when neglecting the temperature independent terms in  $m_y(T)$  and in  $\tilde{m}_y$ ), we obtain that

$$\tau \approx 9.77 \times 10^6 \frac{m_y^3(T)}{\lambda_y^4 T^4}, \quad (3.58)$$

where for the superpotential of the two stage mechanism, we have that  $\lambda_y = 6h^2$ . Based on the previous discussions, we consider the Eckart approximation to be valid when  $\Theta \lesssim 10^{-2}$ , which translates into (using that in the high-temperature limit  $m_y(T) \approx hT/2$ )

$$h \gtrsim 10 \left( \frac{H}{T} \right)^{1/5}. \quad (3.59)$$

One of the conditions for warm inflation is that  $T/H \gtrsim 1$ , therefore, we can easily arrange the condition (3.59) to be satisfied when deep in the warm inflationary regime, particularly in the strong dissipative regime, which can also allow for perturbative values for the coupling  $h$ . The effect of including a causal description of the viscosity is to produce a lower value of the bulk viscous pressure than in the non-causal case with the same coefficient  $C_b$ . The consequence is a shift around the 5% level in the entire parameter spaces shown in the next subsections to higher values of  $C_b$ . This is explicitly verified below for the specific inflaton potential models we have studied.

### 3.4.1 Chaotic model

First we consider a chaotic inflation potential of the form:

$$V(\phi) = \frac{\lambda}{4}\phi^4 \quad (3.60)$$

where we have used  $\lambda = 10^{-14}$ . However this parameter is only relevant for the amplitude of the power spectrum, which we are not interested in here. Using again that  $\Upsilon = C_\phi T^3/\phi^2$ , for the potential (3.60) the slow-roll parameters are given by

$$\eta = 12 \left( \frac{m_P}{\phi} \right)^2, \quad \epsilon = \frac{2}{3}\eta, \quad \beta_\Upsilon = -\frac{2}{3}\eta. \quad (3.61)$$

Therefore, the value of the field decreases during inflation, meanwhile, the dissipative ratio  $Q$  and  $T/H$  both increase. Hence, once the condition on  $T > H$  is fulfilled initially, it is always satisfied. The ratio  $\phi/T$  decreases, but we have checked that it always remains above 10 as long as the other conditions are fulfilled. The parameter  $\epsilon_H$  increases during inflation and, as a consequence, warm inflation ends when  $\epsilon_H = 1$ . Finally, the condition  $\rho_\phi > \rho_r$  is controlled by the stability condition (3.41). It is only necessary to check that the stability condition is positive at the beginning of inflation, as it does not change sign during the evolution. This last statement is true for all the models studied.

The available parameter space is shown in Fig. 3.2. For completeness we have included the parameter space excluded for different values of the hydrodynamic condition  $|\Pi/p_r|$ , namely 0.1, 0.5 and 1. We observe that the enlargement of the parameter space in regions of low  $C_\phi$  is not very efficient. In particular, the minimum value of  $C_\phi$  is reduced from  $2.1 \times 10^6$  up to  $1.6 \times 10^6$ . These values have been confirmed by using the NLCDH description of the bulk viscosity, Eq. (3.25), with a constant  $\tau$  fixed by imposing initially the values  $\Theta = 0.01, 0.9$ . The NLCDH description reduces the bulk viscous pressure associated to a  $C_b$  value when  $\Theta$  grows, which means that higher values of  $C_b$  are allowed before the condition  $|\Pi/p_r|$  is violated. However, at the same time, for the same value of  $C_\phi$ , higher values of  $C_b$  are required to avoid the  $T/H < 1$  exclusion region, therefore the

effects compensate each other and the minimum value of  $C_\phi$  is independent of the initial value  $\Theta$ .

We have also found that the condition  $|\Pi/p_r|$  is the most restrictive one in almost the full parameter space and that the instability regime studied in the previous sections is far beyond the limit imposed by this condition. In the analysis we have fixed the initial values such that the exclusion regions are the least stringent, that is, the upper region is as high as possible and the bottom one, as low as possible. We have fixed initial conditions in this way for the three models studied.

In addition, we separate with black lines the regions where the dissipative ratio at horizon crossing  $Q_*$  is always greater than one from the regions where it is always less than one. In the region between them,  $Q_*$  can be either greater or less than one, depending on the initial value of  $\phi$ . In the regions that were not allowed in the absence of bulk viscosity, its main role is to produce enough e-folds of inflation. In regions allowed with no bulk viscosity, the total number of e-folds is increased. We quantify this effect in terms of the percentage difference  $\Delta N_e$ , defined as

$$\Delta N_e = \frac{N_e^{\text{bulk}} - N_e^{\text{no-bulk}}}{N_e^{\text{no-bulk}}} \times 100, \quad (3.62)$$

where  $N_e^{\text{bulk}}$  is the maximum number of e-folds obtained with bulk viscosity for a certain  $C_\phi$  and  $N_e^{\text{no-bulk}}$  is the equivalent without bulk viscosity. The results are shown in Fig. 3.3.

The bulk viscosity can enhance the number of e-folds through two mechanisms. The first one is, for a given initial value of the field, to reduce the redshift of the radiation energy density by decreasing its total pressure. This effect produces an increase in the value of  $Q$ , which goes as  $\rho_r^{3/4}$  and is related to the number of e-folds via

$$N_e = \int_{\phi_{\text{end}}}^{\phi(0)} \frac{3H^2(1+Q)}{V_\phi} d\phi, \quad (3.63)$$

where  $\phi(0)$  is the initial value of the field and  $\phi_{\text{end}}$ , the value of the field at the end of inflation. Hence, the increase in  $Q$  leads to a larger number of e-folds. However, we have checked that this mechanism is subdominant in the quartic potential, providing an efficiency up to 2%.

The second mechanism allows to increase the initial value of the field. From Eq. (3.63) it can be seen that this produces more e-folds by increasing the integration interval. In the absence of bulk viscosity, there is an upper limit on the value of the field because of the condition  $T/H > 1$ . As the bulk viscosity increases the value of  $T$ , it pushes upwards this limit and, hence, it is possible to use larger values of the field. However, there is a bound to this effect, provided by the condition  $|\Pi/p_r| < 1$ , which translates into a new upper limit to  $\phi(0)$ . Fig. 3.3 shows the increase in the number of e-folds compared to the non-viscous case.

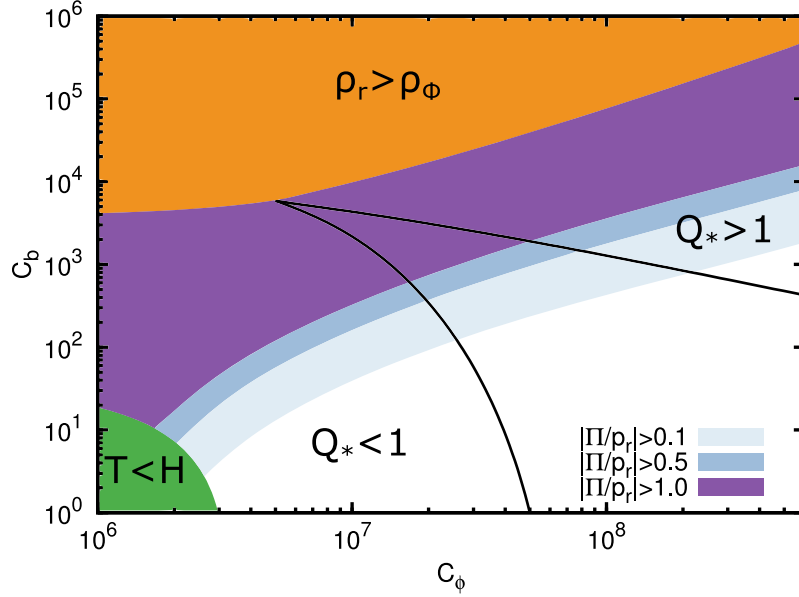


Figure 3.2: Parameter space for the chaotic model. The green regions are excluded because of the violation of the condition written in the plot. The lines separate regions where  $Q_* < 1$  and  $Q_* > 1$  respectively. In the region between them, we can have both  $Q_* < 1$  and  $Q_* > 1$  for different values of  $\phi(0)$ .

From Eq.(3.54) we can obtain the value of  $C_b$  that maximizes this mechanism. Using the values  $|\Pi/p_r| = 1$ ,  $T/H = 1$  and  $g_* = 225.78$  as an example, we find that  $C_b = 8.25$ . This argument is model independent, so that we find the same value of  $C_b$  in the three models studied and independently of the value of  $C_\phi$ .

### 3.4.2 Hybrid models

We consider now small field models of inflation with an inflationary potential given by:

$$V = V_0 \left[ 1 + \frac{\delta}{2} \left( \frac{\phi}{m_P} \right)^2 \right], \quad (3.64)$$

where  $V_0$  is the scale and  $\delta$  a model parameter. Here we have used  $V_0 = 10^{-8} m_P^4$ , and studied the dynamics for two representative values for the parameter  $\delta$ . The slow-roll parameters, in the case of the inflaton potential given by Eq. (3.64), are now given by

$$\eta = \delta, \quad \epsilon = \frac{\delta^2}{2} \left( \frac{\phi}{m_P} \right)^2, \quad \beta_{\text{r}} = -2\eta. \quad (3.65)$$

During the evolution the value of  $\phi$  decreases, while the value of  $Q$  increases. The evolution of the value of  $T/H$  depends on the value of  $Q$ : for  $Q < 1$ ,  $T/H$

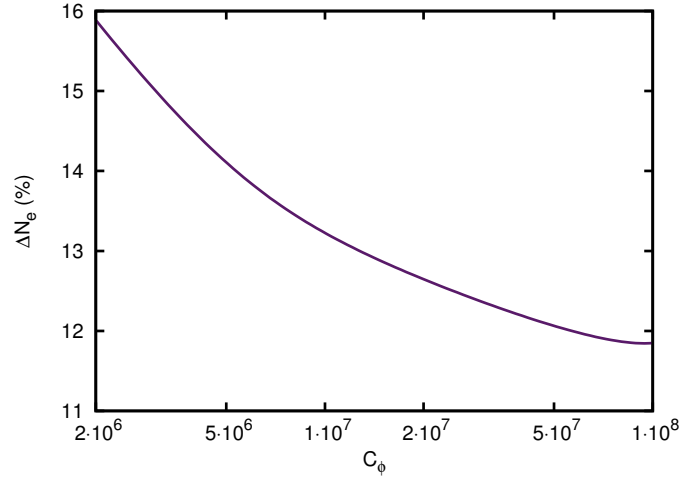


Figure 3.3: Maximum enhancement in the number of e-folds for different values of  $C_\phi$  for the model with quartic potential. The maximum value is obtained for  $C_b=8.25$ .

increases and for  $Q > 1$ , it decreases;  $\phi/T$  always decreases, and  $\epsilon_H$  is not relevant in this model because it is suppressed by a factor  $(\phi/m_P)^2$ , which is usually very small due to the fact that  $\phi \ll m_p$ . Hence,  $\epsilon_H$  is always below one. As a result, inflation ends because the conditions imposed either on  $T/H$  or  $\phi/T$  are violated, or because the field reaches its critical value.

In Fig. 3.4, the parameter space of the hybrid models with  $\delta = 0.1$  (left panel) and  $\delta = 10$  (right panel) are plotted. In the left panel, as in the previous model, the black lines separate regions with different value of the dissipative ratio at horizon crossing. However, in the right panel, the dissipative ratio is always above one. For a higher value of  $\delta$  we can maintain  $\eta/(1+Q)$  below one only for  $Q_* > 1$ . In the left panel the bottom excluded region is forbidden for the same reason as in the chaotic model. Nevertheless, in the right panel we find that the excluded region is forbidden by the  $\phi/T > 10$  condition. This is caused again by the higher value of  $\eta$ . The parameter  $\delta$  in Eq. (3.64) measures the curvature of the potential. Thus, for higher values of  $\delta$  the field evolves faster. As a result, the condition on  $\phi/T$  is reached first than in the case for smaller values for the parameter  $\delta$ .

The minimum value of  $C_\phi$  in this case of inflation with the hybrid type of potential, Eq. (3.64), is reduced from  $3.5 \times 10^4$  up to  $2.6 \times 10^4$ , for  $\delta = 0.1$ , while for  $\delta = 10$  it is reduced from  $5 \times 10^4$  up to  $4.1 \times 10^4$ . Making use of the *NLCDH* description of the bulk with a constant  $\tau$  fixed by imposing the initial values  $\Theta = 0.001, 0.9$ , we found that the minimum value  $C_\phi$  is independent of the initial choice of  $\Theta$ . The effect on the number of e-folds is shown in Fig. 3.5. As in the previous case, the constant field mechanism is subdominant, with an efficiency of around a 3% for the  $\delta = 10$  case and a 6% efficiency for the  $\delta = 0.1$  case.

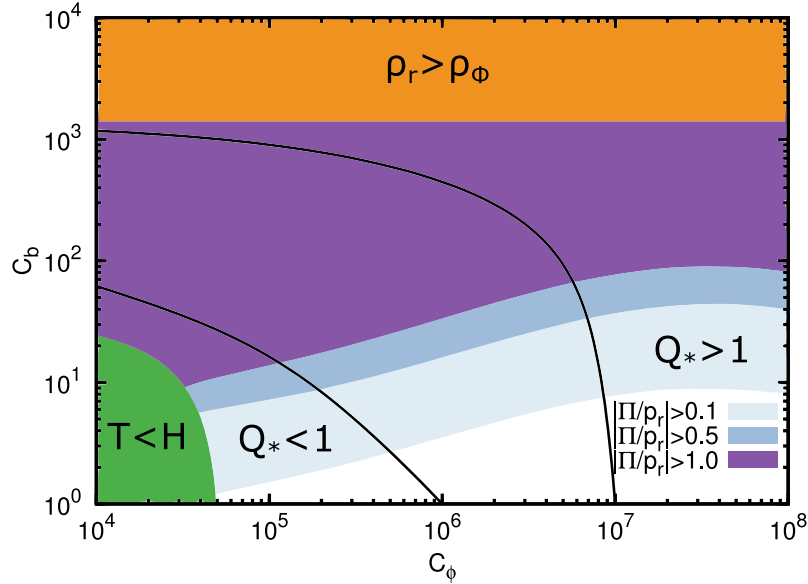
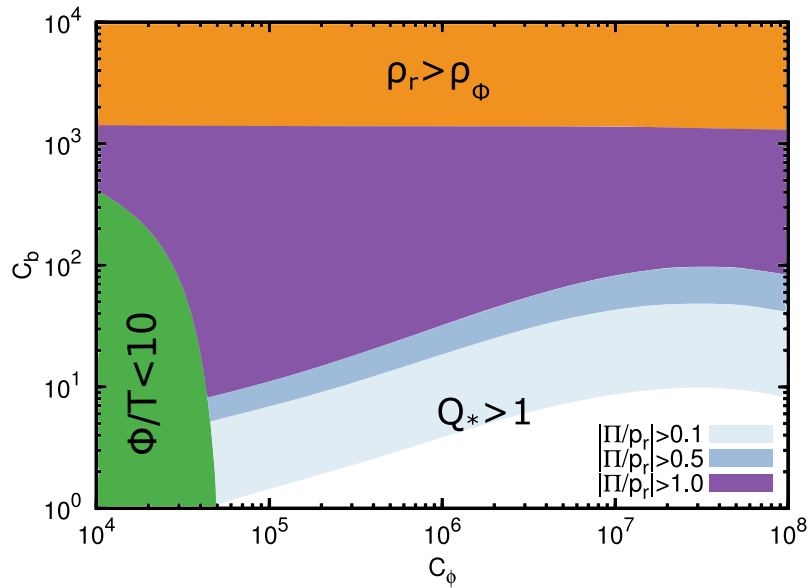
(a)  $\delta = 0.1$ (b)  $\delta = 10$ 

Figure 3.4: Parameter space for the hybrid models with  $\delta = 0.1, 10$ . The green regions are excluded because of the violation of the condition written in the plot. In the left plot the lines separate regions where  $Q_* < 1$  and  $Q_* > 1$  respectively. In the region between them, we can have both  $Q_* < 1$  and  $Q_* > 1$  for different values of  $\phi(0)$ . In the right plot,  $Q_*$  is always above 1.

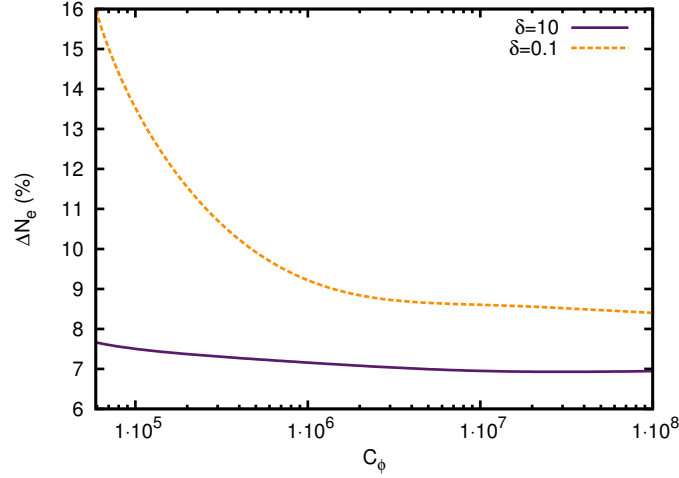


Figure 3.5: Maximum enhancement in the number of e-folds for different values of  $C_\phi$  in the case of the inflaton potential given by Eq. (3.64). The maximum value is obtained for  $C_b = 8.25$ .

### 3.4.3 Hilltop models

We now consider new inflation hilltop type of models, which are characterized by an inflaton potential given by

$$V = V_0 \left[ 1 - \frac{|\delta|}{2} \left( \frac{\phi}{m_P} \right)^2 \right] + \dots, \quad (3.66)$$

where the dots account for higher-order terms and  $V_0 = 10^{-8} m_P^4$ . This is a potential similar to the two previous ones, but with a negative squared inflaton mass. The slow-roll parameters are still given by those in Eq. (3.65), but with the change  $\delta \rightarrow -\delta$ . In these models  $\phi$ ,  $\phi/T$ ,  $T/H$  and  $\epsilon_H$  increase during the evolution, while  $Q$  decreases. Inflation ends when the field reaches a large enough value, so that higher-order terms in the potential start contributing and  $\epsilon_H$  becomes greater than one.

The parameter space for the hilltop model Eq. (3.66) is shown in Fig. 3.7, for the cases of  $\delta = 0.1$  (left panel) and  $\delta = 1$  (right panel). Once again, in the left panel the black curves separate regions with  $Q_*$  greater or less than one at horizon crossing, and in the right panel, the dissipative ratio at horizon crossing is always greater than one due to the large value of  $\eta$ .

Now, the minimum value of  $C_\phi$  is reduced from  $3.3 \times 10^4$  up to  $2.5 \times 10^4$  for  $\delta = 0.1$  and from  $5.9 \times 10^4$  up to  $5.1 \times 10^4$  for  $\delta = 1$ . We have checked these values with the NLCDH description of the bulk with a constant  $\tau$  fixed by imposing

the initial values  $\Theta = 0.001, 0.9$ . The effect on the number of e-folds is shown in Fig. 3.6. As in the other cases studied, the constant field mechanism is subdominant with efficiencies around a 5% and a 3% for the  $\delta = 1$  and the  $\delta = 0.1$  cases respectively. The initial value mechanism works reversely compared with the previous potentials. Here it allows to use lower initial values of the field, however, as the value of the field grows in this case, this reduction implies an increase of the integration interval in Eq. (3.63). In addition, note that in this potential, the lower the value of the field, the larger the value of  $H$  and thus, the lower is the ratio  $T/H$ . This argument also applies to the  $|\Pi/p_r|$  condition, therefore, there are lower limits to  $\phi(0)$  rather than upper ones.

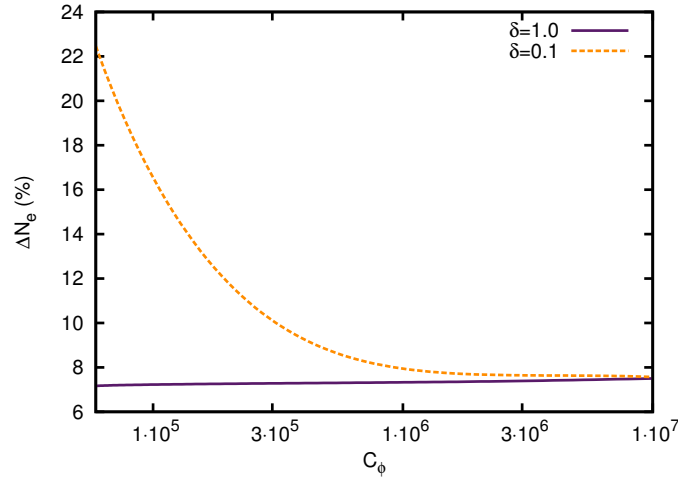


Figure 3.6: Maximum enhancement in the number of e-folds for different values of  $C_\phi$ , for the case of the inflaton potential Eq. (3.66). The maximum value is obtained for  $C_b = 8.25$ .

#### 3.4.4 Bulk viscosity coefficients from quantum field theory

The shear and bulk viscosities describe the properties of a system to return to equilibrium when displaced from it. As explained in [151, 152], at the level of particle physics processes, these viscosities are generally proportional to the mean free path, or equivalently time, of the relevant scattering process. The bulk viscosity is proportional to the mean free path for particle number changing processes in theories with breakdown of scale invariance. In contrast the shear viscosity is proportional to the two-body elastic scattering mean free path. Thus the bulk viscosity roughly has the form

$$\zeta_b \sim \tilde{m}^4 \tau \quad (3.67)$$

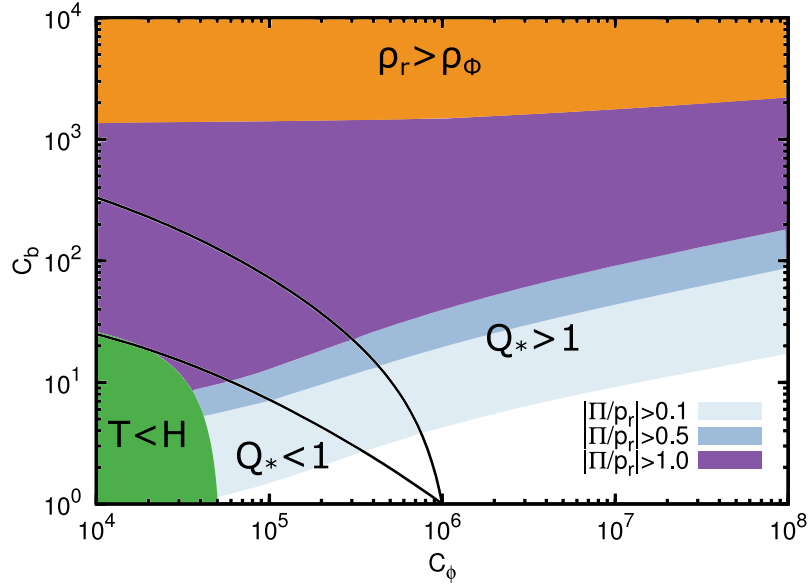
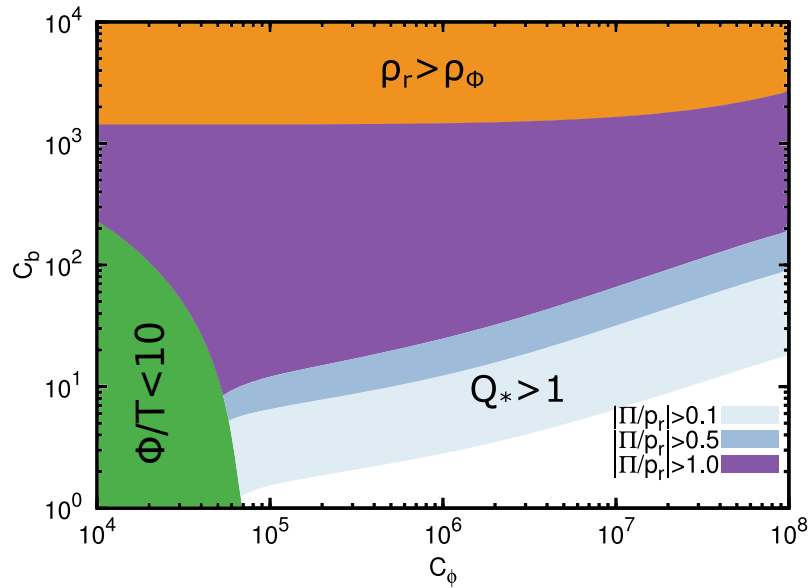
(a)  $\delta = 0.1$ (b)  $\delta = 1$ 

Figure 3.7: Parameter space for the hilltop models with  $\delta = 0.1, 1$ . The green regions are excluded because of the violation of the condition written in the plot. In the left plot the lines separate regions where  $Q_* < 1$  and  $Q_* > 1$  respectively. In the region between them, we can have both  $Q_* < 1$  and  $Q_* > 1$  for different values of  $\phi(0)$ . In the right plot,  $Q_*$  is always above 1.

where  $\tilde{m}$  is a characteristic measure of the violation from scale invariance in the theory and  $\tau$  is the mean free time between number changing inelastic scattering processes.

Explicit expressions for the bulk viscosity have been calculated for a self-interacting  $\lambda_y y^4$  scalar field theory model in [151, 152] for different temperature regimes. The obtained results for the bulk viscosity relevant for us here are [151, 152],

$$\zeta_b \simeq \begin{cases} 5.5 \times 10^4 \frac{\tilde{m}_y^4 m_y^2(T)}{\lambda_y^4 T^3} \ln^2 [1.2465 m_y(T)/T], & m_y \ll T \ll m_y/\lambda_y \\ 8.9 \times 10^{-5} \lambda_y T^3 \ln^2(0.064736 \lambda_y), & T \gg m_y/\lambda_y, \end{cases} \quad (3.68)$$

where  $m_y(T)$  is the scalar  $y$  field thermal mass,  $m_y^2(T) = m_y^2 + \lambda_y T^2/24 [1 + \mathcal{O}(m_y/T)]$ , and  $\tilde{m}_y^2 \equiv m_y^2(T) - T^2(\partial m_y^2(T)/\partial T^2) \simeq m_y^2 - \beta(\lambda_y)T^2/48$ , where  $\beta(\lambda_y) = 3\lambda_y^2/(16\pi^2)$  is the renormalization group  $\beta$ -function. Note that even for a massless scalar field at tree-level,  $m_y = 0$  which is classically scale invariant, the scale invariance is broken by the thermal corrections. The  $\beta$ -function gives a measure of breaking of scale invariance.

The characteristic relaxation time relevant for the bulk viscosity, which also enters in the IS and NLCDH formulas for the bulk pressure, can be extracted from the result for the bulk viscosity in Eq. (3.68) and the formal expression for it in the context of the Kubo formula for  $m_y \ll T$  and in the relaxation time approximation [168],

$$\zeta_b = \frac{1}{T} \int \frac{d^3p}{(2\pi)^3} \frac{\tau(\omega_p)}{\omega_p^2} n(\omega_p) [1 + n(\omega_p)] \left[ \left( \frac{1}{3} - v_s^2 \right) \mathbf{p}^2 - v_s^2 \tilde{m}_y^2 \right]^2, \quad (3.69)$$

where  $n(\omega_p) = 1/[\exp(\omega_p/T) - 1]$  is the Bose-Einstein distribution,  $\omega_p = \sqrt{\mathbf{p}^2 + m_y^2(T)}$  and  $v_s$  is the speed of sound for the radiation bath scalar  $y$  field. Using an on-shell approximation for the relaxation time,  $\tau(\omega_p) \simeq \tau \omega_p/m_y(T)$ , where  $\tau \equiv \tau(m_y(T)) = \text{constant}$ , and the result for the speed of sound for a self-interacting scalar field in the high-temperature approximation  $m_y \ll T$  [151, 152],  $v_s^2 \simeq 1/3 - 5\tilde{m}_y^2/(12\pi^2 T^2)$ , we obtain for the ratio  $\zeta_b/\tau$  the result:

$$\begin{aligned} \frac{\zeta_b}{\tau} &\simeq \tilde{m}_y^4 \frac{1}{m_y(T) T} \int \frac{d^3p}{(2\pi)^3} \frac{1}{\omega_p} n(\omega_p) [1 + n(\omega_p)] \left( \frac{5\mathbf{p}^2}{12\pi^2 T^2} - \frac{1}{3} \right)^2 \\ &\simeq \frac{\tilde{m}_y^4 T}{18\pi^2 m_y(T)} \ln \left( \frac{2T}{m_y(T)} \right). \end{aligned} \quad (3.70)$$

For the above results for the bulk viscosity to be applicable in warm inflation, it is required that the effective mass for the scalar  $y$  field be larger than the Hubble parameter,  $m_y(T) \gg H$ . In this case curvature corrections to the quantum

field expressions defining the bulk viscosity can be neglected and the Minkowski expression (3.68) applies. Also, as already pointed out in the previous sections, a quasi-equilibrium thermal radiation bath requires that the relevant relaxation time, set by  $\tau$  be also short compared to the Hubble time,  $\tau < 1/H$ . We have verified that these conditions can be easily meet for warm inflation.

Let us now briefly discuss the expected values for the bulk viscosity coefficient in the LOTS realization of warm inflation, characterized by  $m_\chi > T$  and  $m_y \ll T$ . The dominant contribution to the bulk viscosity comes from the radiation thermal bath composed of the light  $y$  particles and given by Eq. (3.68). We can see from the expression for the bulk viscosity Eq. (3.68) that the larger values for the bulk coefficient  $C_b = \zeta_b/T^3$  appears in the intermediate temperature regime,  $m_y \ll T \ll m_y/\lambda_y$ , where the  $y$  particles are already in the high-temperature regime, but the temperature is still not too high, such that in the thermal mass  $m_y(T)$  the temperature corrections are subdominant. In this case, neglecting the thermal corrections to the mass, we get the estimate for  $C_b$ ,

$$C_b \approx 5.5 \times 10^4 \frac{1}{\lambda_y^4} \frac{m_y^6}{T^6} \ln^2(1.2465 m_y/T) , \quad (3.71)$$

recalling that for the two stage model,  $\lambda_y = 6h^2$ . Taking  $m_y/T \sim 0.1$ , we obtain  $70 \lesssim C_b \lesssim 1.8 \times 10^4$ , for values of  $h$  between 0.1 and 0.2. This is in the absence of further decay modes, which would increase even more the estimates for  $C_b$  (the bulk viscosity coefficient is proportional to the radiation bath field degeneracy). These values are already within the window of values of the viscosity coefficient observed by the results in Figs. 3.2, 3.4 and 3.7, which allows warm inflation with smaller dissipation as a consequence of including a bulk viscous pressure.



# Perturbations **II**

---



*Ndanke Ndanke moy jiapou golo si ñaye.*

Wolof proverb

# Dynamics of the linear perturbations in warm inflation

In part I of this thesis we have minutely studied some models as examples of the features of the background evolution in warm inflation. In part II we focus our analysis on the dynamics of the linear perturbations of the inflaton field. This subject is of capital importance as the main observables of inflation, the spectral index and the tensor-to-scalar ratio, are calculated from linear perturbation theory.

In cosmological perturbation theory[169], every species is represented as a series of spatially inhomogeneous perturbations around a homogeneous background component. The series is approximated by the background and first-order term in linear perturbation theory. In warm inflation the universe is populated by a multi-component fluid, a mixture of a scalar inflaton field  $\Phi$  interacting with a radiation fluid. Both components exchange energy and momentum through the dissipative term  $\Upsilon$ . Consistency of perturbation theory implies that not only the inflaton, but the energy density and pressure of the radiation bath must be expanded accordingly

$$\Phi(\mathbf{x}, t) = \phi(t) + \delta\phi(\mathbf{x}, t), \quad (4.1)$$

$$\bar{\rho}_r(\mathbf{x}, t) = \rho_r(t) + \delta\rho_r(\mathbf{x}, t), \quad (4.2)$$

$$\bar{p}_r(\mathbf{x}, t) = p_r(t) + \delta p_r(\mathbf{x}, t). \quad (4.3)$$

Perturbations in the matter content of general relativity induce perturbations in the geometry of the space-time, described by the metric. The perturbed FLRW metric, including only scalar perturbations, is given by<sup>1</sup>[170, 171]

$$ds^2 = -(1 + 2\alpha)dt^2 - 2a\partial_i\beta dx^i dt + a^2[\delta_{ij}(1 + 2\varphi) + 2\partial_i\partial_j\gamma]dx^i dx^j, \quad (4.4)$$

where  $\alpha$ ,  $\beta$ ,  $\gamma$  and  $\varphi$  are the spacetime-dependent perturbed-order variables. The evolution equations of the perturbations are calculated from the stress-energy tensors. For the scalar field and a perfect radiation fluid the stress-energy tensors

<sup>1</sup>Latin indexes  $i, j, k, \dots$  are used for the spatial components, and Greek letters for space-time indexes.

read

$$T_{\mu\nu}^{(\phi)} = \nabla_\mu \Phi \nabla_\nu \Phi - \left( \frac{1}{2} \nabla^\alpha \Phi \nabla_\alpha \Phi + V(\Phi) \right) g_{\mu\nu}, \quad (4.5)$$

$$T_{\mu\nu}^{(r)} = (\bar{\rho}_r + \bar{p}_r) u_\mu^{(r)} u_\nu^{(r)} + \bar{p}_r g_{\mu\nu}, \quad (4.6)$$

where  $u_\mu^{(r)}$  is the four velocity of the radiation fluid and  $g_{\mu\nu}$  is the four dimensional metric in Eq.(4.4). The equations of motion follow from the conservation of the stress-energy tensors in Eqs.(4.5,4.6)

$$\nabla^\mu T_{\mu\nu}^{(\alpha)} = Q_\nu^{(\alpha)}, \quad \sum_\alpha Q_\nu^{(\alpha)} = 0, \quad (4.7)$$

where  $Q_\nu$  is the four-vector source term accounting for the exchange of energy and momentum:

$$-Q_\nu^{(\phi)} = Q_\nu^{(r)} = \Upsilon u_{(\phi)}^\mu \nabla_\mu \Phi \nabla_\nu \Phi. \quad (4.8)$$

$u_\phi^\mu$  is the four-velocity of the fluid describing the inflaton field:

$$u_{(\phi)}^\mu = -\frac{\nabla^\mu \Phi}{\sqrt{\rho_\phi + p_\phi}}. \quad (4.9)$$

The four-vector source term contains a source for the energy density  $Q^{(\phi)} = -Q^{(r)}$  and a momentum source  $J_\mu^{(\phi)} = -J_\mu^{(r)}$ ,

$$Q_\mu^{(\phi)} = Q^{(\phi)} u_\mu^{(\phi)} + J_\mu^{(\phi)} \quad (4.10)$$

The energy density source term is given by the projection of the four-vector source term along the direction of the fluid,  $Q^{(r)} = -u_{(\phi)}^\mu Q_\mu^{(\phi)}$ , which at linear order is given by:

$$Q^{(r)} = Q_r + \delta Q_r, \quad (4.11)$$

$$Q_r = \Upsilon \dot{\phi}^2, \quad (4.12)$$

$$\delta Q_r = \delta \Upsilon \dot{\phi}^2 + 2\Upsilon \dot{\phi} \delta \dot{\phi} - 2\alpha \Upsilon \dot{\phi}^2. \quad (4.13)$$

The momentum source term  $J_\mu$  is the orthogonal projection to the fluid velocity  $u^{(\phi)\mu} J_\mu^{(\phi)} = 0$ , vanishing in the background FLRW geometry. At linear order it reads

$$J_i^{(r)} = \partial_i \mathbf{J}_r, \quad (4.14)$$

$$\mathbf{J}_r = -\Upsilon \dot{\phi} \delta \phi. \quad (4.15)$$

Both sources terms  $Q^{(r)}$  and  $J_\mu^{(r)}$  are determined from the dissipative coefficient. We consider a general temperature  $T$  and field  $\phi$  dependence,

$$\Upsilon = C_\phi \frac{T^c}{\phi^{c-1}}, \quad (4.16)$$

$$\delta\Upsilon = \Upsilon \left( c \frac{\delta T}{T} - (c-1) \frac{\delta\phi}{\phi} \right), \quad (4.17)$$

The linear order expansion of Eq.(4.7) gives the evolution equations for the Fourier transform<sup>2</sup> of the radiation fluctuations with wavenumber  $k$  [169, 170, 171, 172]:

$$\delta\dot{\rho}_r + 3H(\delta\rho_r + \delta p_r) = -3(\rho_r + p_r)\dot{\phi} + \frac{k^2}{a^2} [\Psi_r + (\rho_r + p_r)\chi] + \delta Q_r + Q_r\alpha, \quad (4.18)$$

$$\dot{\Psi}_r + 3H\Psi_r = -(\rho_r + p_r)\alpha - \delta p_r + \mathbf{J}_r, \quad (4.19)$$

where  $\Psi_r$  is the radiation momentum perturbation,  $T_j^{0(r)} = -\partial_j\Psi_r/a$  and  $\chi$  is the combination of metric variables

$$\chi = a(\beta + a\dot{\gamma}). \quad (4.20)$$

Thermal fluctuations in the radiation fluid are transferred to the inflaton and become the main source of primordial fluctuations [100, 101, 173, 174, 175, 102, 176]. As a consequence, the evolution of the field fluctuations is governed by the fluctuation-dissipation theorem. In addition to the linear expansion of Eq.(4.7), the effect of the interactions with the thermal bath need to be taken into account. The standard approach is to integrate out the backreaction effect of the thermal bath and represent it through a stochastic source  $\xi_k$ . Hence, the equation of motion of the field perturbations becomes a Langevin equation[100, 101, 102, 177]

$$\begin{aligned} \delta\ddot{\phi} + (3H + \Upsilon)\delta\dot{\phi} + \left( \frac{k^2}{a^2} + V_{\phi\phi} \right) \delta\phi = [2(\Upsilon + H)T]^{1/2} a^{-3/2}\xi_k - \delta\Upsilon\dot{\phi} \\ + \dot{\phi}(\kappa + \dot{\alpha}) + (2\ddot{\phi} + 3H\dot{\phi})\alpha - \Upsilon(\delta\dot{\phi} - \alpha\dot{\phi}), \end{aligned} \quad (4.21)$$

where stochastic source  $\xi_k$  describing the backreaction of the thermal bath can be approximated by a localized gaussian distribution with correlation function:

$$\langle \xi(t, x)\xi(t', x') \rangle = \delta(t - t')\delta^{(3)}(x - x'). \quad (4.22)$$

The relevant quantity extracted from the evolution Eqs. (4.18,4.19,4.21) is the total comoving curvature perturbation. In warm inflation, the comoving curvature perturbation  $\mathcal{R}$  is composed of contributions not only from the metric perturbations

<sup>2</sup>For simplicity, we keep the same notation for the fluctuations  $\delta f(\mathbf{x}, t)$  and their Fourier transform  $\delta f(\mathbf{k}, t)$ .

and the inflaton momentum perturbations, but also from the radiation momentum perturbations,

$$\mathcal{R} = \sum_{i=\phi,r} \frac{\rho_i + p_i}{\rho + p} \mathcal{R}_i, \quad (4.23)$$

$$\mathcal{R}_i = -\varphi - \frac{H}{\rho_i + p_i} \Psi_i, \quad (4.24)$$

with  $\rho = \rho_\phi + \rho_r$ ,  $p = p_\phi + p_r$ . The total comoving curvature perturbation shall be used to evaluate one of the main inflationary observables, the primordial spectrum

$$P_{\mathcal{R}}(k) = \frac{k^3}{2\pi^2} \langle |\mathcal{R}_k|^2 \rangle, \quad (4.25)$$

where “ $\langle \dots \rangle$ ” means average over different realizations of the noise term in Eq. (4.21). The spectral index  $n_s$  measures the scale dependence of the primordial spectrum in Eq. (4.25)

$$\mathcal{P}_{\mathcal{R}}(k) = A_s \left( \frac{k}{k_0} \right)^{n_s-1}, \quad (4.26)$$

where  $A_s$  is the amplitude of the power spectrum at a reference scale  $k_0$ .

The temperature dependence of the dissipative coefficient induces a coupling of the field and radiation fluctuation equations through the term

$$\dot{\phi} \delta\Upsilon = c \frac{H}{\dot{\phi}} \delta\rho_r + \dots \quad (4.27)$$

in Eq. (4.21) as shown in [103]. Previous studies of the primordial spectrum of perturbations in warm inflation [174, 175, 102, 176] did take into account the influence of the thermal fluctuations on the field through the noise term, but not the coupling through the dissipative term itself. In [103] it was shown that in the strong dissipative regime, when  $\Upsilon$  dominates over the Hubble expansion rate, a positive power  $c$  of the temperature in the dissipative coefficient induces a growing mode in the fluctuations before horizon crossing through the coupling term in Eq. (4.27) that can be observed in Fig. 4.1. The outcome of the growing mode is to enhance by several orders of magnitude the amplitude of the primordial perturbations with respect to previous calculations. The effect is strongly scale dependent, thus having a large impact on the spectral index as can be seen from the numerical analysis shown in Fig. 4.2.

In part II of the thesis we are going to explore different ways to avoid the growing mode. In chapter 5 we will follow the line of research initiated in [138], and investigate the effects of non-equilibrium dynamics on the evolution of the warm inflation perturbations. Non-equilibrium effects will induce viscosities in the radiation fluid that may suppress the growth mode when they are large enough.

In chapter 6 we will concentrate on the warm inflation observables in the weak dissipation regime, where the growing mode is not present. We will examine whether warm inflation in that regime modifies the cold inflation predictions for canonical models, and we will compare the results with the observations of the *Planck* n

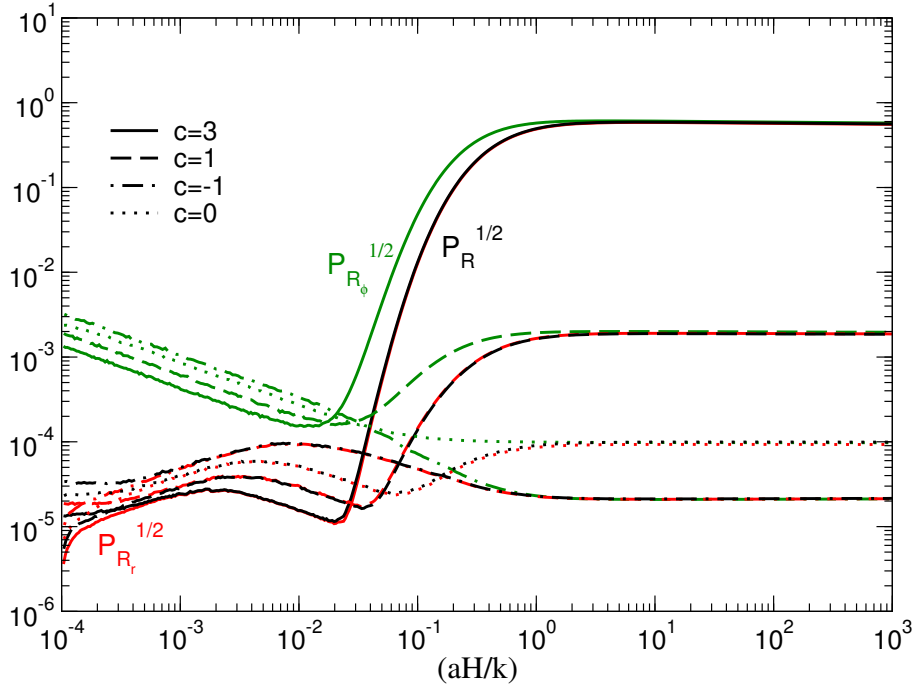


Figure 4.1: Evolution of the total curvature perturbation spectrum  $\mathcal{P}_{\mathcal{R}}^{1/2}$  (black lines), the radiation  $\mathcal{P}_{\mathcal{R}^r}^{1/2}$  (red lines) and the field  $\mathcal{P}_{\mathcal{R}^\phi}^{1/2}$  (green lines) curvature perturbation spectrum for the potential  $V = (\lambda/4)\phi^4$ . The results are shown for different power dependence on  $T$  of the dissipative coefficient:  $c = 3$  (solid lines),  $c = 1$  (dashed lines),  $c = -1$  (dash-dotted lines), and  $c = 0$  (dotted lines) [138]

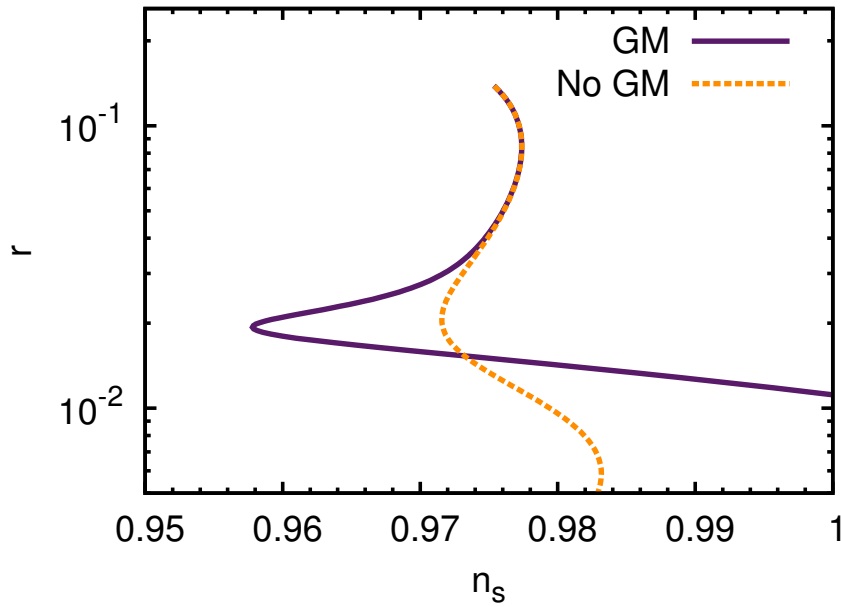


Figure 4.2: Numerical computation of the spectral index as a function of the dissipative ratio at horizon crossing,  $Q_*$ , for the potential  $V = (\lambda/4)\phi^4$  with power dependence on the temperature  $c = 3$ . The solid line shows the values when the growing mode is taken into account while the dashed line represent the prediction in absence of direct coupling between the radiation and inflaton perturbed equations.

*It's the little things citizens do. That's what will  
make the difference. My little thing is planting trees.*

Wangari Maathai

## Viscous effects in warm inflation II: perturbations

---

As we discussed in chapter 3, in warm inflation there may be intrinsic microscopic decay processes in the produced radiation bath itself, causing it to depart from equilibrium. These intrinsic dissipative effects in the radiation fluid itself will cause it not to behave exactly like a perfect fluid during inflation. As the radiation fluid departs from equilibrium, pressure and momentum changes are produced by the particles excitations in the thermal bath, and viscous effects are generated. At the linear perturbative order of the FLRW metric viscosity is described by the bulk and shear viscosities. The presence of these viscous processes during warm inflation may provide a natural solution for the potential problem of generated by the growth modes in warm inflation, as was first studied in [138] considering the effect of the shear viscosity. The viscous effects are characterized by bulk and shear viscosity terms that act like dissipation terms in the fluid itself. In [138] it was found that if the shear viscosity is strong enough it can efficiently damp the radiation perturbations in such a way that prevents the growing modes from emerging, and keeping the power spectrum within the levels obtained in the absence of coupling between radiation and field perturbations. The authors demonstrated this fact with the inclusion of only shear viscous effects, assuming that the bulk viscosity is much smaller than the shear viscosity, as it is the case for common fluids and in quantum field theory calculations in general. For example, in perturbative quantum chromodynamics, which corresponds to the high-temperature quark-gluon phase in the early universe, the bulk viscosity has been estimate to be a factor  $10^{-3}$  to  $10^{-8}$  smaller than the shear viscosity [178]). However, later works [179] gave rise to doubts about the effectiveness of the viscosities in avoiding the growing mode. It was suggested that viscosities are not consistently described only by the shear and bulk viscous terms, on the contrary additional noise terms for each viscosity should be included in the radiation equation. If that is the case the new noise terms reinforce the growth mode and it cannot be eliminated by the presence of viscosities. Nevertheless the subject is still under controversy, therefore we will not introduce such noise terms in our description to contribute to the

discussion.

There have been previous studies on the effect of the bulk viscosity for warm inflation done by the authors in [146, 154], but they have considered only the case of constant dissipation (thus there was no coupling of the radiation bath perturbations with those of the field) and the cases of either a constant bulk viscous pressure or one proportional to the radiation energy density. They have found that these bulk viscous effects could induce a variation in the power spectrum amplitude of only of the order of 4%. Here, however, by including the temperature dependence on both the dissipation and bulk viscosity terms, we find that the effect of the bulk viscous pressure on the power spectrum is significantly much higher, being able to change it by many orders of magnitude, depending on the magnitude of the dissipation term and for physically motivated magnitudes of the bulk viscosity coefficient.

Even though bulk viscosities have in general smaller magnitudes than for the shear viscosities, there are regimes of temperature and field parameters where it can be dominant. For instance, close to phase transitions or phase changes in general, it has been shown that the bulk viscosity can be much larger in magnitude than the shear viscosity [180]. Furthermore, the bulk viscosity, been related to pressure fluctuations, already contributes at the background level, while the shear viscosity, been related to momentum fluctuations, contribute only at the perturbation level. It is then important to investigate not only the possible effects of shear viscosity term on the power spectrum, as done in Ref. [138], but also to study the effects of the bulk viscosity term. In this chapter we will then extend the analysis done in [138] by also including the bulk viscous effects, and by fully accounting for its temperature dependence as motivated from microscopic quantum field theory calculations relevant for the context of warm inflation. Here we will then explore possible regimes where the presence of the bulk viscosity along with the shear viscosity can lead to much efficient damping of the growing modes, preventing them to emerge at all, in addition to possibly lessing the constraints on the inflaton potential for warm inflation. Values for the viscous coefficients are found such that the magnitude of the power spectrum remains controllable, with any growing mode in the spectrum coming from the coupling of the inflaton perturbations with those of the radiation is effectively removed.

## 5.1 Bulk and shear viscous effects in a radiation fluid

In relativistic theory, fluctuation effects in the radiation fluid can be parametrized in general in terms of a shear viscous tensor  $\pi_{ab}$ , an energy flux vector  $q_a$  and a bulk viscous pressure  $\Pi$ , in the stress-energy tensor for the radiation fluid [137,

142, 162, 163],

$$T_{ab}^{(r)} = (\rho_r + p_r + \Pi)u_a^{(r)}u_b^{(r)} + (p_r + \Pi)g_{ab} + q_a^{(r)}u_b^{(r)} + q_b^{(r)}u_a^{(r)} + \pi^{ab}, \quad (5.1)$$

where  $u_a^{(r)}\pi^{ab} = 0 = g_{ab}\pi^{ab}$ ,  $u_a^{(r)}q^a = 0$ . There would be heat flow for example in the presence of conserved charges in the system other than the stress-energy tensor, but we do not consider such possibility in this study, and then set  $q_a = 0$ . The shear viscous tensor vanishes in an homogeneous and isotropic background geometry, but at linear order it is given by [142, 162, 163]:

$$\pi_{ab} \simeq -2\zeta_s\sigma_{ab}, \quad (5.2)$$

where  $\zeta_s$  is the shear viscosity coefficient and  $\sigma_{ab}$  the shear of the radiation fluid:

$$\sigma_{ab} = \nabla_{(a}u_{b)} + u_{(a}u^c\nabla_{c}u_{b)} - \frac{h_{ab}}{3}\nabla^c u_c, \quad (5.3)$$

$\nabla_a$  being the covariant derivative of the metric  $g_{ab}$ . The bulk viscous pressure can be seen as a non-adiabatic pressure contribution, already present at the background level. From the stress-energy tensor (5.1), we see that the bulk viscous pressure enters as a modification of the radiation pressure,  $p_r \rightarrow \bar{p}_r = p_r + \Pi$ . The equation of state for the radiation pressure is still  $p_r = \omega_r\rho_r$ . Despite the dissipation of energy during the interaction between the inflaton and the radiation bath, in warm inflation we still assume close-to-equilibrium conditions. In this case, we can still approximate the radiation bath as a perfect radiative fluid with  $\omega_r \simeq 1/3$ . Then  $\rho_r + p_r + \Pi \simeq 4\rho_r/3 + \Pi$ .

As we showed in chapter 3, in the slow-roll regime the equations of motion for the inflaton and for the radiation energy density, respectively, are

$$3H(1+Q)\dot{\phi} \simeq -V_\phi, \quad (5.4)$$

$$4\rho_r + 3\Pi \simeq 3Q\dot{\phi}^2, \quad (5.5)$$

Typically, for small enough radiation bath relaxation times,  $\tau \ll H^{-1}$ , which is certainly the case for close to equilibrium thermal baths, the bulk viscous pressure is well approximated by the Eckart equation [156],

$$\Pi = -3H\zeta_b, \quad (5.6)$$

where  $\zeta_b$  is the bulk viscosity coefficient. For simplicity in this work we will analyse the regime of low values of  $\tau H$ , where the Eckart theory, Eq. (5.6), is a good approximation for the bulk viscous pressure, as we discussed in chapter 3.

The shear and bulk viscosity coefficients have been computed in the literature and defined through Kubo formulas [165, 166], which are derived in the context

of linear response theory (see also [181]):

$$\zeta_s = \frac{1}{20} \lim_{\omega \rightarrow 0} \frac{1}{\omega} \int d^3x dt e^{i\omega t} \langle [\Pi_{lm}(\mathbf{x}, t), \Pi^{lm}(0)] \rangle, \quad (5.7)$$

$$\zeta_b = \frac{1}{2} \lim_{\omega \rightarrow 0} \frac{1}{\omega} \int d^3x dt e^{i\omega t} \langle [\mathcal{P}(\mathbf{x}, t), \mathcal{P}(0)] \rangle, \quad (5.8)$$

where

$$\Pi_{lm}(x) = T_{lm}(x) - \frac{1}{3} \delta_{lm} T_i^i(x), \quad (5.9)$$

is the traceless part of the stress tensor and

$$\mathcal{P}(x) = -\frac{1}{3} T_i^i(x) + v_s^2 T_{00}(x), \quad (5.10)$$

where  $v_s$  is the local (equilibrium) speed of sound (introduced explicitly in the quantum field theory calculation for consistency, see e.g. [151, 152, 178])

$$v_s^2 = \frac{\partial p}{\partial \rho}. \quad (5.11)$$

The averages in Eqs. (5.7) and (5.8) are again with respect to thermal equilibrium.

Explicit results for both the shear and the bulk viscosity coefficients, starting from Eqs. (5.7) and (5.8), have been obtained for a self-interacting quartic scalar field model,  $\lambda_\sigma \sigma^4/4!$ , in the weak interacting regime  $\lambda_\sigma < 1$ . This is the relevant interaction in the LOTS of realization of warm inflation, where  $\sigma$  represents the scalar components of the  $Y$  superfields [94, 167, 91]. From the results obtained in [151, 152], as showed in chapter3 the expressions for the bulk viscosity are

$$\zeta_b \simeq \begin{cases} 5.5 \times 10^4 \frac{\tilde{m}_\sigma^4 m_\sigma^2(T)}{\lambda_\sigma^4 T^3} \ln^2 [1.2465 m_\sigma(T)/T], & m_\sigma \ll T \ll m_\sigma/\lambda_\sigma \\ 8.9 \times 10^{-5} \lambda_\sigma T^3 \ln^2(0.064736 \lambda_\sigma), & T \gg m_\sigma/\lambda_\sigma, \end{cases} \quad (5.12)$$

while the shear viscosity is the same in the two temperature regimes given in Eq. (5.12),

$$\zeta_s \simeq 3.04 \times 10^3 \frac{T^3}{\lambda_\sigma^2}, \quad (5.13)$$

where, in the above expressions,  $m_\sigma(T)$  is the thermal mass of the  $\sigma$  scalar component of the  $Y$  superfield,  $m_\sigma^2(T) = m_\sigma^2 + \lambda_\sigma T^2/24 [1 + \mathcal{O}(m_\sigma/T)]$ ,  $\tilde{m}_\sigma^2 = m_\sigma^2(T) - T^2(\partial m_\sigma^2(T)/\partial T^2) \simeq m_\sigma^2 - \beta(\lambda_\sigma)T^2/48$ , where  $\beta(\lambda_\sigma) = 3\lambda_\sigma^2/(16\pi^2)$  is the renormalization group  $\beta$ -function.

## 5.2 Perturbations in warm inflation with viscous effects

The system of equations for the perturbations at linear order for the field, radiation energy density and radiation pressure are obtained by expanding these quantities around their background values in a FLRW metric:

$$\Phi(\mathbf{x}, t) = \phi(t) + \delta\phi(\mathbf{x}, t), \quad (5.14)$$

$$\bar{\rho}_r(\mathbf{x}, t) = \rho_r(t) + \delta\rho_r(\mathbf{x}, t), \quad (5.15)$$

$$\bar{p}_r(\mathbf{x}, t) = p_r(t) + \Pi(t) + \delta p_r(\mathbf{x}, t) + \delta\Pi(\mathbf{x}, t), \quad (5.16)$$

and similarly for the dissipative coefficient,  $\bar{\Upsilon}(\mathbf{x}, t) = \Upsilon(t) + \delta\Upsilon(\mathbf{x}, t)$ , and likewise for the bulk viscosity coefficient,  $\bar{\zeta}_b(\mathbf{x}, t) = \zeta_b(t) + \delta\zeta_b(\mathbf{x}, t)$ .

The perturbed FRW metric, including only scalar perturbations, is given by:

$$ds^2 = -(1 + 2\alpha)dt^2 - 2a\partial_i\beta dx^i dt + a^2[\delta_{ij}(1 + 2\varphi) + 2\partial_i\partial_j\gamma]dx^i dx^j, \quad (5.17)$$

where  $\alpha, \beta, \gamma$  and  $\varphi$  are the spacetime-dependent perturbed-order variables. These metric perturbation functions are related by the complete set linear Einstein of equations, which after Fourier transforming to space-momentum are [170, 171]

- Hamiltonian and momentum constraints

$$-\frac{k^2}{a^2}\varphi + H\kappa = -\frac{1}{2m_P^2}\delta\rho, \quad (5.18)$$

$$\kappa - \frac{k^2}{a^2}\chi = -\frac{3}{2m_P^2}\Psi, \quad (5.19)$$

- Evolution equations

$$\dot{\chi} + H\chi - \alpha - \varphi = \frac{1}{m_P^2}\sigma, \quad (5.20)$$

$$\dot{\kappa} + 2H\kappa + \left(3\dot{H} - \frac{k^2}{a^2}\right)\alpha = \frac{1}{2m_P^2}(\delta\rho + 3\delta p), \quad (5.21)$$

where we have defined the new metric variables [170, 171]

$$\chi = a(\beta + a\dot{\gamma}), \quad (5.22)$$

$$\kappa = 3(H\alpha - \dot{\varphi}) + \frac{k^2}{a^2}\chi, \quad (5.23)$$

$\sigma$  is the shear pressure and  $\delta\rho$ ,  $\delta p$  and  $\Psi$  are, respectively, the total density, pressure and momentum perturbations. In our two-fluid system, they are given in terms of the inflaton field and radiation perturbations, e.g.,

$$\delta\rho = \delta\rho_\phi + \delta\rho_r, \quad (5.24)$$

$$\delta p = \delta p_\phi + \delta\bar{p}_r, \quad (5.25)$$

$$\Psi = \Psi_\phi + \Psi_r, \quad (5.26)$$

with  $\delta\rho_\phi = \dot{\phi}\delta\dot{\phi} - \dot{\phi}^2\alpha + V_{,\phi}\delta\phi$ ,  $\delta p_\phi = \dot{\phi}\delta\dot{\phi} - \dot{\phi}^2\alpha - V_{,\phi}\delta\phi$ ,  $\delta\bar{p}_r = \omega_r\delta\rho_r + \delta\Pi$  and  $\Psi_\phi = -\dot{\phi}\delta\phi$ .

The evolution equations for the field and radiation perturbation quantities follow from the conservation of the energy-momentum tensor. The complete equations have been given in [138] (see also Refs.[169, 170, 171, 182]). Working in momentum space, defining the Fourier transform with respect to the comoving coordinates, the equation of motion for the radiation and momentum fluctuations with comoving wavenumber  $k$  are given by

$$\begin{aligned} \delta\dot{\rho}_r + 4H\delta\rho_r + 3H\delta\Pi &= [(1 + \omega_r)\rho_r + \Pi](\kappa - 3H\alpha) + \frac{k^2}{a^2}\Psi_r \\ &+ \delta Q_r + Q_r\alpha, \end{aligned} \quad (5.27)$$

$$\dot{\Psi}_r + 3H\Psi_r + \omega_r\delta\rho_r + \delta\Pi = -[(1 + \omega_r)\rho_r + \Pi]\alpha + \frac{2k^2}{3a^2}\sigma_r + J_r, \quad (5.28)$$

where

$$Q_r = \Upsilon\dot{\phi}^2, \quad (5.29)$$

$$\delta Q_r = \delta\Upsilon\dot{\phi}^2 + 2\Upsilon\dot{\phi}\delta\dot{\phi} - 2\alpha\Upsilon\dot{\phi}^2, \quad (5.30)$$

$$J_r = -\Upsilon\dot{\phi}\delta\phi, \quad (5.31)$$

$$\sigma_r = -2\zeta_s \left[ \frac{\Psi_r}{(1 + \omega_r)\rho_r + \Pi} + \chi \right]. \quad (5.32)$$

Eq. (5.32) is the shear viscous pressure at linear order, with  $\zeta_s$  being the shear viscosity coefficient for the radiation fluid, while in Eqs. (5.27) and (5.28), the bulk pressure at linear order,  $\delta\Pi$ , from Eq. (5.6), is given by

$$\delta\Pi = \zeta_b \left[ \kappa + \frac{k^2}{a^2} \frac{\Psi_r}{(1 + \omega_r)\rho_r + \Pi} - 3H \frac{\delta\zeta_b}{\zeta_b} \right]. \quad (5.33)$$

In addition to Eqs. (5.27) and (5.28), there is also the evolution equation for the field fluctuations  $\delta\phi$ , which is described by a stochastic evolution determined by the Langevin-like equation [100, 101, 102, 177]:

$$\begin{aligned} \delta\ddot{\phi} + 3H\delta\dot{\phi} + \left( \frac{k^2}{a^2} + V_{\phi\phi} \right) \delta\phi &= [2(\Upsilon + H)T]^{1/2} a^{-3/2} \xi_k - \delta\Upsilon\dot{\phi} \\ &+ \dot{\phi}(\kappa + \dot{\alpha}) + (2\ddot{\phi} + 3H\dot{\phi})\alpha - \Upsilon(\delta\dot{\phi} - \alpha\dot{\phi}), \end{aligned} \quad (5.34)$$

where  $\xi_k \equiv \xi(\mathbf{k}, t)$  is a stochastic source that can be well approximated by a localized Gaussian distribution with correlation function given by

$$\langle \xi(\mathbf{k}, t) \xi(\mathbf{k}', t') \rangle = \delta(t - t') \delta^{(3)}(\mathbf{k} - \mathbf{k}'). \quad (5.35)$$

For a general temperature  $T$  and field  $\phi$  dependent dissipative coefficient, its perturbation is given by

$$\delta\Upsilon = \Upsilon \left[ c \frac{\delta T}{T} - (c - 1) \frac{\delta\phi}{\phi} \right]. \quad (5.36)$$

Likewise, the quantum field derivations for the bulk and shear viscosity coefficients,  $\zeta_b$  and  $\zeta_s$ , respectively, show that they can be parametrized in the form

$$\zeta_b = C_b T^d / m_r^{d-3}, \quad (5.37)$$

$$\zeta_s = C_s T^s / m_r^{s-3}, \quad (5.38)$$

where  $m_r$  is just a constant mass scale (typically the renormalized bare mass for the particles in the radiation bath, for example  $m_r \equiv m_\sigma$ ). The temperature exponents  $d$  and  $s$  for the bulk and the shear viscosity coefficients are given by the specific quantum field theory model realization describing the particles in the thermal bath and the specific parameter regime under consideration. For example, from the expressions (5.12) and (5.13) for the viscosity coefficients derived from a thermal  $\lambda_\sigma \sigma^4$  scalar field model, which is the relevant case for warm inflation model building, we have  $d = 3$  in the high temperature regime  $T \gg m_\sigma / \lambda_\sigma$ . In the intermediate temperature regime,  $m_\sigma \ll T \ll m_\sigma / \lambda_\sigma$ , temperature corrections to the thermal mass  $m_\sigma(T)$  are subdominant, and the bulk viscosity seems to behave like  $d = -3$ . In both temperature regimes, from Eq. (5.13), we have  $s = 3$  for the power in the temperature for the shear viscosity coefficients. In this study we will thus work with  $d = 3, 0, -3$  and  $s = 3$ , for the bulk and shear viscosity temperature dependences, respectively. From Eq. (5.37), the perturbation of the bulk viscosity,  $\delta\zeta_b$  reads

$$\delta\zeta_b = d\zeta_b \frac{\delta T}{T}. \quad (5.39)$$

Although dissipation implies departures from thermal equilibrium in the radiation fluid, the system has to be close-to-equilibrium for the calculation of the dissipative coefficient to hold, therefore we assume  $p_r \simeq \rho_r / 3$ .  $\delta T$  can be expressed in terms of the radiation energy density and its perturbation as

$$4 \frac{\delta T}{T} \simeq \frac{\delta \rho_r}{\rho_r}. \quad (5.40)$$

It is convenient to define dimensionless bulk and shear viscosity coefficients,  $\bar{\zeta}_b$  and  $\bar{\zeta}_s$ , respectively, given by

$$\bar{\zeta}_b \equiv \frac{1}{3} \frac{\zeta_b H}{\rho_r + p_r + \Pi}, \quad (5.41)$$

$$\bar{\zeta}_s \equiv \frac{4}{9} \frac{\zeta_s H}{\rho_r + p_r + \Pi}. \quad (5.42)$$

Therefore, the perturbed source, the perturbed bulk viscous pressure and the shear viscous pressure at linear order reads

$$\delta Q_r = \frac{3HQc\dot{\phi}^2}{4\rho_r}\delta\rho_r - \frac{3HQ(c-1)\dot{\phi}^2}{\phi}\delta\phi + 6HQ\dot{\phi}\delta\dot{\phi} - 6HQ\dot{\phi}^2\alpha, \quad (5.43)$$

$$\delta\Pi = \frac{k^2}{a^2}\frac{3\bar{\zeta}_b}{H}\Psi_r - \frac{3d\bar{\zeta}_b}{1+9\bar{\zeta}_b}\delta\rho_r + \frac{4\bar{\zeta}_b\rho_r}{(1+9\bar{\zeta}_b)H}\kappa, \quad (5.44)$$

$$\sigma_r = -\frac{9\bar{\zeta}_s}{2H}\Psi_r - \frac{6\bar{\zeta}_s\rho_r}{(1+9\bar{\zeta}_b)H}\chi. \quad (5.45)$$

Using this results , the system of first-order perturbation equations become

$$\begin{aligned} \delta\ddot{\phi} + 3H(1+Q)\delta\dot{\phi} + \left[ \frac{k^2}{a^2} + V_{\phi\phi} - \frac{3(c-1)HQ\dot{\phi}}{\phi} \right] \delta\phi = \\ = \frac{[2H(1+3Q)T]^{1/2}}{a^{3/2}}\xi_k - \frac{cH}{(1+9\bar{\zeta}_b)\dot{\phi}}\delta\rho_r + \dot{\phi}(\kappa + \dot{\alpha}) + [2\ddot{\phi} + 3H(1+Q)\dot{\phi}]\alpha, \end{aligned} \quad (5.46)$$

$$\begin{aligned} \delta\dot{\rho}_r + H\left(4 - \frac{3cQ\dot{\phi}^2}{4\rho_r} - \frac{9d\bar{\zeta}_b}{1+9\bar{\zeta}_b}\right)\delta\rho_r = \\ = \frac{k^2}{a^2}(1-9\bar{\zeta}_b)\Psi_r + 6HQ\dot{\phi}\delta\dot{\phi} - \frac{3(c-1)HQ\dot{\phi}^2}{\phi}\delta\phi + \left(\frac{1}{3} - 3\bar{\zeta}_b\right)\frac{4\rho_r}{1+9\bar{\zeta}_b}\kappa \\ - 3H\left[Q\dot{\phi}^2 + \frac{4\rho_r}{3(1+9\bar{\zeta}_b)}\right]\alpha, \end{aligned} \quad (5.47)$$

$$\begin{aligned} \dot{\Psi}_r + 3H\left(1 + \frac{k^2}{a^2}\frac{\bar{\zeta}_s + \bar{\zeta}_b}{H^2}\right)\Psi_r = \\ = -3HQ\dot{\phi}\delta\phi + \left(\frac{3d\bar{\zeta}_b}{1+9\bar{\zeta}_b} - \frac{1}{3}\right)\delta\rho_r - \frac{4\rho_r}{1+9\bar{\zeta}_b}\left(\frac{\alpha}{3} + \frac{\bar{\zeta}_b}{H}\kappa + \frac{\bar{\zeta}_s}{H}\frac{k^2}{a^2}\chi\right) \end{aligned} \quad (5.48)$$

Equations (5.46), (5.47) and (5.48) for the field radiation perturbations, together with the metric perturbations Eqs. (5.22) - (5.21), form a complete set of equations in a "gauge-ready" form. From this point on we can either choose to work in terms of gauge-invariant quantities [169, 170, 171], or equivalently choose an appropriate gauge directly. We have tested that a convenient gauge for better stability when numerically integrating the full set of differential equations is the zero shear (or Newtonian slicing) gauge  $\chi = 0$ . In the zero shear gauge, the relevant

equations for this analysis, obtained from Eqs. (5.22) - (5.21), become

$$\kappa = \frac{3}{2m_P^2}(\dot{\phi}\delta\phi - \Psi_r), \quad (5.49)$$

$$\alpha = -\varphi + \frac{9\bar{\zeta}_s}{2Hm_P^2}\Psi_r, \quad (5.50)$$

$$\dot{\varphi} = -H\varphi + \frac{9\bar{\zeta}_s}{2Hm_P^2}\Psi_r - \frac{1}{3}\kappa. \quad (5.51)$$

The comoving curvature perturbation  $\mathcal{R}$  is modified by the bulk viscous pressure as:

$$\mathcal{R} = \sum_{i=\phi,r} \frac{\rho_i + \bar{p}_i}{\rho + \bar{p}} \mathcal{R}_i, \quad (5.52)$$

$$\mathcal{R}_i = -\varphi - \frac{H}{\rho_i + \bar{p}_i} \Psi_i, \quad (5.53)$$

with  $\bar{p} = p_\phi + p_r + \Pi$ ,  $\bar{p}_\phi \equiv p_\phi$  and  $\bar{p}_r = p_r + \Pi$ .

## 5.3 Numerical Results

### 5.3.1 Amplitude of the power spectrum

In this section we study the system numerically using a Rosenbrock integrator method [183] of order four with variable time step-size. The set of equations consists of the system of differential equations (5.46), (5.47) and (5.48) in the zero shear gauge, together with the background evolution equations for the inflaton and the radiation energy density and those for the metric perturbation equations (5.49), (5.50) and (5.51). In the stochastic Langevin evolution equation for the inflaton field perturbation, Eq. (5.46), the stochastic noise term is numerically implemented in the time discretized code with an amplitude given by

$$\xi_k = \frac{1}{\sqrt{dt}} G, \quad (5.54)$$

where  $G$  are random numbers obtained from a zero-mean unit-variance Gaussian distribution [184]. The noise average of the power spectrum is taken over 1000 runs, which was found to be more than enough to get convergent numerical results. Initial conditions for the inflaton field perturbations are taken with respect to a thermal spectrum, as we expected for warm inflation with  $T > H$ , where modes of the inflaton field in  $k$ -space satisfies

$$\langle |\delta\phi(\mathbf{k}, t=0)|^2 \rangle = \frac{T}{k^2 + V_{\phi\phi}}, \quad (5.55)$$

while the momentum modes for the inflaton field is given by

$$\langle |\delta\dot{\phi}(\mathbf{k}, t = 0)|^2 \rangle = T. \quad (5.56)$$

Even though we use these initial conditions for the field, our results are largely insensitive to choice of initial conditions. This is because the noise quickly erases the information of the initial configuration, as is natural in stochastic systems, in just a couple of e-folds of evolution. This can be understood from Eq. (5.46), which can be approximately be seen as a stochastic damped harmonic oscillator equation, where the homogeneous solution, depending on the initial conditions, decays exponentially due to the dissipation term. On the contrary, the non-homogeneous solution, which depends on the two-point noise correlation function, gives the stationary solution.

When analysing the evolution in the presence of the bulk, we account for the possibility of dynamical instability of the background dynamics discussed in chapter 3. As shown there, the condition for stability obtained for the Eckart description of the bulk viscous pressure in Eq. (5.6) is:

$$c + 4 \gtrsim \frac{9\bar{\zeta}_b}{1 + 9\bar{\zeta}_b} \left( c + d + \frac{18\bar{\zeta}_b}{1 + 9\bar{\zeta}_b} \frac{\rho_r}{V + \rho_r} \right). \quad (5.57)$$

Our results for the power spectrum in terms of the bulk viscosity are presented only for values of  $\bar{\zeta}_b$  satisfying the stability condition given by Eq. (5.57). For the parameters we used in the numerical simulations this places a limit for upper values of  $\bar{\zeta}_b \lesssim 1 - 4$ . Results for the effect of the bulk and shear viscosities are shown in Fig. 5.1, where we can then compare the effects of both viscosities on the power spectrum as their magnitude increases. The inflaton potential used is a quartic scalar field potential,  $V(\phi) = (\lambda/4)\phi^4$ , with quartic coupling  $\lambda = 10^{-14}$ . Other type of polynomial potentials and also the hybrid type of potential were studied in Ref. [138], with no significant qualitative change of the behavior of the power spectrum as far shear viscous effects were concerned. We do expect similar behavior here too, so we concentrate on the quartic scalar potential for the inflaton.

Fig. 5.1 displays the results for the (square root) of the amplitude of the total power spectrum, as defined by Eq. (4.25), when it has already crossed the horizon and got frozen at superhorizon scales,  $z = k/(aH) \ll 1$ . We have shown in Fig. 5.1 the most severe case for the growth mode problem, which happens for the  $c = 3$  power on the temperature for the dissipation coefficient. The spectrum is normalized by the value of the  $c = 0$  power, where the growth mode is absent [103, 138]. The growth mode is apparent from the results at vanishing viscosities,  $\bar{\zeta}_s = \bar{\zeta}_b = 0$ , where we see that the ratio  $P_R(c = 3)/P_R(c = 0)$  grows with the dissipation ratio. We see that the bulk viscosity is more efficient than the shear in damping the growth fluctuations for  $\bar{\zeta}_b \gtrsim 10^{-2}$ , suppressing it completely at  $\bar{\zeta}_b \simeq 0.1$ .

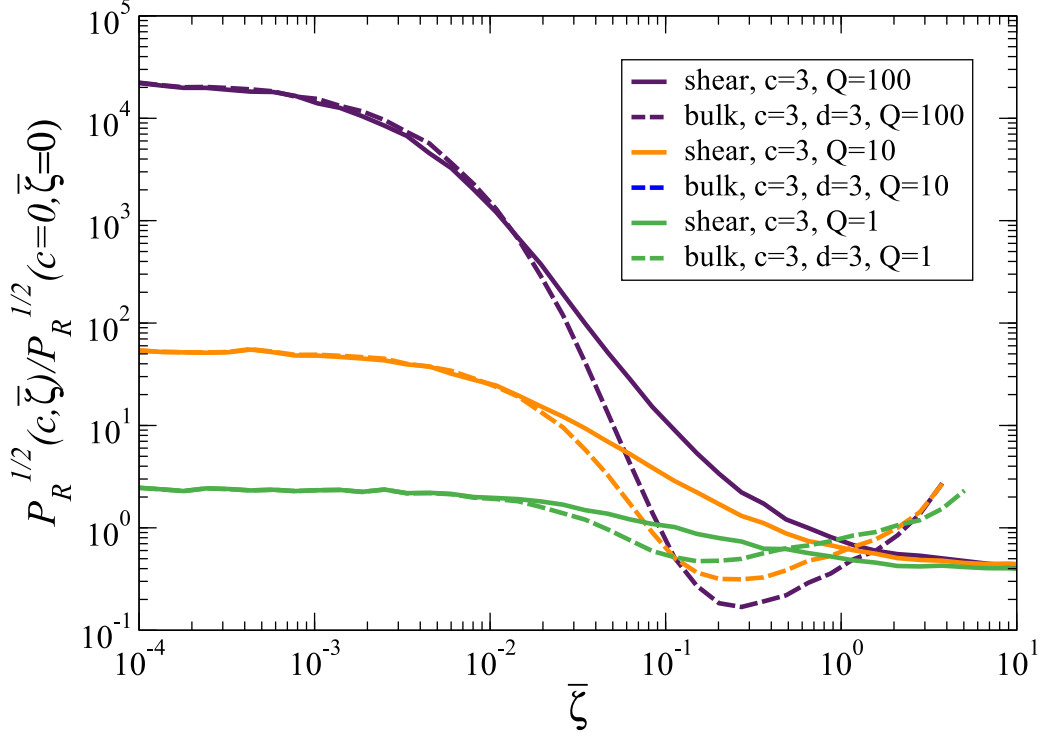


Figure 5.1: The total (square root) amplitude of the power spectrum for the case  $c = 3$  and normalized by its value for  $c = 0$ , as a function of the shear and the bulk viscosities dimensionless parameters  $\bar{\zeta}_{s,b}$ . Three different values for the dissipation ratio  $Q$  are used to illustrate the effect of the viscosities on the growth mode. The wavenumber used was  $k = 10^4 H$ .

The effect of the bulk and shear viscosities can be understood from the evolution equations of the radiation and momentum perturbations, Eqs. (5.47) and (5.48). The dominant effect produced by the shear viscosity comes from the additional friction term in the LHS of the momentum perturbation evolution equation, Eq. (5.48). This term suppresses the amplitude of the momentum fluctuation before the radiation-field system becomes effectively coupled, thus avoiding the appearance of the growing mode. On the contrary, the dominant bulk viscous effect comes from the first term in the RHS of the radiation perturbation evolution equation, Eq. (5.47). The term  $(1 - 9\bar{\zeta}_b) \Psi_r$  decouples the radiation and momentum equations for  $\bar{\zeta}_b \simeq 0.1$ , hence the inflaton perturbations are also decoupled from the momentum evolution and there is no growing mode in the power spectrum. For larger values of the bulk viscosity, the equations are coupled again, but in that case the extra friction term in the momentum equation, Eq. (5.48), damps

the growing mode as in the case of the shear viscosity. In Fig 5.1 it can be seen an increase of the amplitude of the power spectrum for larger values of the bulk viscosity, which comes from the modification in the background evolution caused by the presence of that viscosity. Fig. 5.2 shows the results for the square root for the amplitude of the power spectrum, as a function of the bulk viscosity parameter  $\bar{\zeta}_b$  with different temperature dependences in the bulk and dissipation coefficients, and normalized by the  $c = 0$  and zero viscosities result for the amplitude. We found that for the different powers in the temperature for the dissipation coefficient and for the bulk viscosity considered, the same mechanism of decoupling the evolution equations holds, with the value required to recover the  $c = 0$  case being  $\bar{\zeta}_b \simeq 0.1$  in the 9 cases under consideration.

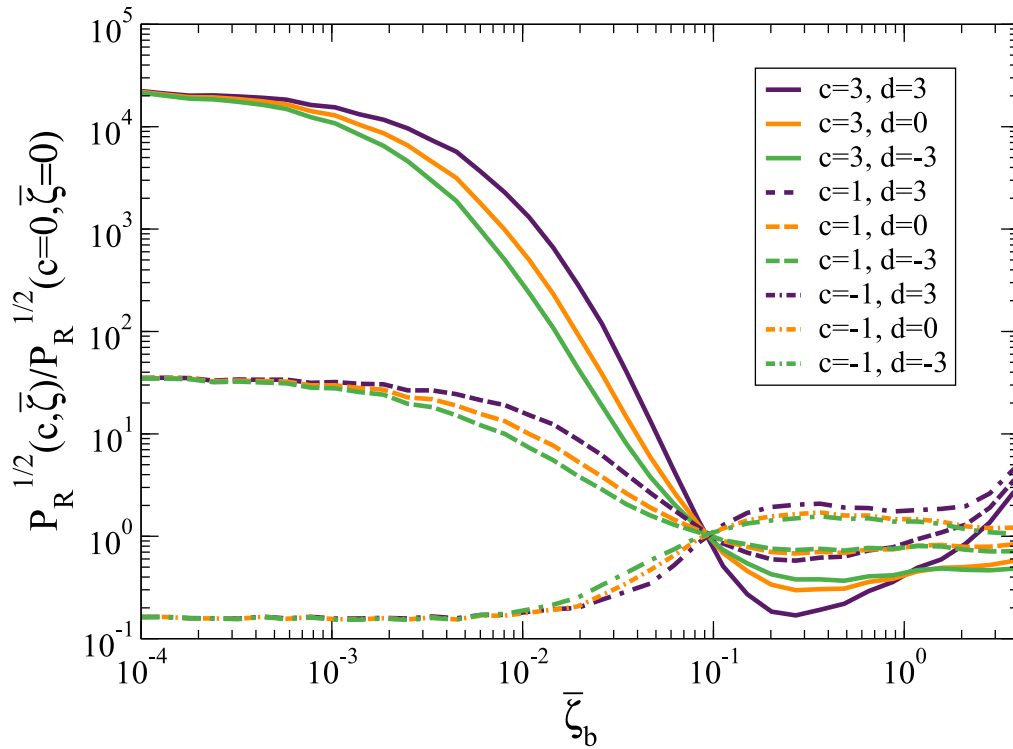


Figure 5.2: The total (square root) normalized amplitude for the power spectrum for the cases  $c = 3, 1, -1$  and for the three cases of temperature dependence for the bulk viscosity,  $d = 3, 0, -3$ , as a function of the dimensionless bulk viscosity parameter  $\bar{\zeta}_b$ . The dissipation ratio used is  $Q = 100$  and wavenumber  $k = 10^4 H$ .

The remaining part of this subsection is focused on the effect of the bulk viscosity without shear viscosity in the case  $c = d = 3$ , as the contribution of these

powers are expected to be dominant from quantum field theory calculations in the LOTS realization of warm inflation [94, 96, 151, 152]. In this case, Eq. (5.48) long after horizon crossing and at zero order in slow-roll reduces to

$$3H\Psi_r \simeq -\frac{1-18\bar{\zeta}_b}{3(1+9\bar{\zeta}_b)}\delta\rho_r - \Upsilon\dot{\phi}\delta\phi. \quad (5.58)$$

We have checked that the first term in the RHS of Eq. (5.58) is negligible, therefore

$$\Psi_r \simeq Q\dot{\phi}\delta\phi. \quad (5.59)$$

As it is show in Ref. [138], this relation implies the simple equality after horizon crossing

$$P_{\mathcal{R}} \simeq P_{\mathcal{R}_r} \simeq P_{\mathcal{R}_\phi}. \quad (5.60)$$

We focus now in the search of a function that fits the amplitude of the power spectrum to have a semianalytic understanding of the effect of the bulk viscosity on this observable, in the same way as it was done for the shear viscosity in Ref. [138]. In order to do that, it is useful to use the dimensionless variable  $y_k$  defined as

$$y_k = \frac{k^{3/2}\delta\phi^{GI}}{[2(H+\Upsilon)T]^{1/2}}, \quad (5.61)$$

where  $\delta\phi$  is the gauge invariant field variable, i.e,

$$\delta\phi^{GI} = \delta\phi - \frac{\dot{\phi}}{H}\varphi. \quad (5.62)$$

The new variable relates with the power spectrum through the relation[138]

$$P_{\mathcal{R}}(k) \simeq \left(\frac{H}{\dot{\phi}}\right)^2 \frac{(H+\Upsilon)T}{\pi^2} \langle y_k^2 \rangle_* \equiv f \langle y_k^2 \rangle_* \quad (5.63)$$

We parametrize the function that fits the amplitude with the following form:

$$\langle y_k^2 \rangle_3 \simeq \langle y_k^2 \rangle_0 F(Q)^{G(\bar{\zeta}_b)}, \quad (5.64)$$

where  $\langle y_k^2 \rangle_3$  is the value of  $\langle y_k^2 \rangle$  in the case under consideration,  $\langle y_k^2 \rangle_0$  is the value of the same variable in the absence of bulk and with  $c = 0$ , which is given by[101]

$$\langle y_k^2 \rangle_0 \simeq \frac{\sqrt{3\pi}}{4} \frac{\sqrt{1+Q}}{1+3Q}, \quad (5.65)$$

and  $F(Q)$ ,  $G(\bar{\zeta}_b)$  are functions of only  $Q$  and  $\bar{\zeta}_b$  respectively that need to be found. In Ref. [138] the authors identified a form of  $F(Q)$  valid for values of  $Q$  larger than 50. However, we need to extend their fit to lower values of  $Q$  for the calculation

of the spectral index that we will perform in the next subsection. Following their procedure we propose the following parametrization:

$$F(Q) = AQ^\alpha + BQ^\beta, \quad (5.66)$$

to fit numerically the amplitude of the spectrum for different values of  $Q$  without any viscosity, and find the values of the different parameters. These values can be found in table 5.1, while Fig. (5.3) shows the accuracy of the fits in its corresponding range of validity.

| Range    | A                    | $\alpha$ | B                    | $\beta$ |
|----------|----------------------|----------|----------------------|---------|
| $Q < 50$ | 13.1                 | 2.14     | $2.7 \times 10^{-2}$ | 4.92    |
| $Q > 50$ | $1.9 \times 10^{-8}$ | 7.5      | $3.4 \times 10^{-6}$ | 7       |

Table 5.1: Values of the parameters of the function 5.66 for different ranges of  $Q$ .

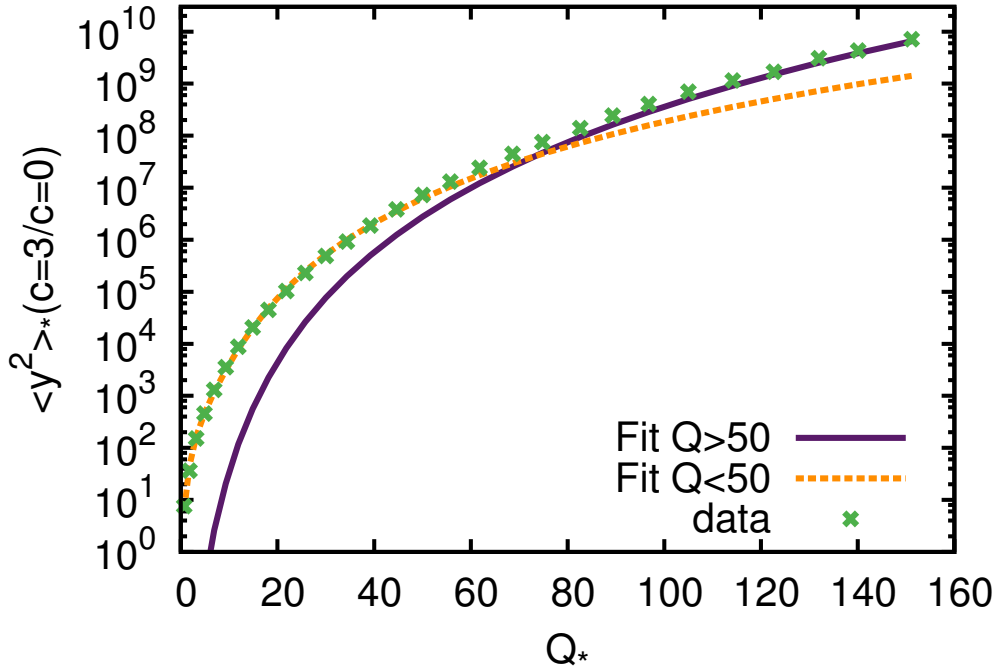


Figure 5.3: Fits of  $\langle y_k^2 \rangle_3$  normalized by  $\langle y_k^2 \rangle_0$  for different ranges of  $Q$ .

Once the function  $F(Q)$  is known, it is possible to use the same procedure to obtain the function  $G(\bar{\zeta}_b)$ . We found that the best fit for this function is given by

$$G(\bar{\zeta}_b) = A_b - B_b \tanh(\log \bar{\zeta}_b - C_b) + D_b (\log \bar{\zeta}_b + E_b)^2 + F_b \tanh(G_b \log \bar{\zeta}_b + H_b), \quad (5.67)$$

with the parameters given in table 5.2. The fit is done with different values of  $Q$  at horizon crossing, namely  $Q_* = 1, 10, 40, 60, 100$ . The last term in Eq. (5.67) has a negligible effect on the amplitude, but it is included to improve the description of the spectral index (see subsection 5.3.2). In Fig. (5.3) it can be seen that there is a little dependence on  $Q_*$  in the function  $G(\bar{\zeta}_b)$ , however for our purposes it is safe to neglect that dependence.

| $A_b$ | $B_b$ | $C_b$ | $D_b$ | $E_b$ | $F_b$ | $G_b$ | $H_b$ |
|-------|-------|-------|-------|-------|-------|-------|-------|
| 0.331 | 0.656 | 3.22  | 0.011 | 4.44  | 0.01  | 25    | 41.2  |

Table 5.2: Values of the parameters of the function 5.67.

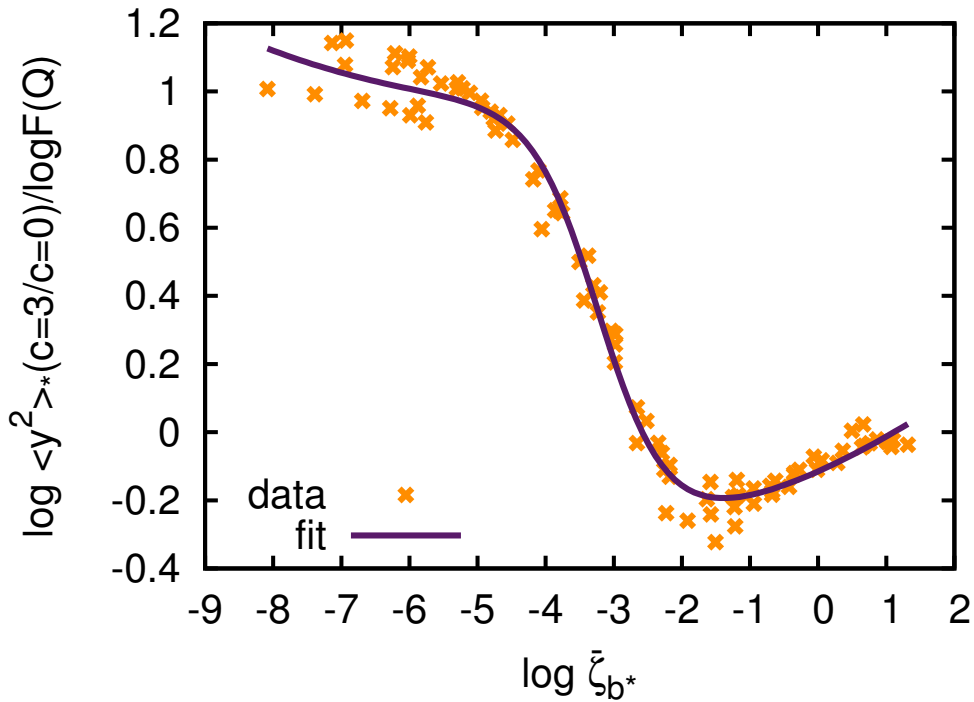


Figure 5.4: Numerical values of  $G(\bar{\zeta}_b)$  in comparison with the fit 5.67 for values  $Q_* = 1, 10, 40, 60, 100$ .

### 5.3.2 Spectral index

At this point it is interesting to study the effects of the bulk and shear viscosities in the spectral index of the power spectrum in the case  $c = d = s = 3$ . The spectral

index measures the dependence of the power spectrum with the scale,

$$P_{\mathcal{R}}(k) = P_{\mathcal{R}} \left( \frac{k}{k_0} \right)^{n_s - 1}, \quad (5.68)$$

where  $P_{\mathcal{R}}$  is the scale-independent amplitude,  $k_0$  is a reference scale and  $n_s$  is the spectral index. From the LHS of Eq. (5.48) it can be observed that there is some scale dependence in the effect of the viscosities in the perturbations, therefore we expect that this effect translates into a modification of the spectral index. Fig. (5.5) shows the effect of the bulk viscosity on the spectral index for  $Q_* = 40$ . The points are the values that were calculated from the numerical integration of the evolution equations Eqs. (5.46)-(5.48) with different values of the wavenumber  $k$  and the same initial conditions. The resulting values were fitted to Eq. (5.68) to find the value of the spectral index for a given  $\bar{\zeta}_b$ . This quantity together with the error of the fit is represented by the dots with error bars. The line shows the derivative of the fit for the amplitude, Eq. (5.64), given by

$$(n_s - 1)_3 = (n_s - 1)_0 + \log F(Q) \frac{dG(\bar{\zeta}_b)}{dNe} + \frac{G(\bar{\zeta}_b)}{F(Q)} \frac{dF(Q)}{dNe} + \frac{d \log f_3/f_0}{dNe}, \quad (5.69)$$

where  $(n_s - 1)_0$  is the spectral index in the case  $c = 0$  without any viscosity (see Appendix B). Eq. (5.69) is a reasonable approximation to the real data in the analyzed range, therefore Fig. (5.5) is also a cross-check for the fit in Eq. (5.67). The last term in Eq. (5.67) was included to improve the description of the peak in the spectral index that can be observed at low bulk viscosity values in Fig. (5.5).

It is possible to get an insight into the effect of the bulk viscosity in the spectral index by looking at the equations Eqs. (5.46)-(5.48). We checked that the peak at low values of  $\bar{\zeta}_b$  is caused by bulk viscous effects at the background level, hence we can regard the spectral index as a monotonically decreasing function of the bulk viscosity at the perturbation level. This behaviour is caused by the viscosity friction term in the LHS of Eq. (5.48) which depends also on the wavenumber  $k$ , therefore for larger values of  $\bar{\zeta}_b$  the dependence on  $k$  increases and as a consequence, the spectral index diminishes. This same effect happens with the shear viscosity, as can be seen in Fig. (5.6). Fig. (5.6) shows that the bulk viscosity is more efficient than the shear viscosity, in concordance with what happens with the amplitude in Fig. (5.1). This effect is due to the term in the RHS of Eq. (5.47) which depends on the bulk viscosity but not on the shear.

Finally in Fig. (5.6) it can be also observed the combined effect of the viscosities. They show an oscillatory behaviour around the dominant viscosity, e.g., in the green line the bulk viscosity is much smaller than the shear viscosity and, as a result, the combined effect are oscillations around the solution with shear viscosity but not bulk viscosity. Therefore, we conclude that viscosities may also suppress the effect of the growth mode in the tilt of the spectrum of scalar perturbations.

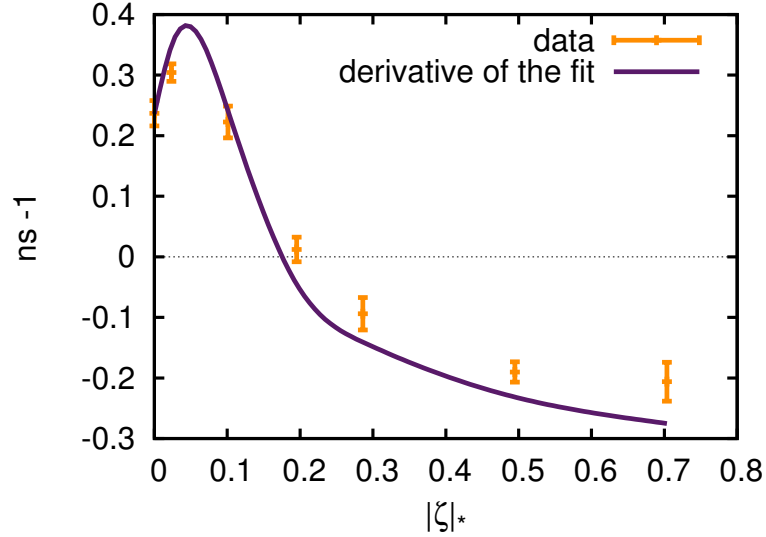


Figure 5.5: Spectral index for  $Q_* = 40$  and different values of  $\bar{\zeta}_b$ . The points represents the numerical values obtained by the direct resolution of the evolution equations, while the line shows the derivative of Eq. (5.64).

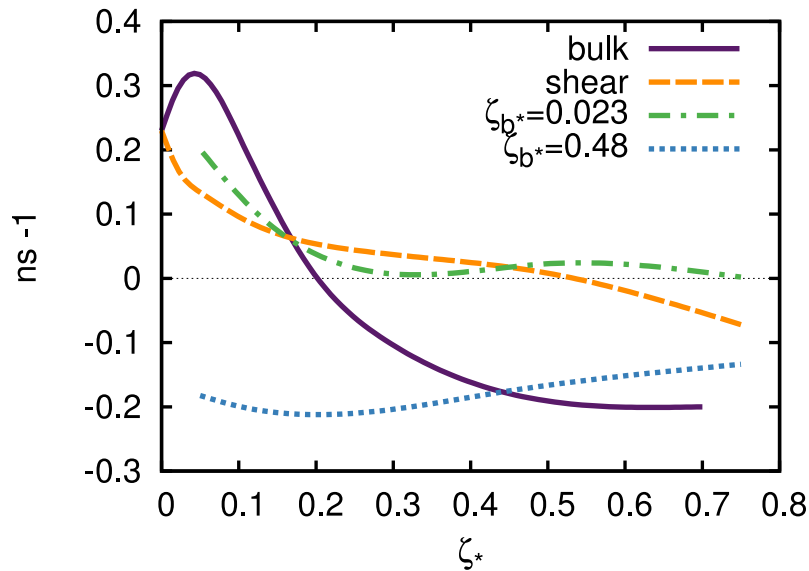


Figure 5.6: Spectral index for  $Q_* = 40$  different values of the bulk and shear viscosities. The purple solid (orange dashed) line corresponds to the variation of the bulk (shear) viscosity with zero shear (bulk) viscosity. The green dashed-dotted (blue dotted) line corresponds to a fixed value of the bulk viscosity  $\bar{\zeta}_b = 0.023$  ( $\bar{\zeta}_b = 0.48$ ) with varying shear viscosity.



*The first problem for all of us, men and women, is not to learn, but to unlearn.*

Gloria Steinem

## Warm inflation in the weak dissipation regime

---

In this chapter we follow a different path to deal with the growing mode of the power spectrum. We restrict our analysis of warm inflation to the regime of weak dissipation,  $Q_* \ll 1$ . In this regime the coupling of the radiation-field evolution equation is not effective, hence the power spectrum does not suffer from a growth mode. Dissipation does not modify the background evolution, but may have a significant impact at the perturbations level due to the thermal origin of the power spectrum, hence producing important observational features for warm inflation.

A very interesting aspect of warm inflation with weak dissipation is the role of the thermodynamical state of the inflaton particles. In [104], the authors realized that strong enough interactions of the inflaton particles can bring the system to a thermalized state. The statistical distribution describing such a system is characterized by non-trivial inflaton occupation numbers, which may have an important influence in the power spectrum of warm inflation. The statistical state of the inflaton particles is of the utmost importance in the weak dissipation regime, whereas it is completely subdominant when dissipation is strong, that is the reason we have not studied it thus far in this thesis.

We will show that even when dissipative effects are still small compared to Hubble damping, the amplitude of scalar curvature fluctuations can be significantly enhanced, while tensor perturbations are generically unaffected due to their weak coupling to matter fields. This generically reduces the tensor-to-scalar ratio with respect to conventional models and also modifies the tilt of the scalar power spectrum, thereby changing observational predictions considerably. These effects are particularly significant when non-trivial inflaton occupation numbers are sustained during inflation.

We performed this analysis after the Planck collaboration released the first cosmological data, hence we could make use of it to compare with the observational predictions of warm inflation. As a first example of the described features of the weak dissipation regime, we show that the simplest model of chaotic inflation,  $V(\phi) = \lambda\phi^4$ , falls well within Planck's observational window for a nearly-

thermalized state in the LOTS realization of warm inflation, whereas it seems in tension with the data in a cold scenario. Then, we will study a model of hill-top inflation to exemplify how the same mechanisms modifying the inflationary observables operate in a different inflationary model.

## 6.1 The weak dissipation regime

The power spectrum or a generic inflaton phase-space distribution  $n(k)$  at the time when observable CMB scales leave the horizon during inflation,  $t_*$ , can be approximated by [100, 87, 101, 102, 104]:

$$\Delta_{\mathcal{R}}^2 = \left(\frac{H_*}{\dot{\phi}_*}\right)^2 \left(\frac{H_*}{2\pi}\right)^2 \left[1 + 2n_* + \left(\frac{T_*}{H_*}\right) \frac{2\sqrt{3}\pi Q_*}{\sqrt{3 + 4\pi Q_*}}\right], \quad (6.1)$$

which yields the standard cold inflation result in the limit  $n_*, Q_*, T_* \rightarrow 0$ . This expression neglects, however, the coupling between inflaton and radiation fluctuations associated with the temperature dependence of the dissipation coefficient. This coupling induces a significant enhancement of the perturbation growth for strong dissipation,  $Q \gtrsim 1$  [103]. Since this coupling is negligible if the relevant scales become super-horizon when dissipation is weak, we can obtain an accurate description of the spectrum by taking the limit  $Q_* \ll 1$  in the expression above, which yields in the slow roll regime:

$$\Delta_{\mathcal{R}}^2 \simeq \left(\frac{H_*}{\dot{\phi}_*}\right)^2 \left(\frac{H_*}{2\pi}\right)^2 \left[1 + 2n_* + 2\pi Q_* \frac{T_*}{H_*}\right]. \quad (6.2)$$

Dissipative processes may maintain a non-trivial distribution of inflaton particles. The heavy fields decay into inflaton particle states through  $\chi \rightarrow yy\phi$ , but this is a sub-leading process, with  $\Gamma(\chi \rightarrow yy\phi) = (g/4\pi)^2 \Gamma(\chi \rightarrow yy)$ , where  $\Gamma(\chi \rightarrow yy) = \alpha_h m_\chi / 16$  [96], with inflaton particles from this process alone typically yielding a negligible component of the radiation bath. However, dissipative particle production destabilizes the local thermal equilibrium of the plasma, triggering decays, inverse decays and thermal scatterings that redistribute the dissipated energy between all the interacting fields and keep the system close to equilibrium if occurring faster than the Hubble rate. In particular, decays and inverse decays of the multiple heavy species in the plasma can be efficient thermalization processes [185, 186] so that, in some parametric regimes, we expect inflaton particles to be sustained in a quasi-thermal state at the ambient temperature  $T$ , with a phase-space distribution that should approach the Bose-Einstein,

$$n_{BE}(k) = (e^{k/aT} - 1)^{-1}. \quad (6.3)$$

Although the details of the thermalization process require solving the system of coupled Boltzmann equations for all the particle species involved, the underlying

physical picture can be understood in simple terms. Starting from an equilibrium configuration where decay and inverse decay processes are occurring at equal rates, dissipation of the inflaton's energy will mainly produce an excess of light particles in the  $Y$  sector, which will enhance the rate of inverse decays and consequently increase the  $X$  sector occupation numbers above their equilibrium value. This in turn enhances the direct decay rate, producing  $Y$  particles and also an excess of inflaton modes. This goes on until the balance between decay and inverse decay rates is restored and the system reaches a new equilibrium configuration. One then expects the energy injected into the system to be distributed amongst all species in the plasma that are produced and annihilated faster than Hubble expansion. The common temperature of these species would decrease due to the dilution effect of expansion but this is compensated by the additional energy, keeping the temperature roughly constant in the slow-roll regime. Species that are not created/destroyed sufficiently fast will decouple from the plasma and their effective temperature will be exponentially redshifted away during inflation, quickly reaching a quasi-vacuum state. A measure of the efficiency of the thermalization processes can then be obtained by comparing the relevant decay rates with the Hubble parameter, as we examine in more detail below in the context of chaotic inflation.

Note that both the second and third terms within the brackets in Eq. (6.2) are positive-definite, the former corresponding to non-trivial inflaton occupation numbers and the latter to the leading effect of fluctuation-dissipation dynamics. Hence, the amplitude of the scalar power spectrum always exceeds the vacuum result in warm inflation scenarios. On the other hand, gravity waves are weakly coupled to the thermal bath and the spectrum of tensor modes retains its vacuum form,  $\Delta_t^2 = (2/\pi^2)(H_*^2/M_P^2)$ . This therefore suppresses the tensor-to-scalar ratio, yielding a modified consistency relation for warm inflation:

$$r \simeq \frac{8|n_t|}{1 + 2n_* + 2\pi Q_* T_*/H_*}, \quad (6.4)$$

where  $n_t = -2\epsilon_*$  is the tensor index. The primordial tensor spectrum can thus be used to distinguish warm from cold inflation scenarios, the former consequently modifying the Lyth bound [187, 135] that relates the value of the tensor-to-scalar ratio to the variation of field, and requires transplanckian excursions for  $r \sim \mathcal{O}(10^{-2})$  (see also [188] for other scenarios where the Lyth bound does not apply). Most importantly, non-trivial inflaton occupation numbers may also generically lower the tensor-to-scalar ratio, which as we illustrate in the following sections may have a very significant effect on inflationary predictions.

In the limit where inflaton particle production is inefficient and  $n_*$  gives a negligible contribution to the power spectrum, the scalar spectral index is nevertheless

modified by the third term in Eq. (6.2), yielding:

$$n_s - 1 \simeq 2\eta_* - 6\epsilon_* + \frac{2\kappa_*}{1 + \kappa_*} (7\epsilon_* - 4\eta_* + 5\sigma_*) , \quad (6.5)$$

where we defined the slow-roll parameter<sup>1</sup>

$$\sigma = m_P^2 \frac{V_\phi}{\phi V} < 1 + Q , \quad (6.6)$$

and we have used the slow-roll equations,  $3H(1 + Q)\dot{\phi} \simeq -V'(\phi)$  and  $\rho_R \simeq (3/4)Q\dot{\phi}^2$ , to determine the variation of  $\kappa \equiv 2\pi QT/H$  as different scales become super-horizon during inflation.

Modifications are, however, more prominent in the opposite limit of nearly-thermal inflaton fluctuations, with  $n_* \simeq n_{BE*}$ . For  $T_* \gtrsim H_*$  and  $Q_* \ll 1$  we then obtain:

$$n_s - 1 \simeq 2\sigma_* - 2\epsilon_* , \quad (6.7)$$

which is, in particular, independent of the curvature of the potential, which only determines its running:

$$n'_s \simeq 2\sigma_*(\sigma_* + 2\epsilon_* - \eta_*) - 4\epsilon_*(2\epsilon_* - \eta_*) . \quad (6.8)$$

In this case, a red-tilted spectrum,  $n_s < 1$ , corresponds to either potentials with a negative slope, such as hill-top models, or large field models where  $\epsilon_* > 2(M_P/\phi_*)^2$ .

## 6.2 Chaotic warm inflation

To illustrate the effects of both dissipation and occupation numbers on observational predictions, we consider the quartic model,  $V(\phi) = \lambda\phi^4$ , which corresponds to a superpotential  $f(\Phi) = \sqrt{\lambda}\Phi^3/3$  and is the canonical model of chaotic inflation [189]. In this case, the slow roll parameters are

$$\epsilon = 2\sigma = \frac{2}{3}\eta = 8 \left( \frac{m_P}{\phi} \right)^2 , \quad (6.9)$$

which from Eq. (6.7) yields for a thermalized inflaton distribution

$$n_s - 1 \simeq -8 \left( \frac{m_P}{\phi_*} \right)^2 . \quad (6.10)$$

---

<sup>1</sup>The slow-roll parameter  $\sigma$  is equivalent to the slow-roll parameter  $\beta_\Upsilon$  used in other chapters. We chose  $\sigma$  in this discussion to simplify the expressions.

This gives a red-tilted spectrum with  $n_s \simeq 0.96$  for  $\phi_* \simeq 14M_P$ , which is superplanckian but smaller than the corresponding field value in the vacuum case,  $\phi_* \simeq 25M_P$ . This also gives

$$r \simeq 8(1 - n_s) \frac{H_*}{T_*}, \quad (6.11)$$

within the upper bound obtained by Planck,  $r < 0.11$  (95% CL), for  $T_* > 2.9H_*$ , as well as a small negative running and a tensor index

$$n'_s = -(n_s - 1)^2 \simeq -0.0016, \quad n_t = 2(n_s - 1) \simeq -0.079, \quad (6.12)$$

The number of e-folds of inflation can be computed by integrating the slow-roll equations, which may be done analytically for the quartic model [190]. In particular, one can use the form of the dissipation coefficient  $\Upsilon = C_\phi T^3/\phi^2$  to express the coupled inflaton and radiation equations in the slow-roll regime as a single equation for the dissipative ratio  $Q$ :

$$\frac{dQ}{dN_e} = C_* \frac{Q^{6/5}(1+Q)^{6/5}}{1+7Q}, \quad (6.13)$$

where  $C_* \simeq 5\epsilon_* Q_*^{-1/5}$  for  $Q_* \ll 1$ . This shows that  $Q$  grows during inflation, so that the system may evolve from the weak to the strong dissipation regime. Inflation ends in this case when  $|\eta| = 1 + Q$ , which yields

$$Q_e \simeq \left[ \frac{2}{3}(1 - n_s) \right]^{5/2} Q_*^{1/2}, \quad (6.14)$$

for a thermal spectrum and hence  $Q_e \gtrsim 1$  for  $Q_* \gtrsim 10^{-6}$ . The relative abundance of radiation will then also grow towards the end of inflation, with

$$\frac{\rho_R}{V(\phi)} \propto Q^{7/5} \quad (6.15)$$

in this case, until it smoothly takes over after slow-roll has ended. Integrating Eq. (6.13) from horizon-crossing to the end of the slow-roll regime, we obtain:

$$N_e \simeq \epsilon_*^{-1} (1 + bQ_*^{1/5}), \quad (6.16)$$

where  $b \simeq 2.81$ . This yields the required 50 – 60 e-folds of inflation with  $n_s \simeq 0.96 - 0.97$  for  $Q_* \simeq 0.001 - 0.01$ . We have checked numerically that the range  $Q_* < 0.01$  is safe from the growth mode of the power spectrum, hence Eq. (6.2) is a good approximation to the power spectrum, as can be seen in Fig. 6.1 For comparison, the spectral index in the standard cold inflation regime is

$$n_s = 1 - \frac{3}{N_e}, \quad (6.17)$$

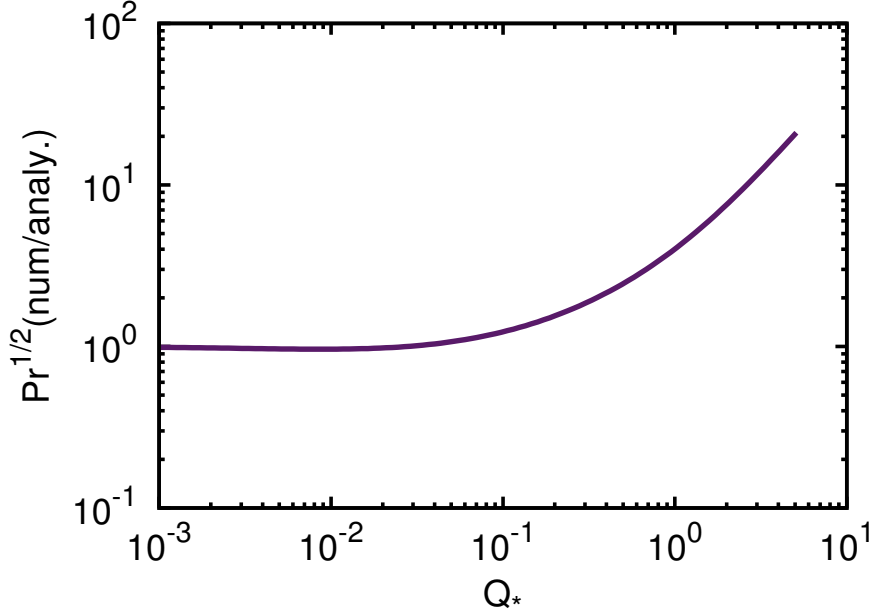


Figure 6.1: Full numerical computation of the power spectrum compared to the analytical approximation in Eq.(6.2) for different values of the dissipative coefficient at horizon crossing.

giving  $n_s = 0.94 - 95$  for  $N_e = 50 - 60$ . This clearly shows that even for weak dissipation at horizon crossing one may obtain substantially different observational results.

For both limits of nearly-thermal and negligible inflaton occupation numbers, one can use the observed amplitude of curvature perturbations,  $\Delta_{\mathcal{R}}^2 \simeq 2.2 \times 10^{-9}$  [191] and the dissipation coefficient to relate the different quantities at horizon-crossing. For instance, in the nearly-thermalized regime

$$Q_* \simeq 2 \times 10^{-8} g_* \left( \frac{H_*}{T_*} \right)^3 . \quad (6.18)$$

This allows one to express both  $n_s$  and  $r$  in terms of the dissipative ratio or temperature at horizon-crossing for a given number of e-folds of inflation and relativistic degrees of freedom, which is illustrated in Fig. 6.2.

As one can see, observational predictions for the quartic model depend on the distribution of inflaton fluctuations,  $n_*$ . For  $n_*, \kappa_* \ll 1$ , the spectrum has the same form as in cold inflation, but from Eq. (6.16) one obtains  $N_e = 50 - 60$  for larger field values than in cold inflation, yielding a larger tensor fraction and a more red-tilted spectrum. When  $\kappa_* \gtrsim 1$ , however, the spectrum becomes more blue-tilted and  $r$  is suppressed, although for weak dissipation it remains too large.

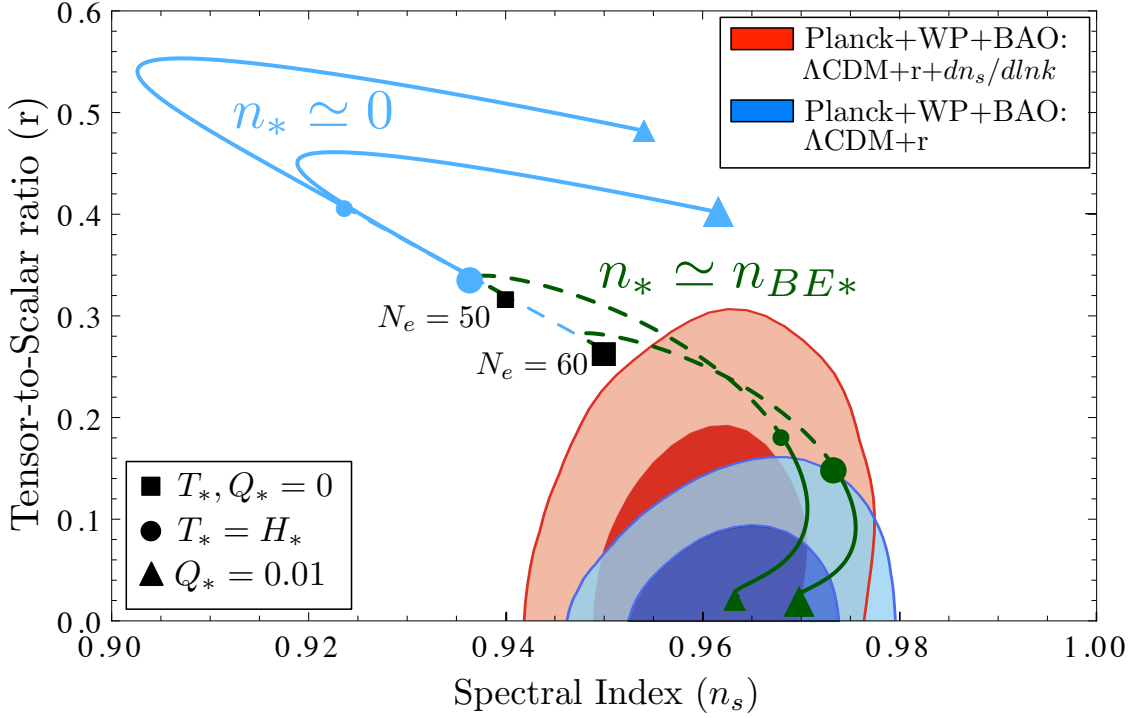


Figure 6.2: Trajectories in the  $(n_s, r)$  plane for  $V(\phi) = \lambda\phi^4$  as a function of the dissipative ratio,  $Q_* < 0.01$ , 50-60 e-folds before the end of inflation, compared with the Planck results [191], for  $g_* = 228.75$  relativistic degrees of freedom. The dark green (light blue) curves correspond to nearly-thermal (negligible) inflaton occupation numbers  $n_*$ , with dashed branches for  $T_* \lesssim H_*$ . Note that corresponding curves converge in the cold inflation limit,  $T_*, Q_* \rightarrow 0$ .

On the other hand, for nearly-thermal inflaton occupation numbers tensor modes are more strongly suppressed and one obtains a remarkable agreement with the Planck results for  $T_* \gtrsim H_*$ . Note that for  $T_* \lesssim H_*$  the concept of thermal equilibrium is ill-defined, since the average particle modes have super-horizon wavelengths, so in Figure 6.2 we represent this regime with dashed curves to nevertheless illustrate the transition from a cold to a warm spectrum. Also, we take the MSSM value  $g_* = 228.75$  only as a reference, with fewer light species further lowering the tensor-to-scalar ratio, since  $T_*/H_*$  is larger.

The results in Fig. 6.2 motivate a closer look at thermalization processes and in particular we can estimate the total production rate of inflaton particles from the decay rate of the  $N_X$  heavy species in the plasma given above. At horizon-crossing, in particular, the inflaton is relativistic. Using that  $m_{\phi_*} \ll T_*$ , we may write this as:

$$\frac{\Gamma_{\phi_*}}{H_*} \simeq 9(\alpha_g \alpha_h)^{3/2} \left(\frac{1-n_s}{0.04}\right)^{3/2} \left(\frac{0.01}{r}\right)^{3/2} \left(\frac{0.005}{Q_*}\right)^{1/2}, \quad (6.19)$$

where  $\alpha_g = g^2 N_Y / 4\pi$ ,  $\alpha_h = h^2 N_Y / 4\pi$  and we assumed  $n_* = n_{BE*}$ . Moreover, finite temperature Bose factors may considerably enhance this for small couplings [192], with e.g. the two-body decay width increasing up to a factor  $T/m_Y \sim \sqrt{12}/h$  [96]. Also,  $\Gamma_\phi/H$  increases during inflation, so that deviations from thermal equilibrium should become less significant. We then expect inflaton particles to be produced sufficiently fast and remain close to thermal equilibrium with the ambient plasma if the effective couplings  $\alpha_{g,h}$  are not too small. Both the inflaton and other light fields could actually be in a pre-inflationary thermal state with  $T \gtrsim H$ , with dissipation and the above mentioned processes maintaining a slowly-varying temperature. Without dissipation, however, thermal effects would be quickly redshifted away, yielding quite different observational features [193].

The agreement with the Planck results is particularly significant, since the quartic potential is the simplest renormalizable model of chaotic inflation, involving no other scales other than the inflaton field value. As originally argued in [189], in large-field models inflation is naturally triggered from a chaotic field distribution following the pre-planckian era, in domains where  $V(\phi) \sim M_P^4$  quickly dominates over gradient and kinetic energy densities. On the other hand, when inflation only occurs for a  $V(\phi) \ll M_P^4$  plateau, the post-planckian universe must be unnaturally smooth, requiring a fine-tuning of initial conditions that the inflationary paradigm is supposed to solve [194].

While other modifications such as a non-minimal coupling to gravity may also bring the quartic model into agreement with observations [195], the renormalizable nature of the interactions leading to dissipation is an attractive feature of warm inflation, with only a few controllable parameters. Note, in particular, that interactions with other bosonic and/or fermionic fields are always required since the vacuum energy of the inflaton field must be transferred into light degrees of freedom at the end of inflation to reheat the universe. In this sense, warm inflation scenarios do not introduce any non-standard modifications to the basic inflationary models but simply correspond to parametric regimes where the universe is kept warm throughout inflation,  $T \gtrsim H$ . For the LOTS realization of warm inflation,

$$\frac{T_*}{H_*} \sim \frac{C_\phi}{g_*} N_e^{-2} \gtrsim 1, \quad (6.20)$$

which may be achieved for  $N_X \gg N_Y \gtrsim 1$  and  $g, h \ll 1$ , while keeping radiative corrections under control. We may express the number of heavy species as:

$$N_X \simeq \frac{8 \times 10^5}{\alpha_h} \left( \frac{0.04}{1 - n_s} \right)^4 \left( \frac{r}{0.01} \right)^2 \left( \frac{Q_*}{10^{-3}} \right), \quad (6.21)$$

where we have assumed a thermal distribution of inflaton perturbations. This large multiplicity of  $X$  species is typical of the form of the dissipation coefficient in the LOTS realization of warm inflation [91, 1], but is expected to be significantly

reduced in other regimes, such as for on-shell  $X$  modes [96]. Large multiplicities may be obtained in D-brane constructions [93], where the  $X$  fields correspond to strings stretched between brane and antibrane stacks and their number thus grows with the square of the brane multiplicity. Due to brane-antibrane annihilation at the end of inflation, these modes will not, however, play a role in the post-inflationary universe. Field multiplicities are also enhanced by the Kaluza-Klein tower in extra-dimensional scenarios [196].

An interesting possibility arises when we consider B- and CP-violating interactions in the two stage superpotential

$$W = g\Phi X^2 + hXY^2 + f(\Phi) , \quad (6.22)$$

with complex couplings and distinct decay channels. In this case, the out-of-equilibrium nature of dissipation can generate a cosmological baryon asymmetry during inflation [197]. The resulting baryon-to-entropy ratio depends on the inflaton field, so that inflaton fluctuations yield both adiabatic and baryon isocurvature (BI) perturbations with a nearly-scale invariant spectrum. For the quartic model with  $n_* \simeq n_{BE*}$ , BI and adiabatic modes are anti-correlated with relative amplitude [198]

$$B_B \simeq 3(n_s - 1) \simeq -0.12 \quad (6.23)$$

and a blue-tilted spectrum [198]

$$n_{iso} \simeq \frac{3 - n_s}{2} \simeq 1.0 \quad (6.24)$$

This then yields for the relative matter isocurvature spectrum

$$\beta_{iso} \simeq \left( \frac{\Omega_b}{\Omega_c} \right)^2 B_B^2 \simeq 4.8 \times 10^{-4} , \quad (6.25)$$

well within the bound  $\beta_{iso} < 0.0087$  obtained by Planck for anti-correlated isocurvature modes with  $n_s \simeq n_{iso}$ , which is in fact the case that best improves the fit to the data [191].

The interactions required to produce a baryon asymmetry through dissipation are analogous to those considered in conventional thermal GUT baryogenesis or leptogenesis models, with the scalar  $X$  fields corresponding to e.g. heavy GUT bosons or right-handed neutrinos [197]. However, since only virtual  $X$  modes are involved in the dissipative processes, baryogenesis may occur below the GUT scale, as opposed to thermal GUT baryogenesis models, avoiding the production of dangerous relics such as monopoles. In particular, we obtain for the temperature at the end of inflation in the quartic model:

$$T_e \simeq 10^{14} \left( \frac{1 - n_s}{0.04} \right)^{\frac{5}{2}} \left( \frac{0.01}{r} \right)^{\frac{1}{2}} \left( \frac{10^{-3}}{Q_*} \right)^{\frac{3}{10}} \text{ GeV} . \quad (6.26)$$

We note that the effective reheating temperature is roughly an order of magnitude lower since radiation typically takes a few e-folds to take over after the end of slow-roll [190]. While gravitinos may still be ubiquitously produced at these temperatures, the inflaton may not decay completely right after inflation if  $Q_e \lesssim 10$  [199], as is the case of the quartic model for  $Q_* < 0.01$ . The inflaton may then come to dominate over the radiation bath at a later stage and the entropy produced by its eventual decay may dilute the excess of gravitinos, thus avoiding the potentially associated cosmological problems [199].

### 6.3 Warm inflation in a hilltop model

In this section we parsimoniously describe the observational characteristics of warm inflation in a different canonical class of inflationary models, in order to demonstrate that the modifications in the spectral index and tensor-to-scalar ratio described in the previous section are not a particularity of the chaotic models. We consider as a working example a hilltop model [73, 72] with a potential

$$V(\phi) = V_0 \left[ 1 - \frac{\gamma}{2} \left( \frac{\phi}{m_p} \right)^2 \right] \quad (6.27)$$

where the values of the field are sub-planckian and the constant term dominates,  $V \simeq V_0$ . The slow roll parameters of this potential reads

$$\epsilon = \frac{\gamma^2}{2} \left( \frac{\phi}{m_p} \right)^2 \quad \eta = \sigma = -\gamma. \quad (6.28)$$

The field rolls away from the origin towards the minimum of the potential, thus increasing with the number of e-folds. Inflation ends when the field is so large that the approximation  $V \simeq V_0$  is no longer valid and slow-roll is violated.

We have solved numerically the full perturbed equations to determine the region of the parameter space where Eq. (6.2) is an accurate description of the amplitude of the power spectrum. Fig. (6.3) shows the result of the numerical computation of the amplitude normalized by Eq. (6.2) for different values of  $Q_*$  and two representative values of  $\gamma$ , for nearly-thermal inflaton occupation numbers. It can be seen that the growing mode begins to have an effect for values of  $Q_* \gtrsim 0.01$ . The evolution of the temperature to Hubble ratio can be computed in slow-roll to be

$$\frac{d \ln T/H}{dN_e} \simeq 2(2\epsilon - \eta + \sigma) = 2\gamma^2 \frac{\phi^2}{m_p^2} > 0, \quad (6.29)$$

therefore  $T/H$  always increases during inflation, therefore the  $T \gtrsim H$  condition only constraint the set of initial conditions. The evolution of the dissipative ratio

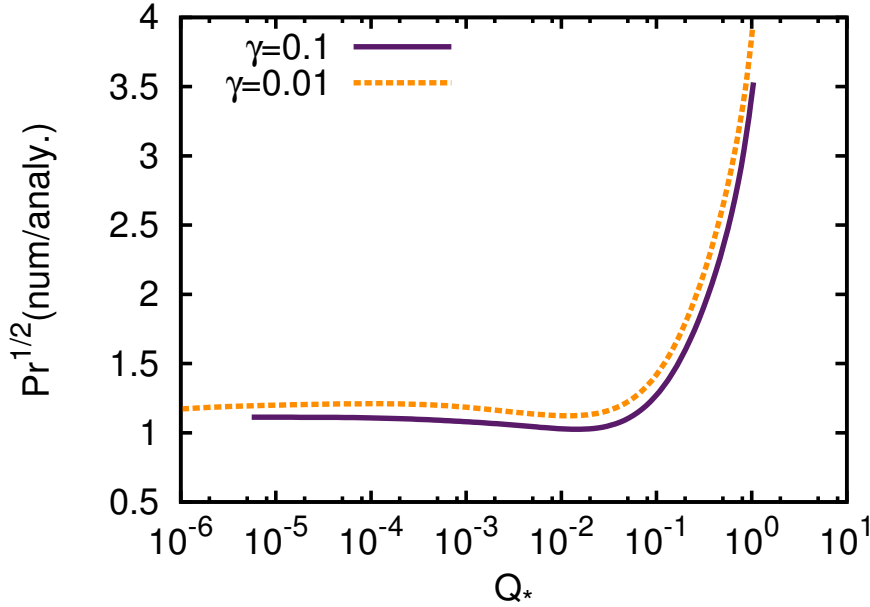


Figure 6.3: Numerical amplitude of the power spectrum normalized by Eq. (6.2) for different values of  $Q_*$  and  $\gamma = 0.1, 0.001$ , for nearly-thermal inflaton occupation numbers.

in slow-roll is

$$\frac{dQ}{dN_e} = Q \left( 5\gamma^2 \frac{\phi^2}{m_p^2} - 2\gamma \right). \quad (6.30)$$

The evolution of  $Q$  depends on the combination of  $\phi, \gamma$ , increasing with the number of e-folds if the condition

$$\frac{\phi^2}{m_p^2} > \frac{2}{5\gamma} \quad (6.31)$$

is fulfilled. In general, for small values of  $\gamma$ , a large value of  $\phi$  is required to obtain 60 e-folds, and  $Q$  grows during inflation. In the limit of large values of  $\gamma$ , we find the opposite situation and  $Q$  decreases. The difference in the behaviour of  $Q$  modifies the observable predictions of warm inflation when the occupation number of the inflaton particles is negligible, as can be seen in Fig. 6.4. In the region where the dissipative ratio grows (decreases), the spectral index moves towards smaller (larger) values compared to the cold inflation result. In the opposite limit of nearly-thermal inflaton fluctuations, the spectral index is roughly independent of the value of the dissipative ratio, while the suppression on the tensor-to-scalar ratio is more important. Fig. 6.4 shows that both nearly-thermal inflaton fluctuations and negligible occupation number limits are consistent with Planck data, proving that the thermalization of the inflaton particles is no a necessary condi-

tion for the consistency of the LOTS realization of warm inflation, but a desirable feature for a certain inflationary models.

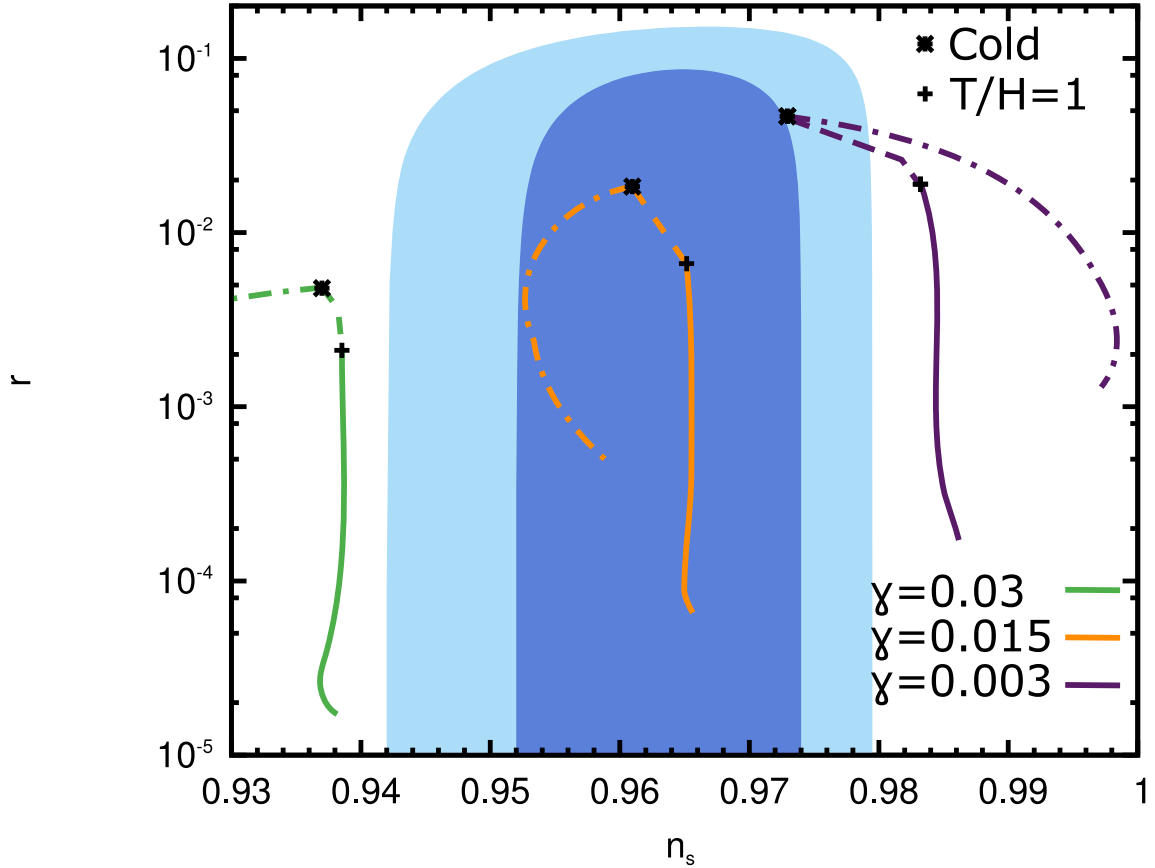


Figure 6.4: Trajectories in the  $(n_s, r)$  plane for the hilltop potential in Eq. (6.27) and different values of the  $\gamma$  parameter as a function of the dissipative ratio,  $Q_* < 0.01$ , 60 e-folds before the end of inflation, compared with the Planck+WP+BAO+ $\Lambda$ CDM+r results [191], for  $g_* = 228.75$  relativistic degrees of freedom. The solid (dashed-dotted) curves correspond to nearly-thermal (negligible) inflaton occupation numbers  $n_*$ , with dashed branches for  $T_* \lesssim H_*$ . Note that corresponding curves converge in the cold inflation limit,  $T_*, Q_* \rightarrow 0$ .

# Reheating

---



*In a spiral galaxy, the ratio of dark-to-light matter is about a factor of ten. That's probably a good number for the ratio of our ignorance-to-knowledge. We're out of kindergarten, but only in about third grade.*

Vera Rubin

# WIMPlaton: inflation and dark matter unification

Inflaton and dark matter candidates in particle physics models share several common features, both being typically assumed to be weakly interacting and neutral fields. The inflaton scalar field must interact weakly with itself and other degrees of freedom in order to ensure the required flatness of the associated scalar potential, which could be spoiled by large radiative corrections. Similarly, dark matter particles should form a stable non-relativistic and non-luminous fluid at late times that accounts for the observed galaxy rotation curves [25, 26], the large scale structure in the universe as inferred from Cosmic Microwave Background [33, 23] and weak-lensing observations [27, 28] (for a detailed review, we refer the reader to [200]). Both inflation and dark matter are essential features in the modern cosmological paradigm and cannot be accounted for within the present framework of the Standard Model of particle physics. It is therefore interesting to consider the possibility that the same field accounts for both accelerated expansion in the early universe and the hidden matter component at late times.

Scalar fields have the interesting property of mimicking fluids with different equations of state depending on the kinematical regime considered. For a homogeneous scalar field  $\phi$  with potential  $V(\phi)$ , we have:

$$\rho_\phi = \frac{1}{2}\dot{\phi}^2 + V(\phi), \quad p_\phi = \frac{1}{2}\dot{\phi}^2 - V(\phi). \quad (7.1)$$

Hence, on the one hand a slowly-varying field,  $\dot{\phi}^2/2 \ll V(\phi)$  acts as an effective cosmological constant, which is the regime typically considered in canonical inflationary models. On the other hand, a field oscillating about the minimum of its potential where  $V(\phi) \simeq m_\phi^2 \phi^2/2$  behaves as non-relativistic matter, with  $\langle \dot{\phi}^2/2 \rangle = -\langle V(\phi) \rangle$  such that  $p_\phi \ll \rho_\phi$  [201]. These two regimes will generically be present in inflationary potentials, which further suggests a common framework for inflation and dark matter. The main difficulty in achieving such a unified description lies, however, in the fact that inflation must end with a transition to a radiation-dominated universe, in order to recover the standard “Big Bang” evolution at least before the freeze-out of light nuclear abundances takes place [202].

An efficient transfer of energy between the inflaton field and radiation generically requires the former to decay into light degrees of freedom following the period of inflationary slow-roll [76, 77, 78, 79], even though other non-perturbative processes such as parametric resonance amplification could contribute significantly to the reheating process [203].

Nevertheless, efficient reheating does not imply the complete decay of the inflaton field and the possibility that a stable remnant is left after inflation has been considered in the literature. Works include models where the decay of the inflaton is blocked by induced thermal masses [204, 205], a second period of thermal inflation diluting the inflaton abundance [206], scalar fields with non-canonical kinetic terms [207, 208], generation of inflaton particles in the thermalization process [209, 210, 211], and singlet scalar inflaton non-minimally coupled to gravity [212, 213]. We propose a concrete realization of the generic idea in quantum field theory, where the decay of the inflaton is truly incomplete, occurring only for a finite period after the end of the slow-roll regime.

We will introduce a simple mechanism based on standard Yukawa coupling between the inflaton and massive fermion fields (and potentially their superpartners), endowed with an appropriate symmetry that protects the full decay of the inflaton field, and discuss the parametric regimes where inflaton decay into such fermions is incomplete. We will analyse the embedding of this generic mechanism in concrete inflationary models, and possible scenarios for the interactions between the fermion fields and the Standard Model degrees of freedom that allow for the presence of the latter in the post-inflationary thermal bath. We will show that the inflaton remnant is not necessarily in the form of a coherent condensate of bosonic particles and that, in particular, for not too small couplings the evaporation of this condensate is inevitable. In this case, the thermalized inflaton particles eventually decouple from the radiation bath and their abundance freezes out, yielding a thermal inflaton relic with properties similar to other WIMP candidates [214]. We suggestively denote this as the “WIMPlaton” scenario.

We will study two dynamically distinct scenarios. Firstly, we will consider a minimal model with a single dynamical scalar field that simultaneously drives inflation, reheats the universe through incomplete decay and leaves a stable non-relativistic remnant. Secondly, we will examine a (supersymmetric) hybrid inflation model with an additional dynamical waterfall sector, which is responsible for ending inflation and reheating of the universe. In this case, we show that despite reheating being ensured by a different field, the inflaton field must decay in order for radiation to fully come to dominate the energy balance in the universe. As in the minimal model, this decay may nevertheless be incomplete and we discuss the parametric regimes in which the inflaton remnant constitutes a suitable dark matter candidate in the hybrid framework.

## 7.1 Minimal model

### 7.1.1 Basic properties and dynamics

The minimal model for inflaton dark matter considers a single dynamical (real) scalar field, the inflaton  $\phi$ , with a potential energy  $V(\phi)$  such that a period of slow-roll can occur for some field range. We take the inflaton field to be coupled to massive fermion fields  $\psi_+$  and  $\psi_-$  through standard Yukawa terms and impose a discrete symmetry<sup>1</sup> [215]  $C_2 \subset \mathbb{Z}_2 \times S_2$  on the Lagrangian such that the scalar inflaton transforms under the  $\mathbb{Z}_2$  group as  $\phi \rightarrow -\phi$  and the fermions are simultaneously interchanged by the permutation symmetry  $\psi_+ \leftrightarrow \psi_-$ . This yields for the resulting Lagrangian density:

$$\begin{aligned} \mathcal{L} = & \frac{1}{2} \partial^\mu \phi \partial_\mu \phi - V(|\phi|) \\ & + \bar{\psi}_+ (i\gamma^\mu \partial_\mu - m_f) \psi_+ + \bar{\psi}_- (i\gamma^\mu \partial_\mu - m_f) \psi_- \\ & - h\phi \bar{\psi}_+ \psi_+ + h\phi \bar{\psi}_- \psi_- , \end{aligned} \quad (7.2)$$

where, as a result of the discrete symmetry, the two fermions have the same tree-level mass  $m_f$  but opposite Yukawa coupling to the inflaton field. The action of the discrete symmetry is restricted to the inflaton-fermion sector, such that all other fields, including the Standard Model fields, are invariant under this symmetry.

This symmetry implies that the inflaton potential is an even function of the field and we assume that it is unbroken at the minimum of the potential, which must therefore lie at the origin,  $\phi = 0$ . As a result, since no other terms linear in  $\phi$  except for the above Yukawa terms are allowed by the discrete symmetry, the only possible decay channels of the inflaton at the minimum are  $\phi \rightarrow \bar{\psi}_\pm \psi_\pm$ . The massive fermions  $\psi_\pm$  must excite other light degrees of freedom for the Standard Model particles to be generated. Nevertheless, such interactions cannot induce additional decay channels of the inflaton through radiative effects or processes mediated by off-shell fermions, as the discrete symmetry causes the cancellation of the contributions of  $\psi_+$  and  $\psi_-$ . Different possibilities for the reheating of the Standard Model will be discussed in section 7.1.3.

If the inflaton mass at the minimum is given by  $m_\phi^2 = V''(0) > 0$  and we require  $m_f > m_\phi/2$ , the decays  $\phi \rightarrow \bar{\psi}_\pm \psi_\pm$  will be kinematically forbidden for  $\phi = 0$  and the inflaton will be stable when it settles at the minimum of its potential. Hence, the discrete symmetry and the mass hierarchy ensure the stability of the inflaton at late times both at tree and loop levels, such that it will contribute to the present dark matter abundance.

The two fermion fields are indistinguishable apart from their coupling to the

<sup>1</sup>This subgroup contains only elements that transform simultaneously under  $\mathbb{Z}_2$  and  $S_2$ .

inflaton, which leads to a mass splitting away from the origin:

$$m_{\pm} = |m_f \pm h\phi|. \quad (7.3)$$

This implies that, although inflaton decay into these fermions is forbidden at late times as the field approaches the origin, that need not be the case if the amplitude of field oscillations after inflation is sufficiently large. In particular, decay will be allowed for field values satisfying:

$$|m_f \pm h\phi| < m_{\phi}/2. \quad (7.4)$$

This implies, in particular, that decay is kinematically allowed for field amplitudes  $|\phi| \gtrsim m_f/h$ . The decay process of the inflaton into the massive fermions as it oscillates around the minimum of the potential follows complex dynamics involving both non-perturbative and perturbative mechanisms [216, 217, 218]. The description of the non-perturbative process strongly depends on the inflationary model under consideration, while the perturbative picture is only sensitive to the low energy behaviour of the model. Therefore, in order to get a model independent estimate of the interesting parameters, we will approximate the full decay mechanism by the perturbative description, and comment on the effects of preheating later. The partial decay widths associated to the two fermionic decay channels are then given by the Born approximation:

$$\Gamma_{\pm} = \frac{h^2}{8\pi} m_{\phi} \left( 1 - \frac{4m_{\pm}^2}{m_{\phi}^2} \right)^{3/2}, \quad (7.5)$$

with  $\Gamma_{\phi} = \Gamma_{+} + \Gamma_{-}$ . Due to the opposite sign of the Yukawa couplings, the inflaton will alternately decay into each fermion species as it oscillates between negative and positive values. The inflaton equation of motion as it oscillates about the minimum of its potential is then given by:

$$\ddot{\phi} + 3H\dot{\phi} + \Gamma_{\phi}\dot{\phi} + m_{\phi}^2\phi = 0, \quad (7.6)$$

where we have assumed that, for the range of field amplitudes involved, the potential can be approximated by  $V(\phi) \simeq (m_{\phi}^2/2)\phi^2$ . We will discuss the consistency of this hypothesis with realistic inflationary models in section 7.3. Eq. (7.6), upon multiplying by  $\dot{\phi}$  is equivalent to:

$$\dot{\rho}_{\phi} + 3H(\rho_{\phi} + p_{\phi}) = -\Gamma_{\phi}\dot{\phi}^2. \quad (7.7)$$

The term on the right hand side gives the rate at which energy density is transferred from the inflaton field into the fermions  $\psi_{\pm}$ . Let us assume that the fermions quickly thermalize, an assumption that we will check *a posteriori*, in the process

exciting  $g_*$  relativistic degrees of freedom and forming a radiation bath at temperature  $T$ , with energy density  $\rho_R = (\pi^2/30)g_*T^4$ . Since the fermion masses oscillate due to the varying inflaton field, they only contribute periodically to the number of relativistic degrees of freedom. These may also include the inflaton for  $T \gtrsim m_\phi$  and other species such as the Standard Model particles. Note that the latter must be excited before the cosmological synthesis of light nuclear elements takes place, as we discuss in more detail in section 7.1.3. For simplicity, we consider a fixed value of  $g_*$ , which is not a bad approximation since, as we will show, our results exhibit only a mild dependence on this parameter.

Energy conservation then implies that the energy lost by the inflaton field in Eq. (7.7) is gained by the radiation bath, which then follows the dynamical equation:

$$\dot{\rho}_R + 4H\rho_R = \Gamma_\phi \dot{\phi}^2. \quad (7.8)$$

Since both the inflaton and the radiation contribute to the energy density in the universe, we may write the Friedmann equation as:

$$H^2 = \frac{\rho_\phi + \rho_R}{3M_P^2} = \frac{\frac{1}{2}\dot{\phi}^2 + \frac{1}{2}m_\phi^2\phi^2 + \rho_R}{3M_P^2}. \quad (7.9)$$

Eqs. (7.6), (7.8) and (7.9) then form a complete set of differential equations that can be solved for given choices of the parameters  $(m_\phi, m_f, h)$  and initial conditions. It is useful to write the fermion tree-level mass as:

$$m_f = \frac{m_\phi}{2}(1 + \delta), \quad (7.10)$$

such that the decay is kinematically forbidden (allowed) at late times for  $\delta > 0$  ( $< 0$ ).

Figure 7.1 shows an example of the results obtained by numerically solving the inflaton-radiation equations for  $m_\phi = 10^{-3}M_P$ ,  $\delta = 0.1$  and  $h = 1$ . In this example we take as initial conditions at  $\phi(t_i) = M_P$ ,  $\dot{\phi}(t_i) = 0$  and  $\rho_R(t_i) = 10^{-16}\rho_\phi(t_i)$ , although the results are essentially unchanged as long as the field value is sufficiently large for the system to undergo some oscillations before the incomplete decay becomes effective and the radiation energy density is initially negligible, as should be expected after 50-60 e-folds of inflation.

The plot in Figure 7.1 (a) illustrates the main dynamical features that are generically obtained. The inflaton field begins to oscillate about the origin with frequency  $m_\phi$  for  $t \sim m_\phi^{-1}$  and behaves initially as cold dark matter,  $\rho_\phi \propto a^{-3}$ , being the dominant energy component such that  $a \propto t^{2/3}$  and  $H = 2/3t$ . While decay is blocked before the onset of oscillations, since  $m_\pm \sim h|\phi| \gg m_\phi$ , it becomes kinematically allowed as soon as the field goes through the origin. Since in this example the amplitude of the field oscillations largely exceeds the tree-level masses,

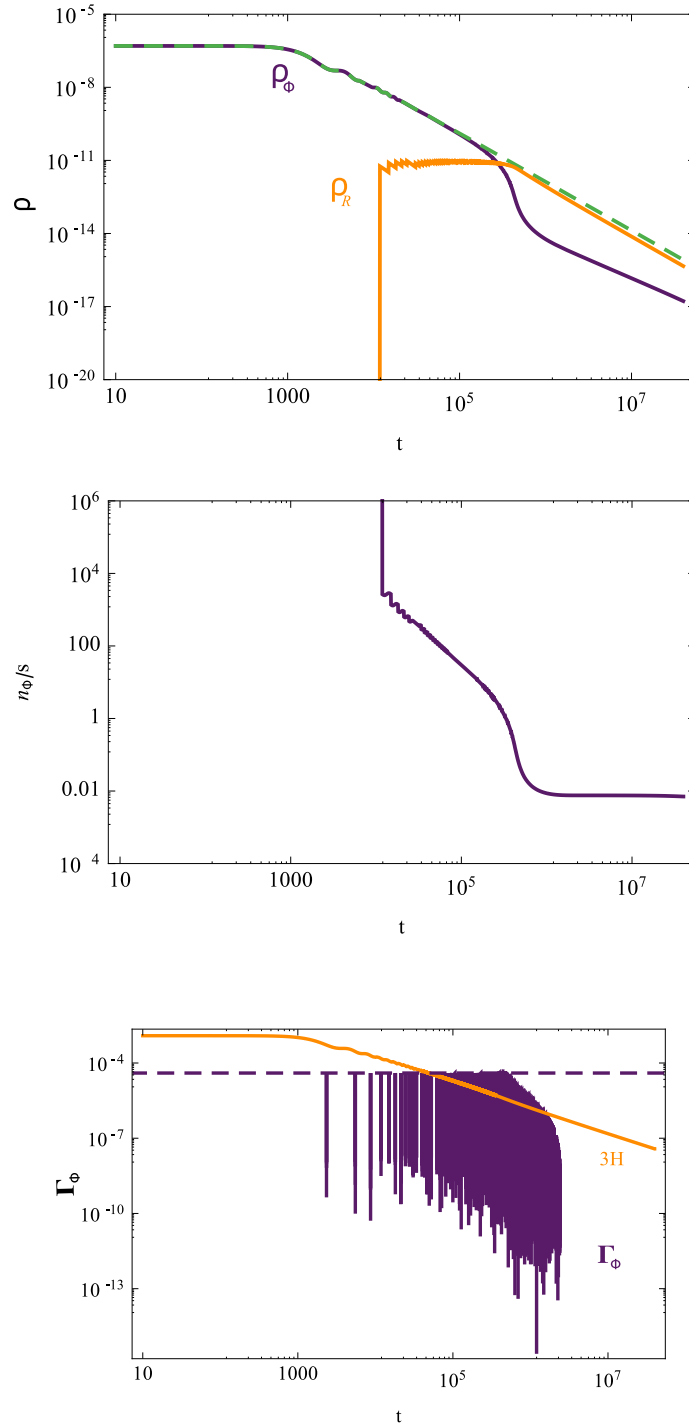


Figure 7.1: Results of the numerical integration of the inflaton-radiation dynamical equations for  $m_\phi = 10^{-3}M_P$ ,  $\delta = 0.1$  and  $h = 1$ , showing the time evolution of (a) the inflaton (solid purple curve) and radiation (solid orange curve) energy densities; (b) the inflaton-to-entropy ratio; and (c) the inflaton decay width (solid purple curve) compared to the Hubble parameter (solid orange curve). The blue dashed curves in (a) and (c) give the evolution of the inflaton energy density in the absence of decay and the maximum value of the decay width, respectively. All quantities are given in Planck units such that  $M_P = 1$ .

with  $h\Phi \gg m_f$ , decay occurs for two narrow field ranges close to (and on both sides of) the origin. The decay width then corresponds to the series of periodic narrow peaks shown in Figure 7.1 (c), with maximum value  $\Gamma_\phi^{max} = (h^2/8\pi)m_\phi$ . While initially  $\Gamma_\phi^{max} \ll 3H$  as illustrated in Figure 7.1 (c), such that the inflaton's energy density remains essentially unaffected by the decay into fermions, the source term in the radiation equation quickly becomes significant, leading to a jump in the value of the radiation energy density. The latter remains approximately constant until the inflaton's energy density is sufficiently redshifted. When they become comparable in magnitude, the inflaton effectively decays and radiation takes over as the dominant component. As the field amplitude decreases, the maximum decay width becomes progressively smaller until decay is finally blocked. The oscillating inflaton then becomes stable and once more behaves as cold dark matter, eventually taking over the radiation as the dominant component at later times.

A peculiar dynamical feature of the evolution is the approximate constancy of the radiation energy density achieved just after the first few oscillations. This is inherent to the fact that inflaton decay occurs in short bursts in each oscillation, which does not occur if the decay were allowed for all field values. Before the effect of decay into fermions becomes significant, for  $t \gtrsim m_\phi^{-1}$  the inflaton behaves as a damped harmonic oscillator with

$$\phi(t) \simeq \Phi(t) \sin(m_\phi t + \alpha_\phi), \quad \Phi(t) = \sqrt{\frac{8}{3}} \frac{M_P}{m_\phi} \frac{1}{t}, \quad (7.11)$$

where  $\alpha_\phi$  is a phase depending on the initial field and velocity values. For  $h\Phi \gg m_f$ , one can easily see that decay into each fermion is allowed during a short period  $\tau_d \simeq (h\Phi)^{-1} \ll 2\pi/m_\phi$  as the field goes through the origin, which occurs twice every oscillation period. Since the average decay width in this interval can be taken as  $\Gamma_\phi^{max}/2$  and the field velocity is  $\dot{\phi} \simeq m_\phi \Phi$ , every half period the radiation energy density increases due to inflaton decay by an amount:

$$\Delta\rho_R^{decay} \simeq \frac{\Gamma_\phi^{max}}{2} (m_\phi \Phi)^2 (2\tau_d) \simeq \frac{h}{8\pi} m_\phi^3 \Phi, \quad (7.12)$$

where we have taken into account the decays into both  $\psi_+$  and  $\psi_-$ . When decay is forbidden, radiation simply redshifts with expansion, which counteracts the enhancement due to decay by an amount:

$$\Delta\rho_R^{Hubble} \simeq -4H\rho_R(\pi/m_\phi). \quad (7.13)$$

Since  $H = 2/3t = (m_\phi/\sqrt{6}M_P)\Phi$ , it is easy to see that the amount of radiation produced by inflaton decay can be balanced exactly by Hubble expansion to yield a constant energy density. Equating  $\Delta\rho_R^{decay} = -\Delta\rho_R^{Hubble}$  then gives:

$$\rho_R \simeq \frac{\sqrt{6}h}{32\pi^2} m_\phi^3 M_P, \quad (7.14)$$

which is in very good agreement with the numerical simulations. Noting that, from Eq. (7.8),  $\dot{\rho}_R \simeq 0$  implies  $4H\rho_R \simeq \Gamma_\phi \dot{\phi}^2 \simeq \Gamma_\phi \rho_\phi$ , we see that that  $\Gamma_\phi \sim 3H$  for  $\rho_R \sim \rho_\phi$ , so that as observed numerically the inflaton energy density is only reduced significantly when it becomes comparable to the radiation energy density.

From Eq. (7.14) we can easily determine the associated temperature, which remains approximately constant up to inflaton-radiation equality and thus constitutes the reheating temperature:

$$\begin{aligned} T_R &\simeq \left( \frac{15\sqrt{6}}{16\pi^4} \right)^{1/4} g_*^{-1/4} h^{1/4} \left( \frac{m_\phi}{M_P} \right)^{3/4} M_P \\ &\simeq 2.7 \times 10^6 g_*^{-1/4} h^{1/4} \left( \frac{m_\phi}{1 \text{ TeV}} \right)^{3/4} \text{ GeV}. \end{aligned} \quad (7.15)$$

From this we conclude, in particular, that the reheating temperature is generically larger than the inflaton mass for:

$$m_\phi < 5.6 \times 10^{16} \frac{h}{g_*} \text{ GeV}. \quad (7.16)$$

After inflaton-radiation equality, the field decays exponentially fast until its amplitude drops sufficiently for decay into fermions to become inefficient. Numerically, we observe that this occurs before the decay becomes kinematically forbidden, for  $\Phi \lesssim m_f/h$ , corresponding roughly to when the (maximum) decay width becomes less than the Hubble rate. Since afterwards the field stabilizes and behaves as non-relativistic matter, it is useful to compare its number density  $n_\phi = \rho_\phi/m_\phi \propto a^{-3}$  with the radiation entropy density:

$$s = \frac{2\pi^2}{45} g_* T^3, \quad (7.17)$$

which redshifts in a similar way up to changes in the number of relativistic degrees of freedom, with  $T \propto a^{-1}$ . As illustrated in Figure 7.1 (b), the ratio  $n_\phi/s$  stabilizes after decay becomes inefficient, and numerically we obtain the following expression:

$$\frac{n_\phi}{s} \simeq 0.5 g_*^{-1/4} h^{-3.6} (m_\phi/M_P)^{1.02} f(\delta)^3, \quad (7.18)$$

where for  $0 < \delta \lesssim 1$ :

$$f(\delta) = 1 + 4.8\sqrt{\delta} + 0.5\delta. \quad (7.19)$$

If no other processes change the inflaton particle number density in the oscillating field, as we investigate below in more detail, this ratio will remain constant until

the present day. Assuming the oscillating inflaton field accounts for all the dark matter in the universe, the present inflaton-to-entropy ratio is given by:

$$\frac{n_{\phi 0}}{s_0} = \frac{3}{4} \frac{T_0}{m_\phi} \frac{\Omega_{c0}}{\Omega_{R0}} \frac{g_{*0}}{g_{*s0}} \simeq 10^{-28} \frac{M_P}{m_\phi}, \quad (7.20)$$

where  $T_0 = 2.73$  K is the present CMB temperature, while  $\Omega_{c0}h^2 = 0.12$  and  $\Omega_{R0}h^2 \simeq 4.17 \times 10^{-5}$  are the present abundances of cold dark matter and radiation, respectively [191]. We have also taken into account the present difference between the number of relativistic degrees of freedom contributing to the radiation and entropy densities,  $g_{*0} \simeq 3.36$ ,  $g_{*s0} \simeq 3.91$ . Equating (7.18) and (7.20), we obtain for the inflaton mass:

$$m_\phi \simeq 72 g_*^{0.12} h^{1.78} f(\delta)^{1.49} \text{ TeV}. \quad (7.21)$$

For fermion masses above the kinematical limit and of the order of the inflaton mass,  $0 < \delta \lesssim 1$ , and taking  $g_* = 10 - 100$ , we conclude from Eq. (7.15) that the reheating temperature is above 100 MeV for Yukawa couplings  $h \gtrsim 10^{-6} - 10^{-5}$ , corresponding to inflaton masses  $m_\phi \gtrsim 10$  keV. For larger (and arguably more natural) couplings  $h \gtrsim 10^{-3} - 10^{-2}$ , the inflaton may account for the dark matter in the universe for masses in the GeV–TeV range, similarly to the mass range obtained for WIMP-like thermal relics. Qualitatively, it is easy to understand the parametric dependence of the required inflaton mass. The (incomplete) decay into fermions is more efficient for larger couplings, which affect both the overall value of the decay width and the effective fermion masses, and lighter fermions, yielding a smaller inflaton-to-entropy ratio at late times and thus allowing for larger inflaton masses to match the present dark matter abundance. On the other hand, smaller couplings and heavier fermions lead to a larger inflaton abundance, which may overclose the universe unless the inflaton is sufficiently light.

We note also that there is no gain in considering finely-tuned fermion masses, i.e.  $\delta \ll 0$ , since even though decay is kinematically allowed for longer as  $\delta$  decreases, decay becomes inefficient when  $\Gamma_\phi \sim H$ , a condition that becomes independent of the tree-level fermion mass in this limit. Although we have restricted the numerical analysis to values of  $\delta \lesssim 1$ , we expect incomplete decay to be efficient as long as  $\Gamma_\phi > H$  for inflaton field values satisfying the kinematical condition in Eq. (7.4). In particular, since the decay width takes its maximum value  $\Gamma_\phi^{max} = (h^2/8\pi)m_\phi$  for  $h|\phi| = m_f$ , i.e. when the fermions are effectively massless, and  $H \sim m_\phi|\phi|/M_P$  during inflaton-domination, we conclude that decay will be efficient for:

$$m_f \lesssim h^3 M_P, \quad (7.22)$$

which allows for quite large fermion masses if the Yukawa coupling is not too suppressed.

### 7.1.2 Condensate evaporation: the WIMPlaton scenario

Although the imposed discrete symmetry protects the inflaton from decaying into any other particles except for the fermions  $\psi_{\pm}$ , the above analysis neglects the effects of additional interactions induced by the Yukawa terms in Eq. (7.2) and which may play an important role as we discuss below.

The classical inflaton field corresponds to a collective state of zero-momentum scalar bosons, assuming that no large field inhomogeneities are formed at the end of the slow-roll inflationary regime. Inflaton particles in this condensate can interact with the fermions that result from its decay and, in particular, these fermions can scatter some of the bosons out of the condensate and promote them to higher-momentum states that become part of the thermal bath. These correspond to scattering processes  $\psi_{\pm}\langle\phi\rangle \rightarrow \psi_{\pm}\phi$ , where we denote by  $\langle\phi\rangle$  and  $\phi$  scalar particles in the zero-momentum condensate and in higher-momentum modes, respectively, and which are mediated through both  $s$ - and  $t$ -channel fermion exchange. Moreover, these processes may occur as soon as the field begins oscillating and decay into  $\psi_{\pm}$  becomes kinematically allowed, potentially leading to the evaporation of the condensate and the transfer of the inflaton particle number into the thermal bath.

As we have seen earlier, soon after the onset of inflaton oscillations, the temperature of the thermal bath rises sharply to a value that remains approximately constant until inflaton-radiation equality and that corresponds to the reheating temperature in Eq. (7.15). In particular, this temperature exceeds the inflaton and fermion (tree-level) masses in the parameter space region that yields the present-day dark matter abundance. Further assuming that local thermal equilibrium is quickly achieved, as we check below, we may then take the phase-space distributions for inflaton and fermion species in the thermal bath to be the relativistic Bose-Einstein and Fermi-Dirac distributions, respectively. Taking into account the above scatterings and the inverse processes, the net condensate evaporation rate is given by [219]:

$$\begin{aligned} \Gamma_{evap} = & \frac{1}{n_{\phi}} \int \prod_{i=1}^4 \frac{d^3\mathbf{p}_i}{(2\pi)^3 2E_i} (2\pi)^4 \delta^4(p_1 + p_2 - p_3 - p_4) \\ & \times |\mathcal{M}|^2 [f_1 f_2 (1 + f_3)(1 - f_4) - f_3 f_4 (1 + f_1)(1 - f_2)] , \end{aligned} \quad (7.23)$$

where  $\mathcal{M}$  is the scattering amplitude for  $\langle\phi\rangle(p_1)\psi_{\pm}(p_2) \leftrightarrow \phi(p_3)\psi_{\pm}(p_4)$  and  $f_i$  the corresponding phase-space distribution factors. Since the condensate is inherently characterized by large occupation numbers  $f_1 \gg 1$ , we obtain to leading order for  $T \gg m_{\phi}, m_{\pm}$ :

$$\Gamma_{evap} \simeq \frac{h^4}{12\pi^3} \left( 1 + \log \left( \frac{T}{m_{\phi}} \right) \right) T , \quad (7.24)$$

where we have taken into account the contribution of both fermion species. Note that this is only valid when the fermions are relativistic, while for non-relativistic fermions in local thermal equilibrium the evaporation rate is exponentially suppressed. This means that during the first few oscillations before the inflaton amplitude is significantly reduced, condensate evaporation only occurs during the short periods where decay is also kinematically allowed. As we have concluded above, for the parameter values yielding the present dark matter abundance we obtain  $T_R \gtrsim m_\phi, m_f$ , and since  $m_\pm \sim m_f$  after reheating the above expression holds until either the inflaton or the fermions become non-relativistic. Since in the radiation era  $H \simeq (\pi/\sqrt{90})g_*^{1/2}T^2/M_P$ , condensate evaporation becomes progressively more efficient as the temperature drops. We may then determine a lower bound on the Yukawa coupling such that condensate evaporation is inefficient for  $T \gtrsim m_\phi, m_f$ . For comparable masses, we obtain:

$$\left. \frac{\Gamma_{evap}}{H} \right|_{T=m_\phi} \simeq \frac{h^4}{4\pi^3} \left( \frac{g_*}{10} \right)^{-1/2} \left( \frac{M_P}{m_\phi} \right) \lesssim 1. \quad (7.25)$$

Using Eq. (7.21) for the inflaton mass, we then obtain for  $\delta = 1$ :

$$h \lesssim 10^{-5} g_*^{0.28}. \quad (7.26)$$

As we had seen above, this is in tension with the lower bound on the coupling required for a reheating temperature above 100 MeV, such that initial conditions for Big Bang Nucleosynthesis (BBN) are already in place after inflaton decay [24]. This conclusion is essentially common to all fermion mass values  $m_f > m_\phi/2$ . Although a more detailed analysis of the Boltzmann equation determining the evolution of the inflaton condensate may be required, this estimate indicates that in the physically interesting parameter range, where the condensate could account for the present dark matter abundance while satisfying the BBN constraint, condensate evaporation is most likely inevitable.

Since evaporation simply transfers the zero-momentum condensate particles into excited states, the conclusion above does not imply that inflaton particles cannot account for dark matter. One can easily check that all 4-body processes involving relativistic inflaton and fermion particles, including scatterings and annihilations, occur at a rate comparable to the evaporation rate obtained in Eq. (7.24). Hence, evaporation of the condensate should lead to a bath of fermions and inflaton particles (as well as other species) in local thermal equilibrium. In fact, this may even occur just after the onset of inflaton oscillations, for  $H \lesssim m_\phi$ , when the temperature reaches an approximately constant value  $T \gtrsim m_\phi, m_f$  as seen above, for  $h \lesssim \mathcal{O}(1)$  couplings. The condensate's energy is in this case quickly transferred

to the thermal bath, increasing its temperature to a maximum value:

$$\begin{aligned} T_R^{max} &= \left(\frac{90}{\pi^2}\right)^{1/4} g_*^{-1/4} \sqrt{M_P m_\phi} \\ &\simeq 8.5 \times 10^{10} g_*^{-1/4} \left(\frac{m_\phi}{1 \text{ TeV}}\right)^{1/2} \text{ GeV} . \end{aligned} \quad (7.27)$$

This value was obtained for  $H = m_\phi$ , which constitutes only an upper bound since fermion particles can be produced for  $H \lesssim m_\phi$  as shown by our numerical simulations. The true reheating temperature will then lie between the value obtained in Eq. (7.15) and this maximum value when the condensate evaporation is more efficient than the incomplete decay. On the contrary, the reheating temperature is given by Eq. (7.15) if condensate evaporation only occurs after it decays significantly, in the radiation era, which corresponds to Yukawa couplings  $h \lesssim 10^{-4}$  for  $\delta \lesssim 1$  and  $g_* = 10 - 100$ . Note that in this parametric regime thermalization of the fermions in the plasma can only be efficient if their interactions with other degrees of freedom are stronger than those induced by the Yukawa terms, while for  $h \gtrsim 10^{-4}$  the latter occur sufficiently fast to maintain local thermal equilibrium, as we analyze in more detail in section 7.1.3.

After reheating, inflaton and fermion particles will be kept in local thermal equilibrium by annihilation and elastic scattering processes. Once these become inefficient, the abundance of inflaton particles will freeze out, as for other conventional WIMP dark matter candidates. Assuming this occurs when both the inflaton and the fermions are non-relativistic, the relevant (fermion  $t$ -channel) annihilation cross section is given by:

$$\sigma_{\phi\phi} \simeq \frac{h^4}{8\pi m_\phi^2} , \quad (7.28)$$

which is independent of the fermion mass in this limit. Following the standard calculation for the thermal relic abundance of a decoupled non-relativistic species, we obtain for the inflaton mass:

$$m_\phi \simeq 1.4 h^2 \left(\frac{\Omega_{\phi 0} h_0^2}{0.1}\right)^{1/2} \left(\frac{g_{*F}}{10}\right)^{1/4} \left(\frac{x_F}{25}\right)^{-3/4} \text{ TeV} , \quad (7.29)$$

where  $g_{*F}$  denotes the number of relativistic degrees of freedom at freeze-out and  $x_F = m_\phi/T_F$ , with  $T_F$  denoting the freeze-out temperature. This is somewhat smaller than the mass values obtained assuming the oscillating inflaton condensate survives until the present day, although in a comparable range and exhibiting a similar dependence on the Yukawa coupling.

This then gives us a more realistic dynamical picture of what we suggestively denote as the ‘‘WIMPlaton’’ scenario. After inflation, the scalar inflaton begins oscillating about the minimum of its potential, decaying into fermions in short

bursts every oscillation. These may thermalize and excite other degrees of freedom in the plasma, and scatter off the inflaton particles in the condensate, leading to its evaporation. Both decay and evaporation increase the relative abundance of radiation and decrease the amplitude of oscillations, until eventually radiation becomes dominant and inflaton decay is no longer kinematically allowed. The stable inflaton particles remain in thermal equilibrium until the temperature drops below their mass and they decouple from the plasma, their frozen abundance yielding the inferred dark matter component of our present universe.

The “WIMPlaton” scenario does not depend on the description of the inflaton decay. Non-perturbative decay of the inflaton field in massive fermions produces non-relativistic fermions with a non-equilibrium number density  $n_f$  and energy density  $\rho_f = m_f n_f$  [216, 217, 220]. Assuming that all particles are non-relativistic in the scattering process, we can estimate the evaporation rate from Eq. (7.23)

$$\Gamma_{evap} \sim \frac{h^4 n_f}{m_f^2}, \quad (7.30)$$

where we considered that the typical momentum of the fermions produced by preheating is  $m_f$ . The Hubble parameter is  $H \sim m_\phi \Phi(t)/m_P$ , hence

$$\frac{\Gamma_{evap}}{H} \sim h^4 \left( \frac{\rho_f}{\rho_\phi} \right) \left( \frac{m_f}{m_\phi} \right) \left( \frac{\Phi(t)}{m_f} \right) \left( \frac{m_P}{m_\phi} \right). \quad (7.31)$$

In the worst case scenario, evaporation is only efficient at the end of preheating, where  $\Phi(t) \sim m_f/h$  and  $\rho_f \lesssim r h o_\phi$ . For the masses under consideration,  $m_\phi \simeq m_f \sim \mathcal{O}(\text{TeV})$ , evaporation will be efficient as long as

$$\frac{\rho_f}{\rho_\phi} \gtrsim h^{-3} \mathcal{O}(10^{-15}), \quad (7.32)$$

a limit which is well below the results for the production of massive fermions by non-perturbative decay [217].

### 7.1.3 Reheating the Standard Model

We have so far assumed that the fermions (or scalars as discussed above) resulting from inflaton decay thermalize and excite other degrees of freedom, and in particular it is crucial that Standard Model particles are generated in the thermal bath at temperatures above  $\sim 100$  MeV so that BBN may occur following the standard freeze-out dynamics of light nuclear abundances.

As we have briefly discussed above, the fermions themselves cannot be treated as fully relativistic degrees of freedom before the inflaton decays sufficiently, since their mass varies between small and large values as the inflaton oscillates about

the origin. For the short periods when they are light and decay is allowed, thermalization through Yukawa interactions can be quite efficient. For example, fermion-fermion scatterings through inflaton  $s$ -channel exchange occurs at a rate:

$$\Gamma_{\psi\psi} \simeq \frac{9\zeta(3)}{16\pi^3} h^4 T . \quad (7.33)$$

Since after the onset of oscillations  $H \lesssim m_\phi$  and taking the temperature value obtained in Eq. (7.15) from inflaton decay, we have:

$$\frac{\Gamma_{\psi\psi}}{H} > \frac{\Gamma_{\psi\psi}}{m_\phi} \simeq 60 g_*^{-1/4} h^{17/4} \left( \frac{m_\phi}{1 \text{ TeV}} \right)^{-1/4} , \quad (7.34)$$

such that for  $\mathcal{O}(1)$  couplings Yukawa interactions can lead to thermalization from the start of oscillations. Recall that, as seen above, evaporation of the condensate occurs at a comparable rate, so that as the temperature rises due to evaporation both processes become progressively more efficient. If the Yukawa couplings are more suppressed, one may also envisage scenarios where for example the fermions are charged under a gauge symmetry that is unbroken at the relevant temperatures and thermalization occurs through gauge boson exchange for sufficiently strong couplings.

Outside the inflaton field range for which the fermions are effectively light, their number density will become Boltzmann-suppressed, and any interactions will necessarily become inefficient in keeping the fermions in local thermal equilibrium. We thus expect them to decouple for most of the oscillation period, transferring their entropy into light degrees of freedom such as the inflaton itself or e.g. gauge bosons. If interactions occur faster than the inflaton oscillation rate  $m_\phi$ , as given in Eq. (7.34) for the Yukawa scattering processes, fermions will drop in and out of local thermal equilibrium as they oscillate between the relativistic and non-relativistic regimes. This will lead to an oscillating  $g_*$ , but as mentioned at the start of our discussion this is of little consequence since our results exhibit only a mild dependence on this parameter.

Since the inflaton is typically taken as a gauge singlet, the structure of the Yukawa interactions implies that  $\psi_\pm$  are non-chiral fermions (either Dirac or Majorana), as opposed to the known SM fermions, being thus unlikely that they are explicitly charged under the SM gauge group. We will discuss two possibilities for exciting the SM degrees of freedom in the plasma either before or after radiation comes to dominate: decay or annihilation of the fermions into the SM particles before they become non-relativistic, and their abundance is Boltzmann-suppressed.

The simplest case is perhaps that of unstable  $\psi_\pm$  fermions decaying into a light scalar and a light fermion, for which the decay width is:

$$\Gamma_{\psi_\pm} = \frac{h_f^2}{16\pi} m_\pm , \quad (7.35)$$

where  $h_f$  denotes the associated coupling constant. Note that this is computed in the fermions' rest frame, whereas in the plasma's frame an additional time dilation factor  $m_{\pm}/T$  suppresses the decay for relativistic fermions. Requiring  $\Gamma_{\psi_{\pm}} \gtrsim H$  for  $T \gtrsim m_f$  in the radiation era (where  $m_{\pm} \simeq m_f$ ), we obtain the following bound on the coupling:

$$h_f \gtrsim 8 \times 10^{-8} g_{*f}^{1/4} \left( \frac{m_f}{1 \text{ TeV}} \right)^{1/2}, \quad (7.36)$$

where  $g_{*f}$  is the number of relativistic degrees of freedom at  $T = m_f$ . In addition, for this to happen before BBN we require  $m_f \gtrsim 100$  MeV. If the inflaton and fermion masses are comparable, this corresponds to  $h \gtrsim 0.01$  according to Eq. (7.29). These light degrees of freedom may correspond to SM particles if, for example, the fermions coupled to the inflaton field correspond to a pair of degenerate sterile neutrinos, which are singlets under the SM gauge group and may decay into a Higgs-lepton pair through Yukawa terms of the form  $h_f H \bar{l} \psi_{\pm}$ . Note that this requires  $m_f > m_H = 125$  GeV [221, 222] and hence  $m_{\phi} < 250$  GeV, which is compatible with the present dark matter abundance for couplings  $h \lesssim 0.7$  from Eq. (7.29).

If the fermions are stable, another possibility for reheating the SM degrees of freedom is through efficient annihilation. A possible scenario is for the fermions to be charged under a hidden  $U(1)_X$  gauge group, which may mediate fermion scatterings and thus improve the thermalization efficiency. This  $U(1)_X$  hidden photon may be kinetically mixed with the SM photon or hypercharge gauge boson  $Y^{\mu}$  through a term of the form  $F_X^{\mu\nu} F_{\mu\nu}^Y$ , which may be generated radiatively if there are fields charged under both gauge groups or simply via gravitational interactions, as happens e.g. in string theory. Diagonalization of the gauge kinetic terms then induces a small electric charge for the fermions  $\psi_{\pm}$ , such that they may annihilate into SM charged particles via  $s$ -channel photon exchange,  $\psi_{\pm} \psi_{\pm} \rightarrow \gamma \rightarrow qq, ll$ . At high temperature the annihilation cross section is given by the Thomson scattering formula and the corresponding interaction rate for relativistic species is then given by:

$$\Gamma_{th} \simeq \frac{4\zeta(3)}{\pi} \epsilon^2 \alpha^2 N_{ch} T, \quad (7.37)$$

where  $\epsilon$  is the "mili-charge" of the fermions  $\psi_{\pm}$ ,  $\alpha$  is the fine-structure constant and  $N_{ch}$  is the effective number of charged species in the final state, which for the full SM is  $N_{ch} = 20/3$ . In the radiation era, since  $H \propto T^2$  annihilation becomes more efficient at smaller temperatures. Requiring that SM species are excited before  $\psi_{\pm}$  become non-relativistic, we obtain the following bound on the mili-charge:

$$\epsilon \gtrsim 5 \times 10^{-7} g_{*f}^{1/4} \left( \frac{N_{ch}}{20/3} \right)^{-1/2} \left( \frac{\alpha^{-1}}{128} \right) \left( \frac{m_f}{1 \text{ TeV}} \right)^{1/2}. \quad (7.38)$$

This bound is not very stringent for fermion masses in the GeV-TeV range, where the main constraints come from direct collider searches (including the LHC) yielding  $\epsilon \lesssim 0.1$  for  $1 \text{ GeV} \lesssim m_f \lesssim \text{few} \times 100 \text{ GeV}$  and indirect bounds from the CMB anisotropy spectrum, which yield  $\epsilon \lesssim 10^{-4}$  for  $\text{few} \times 100 \text{ GeV} \lesssim m_f \lesssim \text{few} \times \text{TeV}$  based on the effect of milli-charged particles on the baryon-photon oscillations (for a gauge coupling  $g_X = 0.1$ ). Note that for masses above the TeV range, milli-charged particles may give a too large contribution to the dark matter abundance in the universe, and more stringent bounds on  $\epsilon$  apply in this case (see [223] and references therein). This thus constitutes a promising scenario with potential for experimental probing in the near future.

The discrete  $C_2 \subset \mathbb{Z}_2 \times S_2$  symmetry protects the inflaton from decaying at late times, thus constituting a viable dark matter candidate. One can consider, however, scenarios where this symmetry is broken and the inflaton is only meta-stable, with a lifetime larger than the age of the universe,  $t_0 \sim 14 \text{ Gyrs}$ . Note that interactions between the fermions  $\psi_{\pm}$  and other light degrees of freedom as in the scenarios outlined above can induce the decay of the inflaton through radiative effects or processes mediated by off-shell fermions. A few examples of these processes are illustrated in Figure 7.2 and in all cases the contribution of  $\psi_+$  and  $\psi_-$  cancels if the discrete symmetry is exact.

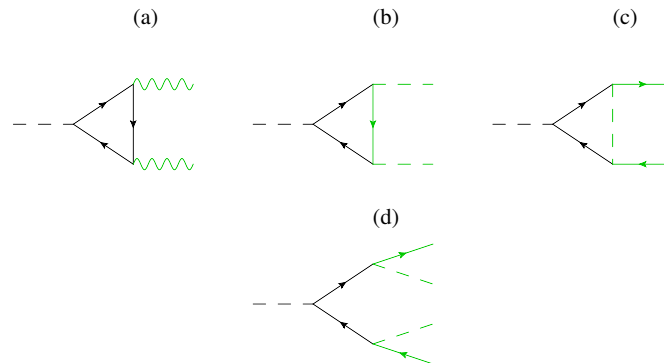


Figure 7.2: Feynman diagrams for the 2-body decay of the inflaton into (a) gauge bosons, (b) light scalars and (c) light fermions, induced at the 1-loop level by gauge and Yukawa interactions of the  $\psi_{\pm}$  fermions. In (d) we also show the 4-body decay of the inflaton induced by the exchange of virtual  $\psi_{\pm}$  modes with Yukawa interactions with other light species. For clarity, all light fields are represented by green lines.

As an example, we have considered the case where  $\psi_{\pm}$  are unstable, decaying into a light fermion and scalar, which induce diagrams (b)-(d) in Figure 7.2. Since these processes have comparable magnitudes, we have computed the inflaton decay width for the 1-loop process (b), where it decays into two light scalars. For concreteness we consider the case where  $\psi_{\pm}$  are slightly non-degenerate with

$m_- = m_f$  and  $m_+ = m_f(1 + \Delta)$ , for  $\Delta \ll 1$ . This gives for  $m_\phi = 2m_f$  ( $\delta = 0$ ):

$$\Gamma_\phi^{(b)} = \frac{h^2 h_f^4}{64\pi^5} m_\phi \Delta^2, \quad (7.39)$$

which is more suppressed for larger values of  $m_f$ .

For  $m_\phi$  yielding the correct relic abundance to account for dark matter and using the lower bound on  $h_f$  obtained in Eq. (7.36), we obtain the following upper bound on the inflaton lifetime:

$$\tau_\phi < 15.7 g_{*f}^{-1} \left( \frac{m_\phi}{10 \text{ GeV}} \right)^{-4} \left( \frac{\Delta}{0.01} \right)^{-2} \text{ Gyrs}, \quad (7.40)$$

where we have taken the reference values for the present dark matter abundance and freeze-out parameters in Eq. (7.29). Hence, we conclude that significant violations of the discrete symmetry can still yield a sufficiently long-lived inflaton for  $100 \text{ MeV} \lesssim m_\phi \lesssim 10 \text{ GeV}$ , such that the fermions  $\psi_\pm$  decay before BBN and while they are still relativistic. For heavier inflaton particles, values of  $\Delta$  below the percent level are required, signaling that the discrete symmetry must hold to a high degree of accuracy in this regime.

It is thus clear from the examples above that if the inflaton field can only decay to the  $\psi_\pm$  fermions for a finite period following the end of the slow-roll regime, becoming (meta-)stable at late times, it may account for the dark matter in the universe while allowing for successful reheating of the SM particles and setting the necessary conditions for BBN.

## 7.2 Hybrid model

### 7.2.1 Basic properties and dynamics

An alternative framework to the one considered in the previous section is the supersymmetric hybrid model [224]. In this scenario, the inflaton decay products need not include or interact with the Standard Model degrees of freedom, since the additional waterfall sector can be responsible for reheating after inflation [225, 226, 227, 228].

For the same reasons exposed in the minimal model, the symmetry  $C_2 \subset \mathbb{Z}_2 \times S_2$  is imposed on the superfield containing the inflaton and all the superfields that it couples directly to. Hence, for the superpotential to be invariant under the action of this group, the inflaton is, as before, coupled to a pair of superfields  $Y_\pm$  which contain the fermions  $\psi_\pm$  with masses  $m_f$ , and to a waterfall sector with a pair of superfields  $X_\pm$ . The group  $C_2$  simultaneously changes  $\Phi \rightarrow -\Phi$  and interchanges the superfields  $Y_+ \leftrightarrow Y_-$  and  $X_+ \leftrightarrow X_-$ .

The discrete symmetry forbids the linear term in the superpotential that is typically considered in SUSY hybrid inflation to generate the constant vacuum energy driving accelerated expansion. This may nevertheless be generated either by a D-term contribution [229, 230], or through a non-vanishing F-term coming from a SUSY breaking sector [231, 232]. In addition, in order to ensure the stability of the inflaton at late times, so that it may account for dark matter, the  $C_2$  symmetry must be preserved in the ground state, implying equal vacuum expectation values for the scalar components of both waterfall fields. One possibility to satisfy this condition and simultaneously generate a constant vacuum energy is to introduce an additional “driving” superfield,  $Z$ , which is not charged under the discrete symmetry and is coupled to the waterfall sector, along the lines proposed in [233, 234]. We thus consider a superpotential of the form:

$$\begin{aligned} W &= \frac{g}{2}\Phi(X_+^2 - X_-^2) + \frac{h}{2}\Phi(Y_+^2 - Y_-^2) + \frac{m_f}{2}(Y_+^2 + Y_-^2) \\ &+ \frac{\kappa}{2}Z(X_+^2 + X_-^2 - M^2) \\ &+ \frac{h_\chi}{2}(X_+ + X_-)Q^2 + \dots, \end{aligned} \quad (7.41)$$

where  $M$  is a constant mass scale and we have included a coupling between the waterfall superfields and additional chiral superfields  $Q$  which give their decay products. The dots indicate additional terms that may be added, involving the inflaton and the superfield  $Z$ . In particular, if the scalar component of the latter has a sufficiently large mass, either from superpotential terms, soft masses from SUSY breaking in other sectors or non-minimal terms in the Kähler potential, its expectation value will be set to zero both during and after inflation. The global minimum of the scalar potential will then lie along the real direction  $\langle X_+ \rangle = \langle X_- \rangle \equiv \chi/\sqrt{2}$ , which preserves the discrete symmetry, and the scalar potential relevant for the inflationary and post-inflationary dynamics has the usual hybrid form:

$$V(\phi, \chi) = \frac{\kappa^2}{4}(\chi^2 - M^2)^2 + \frac{g^2}{2}\phi^2\chi^2 + \dots, \quad (7.42)$$

where  $\phi = \sqrt{2}\langle\Phi\rangle$  is the real inflaton scalar field. We recover the usual SUSY hybrid case for  $\kappa = g/\sqrt{2}$  and for simplicity we will consider this parametric regime, although our analysis can be extended to the generic case.

Inflation takes place for amplitudes of the inflaton field larger than a critical value,  $\phi > \phi_c = M/\sqrt{2}$ , such that the waterfall field is held at the origin  $\chi = 0$ . As the inflaton rolls towards its minimum at  $\phi = 0$ , its amplitude falls below the critical value and the waterfall field can roll to its true vacuum at  $\chi = M$ , thus ending inflation. After that point, both fields start to oscillate around its respective minima, triggering the process of reheating the universe into a radiation era.

In this scenario, the inflaton cannot decay into either the bosonic or fermionic components in the waterfall sector due to kinematical blocking. This is easy to see

at the global minimum, where  $m_\phi = m_\chi = gM$ , but extends to all field values. As in the minimal model, the inflaton can decay into the  $Y_\pm$  fields and the decay will be incomplete for  $m_f > m_\phi/2 = gM/2$ . For simplicity, we assume that the scalar components of the  $Y_\pm$  fields acquire large soft masses from SUSY breaking and focus on the fermionic decay channels, noting that the inclusion of both channels will not change our conclusions significantly.

The waterfall fields will decay into the  $Q$  sector fields and, for similar reasons, we include only the fermionic decay channels in this case as well. We assume that these fields are light, eventually leading to the complete decay of the waterfall sector and reheating the universe. Note that neither the inflaton nor the waterfall field can be completely stable in order to reheat the universe, since they carry a comparable amount of the energy density after inflation. In particular, if the inflaton were completely stable and behaved as dark matter at all times, the decay of the waterfall field would only convert half of the total energy density into radiation. Its incomplete decay will then reduce the inflaton abundance and hence allow for an efficient reheating once the waterfall field decays. For the inflaton to decay incompletely before the waterfall field, we require  $h \gtrsim h_\chi$ , which is the parametric regime on which we will focus henceforth.

The evolution equations driving the post-inflationary dynamics of the inflaton and waterfall fields, as well as their decay products which we assume to quickly thermalize, are then given by:

$$\ddot{\phi} + 3H\dot{\phi} + g^2\chi^2\phi = -\Gamma_\phi\dot{\phi}, \quad (7.43)$$

$$\ddot{\chi} + 3H\dot{\chi} + \frac{g^2}{2}(\chi^2 - M^2 + 2\phi^2)\chi = -\Gamma_\chi\dot{\chi}, \quad (7.44)$$

$$\dot{\rho}_R + 4H\rho_R = \Gamma_\chi\dot{\chi}^2 + \Gamma_\phi\dot{\phi}^2, \quad (7.45)$$

where we assume the Born approximation to compute the decay widths, as discussed in section 7.1.1. Therefore, the decay width of the inflaton is  $\Gamma_\phi = \Gamma_+ + \Gamma_-$ , with  $\Gamma_\pm$  given by Eq. (7.5), while the decay width of the waterfall field is given by:

$$\Gamma_\chi = \frac{h_\chi^2 m_\chi}{8\pi}, \quad (7.46)$$

where we neglect the  $Q$  fermion masses, which we have checked numerically to be a good approximation for couplings  $h_\chi \lesssim 0.1$  in the parameter range of interest to our discussion.

Eqs. (7.43), (7.44) and (7.45), together with the Friedmann equation,

$$H^2 = \frac{\rho_\phi + \rho_\chi + \rho_R}{3M_P^2} = \frac{\frac{1}{2}\dot{\phi}^2 + \frac{1}{2}\dot{\chi}^2 + V(\phi, \chi) + \rho_R}{3M_P^2}, \quad (7.47)$$

form a complete set of differential equations that can be solved numerically given a set of parameters  $(g, M, m_f, h, h_\chi)$  and initial conditions. Fig. 7.3 shows an

example of the numerical solution for the parameter values  $M = 10^{-2}M_P$ ,  $g = 10^{-5}$ ,  $h = 1$ ,  $h_\chi = 10^{-5}$  and  $\delta = 0.02$ , the latter being defined in Eq. (7.10). In this example we have considered initial conditions such that the fields are close to their values at the end of inflation and have small velocities,  $\phi(0) = 1.0001\phi_c$ ,  $\chi(0) = 0$ ,  $\dot{\phi}(0) = \dot{\chi}(0) = -10^{-4}gM^2$ , with  $\rho_R(0) = 0$  since any pre-inflationary radiation should be exponentially diluted by the accelerated expansion. However, we have checked numerically that the results do not show a strong dependence on the choice of initial conditions.

At the beginning of the evolution, both the inflaton and the waterfall field mimic a pair of coupled matter fluids which give a roughly equal contribution to the total energy density. After the incomplete decay of the inflaton becomes efficient, its energy density is transferred into the radiation bath, while the waterfall field evolves as an effective non-interacting matter field in an expanding universe.

Since radiation is diluted more quickly than matter by the cosmological expansion, the universe experiences an era of matter domination until the waterfall field effectively decays and reheats the universe. The system then enters into the standard radiation-dominated era of Big Bang cosmology, with the oscillating inflaton field remnant behaving as a cold dark matter component.

The parameter  $h_\chi$  determines the duration of the reheating process, which is due to the decay of the waterfall field. During that process, there is entropy production [235] and as a consequence the abundance  $n_\phi/s$  will be further reduced, as shown in Fig. 7.3 (b). The dilution factor is given by  $\gamma = S_{eq}/S_R$ , with  $S$  being the entropy and the subscript “eq” denoting the time at which the  $\chi$  thermalized decay products start dominating the radiation bath, at a temperature  $T_{eq} > T_R$ . The dilution factor is then given by:

$$\gamma = \left(\frac{T_R}{T_{eq}}\right)^5 \simeq \frac{5}{3} \left(\frac{T_R}{T_D}\right) \left(\frac{g_{*D}}{g_{*R}}\right), \quad (7.48)$$

with  $T_D$  being the temperature after the effective decay of the inflaton. The smaller the coupling  $h_\chi$ , the longer the reheating process and the smaller  $T_R$ , and the more efficient the reduction of the abundance. Therefore larger inflaton masses are allowed to match the present dark matter abundance.

The temperature after the effective decay of the inflaton,  $T_D$ , can be determined analytically following the same reasoning used in minimal model to compute the reheating temperature, giving:

$$T_D = \left(\frac{15\sqrt{3}}{16\pi^4}\right)^{1/4} g_{*D}^{-1/4} h^{1/4} \left(\frac{m_\phi}{M_P}\right)^{3/4} M_P, \quad (7.49)$$

where  $g_{*D}$  is the effective number of light degrees of freedom when the inflaton effectively decays. Unlike in the minimal model, the reheating temperature is not

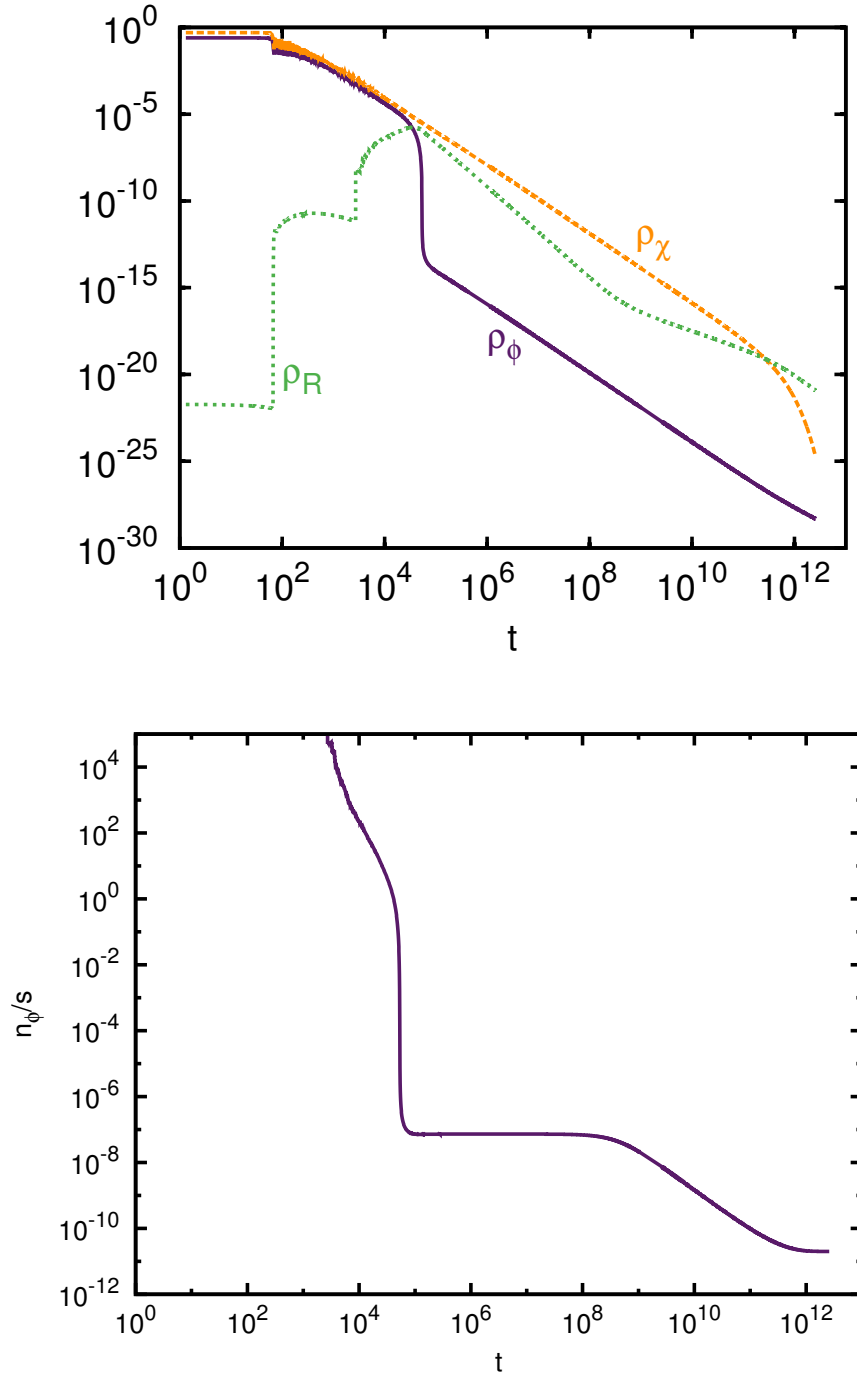


Figure 7.3: Results of the numerical integration of the inflaton-waterfall-radiation dynamical equations for  $M = 10^{-2}M_P$ ,  $g = 10^{-5}$ ,  $h = 1$ ,  $h_\chi = 10^{-5}$  and  $\delta = 0.02$ , showing the time evolution of (a) the inflaton (solid purple curve), the waterfall (dashed orange curve) and radiation (dotted green curve) energy densities; (b) the inflaton-to-entropy ratio. All quantities are given in Planck units such that  $M_P = 1$ .

controlled by the inflaton but rather by the waterfall decay, corresponding to the temperature for which  $\Gamma_\chi = H$ :

$$T_R \simeq 0.23 g_{*R}^{-1/4} h_\chi (m_\phi M_P)^{1/2} , \quad (7.50)$$

with  $g_{*R}$  being the effective number of light degrees of freedom at reheating and where we used  $m_\phi = m_\chi$  since the fields are close to the global minimum at this stage.

The computation of the inflaton dark matter abundance after reheating is more involved than in the minimal scenario due to the larger set of parameters in the hybrid scenario, and the coupling between the inflaton and waterfall fields. The effect of the parameters of the potential in Eq. (7.42),  $g$  and  $M = m_\phi/g$  on the final abundance is shown in Fig. 7.4.

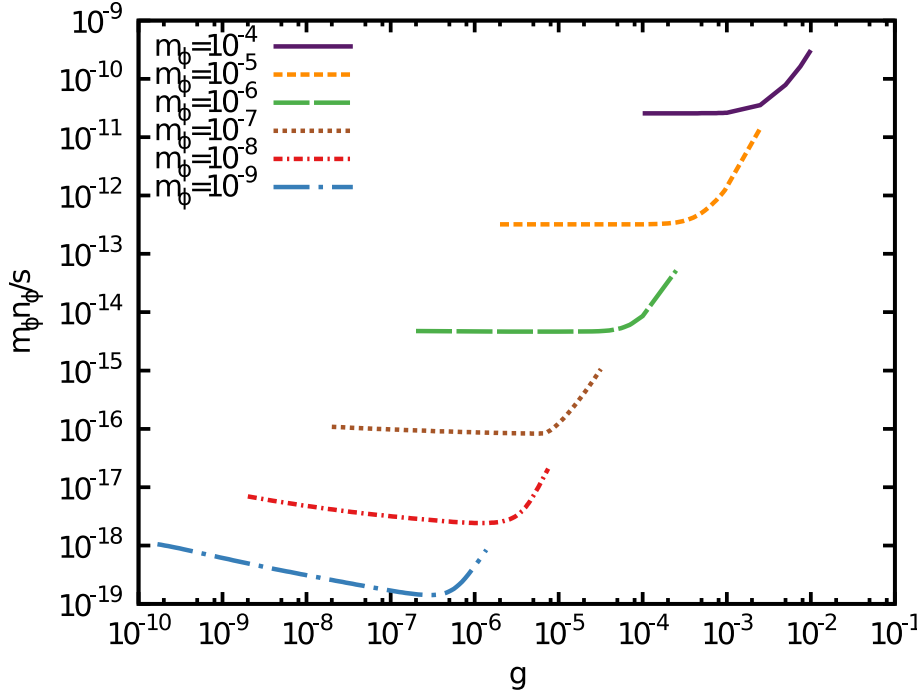


Figure 7.4: Dependence of the inflaton-to-entropy ratio after reheating multiplied by the inflaton mass in Planck units for different values of the parameters in the potential,  $g$ ,  $M$  for  $\delta = 0.02$ ,  $h = 1$  and  $h_\chi = 10^{-5}$ .

For large values of the coupling  $g$ , the inflaton-to-entropy ratio grows with  $g$  since the system is strongly coupled and the waterfall field transfers a significant part of its energy to the inflaton, therefore increasing its abundance. For very low values of the coupling, on the other hand, the inflaton-to-entropy ratio shows a very mild dependence on this coupling. In this case the Hubble parameter  $H \sim$

$m_\phi^2/g$  is very large, so that the condition for the incomplete decay to be efficient,  $\Gamma_\phi > H$ , cannot be maintained for a sufficiently long period and the abundance is not so drastically reduced. Numerically, we take the endpoint of the curves at small  $g$  values such that  $V_0^{1/4} = \sqrt{g}M = m_\phi/\sqrt{g} \sim 10^{16}$  GeV is of the order of the GUT scale, which roughly gives the upper bound on the scale of inflation. The vacuum energy scale therefore diminishes when moving from left to right along each curve of constant  $m_\phi$  in Fig. 7.4.

We will restrict the remainder part of our analysis to the values of  $g$  for which the incomplete decay exhibits its maximal efficiency, therefore yielding the lowest inflaton abundance for a given mass  $m_\phi$ . Numerically, we find these values to be given by:

$$g \simeq 0.04 \left( \frac{m_\phi}{M_P} \right)^{0.57} \delta^{-0.08}. \quad (7.51)$$

With this relation, we obtain for the inflaton-to-entropy ratio from the numerical results:

$$\frac{n_\phi}{s} \simeq 134 g_*^{-1/4} h_\chi h^{-3.42\beta(h)} \delta^{2\gamma(\delta)} \left( \frac{m_\phi}{M_P} \right)^{0.7}, \quad (7.52)$$

$$\beta(h) = 1 - \frac{1}{6} \log_{10} h, \quad (7.53)$$

$$\gamma(\delta) = 1 + 0.115 \log_{10} \delta. \quad (7.54)$$

This expression is equivalent to Eq. (7.18) in the minimal model, with the different powers on the parameters reflecting the more complicated dynamics present in this scenario. Equating (7.20) and (7.52), we then obtain the inflaton mass yielding the observed dark matter abundance:

$$m_\phi \simeq 442 g_*^{0.15} \left( \frac{h_\chi}{10^{-3}} \right)^{-0.6} h^{-0.6\beta(h)} \delta^{-0.6\gamma(\delta)} \text{ GeV}. \quad (7.55)$$

For couplings  $h \sim \mathcal{O}(1)$  and  $h_\chi \sim 10^{-3} - 10^{-5}$ , the inflaton may account for the dark matter in the universe with masses in the GeV-TeV range, similarly to the minimal model, while predicting a reheating temperature well above the BBN constraint. The qualitative dependence of the inflaton mass on the Yukawa coupling  $h$  can be understood using the same arguments as in the minimal realization for inflaton dark matter described earlier in the chapter.

### 7.2.2 Condensate evaporation: the WIMPlaton scenario

The effect of additional processes induced by the Yukawa coupling  $h$  in the evaporation of the condensate of zero-momentum inflaton particles is essentially the same that has been described for the minimal model, with the rate of evaporation given by Eq. (7.24). However, the possibility of the fermions becoming

non-relativistic during the matter era, where the dominant contribution to the energy density comes from the waterfall field, gives a different lower bound on the Yukawa couplings such that evaporation is inefficient for  $T \gtrsim m_\phi, m_f$ :

$$h_\chi \lesssim 5 \times 10^{-10} h^{-\frac{3}{16} \log_{10} h} \left( \frac{g_*}{10} \right)^{13/32}. \quad (7.56)$$

Nevertheless, as we found in the minimal scenario of inflaton dark matter, this bound is in tension with the lower bound on the couplings consistent with a reheating temperature above 100 MeV, as can be seen in Fig. 7.5. Therefore, in the region where the condensate may account for the present dark matter and the reheating temperature is consistent with the BBN constraint, condensate evaporation is most likely inevitable. The evaporation process produces a bath of fermions and inflaton particles kept in local thermal equilibrium by annihilation and elastic scatterings that eventually become inefficient, at which point the inflaton abundance freezes out as in the standard WIMP scenario.

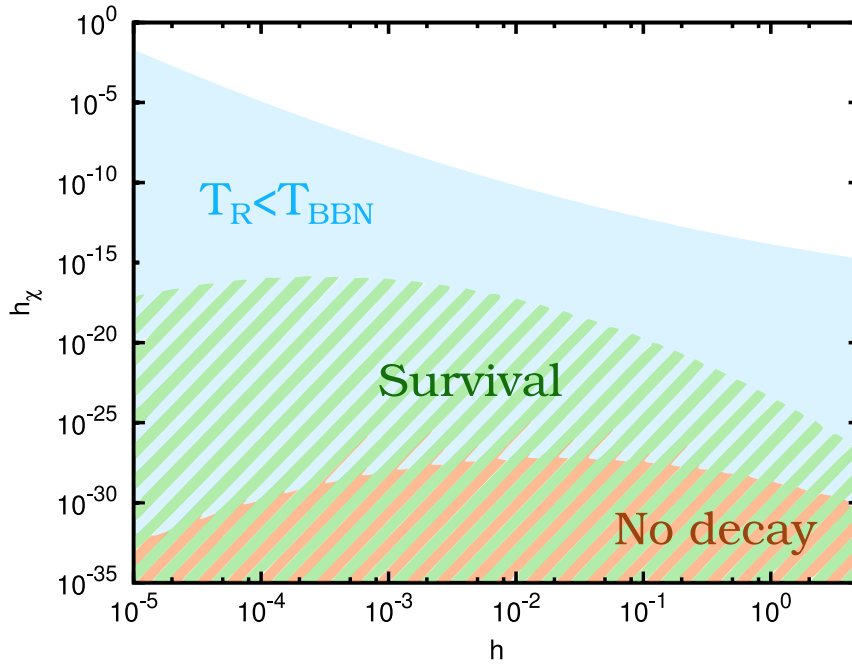


Figure 7.5: Regions in the parameter space  $h_\chi - h$  where the reheating temperature is below the BBN limit (blue), the condensate can survive evaporation (green), and there is no incomplete decay (orange)

If freeze-out occurs after the waterfall field has decayed, i.e. in the radiation-dominated era, we obtain the same value for the inflaton mass as in the minimal model, given in Eq. (7.29). Freeze-out takes place in the waterfall-dominated

matter for values of  $h_\chi$  satisfying:

$$h_\chi \lesssim 4 \times 10^{-9} h \left( \frac{g_{*F}}{10} \right)^{3/8} \left( \frac{x_F}{25} \right)^{-11/8} \left( \frac{\Omega_{\phi 0} h_0^2}{0.1} \right)^{1/4}, \quad (7.57)$$

which then yields an upper bound on the WIMPlaton mass:

$$m_\phi \lesssim 756 h^2 \left( \frac{g_{*F}}{10} \right)^{1/4} \left( \frac{x_F}{25} \right)^{-3/4} \left( \frac{\Omega_{\phi 0} h_0^2}{0.1} \right)^{1/2} \text{ GeV}, \quad (7.58)$$

where the annihilation cross section is given by Eq. (7.28). In Fig. 7.6 we summarize on the plane  $(h, h_\chi)$  the different possibilities for inflaton dark matter in the hybrid model. In both regions where the freeze-out of the inflaton abundance occurs either in the radiation or waterfall era, the inflaton can account for the present dark matter abundance for masses in the GeV-TeV range with the reheating and freeze-out temperatures being well above the limit imposed by BBN. This shows that the WIMPlaton scenario introduced earlier is not an exclusive feature of the minimal model, with a single dynamical field, but also occurs in other models of inflation with additional dynamical fields.

While the inflaton mass values corresponding to the observed dark matter abundance are not very different in the two realizations that we have analyzed, in the hybrid scenario there are novel phenomenological possibilities. In particular, the inflaton decay products need not interact with the SM degrees of freedom, since these may be excited only after the decay of the waterfall field. Either the waterfall sector decays directly into SM particles or its decay products interact with some of the latter. We note that the waterfall fields may be charged under gauge symmetries, in which case the relevant terms in the superpotential are of the form  $\Phi X_\pm \bar{X}_\pm$ , etc, where  $X_\pm$  and  $\bar{X}_\pm$  transform in conjugate representations of the gauge group. This will then open up new avenues for model-building in inflaton dark matter scenarios besides those described in the minimal model.

### 7.3 Embedding in a consistent inflationary model

As we have concluded from the analysis above, the inflaton field can account for dark matter in the universe at late times for masses below or around the TeV scale in the WIMPlaton scenario, with a similar mass range obtained assuming the inflaton condensate does not evaporate. This implies that the inflaton potential cannot be given solely by the terms that we considered in the previous sections. For a quadratic potential, the amplitude of CMB temperature anisotropies would yield for a quadratic potential:

$$m_\phi \simeq \frac{\sqrt{6\pi^2 \Delta_{\mathcal{R}}^2}}{N_e} M_P \simeq 1.4 \times 10^{13} \left( \frac{60}{N_e} \right) \text{ GeV}, \quad (7.59)$$

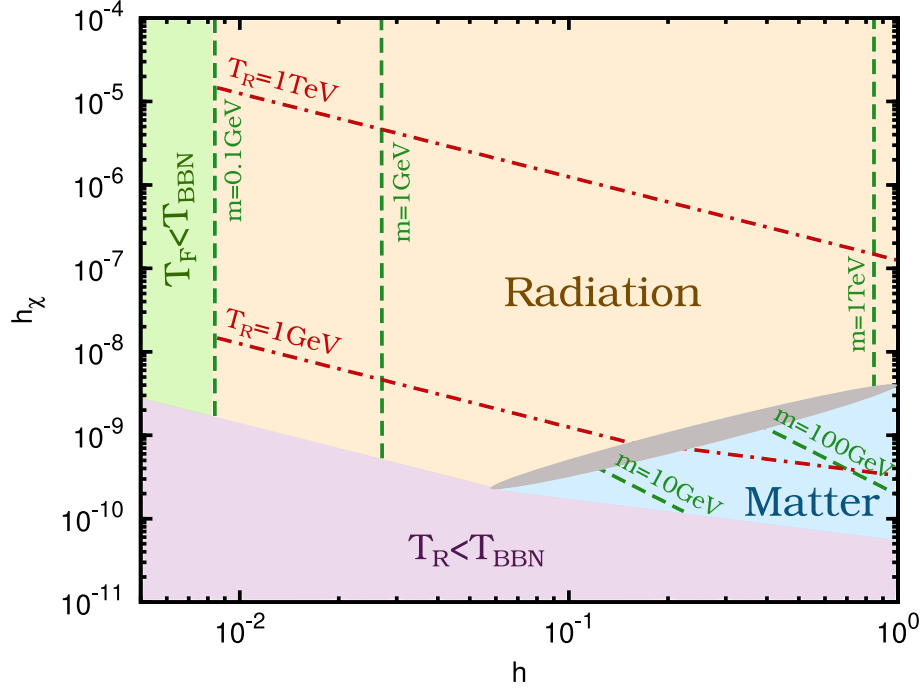


Figure 7.6: Parameter space of the hybrid model of inflaton dark matter with  $\delta = 1$ . In the orange (blue) region the abundance of the inflaton accounts for the present dark matter energy density and the freeze-out occurs in the radiation (waterfall=matter) era. The purple (green) region is excluded because the reheating (freeze-out) temperature is below 100 MeV. Dashed (dashed-dot) lines are curves of constant inflaton mass (reheating temperature). The grey area represents the transition between the regions where the freeze-out takes place in the radiation and waterfall era.

which for 50–60 e-folds of slow-roll inflation largely exceeds the TeV scale. On the other hand, in the standard SUSY hybrid models with minimal Kähler potential, inflation is driven essentially by the constant vacuum energy  $V_0 = g^2 M^4/8$  while the waterfall fields are stabilized at the origin. We may then use the normalization of the scalar curvature power spectrum to obtain the relation:

$$m_\phi \gtrsim 2.5 \times 10^{15} |\eta| \text{GeV} , \quad (7.60)$$

for  $\phi \gtrsim M$ , where  $m_\phi = gM$  is the inflaton mass at the minimum. Since the scalar spectral index  $n_s \simeq 1 + 2\eta \simeq 0.9603 \pm 0.0073$  at 68%CL [23] in these scenarios, we conclude that  $m_\phi \lesssim \text{TeV}$  cannot yield an observationally consistent model. Typically we have from the normalization of the spectrum  $M \sim 10^{13} - 10^{16} \text{ GeV}$ , and then the WIMPlaton scenario requires small couplings  $g \sim 10^{-13} - 10^{-10}$ , which are responsible for the very flat potential during inflation and the scale invariant

spectrum. A non-minimal Kähler potential can yield the observed spectral index for lower values of the coupling, although at the expense of a slight increase in  $M$  [236, 237], which again makes it difficult to achieve the required WIMPlaton mass values.

However, our analysis assumed only that  $m_\phi$  is the inflaton mass as it oscillates about the minimum of the potential at the origin, while the effective inflaton mass can be much larger if slow-roll occurs for significantly larger field values where self-interactions become important. For example, the discrete  $\mathbb{Z}_2$  symmetry allows for quartic self-interactions such that:

$$V(\phi) = \frac{\lambda}{4!} \phi^4 + \dots \quad (7.61)$$

In the minimal model the quartic term dominates for  $|\phi| > \sqrt{12/\lambda} m_\phi$ , while our analysis is valid if the quartic term is sub-dominant for the field values  $|\phi| \sim m_f/h$  at which decay into fermions occurs, which requires:

$$h \gtrsim \sqrt{\frac{\lambda}{12}} \left( \frac{m_f}{m_\phi} \right) \simeq 3 \times 10^{-8} \left( \frac{m_f}{m_\phi} \right), \quad (7.62)$$

where we have used  $\lambda \simeq 10^{-14}$  as imposed by the COBE normalization for inflation with a quartic potential. This is easily satisfied if the fermions are not much heavier than the inflaton given the more stringent bounds on the Yukawa coupling discussed earlier. The discrete  $\mathbb{Z}_2 \times S_2$  symmetry does not protect the scalar potential from radiative corrections, however, for the sake of a clearer presentation of the results, possible solutions to this problem will be discussed in appendix C.

A quartic self-coupling  $\lambda^2 \phi^4/4$  can be easily introduced in SUSY hybrid inflation by a superpotential coupling between the inflaton and an auxiliary field,  $\lambda \Phi^2 Z/2$ . We then have:

$$\frac{\lambda^2 \phi^4}{V_0} \sim 6 \times 10^{16} \left( \frac{\lambda^2}{10^{-14}} \right) \left( \frac{1 \text{ TeV}}{m_\phi} \right)^2 \left( \frac{M_P}{M} \right)^2 \left( \frac{\phi}{M_P} \right)^4, \quad (7.63)$$

so that the quartic term will easily dominate over the vacuum term for superplanckian values and the typical parameters required by the normalization of the spectrum and the WIMPlaton scenario. We note that the vacuum term will come to dominate the energy at small field values, but for  $\phi \gtrsim \phi_c$  we have

$$\eta \sim \lambda^2 \frac{\phi^2}{M^2} \frac{M_P^2}{m_\phi^2} \gtrsim \lambda^2 \frac{M_P^2}{m_\phi^2} \gg 1, \quad (7.64)$$

such that slow-roll inflation never takes place in the small field regime, and inflation may then occur entirely in a chaotic regime.

We note that, in supergravity models, such chaotic inflation scenarios can be obtained by considering a non-minimal Kähler potential for the inflaton, while

taking the canonical one for the other superfields in the model, in particular the  $Z$  field. One possibility is to consider a Kähler potential with a shift symmetry [238, 239, 240], e.g.  $K(\Phi, Z, \dots) = (\Phi + \Phi^\dagger)^2/2 + ZZ^\dagger + \dots$ , with inflation taking place along the imaginary component of the scalar inflaton.

A quartic term is, however, not sufficient to produce a consistent model of inflation, since it predicts a too red-tilted spectrum for curvature perturbations and a tensor-to-scalar ratio already outside the bounds obtained by Planck [23] and BICEP2 [82, 83]. A consistent spectrum may be achieved in warm inflation scenarios, as we discussed in chapter 6. However, as warm inflation naturally leads to radiation becoming the dominant component at the end of the slow-roll regime, the post-inflationary evolution will necessarily differ from the dynamical picture discussed here.

Another interesting possibility is the inclusion of a non-minimal coupling to the gravitational sector, in particular a coupling between the inflaton and Ricci scalar of the form  $\xi\phi^2 R$ , which is compatible with the discrete  $\mathbb{Z}_2$  symmetry. The resulting inflationary scenario yields a perturbation spectrum that smoothly interpolates between the minimal quartic model and the Starobinsky model as the non-minimal coupling constant increases. On the one hand, the latter is characterized by a low tensor-to-scalar ratio and a spectral index  $n_s = 0.96 - 0.97$  in agreement with the Planck results; on the other hand, a small non-minimal coupling constant is preferred to obtain a non-negligible tensor-to-scalar ratio. We refer the reader to [241, 242] and the references therein for a more detailed discussion of these scenarios, since here we are mainly interested in the post-inflationary dynamics. The effect of the non-minimal coupling on the effective scalar potential in the Einstein frame becomes negligible for  $\xi\phi^2/M_P^2 \lesssim 1$ , such that consistency of our analysis implies

$$h \gtrsim \sqrt{\xi} \frac{m_f}{M_P}, \quad (7.65)$$

which is generically less stringent than Eq. (7.62) for masses in the TeV range and  $\xi < 10^{16}$ .

*Let's dare to invent our future.*

Thomas Sankara

## Conclusions

---

The main topic addressed by this thesis is the analysis of the impact of dissipative processes during inflation and reheating. The aim of this work is to deepen the present understanding of the effects of dissipation in both the dynamics and observables of such eras in the early universe. Our study of the inflationary epoch have been done in the context of the warm inflationary scenario, where quantum field theory characterizes the dissipative mechanisms acting during inflation. We have concentrated on the LOTS realization of warm inflation, the particular picture which is best understood in the literature. In our examination of the reheating period, we proposed a mechanism for the incomplete decay of the inflaton field into a radiation bath such that the inflaton can survive the process and remain as a consistent dark matter candidate. Our main results can be summarized as follows:

### ■ Background dynamics of warm inflation

We have broaden the knowledge of the background behaviour of warm inflation in two different directions. We have studied for the first time in the context of warm inflation a class of models characterized by an inflection point in the inflationary potential. Furthermore, we have contributed to the insight of the viscous effects in warm inflation by considering more realistic descriptions of the bulk viscosity based on quantum field theory and causal hydrodynamics.

### ◆ Models with an inflection point

In chapter 2 we have focused on supersymmetric models, where the plethora of available flat directions may be lifted by competing SUSY-breaking effects, producing inflection and even saddle points in the potential, although at the expense of fine-tuning *a priori* unrelated parameters. Our analysis of the dissipative dynamics of inflation in these models have lead us to two main conclusions. Firstly, if dissipative effects are sufficiently strong, a sufficiently long period of inflation may occur independently of the fine-tuning of the parameters in the potential, which was expected since the additional friction alleviates the need for a very flat potential. Secondly, and more surprisingly, the required amount of dissipation does

not decrease arbitrarily for flatter potentials, given that if the scalar potential is too flat and the inflaton evolves too slowly, it becomes more difficult to sustain a radiation bath with a temperature above the Hubble rate, which is required for consistency of our analysis. This results in a field-dependent critical value of the fine-tuning parameter  $\beta$  below which the required dissipation parameter  $C_\phi$  becomes constant. Above this value, the potential is sufficiently steep to ensure that  $T > H$  throughout inflation, with steeper potentials requiring larger values of the dissipation parameter.

#### ◆ Stability with non-negligible viscous effects

In chapter 3 the noncausal theory for the bulk viscous pressure, given by the Eckart hydrodynamics theory, was studied along with two other causal theories, the IS linear theory and the NLCDH theory. We have seen significant differences in the radiation production in each of these different theories as the relaxation time of the radiation fluid increases. Among the three theories for the bulk pressure we have studied, the NLCDH case proved to be the most robust of them as far as stability is concerned. In regards model building, we have shown that accounting for bulk viscous pressure effects in the radiation fluid can relax the requirements on the magnitude of the dissipation coefficient for the inflaton field, especially for a large bulk viscosity coefficient. This range of bulk viscosity coefficients can be realized within the regime of stability requirements in warm inflation, and this range is within reach of realistic model parameters.

#### ■ Growth mode in the LOTS realization of warm inflation

We have analysed two different solutions to the growth mode in the power spectrum, induced by the temperature dependence of the dissipative coefficient in the LOTS realization of warm inflation. We have examined the effectiveness of the viscosities in suppressing the growth mode, and we have extended previous results with the inclusion of the bulk viscosity. Additionally, we have explored the weak dissipation regime of warm inflation, where the growth mode does not emerge. We have shown that the presence of even small dissipative effects at the time when observable scales leave the horizon during inflation may have a significant effect on the spectrum of primordial fluctuations.

#### ◆ Suppressing the growth mode with viscous effects

In chapter 5 we studied the evolution of the linear fluctuations of warm inflation including bulk and shear viscosities. We have concentrated on the LOTS realization of warm inflation, and used expressions for the viscosities computed from quantum field theory. For completeness we have also considered other temperature dependences in the dissipative coefficient and in the bulk viscosity that may

appear in different momentum regimes of the two stage framework of warm inflation. Our main result is the complete suppression of the growth mode in the strong dissipation regime of warm inflation, when viscosity is consistently described by bulk viscous terms. The effect of the bulk viscosity has been compared with previous results for the shear viscosity, and we have found that the bulk viscosity dominates over the shear both in the amplitude and the tilt of the spectrum. We have characterized the impact of the shear and bulk viscosities on the spectral index, considering the modifications at the background and perturbation levels, such that it can be included in future phenomenological studies.

#### ◆ Warm inflation with weak dissipation

In chapter 6 we have proved that warm inflation in the weak dissipation regime lowers the tensor-to-scalar ratio, and yields a modified consistency relation that may be used to distinguish it in a model-independent way from the standard supercooled scenarios if a tensor component is found and accurately measured. The main modifications to the scalar spectrum arise from the presence of dissipative noise that sources inflaton fluctuations, and from the changes in the phase space distribution of inflaton modes as a consequence of inflaton particle production in the plasma. We have shown, in particular, that the latter effect may bring the simplest chaotic inflation scenario with a quartic potential into agreement with the Planck results for a nearly-thermal distribution. Inflation may thus be triggered from chaotic initial conditions at the Planck scale in an observationally consistent way, through simple renormalizable interactions with matter fields that must be present in any inflationary model, as opposed to e.g. a non-minimal coupling to the gravitational sector. The cosmic baryon asymmetry may also be produced during warm inflation, inducing baryon isocurvature perturbations that are within the current Planck bounds for a quartic potential and which may be probed in the near future. Furthermore, we have demonstrated that other low-scale models such as hill-top scenarios are consistent for both the thermal regime and when the fluctuation-dissipation term is dominant.

#### ■ Unification of inflation and dark matter through reheating

In chapter 7 we have shown that the decay of the inflaton following the inflationary slow-roll regime can be incomplete, such that successful reheating is achieved while leaving a stable remnant that can account for the observed dark matter in the universe. By estimating the scattering rate of zero-momentum inflaton particles off thermalized fermions, we concluded that the oscillating condensate will most likely evaporate in parametric regimes where the reheating temperature is above the threshold required for Big Bang Nucleosynthesis. The stable inflaton particles then reach a thermalized state which eventually decouples from the cos-

mological radiation bath and freezes out as a standard WIMP. In this *WIMPlaton* scenario, inflaton masses must lie in the GeV-TeV range to account for the observed dark matter abundance.

In the simplest models with a single dynamical field, the inflaton decay products must interact with the Standard Model (SM) degrees of freedom in order to excite them in the thermal bath. We have explored different possibilities for such interactions, and we have also analysed the alternative possibility of hybrid inflation models, where a dynamical waterfall sector, which is also charged under the discrete symmetry, is responsible for reheating the universe. The entropy produced by the waterfall decay dilutes the inflaton condensate's abundance, however, condensate evaporation will also most likely occur in the viable parametric regimes. A *WIMPlaton* scenario with masses in the GeV-TeV range is again the most probable outcome in hybrid models.

While these mass values may *a priori* seem too low to yield the correct amplitude for the primordial spectrum of curvature perturbations, we have shown that the inflaton mass can be much larger during the slow-roll period than at the minimum of the potential, thus allowing for the embedding in consistent inflationary models.

*Let's dare to invent our future.*

Thomas Sankara

## Conclusiones

---

El tema principal que hemos abordado en esta tesis es el análisis del impacto de los procesos disipativos durante inflación y recalentamiento. El propósito de este trabajo es contribuir al desarrollo conocimiento actual de los efectos de la disipación tanto en la dinámica como en los observables de las eras mencionadas en el universo temprano. Hemos realizado el estudio del periodo inflacionario en el contexto del escenario de inflación templada, donde los mecanismos disipativos que actúan durante inflación se describen en términos de teoría cuántica de campos. Nos hemos enfocado en la realización LOTS de inflación templada, la realización más estudiada en la literatura. En nuestro examen del periodo de recalentamiento propusimos un mecanismo de desintegración del inflatón en un baño de radiación, tal que el inflatón puede sobrevivir al proceso y jugar el papel de un candidato a materia oscura. Nuestros resultados pueden resumirse como sigue:

### ■ Dinámica de inflación templada a orden cero en teoría lineal de perturbaciones

Hemos ampliado el conocimiento del comportamiento a orden cero en teoría lineal de perturbaciones de inflación templada en dos direcciones diferentes. Hemos estudiado por primera vez en el contexto de inflación templada una categoría de modelos caracterizada por la presencia de un punto de inflexión en el potencial inflacionario. Además, hemos contribuido a la intelección de los efectos de viscosidad en inflación templada considerando descripciones más realistas de la viscosidad de volumen basadas en teoría cuántica de campos e hidrodinámica causal.

### ◆ Modelos con puntos de inflexión

En el capítulo 2 nos hemos centrado en modelos supersimétricos, donde la plétora de direcciones planas disponibles pueden ser elevadas por los efectos que compiten para romper SUSY, produciendo puntos de inflexión o incluso de silla, aunque a costa de un ajuste fino de parámetros no relacionados *a priori*. Nuestro análisis de la dinámica disipativa de inflación es esos modelos nos ha conducido a dos conclusiones principales. Primero, si los efectos disipativos son suficientemente

fuertes, puede producirse un periodo de inflación de duración suficiente independientemente del ajuste fino de los parámetros. Este comportamiento tiene sentido puesto que la fricción adicional reduce la necesidad de un potencial muy plano para inflación. Segundo, y más sorprendentemente, la cantidad de disipación necesaria no decrece arbitrariamente para potenciales más planos, puesto que si el potencial escalar es demasiado plano y el inflatón evoluciona muy lentamente, resulta más complicado mantener un baño de radiación a una temperatura superior al parámetro de Hubble, condición necesaria para la consistencia de nuestro análisis. Esto implica que existe un valor crítico del parámetro de ajuste fino  $\beta$  por debajo del cual el parámetro de disipación  $C_\phi$  requerido se hace constante. Por encima de ese valor, el potencial es lo suficientemente inclinado como para asegurar que  $T > H$  durante inflación. Potenciales más inclinados necesitan valores del parámetros de disipación más altos.

#### ◆ Estabilidad con efectos de viscosidad no despreciables

En el capítulo 3 estudiamos la descripción no-causal para la viscosidad de volumen, la teoría hidrodinámica de Eckart, junto con otras dos teorías causales, la teoría linear IS y la teoría NLCDH. Hemos encontrado diferencias significativas en la producción de radiación en cada una de esas teorías cuanto más aumenta el tiempo de relajación del fluido de radiación. Entre las tres teorías para la presión de volumen que hemos estudiado, mostramos que el caso NLCDH es el más robusto en cuanto a estabilidad concierne. En cuanto a construcción de modelos hemos demostrado que los efectos de la presión viscosa de volumen en el fluido de radiación pueden relajar los requisitos para la magnitud del coeficiente disipativo, especialmente para un coeficiente de viscosidad de volumen alto. Este rango de coeficientes de viscosidad de volumen es compatible con el régimen de requisitos de estabilidad de inflación templada y puede obtenerse con parámetros de modelos realistas.

#### ■ Modo creciente en la realización LOTS de inflación templada

Hemos analizado dos soluciones diferentes al modo creciente en el espectro de potencias, que está inducido por la dependencia con la temperatura del coeficiente disipativo en la realización LOTS de inflación templada. Hemos examinado la eficiencia de las viscosidades en la supresión del modo creciente y hemos extendido resultados previos con la inclusión de la viscosidad de volumen. Asimismo, hemos explorado el régimen de disipación débil de inflación templada, en el que el modo creciente no emerge. Hemos demostrado que incluso la presencia de efectos de disipación pequeños en el momento en el que las escalas observables salen del horizonte durante inflación puede tener un efecto importante en el espectro primordial de perturbaciones.

### ◆ Supresión del modo creciente con efectos viscosos

En el capítulo 5 hemos estudiado la evolución de las perturbaciones lineales de inflación templada en presencia de viscosidades de volumen y de cizalla. Nos hemos centrado en la realización LOTS de inflación templada y hemos usado expresiones para las viscosidades calculadas en teoría cuántica de campos. Por completitud también hemos considerado otras dependencias con la temperatura en los coeficientes disipativos y de viscosidad de volumen que pueden aparecer en otros regímenes de momento en la realización en dos etapas de inflación templada. El resultado principal que hemos encontrado es la completa supresión del modo creciente en el régimen de disipación fuerte de inflación templada, cuando describimos la viscosidad en términos de la viscosidad de volumen. Hemos comparado el efecto de la viscosidad de volumen con resultados previos para la viscosidad de cizalla y hemos encontrado que la viscosidad de volumen domina sobre la de cizalla tanto en la amplitud como en el índice espectral del espectro de potencias. Hemos caracterizado el impacto de las viscosidades de volumen y de cizalla en el índice espectral, teniendo en cuenta las modificaciones tanto a orden cero como a orden lineal en teoría de perturbaciones, de modo que pueda ser incluido en futuros estudios fenomenológicos.

### ◆ Inflación templada con disipación débil

En el capítulo 6 hemos demostrado que inflación templada en el régimen de disipación débil disminuye la proporción tensor a escalar e introduce una modificación en la relación de consistencia. Esta modificación puede ser utilizada para diferenciar inflación templada de escenarios fríos independientemente del modelo si se descubre una componente tensorial y se mide de manera precisa. Las principales modificaciones al espectro escalar se deben a la presencia de ruido disipativo que actúa como fuente de las fluctuaciones del inflatón y a los cambios en la distribución en el espacio de las fases de los modos del inflatón, que surge como consecuencia de la producción de partículas inflacionarias en el plasma. Hemos demostrado, en particular, que este último efecto puede aliviar la tensión entre los datos de Planck y el escenario de inflación caótica más simple con un potencial cuártico, cuando la distribución es cercana al equilibrio térmico. En ese caso inflación puede comenzar a partir de condiciones iniciales caóticas a la escala de Planck de manera consistente con las observaciones, a través de simples interacciones renormalizables con campos de materia que deben estar presentes en cualquier modelo inflacionario, en oposición, por ejemplo, a un acoplo no mínimo al sector gravitacional. La asimetría cósmica de bariones puede también ser producida durante inflación templada, de manera que se inducen perturbaciones de isocurvatura en los bariones consistentes con los límites actuales de Planck para un potencial cuadrático y que podrían ser observadas en un futuro cercano. Igualmente, hemos demostrado que otros modelos a escalas bajas, como los escenarios

*hill-top*, son consistentes con Planck tanto en el régimen térmico como cuando el término de fluctuación-disipación es el dominante.

## ■ Unificación de inflación y materia oscura a través de recalentamiento

En el capítulo 7 hemos demostrado que la desintegración del inflatón posterior al régimen inflacionario de rodadura lenta puede ser incompleta, de modo que se complete con éxito el proceso de recalentamiento a la vez que sobrevive un remanente estable que explique la materia oscura en el universo. A partir de la estimación de la tasa de dispersión de inflatones de momento cero con fermiones en el baño térmico, hemos concluido que el condensado oscilante se evaporará en las regiones del espacio de parámetros en las que la temperatura de recalentamiento es superior al umbral necesario para la síntesis de núcleos ligeros. Los inflatones, que son partículas estables, alcanzarán un estado de equilibrio térmico que finalmente se desacoplará del baño cosmológico de radiación y seguirá un proceso de congelación como un WIMP estándar. En este escenario de *WIMPlatón*, las masas del inflatón deben estar en el rango del GeV-TeV para poder describir la abundancia observada de materia oscura.

En los modelos más simples con un sólo campo dinámico, los productos de la desintegración del inflatón deben interactuar con los grados de libertad del modelo estándar para poder excitarlos en el baño térmico. Hemos explorado diferentes posibilidades para esas interacciones y también hemos analizado la posibilidad alternativa de modelos de inflación híbrida, en los que un sector dinámico de cascada, que también está cargado bajo la simetría discreta, es el responsable del recalentamiento del universo. La entropía producida por la desintegración del sector de cascada diluye la abundancia del condensado de inflatones, sin embargo, la evaporación del condensado también se producirá en las regiones viables del espacio de parámetros. Un escenario de *WIMPlatón* con masas en el rango del GeV-TeV vuelve a ser el caso más favorable en los modelos híbridos.

Aunque estos valores de las masas puedan parecer a priori demasiado bajos para producir una amplitud correcta del espectro de perturbaciones, hemos mostrado que la masa del inflatón puede ser mucho mayor durante el periodo de rodadura lenta que en el mínimo del potencial, de modo que es posible incluir el mecanismo en modelos inflacionarios consistentes.

# Stability analysis for the viscosity descriptions

## A.1 Dynamical system for the Eckart case

In the Eckart theory the bulk pressure is simply given by Eq. (3.12),  $\Pi = -3\zeta_b H$ . The dynamical system Eq. (3.36) takes the form,

$$\begin{aligned} u' &= -3H - \Upsilon - V_{,\phi} u^{-1} \equiv f(u, s) , \\ s' &= -3H s u^{-1} + 9\zeta_b H^2 (T u)^{-1} + \Upsilon T^{-1} u \equiv g(u, s) . \end{aligned} \quad (\text{A.1})$$

The Jacobian matrix  $\mathbb{M}$  becomes

$$\mathbb{M}_{\text{Eckart}}(x) = \left. \frac{\partial(f, g)}{\partial(u, s)} \right|_{u=u_0, s=s_0} \equiv \left( \begin{array}{cc} \partial f / \partial u & \partial f / \partial s \\ \partial g / \partial u & \partial g / \partial s \end{array} \right) \Big|_{u=u_0, s=s_0} = \begin{pmatrix} \mathcal{A} & \mathcal{B} \\ \mathcal{C} & \mathcal{D} \end{pmatrix} \quad (\text{A.2})$$

where the matrix elements are evaluated at the slow-roll solutions Eqs. (3.37) and (3.38). The coefficients of the matrix  $\mathbb{M}_{\text{Eckart}}$  become

$$\begin{aligned} \mathcal{A} &= \frac{H}{u} \left\{ -3(1+Q) - \frac{1}{(1+\kappa)^2} \frac{\epsilon}{(1+Q)^2} \right\} , \\ \mathcal{B} &= \frac{H}{s} \left\{ -3(\gamma-1)cQ + 3(\gamma-1)b(1+Q) + \right. \\ &\quad \left. - \frac{1}{(1+\kappa)^2} \frac{Q\epsilon}{(1+Q)^2} + \frac{\sigma}{1+\kappa} \left[ \frac{1}{(1+\kappa)} \frac{Q\epsilon}{(1+Q)^2} - \frac{3}{2} \tilde{\sigma} \right] \right\} , \\ \mathcal{C} &= \frac{Hs}{u^2} \left[ 6 - \frac{1}{(1+\kappa)^2} \frac{\epsilon}{(1+Q)^2} \right] \left\{ 1 + \sigma \frac{[6(1+Q)^2 - 2\epsilon]}{[6(1+Q)^2 - \epsilon]} \right\} , \\ \mathcal{D} &= \frac{H}{u} \left\{ 3(\gamma-1)(c-1) - 3 - \frac{1}{(1+\kappa)^2} \frac{Q\epsilon}{(1+Q)^2} + \right. \\ &\quad \left. + \sigma \left[ 3(\gamma-1)(c-l) - \frac{1}{(1+\kappa)^2} \frac{Q\epsilon}{(1+Q)^2} + \frac{3}{2} \frac{\tilde{\sigma}}{1+\kappa} \right] \right\} , \end{aligned} \quad (\text{A.3})$$

where we have omitted the sub-index “0” of the slow-roll solutions and defined the quantities  $\sigma$  and  $\tilde{\sigma}$  as

$$\sigma = \frac{\Pi}{\gamma\rho_r}, \quad (\text{A.4})$$

$$\tilde{\sigma} = \frac{\Pi}{V}. \quad (\text{A.5})$$

$b$  is the slow-roll parameter ensuring that thermal corrections to the inflation potential are negligible

$$b = \frac{TV_{T\phi}}{V_\phi}. \quad (\text{A.6})$$

The expressions simplify considerably in the strong dissipative regime of warm inflation,  $Q \gg 1$  and neglecting the terms proportional to the slow-roll parameters in Eq. (A.3), we obtain

$$\begin{aligned} \mathcal{A} &= -3Q\frac{H}{u}, \\ \mathcal{B} &= 3(\gamma-1)(b-c)Q\frac{H}{s}, \\ \mathcal{C} &= \frac{Hs}{u^2}6(1+\sigma), \\ \mathcal{D} &= \frac{H}{u} \left\{ 3(\gamma-1)(c-1) - 3 + \left[ 3(\gamma-1)(c-l) + \frac{3}{2}\frac{\tilde{\sigma}}{1+\kappa} \right] \sigma \right\}. \end{aligned} \quad (\text{A.7})$$

Using (A.7), the eigenvalues of  $\mathbb{M}_{\text{Eckart}}$  are

$$\lambda_1^{\text{Eckart}} \simeq -\frac{H}{u} [3Q + 6(1+\sigma)(\gamma-1)(b-c)] + \mathcal{O}(1/Q), \quad (\text{A.8})$$

$$\begin{aligned} \lambda_2^{\text{Eckart}} &\simeq \frac{H}{u} \left\{ 3(\gamma-1)(c-1) - 3 + \left[ 3(\gamma-1)(c-l) + \frac{3}{2}\frac{\tilde{\sigma}}{1+\kappa} \right] \sigma \right. \\ &\quad \left. + 6(1+\sigma)(\gamma-1)(b-c) \right\} + \mathcal{O}(1/Q). \end{aligned} \quad (\text{A.9})$$

Independent of the inflaton dynamics, we then obtain that stability is assured when  $(u/H)\lambda_i < 0$ . In the slow-roll regime we have for  $\sigma = \Pi/(\gamma\rho_r)$  that

$$\sigma \simeq \frac{\Pi}{Qu^2 - \Pi} = \frac{\tilde{\sigma}}{\frac{2Q}{(1+\kappa)(1+Q)}\frac{\epsilon}{1+Q} - \tilde{\sigma}}, \quad (\text{A.10})$$

where we have used the slow-roll equations for the radiation energy density and  $u$ , Eq. (3.37). Note from the above equation that in particular we have that  $|\sigma| < 1$ . Using (A.10) in Eqs. (A.8) and (A.9), the first eigenvalue will always satisfy

the stability condition, while for the second eigenvalue Eq. (A.9), the stability condition implies:

$$(c - 2b)(1 + \sigma) + \frac{\gamma}{(\gamma - 1)} + l\sigma - \frac{1}{2(\gamma - 1)} \frac{\sigma\tilde{\sigma}}{1 + \kappa} > 0, \quad (\text{A.11})$$

or, using  $\gamma = 4/3$ , valid for the quasi-equilibrium thermal bath of warm inflation,

$$(c - 2b)(1 + \sigma) + 4 + l\sigma - \frac{3}{2} \frac{\sigma\tilde{\sigma}}{1 + \kappa} > 0. \quad (\text{A.12})$$

Let us now consider the dynamical system when the bulk pressure  $\Pi$  has an evolution according to the IS theory, Eq. (3.18). The dynamical system, including the evolution equation for the bulk pressure, now becomes

$$\begin{aligned} u' &= -3H - \Upsilon - V_\phi u^{-1} \equiv f(u, s, \Pi), \\ s' &= -3Hsu^{-1} - 3H\Pi(Tu)^{-1} + \Upsilon T^{-1}u \equiv g(u, s, \Pi), \\ \Pi' &= -\frac{\Pi}{\tau}u^{-1} - \frac{3\zeta_b H}{\tau}u^{-1} - \frac{\Pi}{2} \left\{ 3Hu^{-1} + \right. \\ &\quad + \left[ \frac{\tau, \phi}{\tau} - \frac{\zeta_b, \phi}{\zeta_b} + (\gamma - 1) \left( \frac{\tau, T}{\tau} - \frac{\zeta_b, T}{\zeta_b} - 1 \right) \frac{V_{\phi T}}{s} \right] + \\ &\quad \left. - (\gamma - 1) \left( \frac{\tau, T}{\tau} - \frac{\zeta_b, T}{\zeta_b} - 1 \right) \left[ 3Hu^{-1} \left( 1 + \frac{\Pi}{Ts} \right) - \frac{\Upsilon u}{Ts} \right] \right\} \\ &\equiv h(u, s, \Pi), \end{aligned} \quad (\text{A.13})$$

and the Jacobian stability matrix becomes

$$\mathbb{M}_{IS}(x) = \frac{\partial(f, g, h)}{\partial(u, s, \Pi)} \Bigg|_{u=u_0, s=s_0, \Pi=\Pi_0} = \begin{pmatrix} \mathcal{A} & \mathcal{B} & \mathcal{E} \\ \mathcal{C} & \mathcal{D} & \mathcal{F} \\ \mathcal{G} & \mathcal{H} & \mathcal{I} \end{pmatrix}. \quad (\text{A.14})$$

Using the slow-roll solutions, Eqs. (3.37) and (3.38), we obtain for the elements of the matrix  $\mathbb{M}_{IS}$  in the strong dissipation regime and neglecting terms proportional

to the slow-roll coefficients

$$\begin{aligned}
\mathcal{A} &= -3Q\frac{H}{u}, \\
\mathcal{B} &= 3(\gamma-1)(b-c)Q\frac{H}{s}, \\
\mathcal{C} &= \frac{Hs}{u^2}6(1+\sigma), \\
\mathcal{D} &= \frac{H}{u}[3(\gamma-1)(1+\sigma)c-3-3(\gamma-1)], \\
\mathcal{E} &= 0, \\
\mathcal{F} &= -3\frac{H}{Tu}, \\
\mathcal{G} &= \frac{HTs}{u^2}\sigma\left[\frac{3}{2}+3(\gamma-1)\Lambda(1+\sigma)\right], \\
\mathcal{H} &= \frac{HT}{u}\sigma\left\{\frac{(\gamma-1)l}{\Theta}+\frac{3(\gamma-1)^2}{2}c\Lambda(1+\sigma)-\frac{3\gamma(\gamma-1)}{2}\Lambda+\right. \\
&\quad +\frac{3(\gamma-1)}{2}b(1+\sigma)[\Lambda+(\gamma-1)\Sigma]+ \\
&\quad \left.-\frac{\tilde{\sigma}}{2(1+\kappa)}\left[\frac{1}{\Theta}-\frac{3}{2}-3(\gamma-1)\Lambda(1+\sigma)\right]\right\}, \\
\mathcal{I} &= \frac{H}{u}\left\{-\frac{1}{\Theta}-\frac{3}{2}-\frac{3(\gamma-1)}{2}\Lambda[\sigma+b(1+\sigma)]\right\}.
\end{aligned} \tag{A.15}$$

where we have defined the parameters

$$\begin{aligned}
\Theta &= \tau H, \\
\Lambda &= 1+l-\frac{T\tau_{,T}}{\tau}, \\
\Sigma &= \left(1+\frac{T\tau_{,TT}}{\tau T}-\frac{T\tau_{,T}}{\tau}\right)\frac{T\tau_{,T}}{\tau}-\left(1+\frac{T\zeta_{b,TT}}{\zeta_{b,T}}-l\right)l-\Lambda\frac{TV_{\phi TT}}{V_{\phi T}}.
\end{aligned} \tag{A.17}$$

In terms of Eq. (A.16), the eigenvalues of  $\mathbb{M}_{IS}$  are

$$\lambda_1^{\text{IS}} \simeq -\frac{H}{u}[3Q+6(1+\sigma)(\gamma-1)(b-c)], \tag{A.18}$$

$$\lambda_2^{\text{IS}} \simeq -\frac{H}{u}\left\{\frac{1}{\Theta}+3|\sigma|\left[(\gamma-1)l+\frac{|\tilde{\sigma}|}{2(1+\kappa)}\right]\right\}, \tag{A.19}$$

$$\begin{aligned}
\lambda_3^{\text{IS}} &\simeq \frac{1}{2}\left(\mathcal{D}-\frac{\mathcal{BC}}{\mathcal{A}}+\mathcal{I}\right)-\frac{1}{2}\left[(\mathcal{D}-\mathcal{I})\left(\mathcal{D}-\mathcal{I}-2\frac{\mathcal{BC}}{\mathcal{A}}\right)\right. \\
&\quad \left.-4\mathcal{F}\left(\frac{\mathcal{BG}}{\mathcal{A}}-\mathcal{H}\right)+\frac{\mathcal{B}^2\mathcal{C}^2}{\mathcal{A}^2}\right]^{1/2}.
\end{aligned} \tag{A.20}$$

The first eigenvalue above,  $\lambda_1^{\text{IS}}$ , which is the same as the Eckart case,  $\lambda_1^{\text{Eckart}}$ , and the second  $\lambda_2^{\text{IS}}$  satisfy the stability requirement  $(u/H)\lambda_i < 0$ . Hence the stability condition for the IS case then falls on the third eigenvalue  $\lambda_3^{\text{IS}}$ , Eq. (A.20). This is most easily expressed by demanding that the product  $\lambda_2^{\text{IS}}\lambda_3^{\text{IS}} > 0$ , which then leads to the condition

$$\begin{aligned} & \left[ 1 + \frac{2\sigma + 3(\gamma - 1)\Theta b\Lambda(1 + \sigma)^2}{2 + 3\Theta} \right] c + \frac{\gamma}{\gamma - 1} + \frac{2\sigma}{2 + 3\Theta} l \\ & - \frac{1}{2(\gamma - 1)} \frac{\sigma\tilde{\sigma}}{1 + \kappa} \left[ \frac{2 - 3\Theta}{2 + 3\Theta} - \frac{6(\gamma - 1)\Theta\Lambda}{2 + 3\Theta}(1 + \sigma) \right] + \\ & - \left[ 4(1 + \sigma) + 3\Theta(2 + \sigma) - 3\Theta\Lambda(1 + \sigma)^2 + \right. \\ & \left. - 3(\gamma - 1)\Theta(1 + \sigma)(\Lambda + \sigma\Sigma) + 6b(\gamma - 1)\Lambda\Theta(1 + \sigma)^2 \right] \frac{b}{2 + 3\Theta} > 0 \quad (\text{A.21}) \end{aligned}$$

which for the case  $\gamma = 4/3$  becomes

$$\begin{aligned} & \left[ 1 + \frac{2\sigma + \Theta b\Lambda(1 + \sigma)^2}{2 + 3\Theta} \right] c + 4 + \frac{2\sigma}{2 + 3\Theta} l - \frac{3}{2} \frac{\sigma\tilde{\sigma}}{1 + \kappa} \left[ \frac{2 - 3\Theta}{2 + 3\Theta} - \frac{2\Theta\Lambda}{2 + 3\Theta}(1 + \sigma) \right] + \\ & - \left[ 4(1 + \sigma) + 3\Theta(2 + \sigma) - 3\Theta\Lambda(1 + \sigma)^2 - \Theta(1 + \sigma)(\Lambda + \sigma\Sigma) \right. \\ & \left. + 2b\Lambda\Theta(1 + \sigma)^2 \right] \frac{b}{2 + 3\Theta} > 0. \quad (\text{A.22}) \end{aligned}$$

## A.2 Dynamical system for the NLCDH case

Finally, we will now obtain stability condition for the case of the NLCDH theory for the bulk pressure. In the NLCDH case, the evolution equation for the bulk pressure is given by Eq. (3.25). The dynamical system now becomes

$$\begin{aligned} u' &= -3H - \Upsilon - V_\phi u^{-1} \equiv f(u, s, \Pi), \\ s' &= -3Hsu^{-1} - 3H\Pi(Tu)^{-1} + \Upsilon T^{-1}u \equiv g(u, s, \Pi), \\ \Pi' &= -\frac{\Pi}{\tau}u^{-1} - \frac{3\zeta_b H}{\tau}u^{-1} - 3H\Pi u^{-1} \equiv h(u, s, \Pi). \end{aligned} \quad (\text{A.23})$$

The Jacobian stability matrix is similar to the one in the IS case, Eq. (A.14), but now with the functions  $f(u, s, \Pi)$ ,  $g(u, s, \Pi)$ ,  $h(u, s, \Pi)$  obtained from the above equation (A.23). Using again the slow-roll solutions, Eqs. (3.37) and (3.38), we obtain for the elements of the matrix  $\mathbb{M}_{\text{NLCDH}}$  for the NLCDH case in the strong

dissipative regime and to zero order in slow-roll

$$\begin{aligned}
\mathcal{A} &= -3Q \frac{H}{u}, \\
\mathcal{B} &= 3(\gamma - 1)(b - c)Q \frac{H}{s}, \\
\mathcal{C} &= \frac{Hs}{u^2} 6(1 + \sigma), \\
\mathcal{D} &= \frac{H}{u} [3(\gamma - 1)(1 + \sigma)c - 3 - 3(\gamma - 1)], \\
\mathcal{E} &= 0, \\
\mathcal{F} &= -3 \frac{H}{Tu}, \\
\mathcal{G} &= \frac{HTs}{u^2} 3\sigma, \\
\mathcal{H} &= \frac{HT}{u} \sigma \left[ \frac{(\gamma - 1)l}{\Theta} - \frac{1}{2} \left( \frac{1}{\Theta} - 3 \right) \frac{\tilde{\sigma}}{1 + \kappa} \right], \\
\mathcal{I} &= \frac{H}{u} \left( -\frac{1}{\Theta} - 3 \right). \tag{A.24}
\end{aligned}$$

One of the eigenvalues that follow from  $\mathbb{M}_{NLCDH}$  is still the same as the one obtained in the Eckart case, Eq. (A.8), while the other two determine de stability condition for the NLCDH case, similar to Eq. A.21

$$\begin{aligned}
\left( 1 + \frac{\sigma}{1 + 3\Theta} \right) c + \frac{\gamma}{\gamma - 1} + \frac{\sigma}{1 + 3\Theta} l - \frac{1}{2(\gamma - 1)} \frac{\sigma \tilde{\sigma}}{1 + \kappa} \frac{1 - 3\Theta}{1 + 3\Theta} \\
- \left[ 2 + \sigma + \frac{\sigma}{1 + 3\Theta} \right] b > 0. \tag{A.25}
\end{aligned}$$

For  $\gamma = 4/3$  the above equation gives

$$\begin{aligned}
\left( 1 + \frac{\sigma}{1 + 3\Theta} \right) c + 4 + \frac{\sigma}{1 + 3\Theta} l - \frac{3}{2} \frac{\sigma \tilde{\sigma}}{1 + \kappa} \frac{1 - 3\Theta}{1 + 3\Theta} \\
- \left( 2 + \sigma + \frac{\sigma}{1 + 3\Theta} \right) b > 0. \tag{A.26}
\end{aligned}$$

# Semianalytic function for the spectral index with bulk viscosity

In this appendix we write explicitly the form of function for the spectral index Eq. (5.69). The spectral index in the case  $c = 0$  without any viscosity is given by[99]

$$(n_s - 1)_0 = \frac{1}{4(1 + Q)^2} [-(17 + 9Q)\epsilon - (9Q + 1)\beta_\Upsilon + (6 + 6Q)\eta]. \quad (\text{B.1})$$

The derivative of the function  $G(\bar{\zeta}_b)$  is

$$\frac{dG(\bar{\zeta}_b)}{dN_e} = -\frac{4C_r T}{9C_b H} \bar{\zeta}_b \left[ -\frac{\mathcal{B}}{\cosh^2(\log \bar{\zeta}_b - \mathcal{C})} + \frac{\mathcal{F}\mathcal{G}}{\cosh^2(\mathcal{G} \log \bar{\zeta}_b + \mathcal{H})} + 2\mathcal{D}(\log \bar{\zeta}_b + \mathcal{E}) \right] \frac{d \log T/H}{dN_e}. \quad (\text{B.2})$$

The derivative of the function  $F(Q)$  is given by

$$\frac{dF(Q)}{dN_e} = (\alpha A^{\alpha-1} + \beta Q^{\beta-1}) \frac{dQ}{dN_e} \quad (\text{B.3})$$

For a generic  $c$  power, the derivative of the function  $f$  that relates the amplitude of the power spectrum with the  $y_k^2$  variable through Eq. (5.63) is

$$\begin{aligned} \frac{df}{dN_e} = & \left[ \frac{\sqrt{2\epsilon}}{m_P} (3H + (2 + c)\Upsilon) + \frac{H(H + \Upsilon)}{\dot{\phi}} \frac{1}{1 + Q} (\eta - \epsilon) - (c - 1) \frac{\Upsilon}{\dot{\phi}} \right] \left( \frac{H}{\dot{\phi}} \right)^2 \frac{T}{\pi^2} \frac{d\phi}{dN_e} \\ & + \frac{2(H + \Upsilon)T}{\pi^2} \left( \frac{H}{\dot{\phi}} \right)^2 \frac{m_p \sqrt{2\epsilon}}{(1 + Q)^2} \frac{dQ}{dN_e} + \left( \frac{H}{\dot{\phi}} \right)^2 \left[ \frac{(H + \Upsilon)T}{\pi^2} + \frac{cT\Upsilon}{\pi^2} \right] \frac{d \log T/H}{dN_e} \end{aligned} \quad (\text{B.4})$$

The evolution of  $\phi$  with the number of e-folds has the same form independently of the power  $c$  and the presence of bulk viscosity:

$$\frac{d\phi/m_P}{dN_e} = -\frac{\sqrt{2\epsilon}}{1 + Q}. \quad (\text{B.5})$$

The evolution of  $\log T/H$  and  $Q$  with the number of e-folds in the  $c = 0$  case without bulk viscosity is:

$$\left. \frac{d \log(T/H)}{dN_e} \right|_0 = \frac{1}{2} \left( \frac{V_{\phi\phi}}{V_\phi} - \frac{1}{2} \frac{V_\phi}{V} \right) \frac{d\phi}{dN_e} + \frac{1}{4} \left( \frac{1}{Q} - \frac{2}{1+Q} \frac{dQ}{dN_e} \right), \quad (\text{B.6})$$

$$\left. \frac{dQ}{dN_e} \right|_0 = \frac{\sqrt{3} C_\phi m_p}{3\sqrt{V}} \left( 1 - \frac{V_\phi\phi}{2V} \right) \frac{d\phi}{dN_e}. \quad (\text{B.7})$$

The corresponding evolution for  $c = 3$  with bulk is given by:

$$\left. \frac{d \log(T/H)}{dN_e} \right|_3 = \frac{2(1+\sigma)}{1+Q+6Q(1+\sigma)} \left( \frac{2+4Q}{1+Q} \epsilon - \eta + \frac{1-Q}{1+Q} \frac{m_P}{\phi} \sqrt{2\epsilon} \right), \quad (\text{B.8})$$

$$\left. \frac{dQ}{dN_e} \right|_3 = \frac{Q}{1+Q+6Q(1+\sigma)} \left[ 10 \left( 1 + \frac{6}{5} \sigma \right) \epsilon - 6(1+\sigma)\eta + 8 \left( 1 + \frac{3}{4} \sigma \right) \frac{m_P}{\phi} \sqrt{2\epsilon} \right], \quad (\text{B.9})$$

where

$$\sigma = \frac{\Pi}{\rho_r + p_r}. \quad (\text{B.10})$$

# Radiative corrections to the minimal model of inflaton dark matter

An important aspect in embedding the interactions in Eq. (7.2) within a consistent inflationary model is the fact that the discrete  $\mathbb{Z}_2 \times S_2$  symmetry does not protect the scalar potential from radiative corrections. In particular, the Yukawa interactions induce loop-corrections of the Coleman-Weinberg form, which for large inflaton field values take the leading form:

$$\Delta V_f \approx -\frac{h^4 \phi^4}{16\pi^2} \left( \log \left( \frac{h^2 \phi^2}{\mu^2} \right) - \frac{3}{2} \right) \quad (\text{C.1})$$

and therefore induce an effective quartic term in the potential. The effect of this term does not necessarily spoil the predictions of the non-minimally coupled quartic model, as discussed in [243], although one must ensure that the observed normalization of the perturbation spectrum is obtained. While for  $\xi \ll 1$  the effective quartic coupling must have approximately the same value as in the minimally coupled case, which requires  $h \lesssim 10^{-3}$ , significantly larger values can be accommodated for large non-minimal couplings.

Radiative corrections can, however, be significantly reduced in supersymmetric scenarios, and a supersymmetric version of the model in Eq. (7.2) with a  $C_2 \subset \mathbb{Z}_2 \times S_2$  symmetry can be easily obtained by considering a superpotential of the form:

$$\begin{aligned} W &= \frac{h}{2} \Phi (Y_+^2 - Y_-^2) + \frac{m_f}{2} (Y_+^2 + Y_-^2) + \\ &+ \frac{m_\phi}{2} \Phi^2 + \frac{\lambda}{2} \Phi^2 Z, \end{aligned} \quad (\text{C.2})$$

where the inflaton and fermions  $\psi_\pm$  are embedded within the chiral superfields  $\Phi$  and  $Y_\pm$ , respectively, and the auxiliary superfield  $Z$  induces the quartic term in the inflaton potential (noting that the discrete symmetry forbids cubic inflaton terms in the superpotential). Supersymmetry then cancels the leading contributions of

scalars and bosons to the 1-loop Coleman-Weinberg potential, which becomes:

$$\Delta V_{SUSY} \approx \frac{h^2}{16\pi^2} \log\left(\frac{h^2\phi^2}{\mu^2}\right) V(\phi). \quad (\text{C.3})$$

This contribution is thus necessarily smaller than the tree-level potential  $V(\phi) \simeq \lambda^2|\phi|^4/4$  for  $h \lesssim 1$ , therefore avoiding the generation of large effective self-interactions during inflation.

Besides the Yukawa terms considered so far, the supersymmetric model also yields scalar interactions between the inflaton and the scalar partners  $y_{\pm}$  of the fermions  $\psi_{\pm}$ , which apart from SUSY splittings that vanish at the origin have the same mass  $m_{\pm} = |m_f + h\phi|$ . Trilinear terms in the scalar potential also lead to the decay  $\phi \rightarrow y_{\pm}y_{\pm}$ , with analogous kinematics and comparable widths to the fermionic decay channels, therefore yielding a similar incomplete decay of the inflaton as analyzed above. We note that the incomplete decay dynamics can be fully described in terms of scalar fields and is therefore not exclusive of fermion Yukawa couplings, although the required form of the scalar mass terms is more naturally motivated within a supersymmetric context. We also note the existence of quartic terms in the scalar potential which induce the 3-body decay  $\phi \rightarrow zy_{\pm}y_{\pm}$ , where  $z$  is the scalar component of the  $Z$  chiral multiplet. The associated couplings have opposite signs for  $y_{\pm}$  and proportional to  $\lambda$ , so that they are typically sub-dominant with respect to the 2-body decays and they are also kinematically forbidden at late times, so that they do not affect our earlier conclusions.

## List of Figures

---

|     |                                                                                                                                                                                                                                                                                                                                                              |    |
|-----|--------------------------------------------------------------------------------------------------------------------------------------------------------------------------------------------------------------------------------------------------------------------------------------------------------------------------------------------------------------|----|
| 2.1 | Normalized scalar potential for different values of the fine-tuning parameter $\beta$ . . . . .                                                                                                                                                                                                                                                              | 20 |
| 2.2 | Values of $C_\phi$ and $\beta$ required to obtain $N_e \in [40, 60]$ for $g_* = 100$ and $\phi_0/m_P = 10^{-4}, 10^{-2}, 1$ from top to bottom. . . . .                                                                                                                                                                                                      | 24 |
| 2.3 | Evolution with the number of e-folds of $(\phi - \phi_0)/\phi_0$ , $\epsilon_H$ , $\rho_r/\rho_\phi$ and $T/H$ for $\phi/m_P = 10^{-2}$ , $g_* = 100$ and $\beta = 10^{-7}$ when inflation lasts 40 e-folds. . . . .                                                                                                                                         | 26 |
| 2.4 | Evolution with the number of e-folds of $(\phi - \phi_0)/\phi_0$ , $\epsilon_H$ , $\rho_r/\rho_\phi$ and $T/H$ for $\phi/m_P = 10^{-2}$ , $g_* = 100$ and $\beta = 10^{-2}$ when inflation lasts 40 e-folds. . . . .                                                                                                                                         | 27 |
| 2.5 | Values of $C_\phi$ and $\beta$ required to obtain $N_e \in [40, 60]$ for $\phi_0/m_P = 1$ and $g_* = 1, 10^4$ . . . . .                                                                                                                                                                                                                                      | 28 |
| 3.1 | The stability condition (left) and the results (right) for the radiation energy density, $\rho_r$ (purple curves), and bulk pressure, $\Pi$ (orange curves), normalized by the total energy density. The solid curves are for the Eckart case, the dashed curves are for IS and the dash-dotted curves are for NLCDH. In all cases $\Theta = 0.01$ . . . . . | 45 |
| 3.2 | Parameter space for the chaotic model. The green regions are excluded because of the violation of the condition written in the plot. The lines separate regions where $Q_* < 1$ and $Q_* > 1$ respectively. In the region between them, we can have both $Q_* < 1$ and $Q_* > 1$ for different values of $\phi(0)$ . . . . .                                 | 50 |
| 3.3 | Maximum enhancement in the number of e-folds for different values of $C_\phi$ for the model with quartic potential. The maximum value is obtained for $C_b=8.25$ . . . . .                                                                                                                                                                                   | 51 |

- 3.4 Parameter space for the hybrid models with  $\delta = 0.1, 10$ . The green regions are excluded because of the violation of the condition written in the plot. In the left plot the lines separate regions where  $Q_* < 1$  and  $Q_* > 1$  respectively. In the region between them, we can have both  $Q_* < 1$  and  $Q_* > 1$  for different values of  $\phi(0)$ . In the right plot,  $Q_*$  is always above 1. . . . . 52
- 3.5 Maximum enhancement in the number of e-folds for different values of  $C_\phi$  in the case of the inflaton potential given by Eq. (3.64). The maximum value is obtained for  $C_b = 8.25$ . . . . . 53
- 3.6 Maximum enhancement in the number of e-folds for different values of  $C_\phi$ , for the case of the inflaton potential Eq. (3.66). The maximum value is obtained for  $C_b = 8.25$ . . . . . 54
- 3.7 Parameter space for the hilltop models with  $\delta = 0.1, 1$ . The green regions are excluded because of the violation of the condition written in the plot. In the left plot the lines separate regions where  $Q_* < 1$  and  $Q_* > 1$  respectively. In the region between them, we can have both  $Q_* < 1$  and  $Q_* > 1$  for different values of  $\phi(0)$ . In the right plot,  $Q_*$  is always above 1. . . . . 55
- 4.1 Evolution of the total curvature perturbation spectrum  $\mathcal{P}_{\mathcal{R}}^{1/2}$  (black lines), the radiation  $\mathcal{P}_{\mathcal{R}}^{1/2}$  (red lines) and the field  $\mathcal{P}_{\mathcal{R}}^{1/2}$  (green lines) curvature perturbation spectrum for the potential  $V = (\lambda/4)\phi^4$ . The results are shown for different power dependence on  $T$  of the dissipative coefficient:  $c = 3$  (solid lines),  $c = 1$  (dashed lines),  $c = -1$  (dash-dotted lines), and  $c = 0$  (dotted lines)[138] . . . . . 65
- 4.2 Numerical computation of the spectral index as a function of the dissipative ratio at horizon crossing,  $Q_*$ , for the for the potential  $V = (\lambda/4)\phi^4$  with power dependence on the temperature  $c = 3$ . The solid line shows the values when the growing mode is taken into account while the dashed line represent the prediction in absence of direct coupling between the radiation and inflaton perturbed equations. . . . . 66
- 5.1 The total (square root) amplitude of the power spectrum for the case  $c = 3$  and normalized by its value for  $c = 0$ , as a function of the shear and the bulk viscosities dimensionless parameters  $\bar{\zeta}_{s,b}$ . Three different values for the dissipation ratio  $Q$  are used to illustrate the effect of the viscosities on the growth mode. The wavenumber used was  $k = 10^4 H$ . . . . . 77

|     |                                                                                                                                                                                                                                                                                                                                                                                                                                                                                                                                                                                                                    |    |
|-----|--------------------------------------------------------------------------------------------------------------------------------------------------------------------------------------------------------------------------------------------------------------------------------------------------------------------------------------------------------------------------------------------------------------------------------------------------------------------------------------------------------------------------------------------------------------------------------------------------------------------|----|
| 5.2 | The total (square root) normalized amplitude for the power spectrum for the cases $c = 3, 1, -1$ and for the three cases of temperature dependence for the bulk viscosity, $d = 3, 0, -3$ , as a function of the dimensionless bulk viscosity parameter $\bar{\zeta}_b$ . The dissipation ratio used is $Q = 100$ and wavenumber $k = 10^4 H$ . . . . .                                                                                                                                                                                                                                                            | 78 |
| 5.3 | Fits of $\langle y_k^2 \rangle_3$ normalized by $\langle y_k^2 \rangle_0$ for different ranges of $Q$ . . . . .                                                                                                                                                                                                                                                                                                                                                                                                                                                                                                    | 80 |
| 5.4 | Numerical values of $G(\bar{\zeta}_b)$ in comparison with the fit 5.67 for values $Q_* = 1, 10, 40, 60, 100$ . . . . .                                                                                                                                                                                                                                                                                                                                                                                                                                                                                             | 81 |
| 5.5 | Spectral index for $Q_* = 40$ and different values of $\bar{\zeta}_b$ . The points represents the numerical values obtained by the direct resolution of the evolution equations, while the line shows the derivative of Eq. (5.64). . . . .                                                                                                                                                                                                                                                                                                                                                                        | 83 |
| 5.6 | Spectral index for $Q_* = 40$ different values of the bulk and shear viscosities. The purple solid (orange dashed) line corresponds to the variation of the bulk (shear) viscosity with zero shear (bulk) viscosity. The green dashed-dotted (blue dotted) line corresponds to a fixed value of the bulk viscosity $\bar{\zeta}_b = 0.023$ ( $\bar{\zeta}_b = 0.48$ ) with varying shear viscosity. . . . .                                                                                                                                                                                                        | 83 |
| 6.1 | Full numerical computation of the power spectrum compared to the analytical approximation in Eq.(6.2) for different values of the dissipative coefficient at horizon crossing. . . . .                                                                                                                                                                                                                                                                                                                                                                                                                             | 90 |
| 6.2 | Trajectories in the $(n_s, r)$ plane for $V(\phi) = \lambda\phi^4$ as a function of the dissipative ratio, $Q_* < 0.01$ , 50-60 e-folds before the end of inflation, compared with the Planck results [191], for $g_* = 228.75$ relativistic degrees of freedom. The dark green (light blue) curves correspond to nearly-thermal (negligible) inflaton occupation numbers $n_*$ , with dashed branches for $T_* \lesssim H_*$ . Note that corresponding curves converge in the cold inflation limit, $T_*, Q_* \rightarrow 0$ . . . . .                                                                            | 91 |
| 6.3 | Numerical amplitude of the power spectrum normalized by Eq. (6.2) for different values of $Q_*$ and $\gamma = 0.1, 0.001$ , for nearly-thermal inflaton occupation numbers. . . . .                                                                                                                                                                                                                                                                                                                                                                                                                                | 95 |
| 6.4 | Trajectories in the $(n_s, r)$ plane for the hilltop potential in Eq. (6.27) and different vales of the $\gamma$ parameter as a function of the dissipative ratio, $Q_* < 0.01$ , 60 e-folds before the end of inflation, compared with the Planck+WP+BAO+ $\Lambda$ CDM+r results [191], for $g_* = 228.75$ relativistic degrees of freedom. The solid (dashed-dotted) curves correspond to nearly-thermal (negligible) inflaton occupation numbers $n_*$ , with dashed branches for $T_* \lesssim H_*$ . Note that corresponding curves converge in the cold inflation limit, $T_*, Q_* \rightarrow 0$ . . . . . | 96 |

- 7.1 Results of the numerical integration of the inflaton-radiation dynamical equations for  $m_\phi = 10^{-3}M_P$ ,  $\delta = 0.1$  and  $h = 1$ , showing the time evolution of (a) the inflaton (solid purple curve) and radiation (solid orange curve) energy densities; (b) the inflaton-to-entropy ratio; and (c) the inflaton decay width (solid purple curve) compared to the Hubble parameter (solid orange curve). The blue dashed curves in (a) and (c) give the evolution of the inflaton energy density in the absence of decay and the maximum value of the decay width, respectively. All quantities are given in Planck units such that  $M_P = 1$ . . . . . 104
- 7.2 Feynman diagrams for the 2-body decay of the inflaton into (a) gauge bosons, (b) light scalars and (c) light fermions, induced at the 1-loop level by gauge and Yukawa interactions of the  $\psi_\pm$  fermions. In (d) we also show the 4-body decay of the inflaton induced by the exchange of virtual  $\psi_\pm$  modes with Yukawa interactions with other light species. For clarity, all light fields are represented by green lines. . . . . 114
- 7.3 Results of the numerical integration of the inflaton-waterfall-radiation dynamical equations for  $M = 10^{-2}M_P$ ,  $g = 10^{-5}$ ,  $h = 1$ ,  $h_\chi = 10^{-5}$  and  $\delta = 0.02$ , showing the time evolution of (a) the inflaton (solid purple curve), the waterfall (dashed orange curve) and radiation (dotted green curve) energy densities; (b) the inflaton-to-entropy ratio. All quantities are given in Planck units such that  $M_P = 1$ . . . . . 119
- 7.4 Dependence of the inflaton-to-entropy ratio after reheating multiplied by the inflaton mass in Planck units for different values of the parameters in the potential,  $g$ ,  $M$  for  $\delta = 0.02$ ,  $h = 1$  and  $h_\chi = 10^{-5}$ . 120
- 7.5 Regions in the parameter space  $h_\chi - h$  where the reheating temperature is below the BBN limit (blue), the condensate can survive evaporation (green), and there is no incomplete decay (orange) . . 122
- 7.6 Parameter space of the hybrid model of inflaton dark matter with  $\delta = 1$ . In the orange (blue) region the abundance of the inflaton accounts for the present dark matter energy density and the freeze-out occurs in the radiation (waterfall=matter) era. The purple (green) region is excluded because the reheating (freeze-out) temperature is below 100 MeV. Dashed (dashed-dot) lines are curves of constant inflaton mass (reheating temperature). The grey area represents the transition between the regions where the freeze-out takes place in the radiation and waterfall era. . . . . 124





## List of Tables

---

|     |                                                                                                                                                                              |    |
|-----|------------------------------------------------------------------------------------------------------------------------------------------------------------------------------|----|
| 1.1 | Chirality and gauge quantum numbers of one family of fermions of the SM. . . . .                                                                                             | 2  |
| 1.2 | 68% limits on the cosmological parameter values measured by <i>Planck</i> using the CMB power spectra in combination with lensing reconstruction. . . . .                    | 3  |
| 3.1 | The critical values for the bulk viscosity constant $C_b$ . The Eckart case is independent of $\Theta$ , therefore the value for its critical $C_b$ does not change. . . . . | 43 |
| 3.2 | The increase of the critical value of $C_b$ for the causal theories with respect to the Eckart theory. . . . .                                                               | 43 |
| 5.1 | Values of the parameters of the function 5.66 for different ranges of $Q$ . . . . .                                                                                          | 80 |
| 5.2 | Values of the parameters of the function 5.67. . . . .                                                                                                                       | 81 |



## Bibliography

---

- [1] R. Cerezo and J. G. Rosa, *Warm Inflection*, JHEP **1301**, 024 (2013), arXiv:1210.7975.
- [2] M. Bastero-Gil, A. Berera, R. Cerezo, R. O. Ramos, and G. S. Vicente, *Stability analysis for the background equations for inflation with dissipation and in a viscous radiation bath*, JCAP **1211**, 042 (2012), arXiv:1209.0712.
- [3] S. Bartrum *et al.*, *The importance of being warm (during inflation)*, Phys.Lett. **B732**, 116 (2014), arXiv:1307.5868.
- [4] M. Bastero-Gil, R. Cerezo, and J. G. Rosa, *Inflaton dark matter from incomplete decay*, (2015), arXiv:1501.05539.
- [5] S. Glashow, *Partial Symmetries of Weak Interactions*, Nucl.Phys. **22**, 579 (1961).
- [6] S. Weinberg, *A Model of Leptons*, Phys.Rev.Lett. **19**, 1264 (1967).
- [7] A. Salam, *Weak and Electromagnetic Interactions*, Conf.Proc. **C680519**, 367 (1968).
- [8] P. W. Higgs, *Broken symmetries, massless particles and gauge fields*, Phys.Lett. **12**, 132 (1964).
- [9] F. Englert and R. Brout, *Broken Symmetry and the Mass of Gauge Vector Mesons*, Phys.Rev.Lett. **13**, 321 (1964).
- [10] G. Guralnik, C. Hagen, and T. Kibble, *Global Conservation Laws and Massless Particles*, Phys.Rev.Lett. **13**, 585 (1964).
- [11] T. Kibble, *Symmetry breaking in nonAbelian gauge theories*, Phys.Rev. **155**, 1554 (1967).
- [12] Particle Data Group, K. Olive *et al.*, *Review of Particle Physics*, Chin.Phys. **C38**, 090001 (2014).

- [13] SNO Collaboration, Q. Ahmad *et al.*, *Measurement of the rate of  $\nu_e + d \rightarrow p + p + e^-$  interactions produced by  $^8B$  solar neutrinos at the Sudbury Neutrino Observatory*, Phys.Rev.Lett. **87**, 071301 (2001), arXiv:nucl-ex/0106015.
- [14] Super-Kamiokande Collaboration, Y. Fukuda *et al.*, *Evidence for oscillation of atmospheric neutrinos*, Phys.Rev.Lett. **81**, 1562 (1998), arXiv:hep-ex/9807003.
- [15] KamLAND Collaboration, A. Gando *et al.*, *Constraints on  $\theta_{13}$  from A Three-Flavor Oscillation Analysis of Reactor Antineutrinos at KamLAND*, Phys.Rev. **D83**, 052002 (2011), arXiv:1009.4771.
- [16] K2K Collaboration, M. Ahn *et al.*, *Measurement of Neutrino Oscillation by the K2K Experiment*, Phys.Rev. **D74**, 072003 (2006), arXiv:hep-ex/0606032.
- [17] A. Einstein, *The Foundation of the General Theory of Relativity*, Annalen Phys. **49**, 769 (1916).
- [18] A. Friedman, *On the Curvature of space*, Z.Phys. **10**, 377 (1922).
- [19] E. Hubble, *A relation between distance and radial velocity among extragalactic nebulae*, Proc.Nat.Acad.Sci. **15**, 168 (1929).
- [20] G. Gamow, *Expanding universe and the origin of elements*, Phys.Rev. **70**, 572 (1946).
- [21] R. Alpher, H. Bethe, and G. Gamow, *The origin of chemical elements*, Phys.Rev. **73**, 803 (1948).
- [22] A. A. Penzias and R. W. Wilson, *A Measurement of excess antenna temperature at 4080-Mc/s*, Astrophys.J. **142**, 419 (1965).
- [23] Planck Collaboration, P. Ade *et al.*, *Planck 2015 results. XIII. Cosmological parameters*, (2015), arXiv:1502.01589.
- [24] K. A. Olive, G. Steigman, and T. P. Walker, *Primordial nucleosynthesis: Theory and observations*, Phys.Rept. **333**, 389 (2000), arXiv:astro-ph/9905320.
- [25] V. C. Rubin and J. Ford, W. Kent, *Rotation of the Andromeda Nebula from a Spectroscopic Survey of Emission Regions*, Astrophys.J. **159**, 379 (1970).
- [26] A. Borriello and P. Salucci, *The Dark matter distribution in disk galaxies*, Mon.Not.Roy.Astron.Soc. **323**, 285 (2001), arXiv:astro-ph/0001082.
- [27] J. Tyson, R. Wenk, and F. Valdes, *Detection of systematic gravitational lens galaxy image alignments - Mapping dark matter in galaxy clusters*, Astrophys.J. **349**, L1 (1990).

- [28] H. Hoekstra, H. Yee, and M. Gladders, *Current status of weak gravitational lensing*, *New Astron.Rev.* **46**, 767 (2002), arXiv:astro-ph/0205205.
- [29] L. A. Moustakas and R. B. Metcalf, *Detecting dark matter substructure spectroscopically in strong gravitational lenses*, *Mon.Not.Roy.Astron.Soc.* **339**, 607 (2003), arXiv:astro-ph/0206176.
- [30] Supernova Search Team, A. G. Riess *et al.*, *Observational evidence from supernovae for an accelerating universe and a cosmological constant*, *Astron.J.* **116**, 1009 (1998), arXiv:astro-ph/9805201.
- [31] Supernova Cosmology Project, S. Perlmutter *et al.*, *Measurements of Omega and Lambda from 42 high redshift supernovae*, *Astrophys.J.* **517**, 565 (1999), arXiv:astro-ph/9812133.
- [32] SDSS Collaboration, W. J. Percival *et al.*, *Baryon Acoustic Oscillations in the Sloan Digital Sky Survey Data Release 7 Galaxy Sample*, *Mon.Not.Roy.Astron.Soc.* **401**, 2148 (2010), arXiv:0907.1660.
- [33] WMAP, G. Hinshaw *et al.*, *Nine-Year Wilkinson Microwave Anisotropy Probe (WMAP) Observations: Cosmological Parameter Results*, *Astrophys.J.Suppl.* **208**, 19 (2013), arXiv:1212.5226.
- [34] S. Ho, C. Hirata, N. Padmanabhan, U. Seljak, and N. Bahcall, *Correlation of CMB with large-scale structure: I. ISW Tomography and Cosmological Implications*, *Phys.Rev.* **D78**, 043519 (2008), arXiv:0801.0642.
- [35] T. Giannantonio *et al.*, *Combined analysis of the integrated Sachs-Wolfe effect and cosmological implications*, *Phys.Rev.* **D77**, 123520 (2008), arXiv:0801.4380.
- [36] H. Goldberg, *Constraint on the Photino Mass from Cosmology*, *Phys. Rev. Lett.* **50**, 1419 (1983).
- [37] J. R. Ellis, J. Hagelin, D. V. Nanopoulos, K. A. Olive, and M. Srednicki, *Supersymmetric Relics from the Big Bang*, *Nucl.Phys.* **B238**, 453 (1984).
- [38] N. Arkani-Hamed, S. Dimopoulos, and G. Dvali, *The Hierarchy problem and new dimensions at a millimeter*, *Phys.Lett.* **B429**, 263 (1998), arXiv:hep-ph/9803315.
- [39] N. Arkani-Hamed, S. Dimopoulos, and G. Dvali, *Phenomenology, astrophysics and cosmology of theories with submillimeter dimensions and TeV scale quantum gravity*, *Phys.Rev.* **D59**, 086004 (1999), arXiv:hep-ph/9807344.

- 
- [40] L. Randall and R. Sundrum, *A Large mass hierarchy from a small extra dimension*, Phys.Rev.Lett. **83**, 3370 (1999), arXiv:hep-ph/9905221.
- [41] Y. Fujii, *Origin of the Gravitational Constant and Particle Masses in Scale Invariant Scalar - Tensor Theory*, Phys.Rev. **D26**, 2580 (1982).
- [42] L. Ford, *COSMOLOGICAL CONSTANT DAMPING BY UNSTABLE SCALAR FIELDS*, Phys.Rev. **D35**, 2339 (1987).
- [43] C. Wetterich, *Cosmology and the Fate of Dilatation Symmetry*, Nucl.Phys. **B302**, 668 (1988).
- [44] B. Ratra and P. Peebles, *Cosmological Consequences of a Rolling Homogeneous Scalar Field*, Phys.Rev. **D37**, 3406 (1988).
- [45] S. Capozziello, *Curvature quintessence*, Int.J.Mod.Phys. **D11**, 483 (2002), arXiv:gr-qc/0201033.
- [46] S. Capozziello, S. Carloni, and A. Troisi, *Quintessence without scalar fields*, Recent Res.Dev.Astron.Astrophys. **1**, 625 (2003), arXiv:astro-ph/0303041.
- [47] G. Dvali, G. Gabadadze, and M. Porrati, *4-D gravity on a brane in 5-D Minkowski space*, Phys.Lett. **B485**, 208 (2000), arXiv:hep-th/0005016.
- [48] G. Steigman, *Observational tests of antimatter cosmologies*, Ann.Rev.Astron.Astrophys. **14**, 339 (1976).
- [49] PAMELA Collaboration, O. Adriani *et al.*, *PAMELA results on the cosmic-ray antiproton flux from 60 MeV to 180 GeV in kinetic energy*, Phys.Rev.Lett. **105**, 121101 (2010), arXiv:1007.0821.
- [50] AMS-01 Collaboration, M. Aguilar *et al.*, *Cosmic-ray positron fraction measurement from 1 to 30-GeV with AMS-01*, Phys.Lett. **B646**, 145 (2007), arXiv:astro-ph/0703154.
- [51] O. Reimer, M. Pohl, P. Sreekumar, and J. Mattox, *Egret upper limits on the high-energy gamma-ray emission of galaxy clusters*, Astrophys.J. **588**, 155 (2003), arXiv:astro-ph/0301362.
- [52] G. Steigman, *When Clusters Collide: Constraints On Antimatter On The Largest Scales*, JCAP **0810**, 001 (2008), arXiv:0808.1122.
- [53] Planck Collaboration, P. Ade *et al.*, *Planck 2013 results. XVI. Cosmological parameters*, Astron.Astrophys. **571**, A16 (2014), arXiv:1303.5076.
- [54] G. Steigman, *Primordial Nucleosynthesis: The Predicted and Observed Abundances and Their Consequences*, PoS **NICXI**, 001 (2010), arXiv:1008.4765.

- [55] C. Wu, E. Ambler, R. Hayward, D. Hoppes, and R. Hudson, *Experimental Test of Parity Conservation in Beta Decay*, Phys.Rev. **105**, 1413 (1957).
- [56] J. Christenson, J. Cronin, V. Fitch, and R. Turlay, *Evidence for the  $2\pi$  Decay of the  $k(2)0$  Meson*, Phys.Rev.Lett. **13**, 138 (1964).
- [57] A. Sakharov, *Violation of CP Invariance, C Asymmetry, and Baryon Asymmetry of the Universe*, Pisma Zh.Eksp.Teor.Fiz. **5**, 32 (1967).
- [58] V. Kuzmin, V. Rubakov, and M. Shaposhnikov, *On the Anomalous Electroweak Baryon Number Nonconservation in the Early Universe*, Phys.Lett. **B155**, 36 (1985).
- [59] M. Shaposhnikov, *Possible Appearance of the Baryon Asymmetry of the Universe in an Electroweak Theory*, JETP Lett. **44**, 465 (1986).
- [60] M. Shaposhnikov, *Baryon Asymmetry of the Universe in Standard Electroweak Theory*, Nucl.Phys. **B287**, 757 (1987).
- [61] A. Pilaftsis, *CP violation and baryogenesis due to heavy Majorana neutrinos*, Phys.Rev. **D56**, 5431 (1997), arXiv:hep-ph/9707235.
- [62] A. Pilaftsis, *Heavy Majorana neutrinos and baryogenesis*, Int.J.Mod.Phys. **A14**, 1811 (1999), arXiv:hep-ph/9812256.
- [63] E. K. Akhmedov, V. Rubakov, and A. Y. Smirnov, *Baryogenesis via neutrino oscillations*, Phys.Rev.Lett. **81**, 1359 (1998), arXiv:hep-ph/9803255.
- [64] T. Asaka and M. Shaposhnikov, *The nuMSM, dark matter and baryon asymmetry of the universe*, Phys.Lett. **B620**, 17 (2005), arXiv:hep-ph/0505013.
- [65] C. W. Misner, *The Isotropy of the universe*, Astrophys.J. **151**, 431 (1968).
- [66] R. H. Dicke, *Gravitation and The Universe: The Jayne Lectures for 1969* (American Philosophical Institute, Philadelphia, 1979).
- [67] R. H. Dicke and J. Peebles, *The big bang cosmology-enigmas and nostrums*, in *General Relativity: An Einstein Centenary Survey*, p. 1979, Cambridge University Press, 506-508.
- [68] Boomerang Collaboration, P. de Bernardis *et al.*, *A Flat universe from high resolution maps of the cosmic microwave background radiation*, Nature **404**, 955 (2000), arXiv:astro-ph/0004404.
- [69] S. Hanany *et al.*, *MAXIMA-1: A Measurement of the cosmic microwave background anisotropy on angular scales of 10 arcminutes to 5 degrees*, Astrophys.J. **545**, L5 (2000), arXiv:astro-ph/0005123.

- [70] G. F. Smoot *et al.*, *Structure in the COBE differential microwave radiometer first year maps*, *Astrophys.J.* **396**, L1 (1992).
- [71] A. H. Guth, *The Inflationary Universe: A Possible Solution to the Horizon and Flatness Problems*, *Phys.Rev.* **D23**, 347 (1981).
- [72] A. Albrecht and P. J. Steinhardt, *Cosmology for Grand Unified Theories with Radiatively Induced Symmetry Breaking*, *Phys.Rev.Lett.* **48**, 1220 (1982).
- [73] A. D. Linde, *A New Inflationary Universe Scenario: A Possible Solution of the Horizon, Flatness, Homogeneity, Isotropy and Primordial Monopole Problems*, *Phys.Lett.* **B108**, 389 (1982).
- [74] A. R. Liddle and D. H. Lyth, *COBE, gravitational waves, inflation and extended inflation*, *Phys.Lett.* **B291**, 391 (1992), arXiv:astro-ph/9208007.
- [75] A. R. Liddle and D. H. Lyth, *The Cold dark matter density perturbation*, *Phys.Rept.* **231**, 1 (1993), arXiv:astro-ph/9303019.
- [76] A. Albrecht, P. J. Steinhardt, M. S. Turner, and F. Wilczek, *Reheating an Inflationary Universe*, *Phys.Rev.Lett.* **48**, 1437 (1982).
- [77] A. Dolgov and A. D. Linde, *Baryon Asymmetry in Inflationary Universe*, *Phys.Lett.* **B116**, 329 (1982).
- [78] L. Abbott, E. Farhi, and M. B. Wise, *Particle Production in the New Inflationary Cosmology*, *Phys.Lett.* **B117**, 29 (1982).
- [79] L. Kofman, A. D. Linde, and A. A. Starobinsky, *Reheating after inflation*, *Phys.Rev.Lett.* **73**, 3195 (1994), arXiv:hep-th/9405187.
- [80] A. R. Liddle and D. Lyth, *Cosmological inflation and large scale structure*, (2000).
- [81] Boomerang Collaboration, A. H. Jaffe *et al.*, *Cosmology from MAXIMA-1, BOOMERANG and COBE / DMR CMB observations*, *Phys.Rev.Lett.* **86**, 3475 (2001), arXiv:astro-ph/0007333.
- [82] BICEP2 Collaboration, P. Ade *et al.*, *Detection of B-Mode Polarization at Degree Angular Scales by BICEP2*, *Phys.Rev.Lett.* **112**, 241101 (2014), arXiv:1403.3985.
- [83] BICEP2 Collaboration, Planck Collaboration, P. Ade *et al.*, *A Joint Analysis of BICEP2/Keck Array and Planck Data*, *Phys.Rev.Lett.* (2015), arXiv:1502.00612.

- 
- [84] A. Berera, *Warm inflation*, Phys.Rev.Lett. **75**, 3218 (1995), arXiv:astro-ph/9509049.
- [85] A. Berera, *Thermal properties of an inflationary universe*, Phys.Rev. **D54**, 2519 (1996), arXiv:hep-th/9601134.
- [86] L. Fang, *Entropy Generation in the Early Universe by Dissipative Processes Near the Higgs' Phase Transitions*, Phys.Lett. **B95**, 154 (1980).
- [87] I. Moss, *Primordial Inflation With Spontaneous Symmetry Breaking*, Phys.Lett. **B154**, 120 (1985).
- [88] A. Berera, M. Gleiser, and R. O. Ramos, *Strong dissipative behavior in quantum field theory*, Phys.Rev. **D58**, 123508 (1998), arXiv:hep-ph/9803394.
- [89] J. Yokoyama and A. D. Linde, *Is warm inflation possible?*, Phys.Rev. **D60**, 083509 (1999), arXiv:hep-ph/9809409.
- [90] A. Berera and R. O. Ramos, *The Affinity for scalar fields to dissipate*, Phys.Rev. **D63**, 103509 (2001), arXiv:hep-ph/0101049.
- [91] M. Bastero-Gil and A. Berera, *Warm inflation model building*, Int.J.Mod.Phys. **A24**, 2207 (2009), arXiv:0902.0521.
- [92] L. M. H. Hall and I. G. Moss, *Thermal effects on pure and hybrid inflation*, Phys.Rev. **D71**, 023514 (2005), arXiv:hep-ph/0408323.
- [93] M. Bastero-Gil, A. Berera, and J. G. Rosa, *Warming up brane-antibrane inflation*, Phys.Rev. **D84**, 103503 (2011), arXiv:1103.5623.
- [94] M. Bastero-Gil, A. Berera, and R. O. Ramos, *Dissipation coefficients from scalar and fermion quantum field interactions*, JCAP **1109**, 033 (2011), arXiv:1008.1929.
- [95] I. G. Moss and C. Xiong, *Dissipation coefficients for supersymmetric inflatary models*, (2006), arXiv:hep-ph/0603266.
- [96] M. Bastero-Gil, A. Berera, R. O. Ramos, and J. G. Rosa, *General dissipation coefficient in low-temperature warm inflation*, JCAP **1301**, 016 (2013), arXiv:1207.0445.
- [97] M. Bastero-Gil, A. Berera, T. P. Metcalf, and J. G. Rosa, *Delaying the waterfall transition in warm hybrid inflation*, JCAP **1403**, 023 (2014), arXiv:1312.2961.
- [98] G. W. Anderson and L. J. Hall, *The Electroweak phase transition and baryogenesis*, Phys.Rev. **D45**, 2685 (1992).

- 
- [99] I. G. Moss and C. Xiong, *On the consistency of warm inflation*, JCAP **0811**, 023 (2008), arXiv:0808.0261.
- [100] A. Berera and L.-Z. Fang, *Thermally induced density perturbations in the inflation era*, Phys.Rev.Lett. **74**, 1912 (1995), arXiv:astro-ph/9501024.
- [101] A. Berera, *Warm inflation at arbitrary adiabaticity: A Model, an existence proof for inflationary dynamics in quantum field theory*, Nucl.Phys. **B585**, 666 (2000), arXiv:hep-ph/9904409.
- [102] L. M. H. Hall, I. G. Moss, and A. Berera, *Scalar perturbation spectra from warm inflation*, Phys.Rev. **D69**, 083525 (2004), arXiv:astro-ph/0305015.
- [103] C. Graham and I. G. Moss, *Density fluctuations from warm inflation*, JCAP **0907**, 013 (2009), arXiv:0905.3500.
- [104] R. O. Ramos and L. da Silva, *Power spectrum for inflation models with quantum and thermal noises*, JCAP **1303**, 032 (2013), arXiv:1302.3544.
- [105] D. Baumann and L. McAllister, *Advances in Inflation in String Theory*, Ann.Rev.Nucl.Part.Sci. **59**, 67 (2009), arXiv:0901.0265.
- [106] T. Gherghetta, C. F. Kolda, and S. P. Martin, *Flat directions in the scalar potential of the supersymmetric standard model*, Nucl.Phys. **B468**, 37 (1996), arXiv:hep-ph/9510370.
- [107] R. Allahverdi, K. Enqvist, J. Garcia-Bellido, and A. Mazumdar, *Gauge invariant MSSM inflaton*, Phys.Rev.Lett. **97**, 191304 (2006), arXiv:hep-ph/0605035.
- [108] R. Allahverdi, A. Kusenko, and A. Mazumdar, *A-term inflation and the smallness of neutrino masses*, JCAP **0707**, 018 (2007), arXiv:hep-ph/0608138.
- [109] J. Bueno Sanchez, K. Dimopoulos, and D. H. Lyth, *A-term inflation and the MSSM*, JCAP **0701**, 015 (2007), arXiv:hep-ph/0608299.
- [110] R. Allahverdi, K. Enqvist, J. Garcia-Bellido, A. Jokinen, and A. Mazumdar, *MSSM flat direction inflation: Slow roll, stability, fine tuning and reheating*, JCAP **0706**, 019 (2007), arXiv:hep-ph/0610134.
- [111] R. Allahverdi, B. Dutta, and A. Mazumdar, *Probing the parameter space for an MSSM inflation and the neutralino dark matter*, Phys.Rev. **D75**, 075018 (2007), arXiv:hep-ph/0702112.
- [112] R. Allahverdi, B. Dutta, and A. Mazumdar, *Unifying inflation and dark matter with neutrino masses*, Phys.Rev.Lett. **99**, 261301 (2007), arXiv:0708.3983.

- 
- [113] Z. Lalak and K. Turzynski, *Back-door fine-tuning in supersymmetric low scale inflation*, Phys.Lett. **B659**, 669 (2008), arXiv:0710.0613.
- [114] R. Allahverdi, B. Dutta, and Y. Santoso, *MSSM inflation, dark matter, and the LHC*, Phys.Rev. **D82**, 035012 (2010), arXiv:1004.2741.
- [115] K. Enqvist, A. Mazumdar, and P. Stephens, *Inflection point inflation within supersymmetry*, JCAP **1006**, 020 (2010), arXiv:1004.3724.
- [116] R. Allahverdi, S. Downes, and B. Dutta, *Constructing Flat Inflationary Potentials in Supersymmetry*, Phys.Rev. **D84**, 101301 (2011), arXiv:1106.5004.
- [117] A. Chatterjee and A. Mazumdar, *Tuned MSSM Higgses as an inflaton*, JCAP **1109**, 009 (2011), arXiv:1103.5758.
- [118] C. Boehm, J. Da Silva, A. Mazumdar, and E. Pukartas, *Probing the Supersymmetric Inflaton and Dark Matter link via the CMB, LHC and XENON1T experiments*, Phys.Rev. **D87**, 023529 (2013), arXiv:1205.2815.
- [119] S. Hotchkiss, A. Mazumdar, and S. Nadathur, *Inflection point inflation: WMAP constraints and a solution to the fine-tuning problem*, JCAP **1106**, 002 (2011), arXiv:1101.6046.
- [120] K. Enqvist, L. Mether, and S. Nurmi, *Supergravity origin of the MSSM inflation*, JCAP **0711**, 014 (2007), arXiv:0706.2355.
- [121] A. Mazumdar, S. Nadathur, and P. Stephens, *Inflation with large supergravity corrections*, Phys.Rev. **D85**, 045001 (2012), arXiv:1105.0430.
- [122] R. Allahverdi, A. R. Frey, and A. Mazumdar, *Graceful exit from a stringy landscape via MSSM inflation*, Phys.Rev. **D76**, 026001 (2007), arXiv:hep-th/0701233.
- [123] S. Kachru *et al.*, *Towards inflation in string theory*, JCAP **0310**, 013 (2003), arXiv:hep-th/0308055.
- [124] D. Baumann, A. Dymarsky, S. Kachru, I. R. Klebanov, and L. McAllister, *Holographic Systematics of D-brane Inflation*, JHEP **0903**, 093 (2009), arXiv:0808.2811.
- [125] D. Baumann, A. Dymarsky, S. Kachru, I. R. Klebanov, and L. McAllister, *Compactification Effects in D-brane Inflation*, Phys.Rev.Lett. **104**, 251602 (2010), arXiv:0912.4268.
- [126] D. Baumann, A. Dymarsky, S. Kachru, I. R. Klebanov, and L. McAllister, *D3-brane Potentials from Fluxes in AdS/CFT*, JHEP **1006**, 072 (2010), arXiv:1001.5028.

- [127] A. Ali, A. Deshamukhya, S. Panda, and M. Sami, *Inflation with improved D3-brane potential and the fine tunings associated with the model*, Eur.Phys.J. **C71**, 1672 (2011), arXiv:1010.1407.
- [128] N. Agarwal, R. Bean, L. McAllister, and G. Xu, *Universality in D-brane Inflation*, JCAP **1109**, 002 (2011), arXiv:1103.2775.
- [129] J. Blanco-Pillado *et al.*, *Racetrack inflation*, JHEP **0411**, 063 (2004), arXiv:hep-th/0406230.
- [130] A. D. Linde and A. Westphal, *Accidental Inflation in String Theory*, JCAP **0803**, 005 (2008), arXiv:0712.1610.
- [131] J. J. Blanco-Pillado, M. Gomez-Reino, and K. Metallinos, *Accidental Inflation in the Landscape*, JCAP **1302**, 034 (2013), arXiv:1209.0796.
- [132] S. Choudhury, A. Mazumdar, and S. Pal, *Low & High scale MSSM inflation, gravitational waves and constraints from Planck*, JCAP **1307**, 041 (2013), arXiv:1305.6398.
- [133] A. Berera and T. W. Kephart, *The Ubiquitous Inflaton in String-Inspired Models*, Phys.Rev.Lett. **83**, 1084 (1999), arXiv:hep-ph/9904410.
- [134] M. Bastero-Gil, A. Berera, J. B. Dent, and T. W. Kephart, *Towards Realizing Warm Inflation in String Theory*, (2009), arXiv:0904.2195.
- [135] Y.-F. Cai, J. B. Dent, and D. A. Easson, *Warm DBI Inflation*, Phys.Rev. **D83**, 101301 (2011), arXiv:1011.4074.
- [136] WMAP Collaboration, E. Komatsu *et al.*, *Seven-Year Wilkinson Microwave Anisotropy Probe (WMAP) Observations: Cosmological Interpretation*, Astrophys.J.Suppl. **192**, 18 (2011), arXiv:1001.4538.
- [137] S. Weinberg, *Cosmology* (Oxford University Press Inc., New York, 2008).
- [138] M. Bastero-Gil, A. Berera, and R. Ramos, *Shear viscous effects on the primordial power spectrum from warm inflation*, JCAP **1107**, 030 (2011), arXiv:1106.0701.
- [139] G. Murphy, *Big-bang model without singularities*, Phys.Rev. **D8**, 4231 (1973).
- [140] Y. Zeldovich, *Particle production in cosmology*, Pisma Zh.Eksp.Teor.Fiz. **12**, 443 (1970).
- [141] I. Waga, R. C. Falcao, and R. Chanda, *A BULK VISCOSITY DRIVEN INFLATIONARY MODEL*, Phys.Rev. **D33**, 1839 (1986).

- [142] R. Maartens, *Dissipative cosmology*, *Class.Quant.Grav.* **12**, 1455 (1995).
- [143] W. Zimdahl, D. Pavon, and J. Triginer, *Cosmology with bulk pressure*, *Helv.Phys.Acta* **69**, 225 (1996), arXiv:astro-ph/9608060.
- [144] W. Zimdahl, *Cosmological particle production, causal thermodynamics, and inflationary expansion*, *Phys.Rev.* **D61**, 083511 (2000), arXiv:astro-ph/9910483.
- [145] M. Giovannini, *Cosmological perturbations for imperfect fluids*, *Class.Quant.Grav.* **22**, 5243 (2005), arXiv:astro-ph/0504655.
- [146] S. del Campo, R. Herrera, and D. Pavon, *Cosmological perturbations in warm inflationary models with viscous pressure*, *Phys.Rev.* **D75**, 083518 (2007), arXiv:astro-ph/0703604.
- [147] J.-S. Gagnon and J. Lesgourgues, *Dark goo: Bulk viscosity as an alternative to dark energy*, *JCAP* **1109**, 026 (2011), arXiv:1107.1503.
- [148] I. Brevik, E. Elizalde, S. Nojiri, and S. Odintsov, *Viscous Little Rip Cosmology*, *Phys.Rev.* **D84**, 103508 (2011), arXiv:1107.4642.
- [149] O. F. Piattella, J. C. Fabris, and W. Zimdahl, *Bulk viscous cosmology with causal transport theory*, *JCAP* **1105**, 029 (2011), arXiv:1103.1328.
- [150] C. Bogdanos, A. Dimitriadis, and K. Tamvakis, *Dark energy from bulk matter*, *Phys.Rev.* **D75**, 087303 (2007), arXiv:hep-th/0611094.
- [151] S. Jeon, *Hydrodynamic transport coefficients in relativistic scalar field theory*, *Phys.Rev.* **D52**, 3591 (1995), arXiv:hep-ph/9409250.
- [152] S. Jeon and L. G. Yaffe, *From quantum field theory to hydrodynamics: Transport coefficients and effective kinetic theory*, *Phys.Rev.* **D53**, 5799 (1996), arXiv:hep-ph/9512263.
- [153] H. de Oliveira and R. O. Ramos, *Dynamical system analysis for inflation with dissipation*, *Phys.Rev.* **D57**, 741 (1998), arXiv:gr-qc/9710093.
- [154] S. del Campo, R. Herrera, D. Pavon, and J. R. Villanueva, *On the consistency of warm inflation in the presence of viscosity*, *JCAP* **1008**, 002 (2010), arXiv:1007.0103.
- [155] J. P. Mimoso, A. Nunes, and D. Pavon, *Asymptotic behavior of the warm inflation scenario with viscous pressure*, *Phys.Rev.* **D73**, 023502 (2006), arXiv:gr-qc/0512057.

- [156] C. Eckart, *The Thermodynamics of irreversible processes. 3.. Relativistic theory of the simple fluid*, Phys.Rev. **58**, 919 (1940).
- [157] W. Israel, *Nonstationary irreversible thermodynamics: A Causal relativistic theory*, Annals Phys. **100**, 310 (1976).
- [158] W. Israel and J. Stewart, *Transient relativistic thermodynamics and kinetic theory*, Annals Phys. **118**, 341 (1979).
- [159] G. Denicol, T. Kodama, T. Koide, and P. Mota, *Extensivity of irreversible current and stability in causal dissipative hydrodynamics*, J.Phys. **G36**, 035103 (2009).
- [160] R. Maartens and V. Mendez, *Nonlinear bulk viscosity and inflation*, Phys.Rev. **D55**, 1937 (1997), arXiv:astro-ph/9611205.
- [161] P. Ilg and H. C. Ottinger, *Nonequilibrium relativistic thermodynamics in bulk viscous cosmology*, Phys.Rev. **D61**, 023510 (2000).
- [162] R. Maartens, *Causal thermodynamics in relativity*, (1996), arXiv:astro-ph/9609119.
- [163] R. Maartens and J. Triginer, *Density perturbations with relativistic thermodynamics*, Phys.Rev. **D56**, 4640 (1997), arXiv:gr-qc/9707018.
- [164] W. Hiscock and L. Lindblom, *Stability and causality in dissipative relativistic fluids*, Annals Phys. **151**, 466 (1983).
- [165] R. Kubo and K. Tomita, *A General Theory of Magnetic Resonance Absorption*, J. Phys. Soc. Jpn. **9**, 888 (1954).
- [166] H. Nakano, *A Method of Calculation of Electrical Conductivity*, Prog. Theor. Phys. **15**, 77 (1956).
- [167] A. Berera, I. G. Moss, and R. O. Ramos, *Warm Inflation and its Microphysical Basis*, Rept.Prog.Phys. **72**, 026901 (2009), arXiv:0808.1855.
- [168] P. Chakraborty and J. Kapusta, *Quasi-Particle Theory of Shear and Bulk Viscosities of Hadronic Matter*, Phys.Rev. **C83**, 014906 (2011), arXiv:1006.0257.
- [169] H. Kodama and M. Sasaki, *Cosmological Perturbation Theory*, Prog.Theor.Phys.Suppl. **78**, 1 (1984).
- [170] J.-c. Hwang, *Perturbations of the Robertson-Walker space - Multicomponent sources and generalized gravity*, Astrophys.J. **375**, 443 (1991).

- [171] J.-c. Hwang and H. Noh, *Cosmological perturbations with multiple fluids and fields*, *Class.Quant.Grav.* **19**, 527 (2002), arXiv:astro-ph/0103244.
- [172] K. A. Malik, D. Wands, and C. Ungarelli, *Large scale curvature and entropy perturbations for multiple interacting fluids*, *Phys.Rev.* **D67**, 063516 (2003), arXiv:astro-ph/0211602.
- [173] A. Taylor and A. Berera, *Perturbation spectra in the warm inflationary scenario*, *Phys.Rev.* **D62**, 083517 (2000), arXiv:astro-ph/0006077.
- [174] H. De Oliveira and S. Joras, *On perturbations in warm inflation*, *Phys.Rev.* **D64**, 063513 (2001), arXiv:gr-qc/0103089.
- [175] H. De Oliveira, *Density perturbations in warm inflation and COBE normalization*, *Phys.Lett.* **B526**, 1 (2002), arXiv:gr-qc/0202045.
- [176] T. Matsuda, *Evolution of the curvature perturbations during warm inflation*, *JCAP* **0906**, 002 (2009), arXiv:0905.0308.
- [177] E. Calzetta and B. Hu, *Nonequilibrium Quantum Fields: Closed Time Path Effective Action, Wigner Function and Boltzmann Equation*, *Phys.Rev.* **D37**, 2878 (1988).
- [178] P. B. Arnold, C. Dogan, and G. D. Moore, *The Bulk Viscosity of High-Temperature QCD*, *Phys.Rev.* **D74**, 085021 (2006), arXiv:hep-ph/0608012.
- [179] M. Bastero-Gil, A. Berera, I. G. Moss, and R. O. Ramos, *Cosmological fluctuations of a random field and radiation fluid*, *JCAP* **1405**, 004 (2014), arXiv:1401.1149.
- [180] A. Onuki, *Dynamic equations and bulk viscosity near the gas-liquid critical point*, *Phys. Rev. E* **55**, 403 (1997).
- [181] D. N. Zubarev, *Non-equilibrium statistical thermodynamics* (Consultants Bureau, New York, 1974).
- [182] I. G. Moss and C. Xiong, *Non-Gaussianity in fluctuations from warm inflation*, *JCAP* **0704**, 007 (2007), arXiv:astro-ph/0701302.
- [183] E. Hairer and G. Wanner, *Solving Ordinary Differential Equations II. Stiff and Differential-Algebraic Problems*, (Springer-Verlag, 1996).
- [184] W. Press, S. Teukolsky, W. Vetterling, and B. Flannery, *Numerical Recipes 3rd Edition: The Art of Scientific Computing* (Cambridge University Press, Cambridge, 2007).

- [185] H. A. Weldon, *Simple Rules for Discontinuities in Finite Temperature Field Theory*, Phys.Rev. **D28**, 2007 (1983).
- [186] A. Anisimov, W. Buchmuller, M. Drewes, and S. Mendizabal, *Nonequilibrium Dynamics of Scalar Fields in a Thermal Bath*, Annals Phys. **324**, 1234 (2009), arXiv:0812.1934.
- [187] D. H. Lyth, *What would we learn by detecting a gravitational wave signal in the cosmic microwave background anisotropy?*, Phys.Rev.Lett. **78**, 1861 (1997), arXiv:hep-ph/9606387.
- [188] S. Hotchkiss, A. Mazumdar, and S. Nadathur, *Observable gravitational waves from inflation with small field excursions*, JCAP **1202**, 008 (2012), arXiv:1110.5389.
- [189] A. D. Linde, *Chaotic Inflation*, Phys.Lett. **B129**, 177 (1983).
- [190] S. Bartrum, A. Berera, and J. G. Rosa, *Gravitino cosmology in supersymmetric warm inflation*, Phys.Rev. **D86**, 123525 (2012), arXiv:1208.4276.
- [191] Planck, P. Ade *et al.*, *Planck 2013 results. XXII. Constraints on inflation*, Astron.Astrophys. **571**, A22 (2014), arXiv:1303.5082.
- [192] M. Drewes and J. U. Kang, *The Kinematics of Cosmic Reheating*, Nucl.Phys. **B875**, 315 (2013), arXiv:1305.0267.
- [193] K. Bhattacharya, S. Mohanty, and R. Rangarajan, *Temperature of the inflation and duration of inflation from WMAP data*, Phys.Rev.Lett. **96**, 121302 (2006), arXiv:hep-ph/0508070.
- [194] A. Ijjas, P. J. Steinhardt, and A. Loeb, *Inflationary paradigm in trouble after Planck2013*, Phys.Lett. **B723**, 261 (2013), arXiv:1304.2785.
- [195] R. Kallosh and A. Linde, *Superconformal generalization of the chaotic inflation model  $\frac{\lambda}{4}\phi^4 - \frac{\xi}{2}\phi^2 R$* , JCAP **1306**, 027 (2013), arXiv:1306.3211.
- [196] T. Matsuda, *Particle production and dissipation caused by the Kaluza-Klein tower*, Phys.Rev. **D87**, 026001 (2013), arXiv:1212.3030.
- [197] M. Bastero-Gil, A. Berera, R. O. Ramos, and J. G. Rosa, *Warm baryogenesis*, Phys.Lett. **B712**, 425 (2012), arXiv:1110.3971.
- [198] S. Bartrum, A. Berera, and J. G. Rosa, *Warming up for Planck*, JCAP **1306**, 025 (2013), arXiv:1303.3508.

- [199] J. C. Bueno Sanchez, M. Bastero-Gil, A. Berera, K. Dimopoulos, and K. Kohri, *The gravitino problem in supersymmetric warm inflation*, JCAP **1103**, 020 (2011), arXiv:1011.2398.
- [200] M. Taoso, G. Bertone, and A. Masiero, *Dark Matter Candidates: A Ten-Point Test*, JCAP **0803**, 022 (2008), arXiv:0711.4996.
- [201] M. S. Turner, *Coherent Scalar Field Oscillations in an Expanding Universe*, Phys.Rev. **D28**, 1243 (1983).
- [202] A. R. Liddle and L. A. Urena-Lopez, *Inflation, dark matter and dark energy in the string landscape*, Phys.Rev.Lett. **97**, 161301 (2006), arXiv:astro-ph/0605205.
- [203] L. Kofman, A. D. Linde, and A. A. Starobinsky, *Towards the theory of reheating after inflation*, Phys.Rev. **D56**, 3258 (1997), arXiv:hep-ph/9704452.
- [204] V. H. Cardenas, *Inflation, Reheating and Dark Matter*, Phys.Rev. **D75**, 083512 (2007), arXiv:astro-ph/0701624.
- [205] G. Panotopoulos, *A Brief note on how to unify dark matter, dark energy, and inflation*, Phys.Rev. **D75**, 127301 (2007), arXiv:0706.2237.
- [206] A. R. Liddle, C. Pahud, and L. A. Urena-Lopez, *Triple unification of inflation, dark matter, and dark energy using a single field*, Phys.Rev. **D77**, 121301 (2008), arXiv:0804.0869.
- [207] N. Bose and A. Majumdar, *A k-essence Model Of Inflation, Dark Matter and Dark Energy*, Phys.Rev. **D79**, 103517 (2009), arXiv:0812.4131.
- [208] J. De-Santiago and J. L. Cervantes-Cota, *Generalizing a Unified Model of Dark Matter, Dark Energy, and Inflation with Non Canonical Kinetic Term*, Phys.Rev. **D83**, 063502 (2011), arXiv:1102.1777.
- [209] N. Okada and Q. Shafi, *WIMP Dark Matter Inflation with Observable Gravity Waves*, Phys.Rev. **D84**, 043533 (2011), arXiv:1007.1672.
- [210] A. de la Macorra, *Dark Matter from the Inflaton Field*, Astropart.Phys. **35**, 478 (2012), arXiv:1201.6302.
- [211] K. Mukaida and K. Nakayama, *Dark Matter Chaotic Inflation in Light of BICEP2*, JCAP **1408**, 062 (2014), arXiv:1404.1880.
- [212] R. N. Lerner and J. McDonald, *Gauge singlet scalar as inflaton and thermal relic dark matter*, Phys.Rev. **D80**, 123507 (2009), arXiv:0909.0520.

- [213] V. V. Khoze, *Inflation and Dark Matter in the Higgs Portal of Classically Scale Invariant Standard Model*, JHEP **1311**, 215 (2013), arXiv:1308.6338.
- [214] G. Steigman and M. S. Turner, *Cosmological Constraints on the Properties of Weakly Interacting Massive Particles*, Nucl.Phys. **B253**, 375 (1985).
- [215] W.-K. Tung, *Group Theory in Physics* (World Scientific Publishing Co. Pte. Ltd., 1985).
- [216] P. B. Greene and L. Kofman, *Preheating of fermions*, Phys.Lett. **B448**, 6 (1999), arXiv:hep-ph/9807339.
- [217] G. Giudice, M. Peloso, A. Riotto, and I. Tkachev, *Production of massive fermions at preheating and leptogenesis*, JHEP **9908**, 014 (1999), arXiv:hep-ph/9905242.
- [218] I. Rudenok, Y. Shtanov, and S. Vilchinskii, *Post-inflationary preheating with weak coupling*, Phys.Lett. **B733**, 193 (2014), arXiv:1401.7298.
- [219] E. W. Kolb and M. S. Turner, *The Early Universe* (Addison-Wesley, Redwood City, USA, 1988).
- [220] D. J. Chung, E. W. Kolb, A. Riotto, and I. I. Tkachev, *Probing Planckian physics: Resonant production of particles during inflation and features in the primordial power spectrum*, Phys.Rev. **D62**, 043508 (2000), arXiv:hep-ph/9910437.
- [221] ATLAS, G. Aad *et al.*, *Observation of a new particle in the search for the Standard Model Higgs boson with the ATLAS detector at the LHC*, Phys.Lett. **B716**, 1 (2012), arXiv:1207.7214.
- [222] CMS, S. Chatrchyan *et al.*, *Observation of a new boson at a mass of 125 GeV with the CMS experiment at the LHC*, Phys.Lett. **B716**, 30 (2012), arXiv:1207.7235.
- [223] H. Vogel and J. Redondo, *Dark Radiation constraints on minicharged particles in models with a hidden photon*, JCAP **1402**, 029 (2014), arXiv:1311.2600.
- [224] G. Dvali, Q. Shafi, and R. K. Schaefer, *Large scale structure and supersymmetric inflation without fine tuning*, Phys.Rev.Lett. **73**, 1886 (1994), arXiv:hep-ph/9406319.
- [225] A. D. Linde, *Eternal extended inflation and graceful exit from old inflation without Jordan-Brans-Dicke*, Phys.Lett. **B249**, 18 (1990).

- [226] A. D. Linde, *Axions in inflationary cosmology*, Phys.Lett. **B259**, 38 (1991).
- [227] A. D. Linde, *Hybrid inflation*, Phys.Rev. **D49**, 748 (1994), arXiv:astro-ph/9307002.
- [228] E. J. Copeland, A. R. Liddle, D. H. Lyth, E. D. Stewart, and D. Wands, *False vacuum inflation with Einstein gravity*, Phys.Rev. **D49**, 6410 (1994), arXiv:astro-ph/9401011.
- [229] P. Binetruy and G. Dvali, *D term inflation*, Phys.Lett. **B388**, 241 (1996), arXiv:hep-ph/9606342.
- [230] E. Halyo, *Hybrid inflation from supergravity D terms*, Phys.Lett. **B387**, 43 (1996), arXiv:hep-ph/9606423.
- [231] M. Bastero-Gil and S. King, *A Next-to-minimal supersymmetric model of hybrid inflation*, Phys.Lett. **B423**, 27 (1998), arXiv:hep-ph/9709502.
- [232] M. Bastero-Gil and S. King, *F term hybrid inflation in effective supergravity theories*, Nucl.Phys. **B549**, 391 (1999), arXiv:hep-ph/9806477.
- [233] S. Antusch, K. Dutta, and P. M. Kostka, *SUGRA Hybrid Inflation with Shift Symmetry*, Phys.Lett. **B677**, 221 (2009), arXiv:0902.2934.
- [234] S. Antusch, K. Dutta, and P. M. Kostka, *Tribrid Inflation in Supergravity*, AIP Conf.Proc. **1200**, 1007 (2010), arXiv:0908.1694.
- [235] R. J. Scherrer and M. S. Turner, *Primordial Nucleosynthesis with Decaying Particles. 1. Entropy Producing Decays. 2. Inert Decays*, Astrophys.J. **331**, 19 (1988).
- [236] M. Bastero-Gil, S. King, and Q. Shafi, *Supersymmetric Hybrid Inflation with Non-Minimal Kahler potential*, Phys.Lett. **B651**, 345 (2007), arXiv:hep-ph/0604198.
- [237] M. ur Rehman, V. N. Senoguz, and Q. Shafi, *Supersymmetric And Smooth Hybrid Inflation In The Light Of WMAP3*, Phys.Rev. **D75**, 043522 (2007), arXiv:hep-ph/0612023.
- [238] M. Kawasaki, M. Yamaguchi, and T. Yanagida, *Natural chaotic inflation in supergravity*, Phys.Rev.Lett. **85**, 3572 (2000), arXiv:hep-ph/0004243.
- [239] P. Brax and J. Martin, *Shift symmetry and inflation in supergravity*, Phys.Rev. **D72**, 023518 (2005), arXiv:hep-th/0504168.
- [240] R. Kallosh and A. Linde, *New models of chaotic inflation in supergravity*, JCAP **1011**, 011 (2010), arXiv:1008.3375.

- 
- [241] A. Barvinsky, A. Y. Kamenshchik, and A. Starobinsky, *Inflation scenario via the Standard Model Higgs boson and LHC*, JCAP **0811**, 021 (2008), arXiv:0809.2104.
- [242] F. L. Bezrukov and M. Shaposhnikov, *The Standard Model Higgs boson as the inflaton*, Phys.Lett. **B659**, 703 (2008), arXiv:0710.3755.
- [243] N. Okada, M. U. Rehman, and Q. Shafi, *Tensor to Scalar Ratio in Non-Minimal  $\phi^4$  Inflation*, Phys.Rev. **D82**, 043502 (2010), arXiv:1005.5161.